Physical and Numerical Modelling Study of Meandering in Fluvial Rivers

A thesis submitted to Cardiff University for the degree of

Doctor of Philosophy

by

Hongwei Kuang

Division of Civil Engineering, Cardiff School of Engineering

Cardiff University

Sep 2011

DECLARATION

This work has not previously been accepted in substance for any degree and is not concurrently submitted in candidature for any degree.

Signed: Kuang Hongwei 匡宏维 (Hongwei Kuang) Date: 2011.11.29

STATEMENT 1

This thesis is being submitted in partial fulfillment of the requirements for the degree of Doctor of Philosophy.

Signed: Kuang Hongwei 匡宏维 (Hongwei Kuang) Date: 2011.11.29

STATEMENT 2

This thesis is the result of my own independent work/investigation, except where otherwise stated. Other sources are acknowledged by explicit references.

Signed: Kuang Hongwei 匡宏维 (Hongwei Kuang) Date: 2011.11.29

STATEMENT 3

I hereby give consent for my thesis, if accepted, to be available for photocopying and for inter-library loan, and for the title and summary to be made available to outside organisations.

Signed: Kuang Hongwei 匡宏维 (Hongwei Kuang) Date: 2011.11.29

ACKNOWLEDGEMENTS

This study would not be possible to finish without the support, help and encouragement that I got in the past from many people and organisations.

In particular I would like to express my thanks to my supervisor Professor Binliang Lin and Professor Roger A Falconer, their continued help advice, support and encouragement throughout the period of this research project. And also thanks for their review and key advice on the original manuscript.

I would like to thank everyone who helped during the period of this study, in particular colleagues in the Hydro-environmental Research Centre and friends in Cardiff University. Thanks for sharing with me their expertise and friendship. Their helps are invaluable. My sincere thanks are to all of them.

I also express my thanks to the technical staff of the Hydraulics and Soil Mechanics Laboratories, for their assistance on technical matters in the laboratory and to the administrative staff in Research Office in School of Engineering.

Finally, I am indebted to my father, mother, brother and sisters, my wife, for their continuous love, understanding, and support at all times.

ABSTRACT

A study has been taken to investigate the channel development especially fluvial river with meandering thalweg. The study included the physical model with steady inflow and unsteady inflow in the lab, and numerical model to simulate the development process, considering the bank erosion and secondary flow.

In the study of channel development with physical model, a series of tests have been carried out to model the fluvial river with different flume slope, flow rate and channel section size. The meandering thawleg channel development process was carefully observed and from results in the lab, channels only had curved boundaries with meandering thalweg, not the real meandering river. Many characteristics of fluvial river in the nature like ripple- pool unit, point bar have been modelled successfully. Then different parameters like slope, flow rate and channel size were tested independently to see their effect on channel morphology. From experiments, it is confirmed that slope is key factor to distinguish straight, meandering and braided channels. Flow rate and section size were also discussed. From the discussion of different controlling parameters, it is found that the essential control factor is Froude number.

Tests with unsteady inflow were then carried out to model the real hydrology process as that in nature. Gradually varied unsteady inflow and rapidly varied unsteady inflow were achieved by controlling the frequency of pump. Bed profile of channel after operation was recorded by Bed Profiler. Developments tell that steady inflow could deep channel and unsteady inflow has more effect on bank erosion and makes channel wider. It is concluded from bed profiles, steady inflow produces stable ripples, smooth point bars, curved channel banks. Rapidly varied flow got straight channel, wider upstream. Gradually varied flow got unstable ripple in the main channel and deepest pools.

Finally numerical modelling considering bank erosion and secondary flow was developed to simulate the tests. Bank erosion model comes from previous research and secondary flow was considered based on the balance of force in the transverse direction on Cartesian coordinate system without the constraint of constant radius of curvature. The modelling results have a good agreement with physical model for steady inflow and unsteady inflow with different channel size and slope.

CONTENTS

Chapter 4: Experimentation methods

Chapter 5: Results of physical experiment

Chapter 6: Governing equations

Chapter 7: Development of 2-D numerical model

Chapter 8: Numerical model results and comparison with experiments

LIST OF FIGURES

Chapter 5: Physical experiment results

Chapter 8: Numerical model results and comparison with experiments

LIST OF TABLES

NOTATIONS

a	maximum diameter to describe the shape of a particle, reference level of sediment profile and equals to the roughness height
A	width of channel, cross section area
B	intermediate diameter to describe the shape of a particle
B	channel width
B_C	calculated width
Bm	thalweg width
Br	channel width
Br	degree of braiding
c	volumetric concentration, time averaged concentration, minimum diameter to describe the shape of a particle, volumetric concentration
c_a	reference concentration
C	coefficient in the equation, Chezy roughness coefficient, a maximum Courant number for the ADI method
C'	Chezy coefficient
C_d	experimentally derived coefficient between Q and Q_{ideal}
C_w	air/fluid resistence coefficient
C_D	drag coefficient
d^*	bed depth
D	mean flow depth, the deposition, depth of sand
D	spherical sediment diameter, bed material size
D_n	a nominal diameter

D_s	diameter of circumscribed circle which is equivalent to the maximum dimension of the particle
$D_{15.9}$	sediment diameter for which 15.9% of bed material being finer
D_{50}	sediment diameter for which 50% of bed material being finer
$D_{84.1}$	sediment diameter for which 84.1% of bed material being finer
D_{90}	sediment diameter for which 90% of bed material being finer
D_*	non-dimensional particle size, $D_* = (\Delta g D^3 / \upsilon^2)^{1/3}$
D_{xx}, D_{xy}, D_{yx}, D_{yy}	the depth- averaged dispersion- diffusion coefficients in the x and y directions respectively
E	the erosion rates, values of the depth averaged turbulent eddy viscosity, the net erosion flux per unit area of bed
f	the friction factor, Coriolis parameter due to earth's rotation, the Darcy-Weisbach friction coefficient
F	drag force, factor in calculation of suspended sediment load
F_b	one factor in Bench's equation
F_{bc}	bed factor
Fr	Froude number
F_s	side factor
g	gravitational acceleration
h	Water depth, channel depth, the depth of water at the centre of the control volume, water depth between bed level and datum
h'	the distance between the datum and base line
h1	depth of water measurement
h2	length between water surface and position of moving rack

h_C, h_L, h_R, h_B, h_T the bed elevations at the central, left, right, bottom and top cells

H height from bottom of flume to the position of moving rack, water depth with vee weir, total water depth

I the net inflow for the control volume

I_{ABCD} the volume of water across face ABCD

I_{EFGH} the volume of water across the opposite face EFGH

I_x net inflow in the x direction in time Δt

I_y the net inflow in the y direction in time Δt

I_z the net inflow in the z direction in time Δt

J flowing slope

κ constant of Von Karman (κ=0.4)

k a factor multiplied on right-hand side of the slope equation (3.36c) in Blench's equation for meandering channels

$k1$ viscous drag coefficient

$k2$ form drag coefficient

k_s the Nikuradse equivalent sand roughness size

L Length of thalweg of one wave, river length (path wave length)

M empirical constant, weighted silt- clay index, the net mass increase during time step Δt

M_s mass of solid particle

m the velocity profile exponent, representing the effect of friction

n the Manning roughness coefficient

$\vec{n}$ the direction normal to $\vec{\tau}$

N_*	a coefficient representing the strength of the secondary flow related to the vertical profile of velocity
p	discharges per unit width in the x direction
P	wetted perimeter
q	flow rate, discharges per unit width in the y direction
q_b	volumetric bed-load transport rate
q_{bx}	components of bed load transport (kg/m/s) in the x direction
q_{by}	components of bed load transport (kg/m/s) in the y direction
q_m	source discharge per unit horizontal area
q_s	depth-integrated suspended load transport rate
q_t	total sediment discharge
q_{tx}	total volumetric sediment transport rate in positive x directions
q_{ty}	total volumetric sediment transport rate in positive y directions
q_x	flow per unit width in the x direction
q_y	flow per unit width in the y direction
Q	flow rate, discharge, bankfull discharge, volume of sand transported per unit width of bed per unit time
Q_b	bank full discharge
Q_{ideal}	ideal flow rate
Q_m	mean annual flow rate
Q_{ma}	mean annual flood flow rate
Qs	sediment discharge
Q_w	flow in straight channels in medium sand by Ackers (1964)

r	the radius of curvature of the streamline
r_c	meander-bend radius
R	hydraulic radius
R_b	the hydraulic mean radius for the bed
Re	Reynolds number
Re_*	grain Reynolds number, $\mathrm{Re}_* = u_{*cr} D / \upsilon$
R_m	minimum radius of curvature.
s	ratio of densities of grain and water, $s = \rho_s / \rho$
S	water surface gradient, slope of flume, Sinuosities, bed slope, the concentration of suspended sediment
S_b	near bed cohesive sediment concentration, percentage of silt and clay in channel banks
S_c	percentage of silt and clay in channel bed
S_{cr}	the critical slope
S_{e}	the depth-integrated equilibrium concentration
$S_{\mathrm{I}}, S_{\mathrm{II}}, S_{\mathrm{III}}, S_{\mathrm{IV}}$	four quadrants in schematic diagram of modelling the bank failure
$S_{\mathrm{L}}, S_{\mathrm{R}}, S_{\mathrm{B}}, S_{\mathrm{T}}$	the bed slopes along the cell system, named as the left ,right, bottom and top slopes
$S_{\max}$	the maximum bed slope around a cell
S_0	the initial bank slope
Sr	a specific value for slope when carrying a particular discharge and sediment load is stable only
Sv	valley slope

T	temperature by ^{O}C, the transport parameter, the transport stage parameter, time
u_{*cr}	the critical shear velocity according to Shields' diagram
μ	dynamic viscosity
υ	kinematics viscosity of water, $\upsilon = \mu / \rho$
u	velocity, local velocity, the horizontal velocity
u_*	overall bed-shear velocity
$u_*^{'}$	effective bed shear velocity
U	mean velocity, depth averaged velocity components in the x direction
U_c, U_{cr}	threshold (critical) depth- averaged speed
$U_\tau^{\mathrm{p}}(\tau,n,t)$	the depth-averaged horizontal velocity components in the $\vec{\tau}$ directions
$U_n^{\mathrm{p}}(\tau,n,t)$	the depth-averaged horizontal velocity components in the $\vec{n}$ directions
v	velocity,
v^s	the near-bed secondary flow speed
V	the total volume of sediment including solid particle volume (V_s) and pore-space volume (V_p), flowing velocity, depth averaged velocity components in the y direction
V_p	pore-space volume
V_s	volume of solid particle
V_C	calculated velocity
w	Width,width of river
w	fall velocity for a single particle, the vertical velocity
w_{O}	fall velocity of particle in a concentration

w_s particle fall velocity of suspended sediment, apparent sediment setting velocity, the settling velocity of particles

W the submerged weight, channel width

W_s the wind speed measured at 10m above the water surface

W_x the wind velocity component in the x direction at 10m above the water surface

W_y the wind velocity component in the y direction at 10m above the water surface

W^* mean width

y_0 depth

y_{0C} calculated depth

z suspension parameter which expresses the influence of the upward turbulent fluid forces and the downward gravitational forces, vertical coordinate

θ angle of vee weir, channel direction or orientation angle

θ_{cr} threshold Shields parameter

θ_m maximum angle between a channel segment and the mean down valley axis

θ_r the submerged angle of repose

τ shear stress

$\bar{\tau}$ the primary flow direction

τ_0 shear stress on bed surface

τ_b bed shear stress

τ_{cr} threshold bed shear-stress

τ_d critical shear stress for deposition

τ_f a characteristic time scale for bank erosion

τ_{xb} the bed shear stress

τ_e	critical shear stress for erosion
ρ	density of water
ρ_a	air density
ρ_s	density of sediment
γ	$g\rho$, air- water resistance coefficient, an adjustment coefficient
γ_s	$g\rho_s$
Λ	amplitude of meandering, sphericity of a sediment particle, meander length
λ	meander wavelength, scale parameter of secondary flow
β	factor for the fall velocity by sediment concentration, a function of Re, coefficient related to diffusion of sediment particles, momentum correction factor for a non-uniform vertical velocity profile
β'	a coefficient used to describe the friction coming from both the bed and the upper layer water
Δ	$\Delta = (\rho_s - \rho)/\rho$, apparent roughness
Δh_{B}, Δh_{R}	the sediment volumes transferred to the two parts are expressed by the variation of bed elevation
Δx	grid sizes in x direction
Δy	grid sizes in y direction
ΔS	the difference between the maximum bed slope $S_{\max}$ and the critical bed slope S_{cr}
$\Delta\widetilde{S}$	the slope to be adjusted for bank erosion
Δt	the time step
$\Delta\theta_{\mathrm{r}}$	an additional angle for the special location

ψ	correction factor representing all additional effects such as the volume occupied by particles, reduction of particle fall velocity and turbulence damping effect
δ_b	saltation height
Φ	the transport function is for the total transport
ε	porosity of bed, depth averaged turbulent eddy viscosity
ω	angle rotation speed of the earth
φ	geographical angle of latitude of site
α	the proportion of near bed water column
ζ	bed level, relative to an arbitrary datum, distance between the sand bed surface and base line
η	water surface elevation above datum, the porosity of bed sediment

ABBREVIATIONS

ADI	Alternating Direction Implicit
ADV	Acoustic Doppler Velocimeter
AutoCAD	A software for design and drawing
BS	British Standard
BOD	Biochemical Oxygen Demand
CAIC	A small software to get position from AutoCAD to Excel
CFD	Computational Fluid Dynamics
COR	the value of signal correlation coefficient
DB	Unit for COR
DIVAST	Depth Integrated Velocity And Solute Transport
DO	Dissoloved Oxygen
FORTRAN	A programming language suited to numeric computation and scientific computing
HZ	Hertz, the unit of frequency
ISO	International Organization for Standardization
SF	Shape Factor
SIMENS	A German engineering conglomerate, the largest of this kind in Europe
SNR	Signal- to- Noise Ratio
TECPLOT	The name of a family of visualization software tools developed by Tecplot, Inc.
WIHEE	Wuhan Institute of Hydraulics and Electrical Engineering
WBB	The name of Providers of industrial minerals

Chapter 1

Introduction

1.1 Introduction

Alluvial rivers play an important role in people's living. There are three types of alluvial rivers: straight, meandering and braided (see Figure 1.1). Among the various river planforms, meandering is a very common type observed in natural rivers (Dulal and Shimizu, 2010). Morphology development of meandering rivers involves not only sand erosion and deposition in the vertical direction, but also retreat and advance in the lateral direction. Large population tends to live in close proximity to meandering rivers because of the fertile land, easy transportation and flat terrain. Meandering development could have negative impacts to flooding defence projects, ports, roads, bridges and navigation. It is very important to understand the meandering phenomenon before any new construction work such as bridges, ports, pipe line crossings, etc. (Parker, 1998) and/or dealing with problems like sediment transport, river ecology, re-naturalization, etc. (Crosato, 2008). Construction works would also affect the meandering development.

(a): A meandering section of the Amazon River. (b): A braided river in New Zealand.

Figure 1.1: River forms: (a) a meandering river and (b) a braided river from Google map.

Physical experiment has shown to be a useful method to study the meandering process by many researchers. In the laboratory it is easy to control the flow rate, flume slope, channel size and sand material type thus to understand their effects on channel morphology development. Experiments undertaken in the laboratory can be used not only to model real natural rives, but also to provide calibration data for numerical model development.

1.2 Aims and objectives

From the review in Chapter 2, it is clear that physical experiment in the laboratory is an important method to study morphological development in fluvial rivers. There are a lot of experiments being carried out to study meandering and braided rivers since the pioneering work by Friedkin in 1945. Most of these researches involved only the condition of steady inflow. There are very few unsteady inflow experiments. One of the main objectives of this research was to cover this gap by modelling fluvial rivers with unsteady inflow. Non-cohesive silica sands with size D50 = 0.268 mm were used in this study. This size range is similar to those used in previous studies. A two dimensional sediment transport model developed by Sun and Tao (2010) was modified and used to model the channel development.

The main objectives and key problems can be summarized as follows:

1. To improve the understanding of the fundamental processes of river planform evolution like bank erosion processes, meander evolution and cut-offs, which are important for the fixing of river bend or the creation of an artificial cut-off.

2. To undertake physical modelling of fluvial rivers in the laboratory with a different grain size from existing studies.
3. To test the different effects of some key parameters on the morphological development, such as channel size, flume slope and flow rate. Since different parameters have different roles in the channel development.
4. To undertake experiments with unsteady inflow. To compare results from experiments by unsteady inflow with experiment results by steady inflow.
5. To analyse the meandering development process in fluvial rivers. Most previous experiments focused on the final results but did not mention the process of development. Here the observation of process development could provide foundation of analysis in natural rivers.
6. To undertake numerical model simulations to predict lateral channel development. The experimental data obtained from the laboratory will be used to assist the numerical model development.

1.3 Outline of thesis

The details of the remaining chapters in this study can be summarised as follows:

Chapter 2 reviews recent physical experiments and numerical modelling on meandering rivers and the phenomenon of meandering development.

Chapter 3 introduces the properties of sands, sediment transport model and some theories of river morphology, including channel types and regime theory.

Chapter 4 demonstrates the experimentation methods including experiment planning, water supply system, equipment, model set up, operation and data processing.

Chapter 5 presents physical experiment results, first with steady inflows and then with unsteady inflows. Tests for straight, meandering and braided channels are introduced. Comparisons are made between tests with different flow rates, slopes and channel sizes. The reproducibility is discussed. In the second part, tests with gradually varied inflow and rapidly varied inflow are outlined to compare with tests having steady inflow. Results from the experiments are also compared with theoretical calculations.

Chapter 6 provides details of the governing equations used to represent the hydrodynamic and sediment transport processes.

Chapter 7 introduced the development of numerical model which includes the numerical solution methods, bank erosion and secondary flow. The developed model would be used to model the experiments in the lab.

In chapter 8, numerical model predictions are compared with results from the physical experiments.

Chapter 9 draws conclusions for this research and also provides recommendations for future study.

The appendices contain source code for processing data collected from the laboratory experiments. Comparisons between results from the physical experiments and results from several regime theories are also included.

Chapter 2

Literature review

2.1 Introduction

Meandering migration is a complex process involving water flow, sediment transport and bank movement. Many researchers have investigated this process in order to prevent potential damages. Physical experiments and numerical modelling are two basic research methods in this field and many useful progresses have been made.

2.2 Phenomena study

Before undertaking any numerical modelling on meander migration, it is important to understand physical processes that are causing meandering migration to take place.

Water Flow

Flow characteristics and their interaction with channel geometry and planform are central to all problems of river engineering (Thorne et al., 1997). A spiral flow occurs in the channel bend, combining a primary flow and a secondary flow. It affects the flow velocity distribution, sediment transportation, bed and bank erosion and deposition and, as a result, affects the development of channel morphology, dispersion of contaminants and sorting of sediments.

Knighton (1998) and Chang (1988) pointed out that the flow phenomenon under the influence of centrifugal acceleration includes:

(1) superelevation of the water surface against the concave bank.

(2) transverse current towards the outer bank at the surface and towards the inner bank at the bed to give a secondary circulation additional to the main downstream flow.

(3) a maximum velocity current, which moves from near the inner bank at the bend entrance to near the outer bank at the bend exit, crossing the channel through the zone of greatest curvature.

De Vriend (1979), Bathurst et al. (1979) and Thorne et al. (1997) indicated that the circulation pattern may also include a small cell of reverse circulation at the steep outside bank and a dominance of outward flow near the inside bank caused by a progressive longstream decrease in depth along the point bar, see Figure 2.1. Rozovskii (1957) concluded that the small cell is a wall effect, extending over a region of one or two depths from the bank, but negligible in bends with large width/depth ratios.

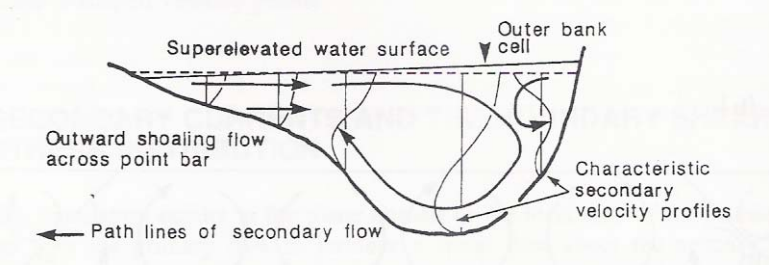

Figure 2.1: Secondary circulation pattern at a river bend cross-section, with main circulation cell near the inside bank and small cell of reverse circulation at the outside bank. (From Thorne et al., 1997)

Secondary flow

Just as mentioned above: a spiral flow occurs in the channel bend, combining a primary flow and a secondary flow. The secondary flow is an important process in river morphology. Below is a brief review of the secondary flow.

Secondary flow is a field of fluid motion which can be considered as superimposed on a primary field of motion. It is relatively minor flow when compared with the primary flow. There are several types of secondary flows. The most common type occurs when fluid follows a curved path (Taylor, 1968). Another type is generated through the action of friction, usually in the vicinity of solid boundaries, thus it is also known as frictional secondary flow (McGraw-Hill of Science and Technology Dictionary, 2003). In some instances, the secondary flow is in a region separated from the primary flow by a streamline that attaches to smooth surfaces or sharp edges (Lewalle, 2006).

A classic example is that a cup of tea is stirred to give a circular motion. Tea leaves tend to gather at the centre bottom of tea cup, not at the perimeter. The water is a little deeper at the perimeter than at the centrer. There is a pressure gradient from the perimeter toward the centre. This pressure gradient provides the centripetal force for the circular motion of water. The pressure gradient also accounts for a secondary flow flowing toward the axis of circulation of the water across the floor of the cup. On reaching the center the secondary flow is then upward toward the surface, progressively mixing with the primary flow. Near the surface there may also be a slow secondary flow outward toward the perimeter.

The secondary flow at a river bend is a similar type which will be emphasized in this chapter. The water surface is slightly higher near the concave bank than near the convex bank. As a result, the water pressure is slightly higher near the concave bank than near the convex bank. There is a secondary flow along the floor of the river bed from the concave bank toward the convex bank, driven by the pressure gradient. The secondary flow is then upward toward the surface where it mixes with the primary flow or moves slowly across the surface, back toward the concave bank.

On the floor the secondary flow sweeps sand across the river and deposits sediment near the convex bank just like tea leaves being swept toward the center of a cup as described above.

In nature, there are other types of secondary flow existing around us, for example the tropical cyclones, tornadoes and dust devils. Secondary flow also occurs in machines like turbines and other turbomachinery.

Sand transportation

'Pool- bar unit' is the basic morphological unit in meandering rivers because of the spiral current. The shear stress is linked to velocity. When shear stress is larger than the critical shear stress, bed material would begin to move first as bed load, then suspended load. Due to the spiral motion in the flow, the pool is scoured near the outer bank and bed material would be transported from the outer bank to the inner bank, and clear water would be transported from the inner bank to the outer bank. The above processes enhance erosion of the outer bank and growth of point bar. The maximum sediment transport follows the maximum shear stress and the distribution of shear stress affects sediment sorting. The coarser material would be found in the outer bank and finer material is found in the inner bank.

Bank erosion and collapse

With the erosion at the outer bank, and deposition at the inner bank, the out bank retreats and point bar advances. Chen and Duan (2006), Nagata et al. (2000) recognized that bank erosion of non-cohesive material consisted of two interactive physical processes: basal erosion and bank

collapse. The bank material at the bank toe is transported by the flowing water and then the bank collapses by its gravity and sediment is accumulated or transported away from bank toe.

Ikeda et al. (1981) assumed that the rate of bank erosion rate is linearly related to the near bank velocity perturbation, a difference between depth- averaged velocity and cross- sectional mean velocity (Chen and Duan, 2006). The distribution of velocity and shear stress and local turbulence characteristics have an important influence on the erosive potential of hydraulic action, which in many instances is the major process (Knighton, 1973; Hooke, 1979). The bank collapse by mass failure depends on bank geometry, structure and material properties. Thorne (1982) recognized that the moisture conditions play an important role in the processes of weakening of bank material strength and bank stability. There are many factors that influence the bank erosion, including: stream power, shear stress by the primary current and secondary current, local slope, bend, bank composition, vegetation, bank moisture content, bank height and angle.

The collapse of bank makes bank line retreat. Thorne et al. (1997) pointed out that the balance between the rates of supply from bank processes and removal by fluvial entrainment decides the amount and duration of basal sediment storage and then decides the bank retreat and advance.

Meander migration

Lateral migration in meandering rivers results from the erosion of the outer bank combined with equivalent sedimentation near the inner bank. The migration rate depends on the erosion rate and erosion rate depends on the bank material strength, cohesion, armouring and vegetation (Julien, 2002). The rate of migration is controlled to a large extent by bend geometry and in particular by channel curvature (r_c / w, where r_c is meander-bend radius and w channel width) (Knighton,

1998). The relative migration rate is defined as the annual migration rate divided by the channel width. Nanson and Hickin (1986) found that the rate of migration reaches a maximum when $2 < r_c / w < 4$, decreasing rapidly on either side of this range.

Migration has various movements: translation, extension, rotation and lobbing and compound growth. Hooke (2007) offered an insight into the geomorphological instability and evolution of landscape by 20 years of observation of an active natural meandering channel.

The lateral migration rate increases as channel sinuosity increases. When sinuosity and bend amplitude become very large, the downstream transport capacity, channel slope and flow velocity are reduced. A threshold sinuosity may be reached and the concerned river can no longer maintain its shape, then a cut- off develops. Cut-off includes neck cut-off and chute cut-off. Cut-offs cause a decrease in the sinuosity, and an increase in the slope and velocity.

2.3 Theory analysis

Many scientists studied the meandering river, not only through physical experiment and field observation, but also through theoretical analysis.

According to Ikeda et al. (1981), the rate of bank erosion is linearly related to the magnitude of near bank velocity perturbation, a difference between depth- averaged velocity and cross-sectional mean velocity, bank advances if the near bank perturbation velocity is greater than zero, and it retreats otherwise (Duan, Wang and Jia, 2001). This method had been used by many other researchers: Sun et al. (1996, 2001a, b), Johannesson and Parker (1989), Odgaard (1989) and Parker (1983). This assumption has its own limitation when it is used to simulate meander

migration. Other investigators have developed a few analytical models, such as El-Khudairy (1970), Engelund (1974), Kikkawa et al. (1976), Zimmermann and Kennedy (1978) and Odgaard (1981), Kassem and Chaudhry (2002). These models can be applied to simple bed- flow conditions due to their simple assumptions.

Empirical regime theory developed from field observation and analysis has been used to predict geometry of equilibrium channels with flowing characteristics.

Ackers (1964) found the best-fit relations describing the morphology of straight channels in medium sands, and Ackers and Charlton (1970a) indicated that meandering channels on average are twice the width of straight channels. Lacey in 1929 obtained relationships between wet perimeter and discharge in the channel. Leopold and Maddock (1953) recognized that the regime concept could be used to describe natural alluvial rivers, based on the bankfull discharge. Julien and Wargadalam (1995) took the discharge, grain size and channel slope into consideration. Leopold et al. (1960) obtained a relationship between the meander length, width and radius of curvature. Bettess and White (1983) developed an analytical regime theory to decide the channel patterns.

Extremal hypotheses with more physical basis have also been proposed. These theories include: the minimum unit stream power (Yang, 1976), the minimum stream power (Chang, 1979), the maximum sediment transport rate (Kirkby, 1977; White et al., 1982), the minimum variance hypothesis, the minimum energy dissipation rate (Yang et al., 1981), the minimum Froude number (Jia, 1990) and other theories.

2.4 Physical experiment study

Steady inflow

Many physical experiments have been undertaken to investigate the flow velocity, channel bed form and channel morphology development.

Many experiments have been carried out since the pioneering work by Friedkin in 1945. Most researchers chose non-cohesive silica sand as the bed and bank materials, such as Friedkin (1945), Schumm et al. (1987), Jang and Shimizu (2005), Gran and Paola (2001) and Federici and Paola (2003). The results were either the braided channels or the straight channels with meandering thalwegs. Madej et al. (2009) carried out experiments to examine how sediment transport capacity changes during aggradation and degradation while changing sediment loads.

Smith (1998) used light, fine grained materials to simulate the formation of well defined, highly sinuous meanders in a small flume. Jin and Schumm (1986) did experiments with kaolinite clay as top layer and floodplain as base of sand. Ouchi (1985) conducted physical experimentation with a mixture of moderately sorted medium sand and a small amount of kaolinite to examine the effects of both uplift and subsidence on braided and meandering channels. And for the braided channel, additional sand was fed into the head of channel by a sand feeder and a mixture of clay and water was circulated by a pump for the meandering channel. Gardner (1983) carried out physical experiments to simulate knickpoint retreat and stable alluvial meander phase developed within 150 hours. Kleinhans et al. (2009) modeled estuarine meandering channels with highly cohesive sediment and found that the channel bed was eroded by backward migrating steps.

Other researchers did experiments with the sine- generated channel to see the morphological change. Silva (1995) used a channel with an initial angle of 30 degree; Nagata et al. (2000) took the initial meandering channel form with 2 m wavelength. In these experiments non- cohesive uniform silica sand was used. Shepherd and Schumm (1974) carried out experiments to study the incision in straight and sinuous channels.

These researchers carried out many experiments with different materials. However, they mainly focused on the last stage of channel development, with little attention being focused on the actual processes and also the relationship between the meander length, width and amplitude. This paper is to fill this gap.

Unsteady inflow

Most experiments carried out before were using different materials, such as cohesive sediment (Smith, 1998; Kleinhans et al., 2009; Dulal and Shimizu, 2010) or non-cohesive sediment (Friedkin, 1945; Ackers, 1964), but they were only involving steady inflow conditions. Experiments with unsteady inflow conditions are rare. The only previous laboratory work on unsteady inflows is limited to some experiments where, for example, Tominaga, Liu, Nagao and Nezu (1995) studied the hydraulic response of flash floods with fixed boundaries, and Kabir (1993), Graf and Song (1995) and Bestawy (1997) studied sediment transport and velocity distributions in flash floods in laboratory conditions with mobile beds. (Valentine and Ershadi, 2003). Hong et al. (1987) did experiments with flooding modelling in the lab and analysed its impact on meandering. Unsteady inflows include gradually varied and rapidly varied flows. Experiments with steady inflow in the laboratory show a lot of similarity to rivers in nature and

also have some differences. These have been analysed by many researchers. In this study, a series of physical experiments were carried out, using non-cohesive sediment, to understand the influence of unsteady inflow on the development of channel form.

2.5 Numerical modelling

Ikeda et al. (1981) developed a model to predict the meander formation and migration, in which the bank erosion rate is assumed to be proportional to the near bank flow velocity. Such process-based bank erosion models could be used to predict long term development of meandering forms. And this model is used by many researchers (Parker et al., 1982; Odgaard, 1989; Parker and Andrew, 1986; Sun et al., 1996, 2001a, b). However, according to Darby et al. (2002), these models are limited to predict the meandering processes over a short time period. Because:

1. the erodibility coefficient is empirical and decided by calibration not by sand characteristics.
2. some models set the river as regular planform, which is different from rivers found in the natural world.
3. many meander channel models (Odgaard, 1989; Sun et al., 1996, 2001a, b) neglected the adjustment of channel width. The bank advance or retreat is the result of bank erosion and near bank sediment transportation. Thus over simplification may cause inaccuracy in the predictions of flow, sediment transport and bed-level change in rivers with erodible banks.

To overcome this disadvantage, a physically based model was developed by Osman and Thorne (1988). In this model the sediment transport and bank erosion rates were calculated to assess the advance or retreat of a channel bank line. Then Mosselman (1998), Nagata et al. (2000), Duan et

al. (2001) and Darby et al. (2002) presented 2-D depth averaged models of flow and bed topography in movable computational grids. The advantages of this physically based model are that:

1. the model of bank erosion, collapse and deposition could allow further insight into the influence of sedimentary characteristics on meander evolution (Osman and Thorne, 1988).
2. the model is a dynamic model and not restricted to steady conditions.
3. the coordinate system of 2-D physically based model could be used to model the natural irregular rivers.

However, Mosselman (1998), Duan et al. (2001) neglected the bank failure process, Nagata et al. (2000) neglected the difference between basal erosion and bed degradation. Mosselman (1998) concluded that the empirical formula which was used to calculate the helical flow in the bending section was the main reason for the shortcoming in his model. And Shimizu et al. (1996) and Nagata et al. modelled the meandering evolution with uniform non- cohesive banks in the laboratory while Sun and Darby's model included mixed materials for natural rivers.

A 3-D model was also developed to predict the meander evolution by Olsen (2003) and Rüther and Olsen (2003, 2005a, b). With a 3-D model, the domain is also discretised over the depth and velocities in all the three directions are calculated in each cell of the domain (Rüther and Olsen, 2007). It does not need the empirical formulae like the 2-D model to calculate the helical flow in the bending section. The advantage for these models is that the cells could keep dimensions and would not be distorted while channel narrowing or widening. The main disadvantage of a 3-D model is that it is time consuming.

Some other researchers (Murray and Paola, 1994 and 1997) used a simple cellular numerical model in a fixed grid system to reproduce the braided river's features. Cellular modelling has its advantage on the range of spatial scales (1–100 km^2) and time periods (1–100 years) that are especially relevant to contemporary management and fluvial studies (Coulthard, Hicks and Van De Wiel, 2007), and disadvantage on the restrictions on computational stability and routing water velocity limitation.

2.6 Spur dike

A spur dike may be defined as a structure extending outward from the bank of a stream for the purpose of deflecting the current away from the bank to protect it from erosion. (Kuhnle1 et al, 2008) River spur dikes are often constructed nearly perpendicular to the riverbanks, beginning at a riverbank with a root and ending at the regulation line with a head. They maintain a channel to prevent ice jamming, and more generally improve navigation and control over lateral erosion, that would form from meanders. Spur dikes have a major impact on the river morphology: they cause autonomous degradation of the river.

2.7 Summary

This chapter introduces the phenomena study, theory analysis and sediment transport, physical experiment study and numerical modelling of meandering rivers. Previous physical experiments did not show details on the morphology change due to bed slope and cross sections development, and the current research would cover this gap. This research with unsteady inflow is a new aspect

to doing meandering research in the laboratory. And the physical experiment is the foundation for calibration of the 2-D depth average model development.

Chapter 3

Sediment transport and river morphology

3.1 Introduction

Sediment is important to river morphology and the environment which affect people's living conditions. The river form is influenced by sediment transport, including erosion and deposition. Sediment is generally transported in two forms: bed load and suspended load. In the following, the sediment characteristics will be first introduced and then details of two main river forms, meandering and braided rivers, and the regime theory are presented. The sediment transport equation will be described with details in Chapter 6.

3.2 Sediment properties and characteristics

It is important to understand the physical properties and characteristics of sediment that control the transportation rate. It will help in interpreting results obtained from physical and numerical modelling studies.

3.2.1 Density and porosity

The mass density of a solid particle could be described as the solid mass per unit volume.

$$\rho_s = \frac{M_s}{V_s} \qquad 3.1$$

where ρ_s = sediment density, M_s = mass of solid particle, V_s = volume of solid particle.

The mass density for a quartz particle is $2650\,kg/m^3$. It does not vary significantly with the temperature. Other materials can be different, for example: heavy materials have large mass density, plastic sediments are usually lighter.

The specific gravity is another parameter used to describe the density.

$$s = \frac{\rho_s}{\rho} \qquad 3.2$$

where s = specific gravity, ρ = density of fluid at reference temperature, usually taken as 1000 kg/m^3 when the temperature is at $4^{O}C$. In this way, the specific gravity for a quartz particle is 2.65.

Porosity is the ratio of pore-space volume to total volume of sediment. The equation used to describe its value is given as:

$$\text{Porosity} = \frac{V_p}{V} = \frac{V_p}{V_p + V_s} \qquad 3.3$$

where V_p = the pore-space volume, V_s = the solid volume, V = the total volume of sediment including solid particle volume (V_s) and pore- space volume (V_p).

The porosity is a measure of the closeness of contact between particles. It is influenced by sediment shape, size, uniformity and pattern of deposition.

The value of porosity tends to reduce after sediments travel a long distance, because the shape would become round. Sediments with different sizes have smaller porosity compared with the uniform sediments. Fine sediment particles have fewer voids than coarse particles.

3.2.2 Shape

Sediment comes from rocks which became small parts by outer forces such as temperature, collision. These parts have different shapes and sizes. Then with transportation in the river, particles become smaller and their surfaces become smoother from upstream to downstream. Different shapes and sizes would have important impact on their transportation.

One of the definitions in use is named shape factor (Raudkivi, 1998):

$$SF = \frac{c}{(ab)^{1/2}} \qquad 3.4$$

where SF = shape factor, a, b and c = maximum, intermediate and minimum diameters of a particle, respectively.

The sphericity is also used to describe shape:

$$\Lambda = \frac{D_n}{D_s} \qquad 3.5$$

where Λ = sphericity of a sediment particle, D_n = a nominal diameter, D_s = diameter of circumscribed circle which is equivalent to the maximum dimension of the particle.

3.2.3 Size

Size is another important physical property of a sediment particle. According to the size, sediment is clarified as boulder, cobble, gravel, sand, silt and clay. Details of classification are shown in Table 3.1.

Table 3.1: Sediment classification according to particle size, BS 1377: 1975.

Class name	Particle diameter D (mm)	Class name	Particle diameter D (mm)
Boulder		**Sand**	
Very large	>2048	Coarse	0.500< D< 1
large	1024< D <2048	Medium	0.250< D <0.500
medium	512< D <1024	Fine	0.125< D< 0.250

small	256< D <512	Very fine	0.062< D <0.125
Cobble		**Silt**	
Large	128< D <256	Coarse	0.031< D <0.062
Small	64< D <128	Medium	0.016< D <0.031
Gravel		Fine	0.008< D <0.016
Very coarse	32 < D <64	Very fine	0.004< D <0.008
Coarse	16< D <32	**Clay**	
Medium	8< D <16	Coarse	0.0020< D <0.004
Fine	4< D <8	Medium	0.0010< D <0.0020
Very fine	2< D <4	Fine	0.0005< D <0.0010
Sand		Very fine	0.00024< D <0.0005
Very coarse	1< D <2		

The sediments become cohesive when their size is smaller enough. The shape of sediment particles are different in nature, thus specific methods have been developed to measure the size. There are a number of ways to define the particle size (Shao and Wang, 2005):

1. The nominal diameter refers to the diameter of a sphere with the same volume as that of particle, usually measured by the displaced volume of a submerged particle.
2. The sieve diameter is the minimum length of the square sieve opening through which a particle will fall.
3. The fall diameter is the diameter of an equivalent sphere of specific gravity $s = 2.65$ having the same fall velocity in water at $24^{O}C$.

4. D_{50} (medium size) is usually taken as the representative diameter, which means sediment coarser and finer than that diameter both have 50% of the total weight.

3.2.4 Angle of repose for sediments

When sediments are poured together in still water the angle between the edge of the pile and the horizontal surface is called the angle of repose. The angle of repose varies with grain size and angularity of the material.

The value of the angle of repose for material coarser than medium silt would be between 30^{O} and 42^{O}. Different shaps lead to different values. If particles have sharp edges and are angular, then they will have a larger angle of repose than normal, sometimes 5^{O} to 10^{O} higher.

3.2.5 Fall velocity

The fall velocity of sediment particles is an important property for sediment transport. It is also known as setting velocity or terminal velocity. The concept is straightforward, but not easy to evaluate. Many factors such as size, shape, density and viscosity decide its value.

The fall velocity of single particle in still water

For a spherical particle in stationary fluid, falling would reach a constant velocity when the submerged weight (W) of the particle is equal to the drag (F):

$$W = F \qquad 3.6a$$

$$W = \frac{\pi D^3}{6} g(\gamma_s - \gamma), F = C_D \frac{\pi D^2}{4} \frac{\rho \omega^2}{2} \qquad 3.6b$$

where C_D = drag coefficient, which is a function of grain specify Reynolds number, D = spherical sediment diameter, υ = kinematic viscosity, g = gravitational acceleration and ω = falling velocity.

$$\omega = \left[\frac{4}{3}\frac{1}{C_D}\frac{\gamma_s - \gamma}{\gamma} gD\right]^{1/2} \qquad 3.7$$

When Reynolds number is less than 0.4, the drag coefficient can be obtained from a relationship given by Stokes:

$$F = 3\pi\mu D\omega \qquad 3.8$$

So, $$3\pi\mu D\omega = C_D \frac{\pi D^2}{4}\frac{\rho\omega^2}{2} \qquad 3.9$$

and $$C_D = \frac{24}{\mathrm{Re}_*} \qquad 3.10$$

where μ = dynamic viscosity, and

$$\omega = \frac{1}{18}\frac{\gamma_s - \gamma}{\gamma}\frac{gD^2}{\upsilon} \qquad 3.11$$

For natural sands, the fall velocity would have a coefficient less than 1. WIHEE (Wuhan Institute of Hydraulics and Electrical Engineering) uses $\frac{1}{25.6}$ (Shao and Wang, 2005) instead of $\frac{1}{18}$ when some researchers use $\frac{1}{24}$.

The above equation applies when Re_* < 0.4.Most researchers think that Stokes solution works if Re_* <= 1.

For $\mathrm{Re}_* \le 2$, Goldstein (Raudkivi, 1998) got:

$$C_D = \frac{24}{\mathrm{Re}_*}\left(1 + \frac{3}{16}\mathrm{Re}_* - \frac{19}{1280}\mathrm{Re}_*^{\,2} + \frac{71}{20480}\mathrm{Re}_*^{\,3} ...\right) \qquad 3.12$$

Oseen solution is the first two terms in brackets (Raudkivi, 1998).

If Re_* > 1000, the viscous force is negligible and $C_D = 0.45$,

$$\omega = 1.72\sqrt{\frac{\gamma_s - \gamma}{\gamma} gD} \qquad 3.13$$

The corresponding diameter is larger than 4.0 mm. For natural sands, the fall velocity would have a coefficient less than 1. For WIHEE the coefficient 1.72 would become 1.044, other researchers use different coefficients.

If Re_* is between 0.4 and 1000, both the inertia and viscous forces have significant effects. For this transitional region, both the viscous drag and form drag exist, with different terms being used to represent them:

$$(\gamma_s - \gamma)\frac{\pi D^3}{6} = k_1 \frac{\pi D^2}{4}\frac{\rho\omega^2}{2} + k_2 \pi D \mu \omega \qquad 3.14a$$

$$\omega = -4\frac{k_2}{k_1}\frac{\upsilon}{D} + \sqrt{(4\frac{k_2}{k_1}\frac{\upsilon}{D})^2 + \frac{4}{3k_1}\frac{\gamma_s - \gamma}{\gamma} gD} \qquad 3.14b$$

where k_1 and k_2 are two coefficients. For natural sands, Rubey chose $k_1 = 2, k_2 = 3$ and WIHEE chose $k_1 = 1.223, k_2 = 4.266$.

The effect of shape on the fall velocity

The shape of a particle is another factor that has a significant effect on the fall velocity. Analytical solutions exist for the Stokes range, but only experimental information is available when the Re is outside of the Stoke range. The effect of shape on the fall velocity is far from being completely understood.

Cheng (1997) proposed a formula:

$$\frac{\omega D}{\upsilon} = \left[(25 + 1.2D_*^2)^{1/2} - 5\right]^{1.5} \qquad 3.15$$

Zanke (1982) developed a relationship for determining the fall velocity of grains with a SF ≈ 0.7 (SF is shape factor, see Equation 3.4).

$$\omega = \frac{11\upsilon}{D}\left[(1+0.01D_*^3)^{0.5}-1\right] \qquad 3.16$$

For isolated sand grains in still water, the formulae of van Rijn (1984a) for natural sand are widely used:

$$\omega = \frac{1}{18}\frac{\upsilon D_*^3}{D} \quad \text{when} \quad D_* \le 16.187 \qquad 3.17a$$

$$\omega = \frac{10\upsilon}{D}\left[(1+0.01D_*^3)^{0.5}-1\right] \quad \text{when} \quad 16.187 \le D_* \le 16187 \qquad 3.17b$$

$$\omega = \frac{1.1\upsilon D_*^{1.5}}{D} \quad \text{when} \quad D_* \ge 16187 \qquad 3.17c$$

in which $D_* = (\frac{\Delta g D^3}{\upsilon^2})^{1/3}$, and $\Delta = (\rho_s - \rho)/\rho$.

Effect of temperature on fall velocity

Temperature affects the fall velocity since the kinematic viscosity υ of water changes with temperature. For small size particles the effect of temperature is more significant. A 0.2 mm grain in water at 20 ^{O}C has an approximately 20% higher fall velocity than at 10 ^{O}C (Raudkivi, 1998).

The average values for quartz sands in water at 20 ^{O}C are well described by Equation 3.18.

$\omega(mm/s) = 663D^2(mm)$, $D < 0.15$mm 3.18a

$\omega(mm/s) = 134.5D^{0.52} \cong 134.5\sqrt{D}(mm)$, $D > 1.5$mm 3.18b

In the transition region, i.e., $0.15mm \le D \le 1.5mm$, the value of fall velocity is shown in Table 3.2.

Table 3.2: Fall velocities of quartz grains of $0.15mm \le D \le 1.5mm$ at $20^{O}C$, from Raudkivi (1998).

D (mm)	0.15	0.2	0.3	0.4	0.5	0.6
ω (mm/s)	14.8	21.1	36.1	50.0	64.0	76.4
D (mm)	0.7	0.8	0.9	1.0	1.2	1.5
ω (mm/s)	88.6	99.0	110.0	121.0	137.3	166.0

The kinematic viscosity could be calculated by an empirical formula:

$$\upsilon = \frac{0.01775}{1 + 0.0337T + 0.000221T^2} \qquad 3.19$$

in which T is in ^{O}C, and υ is in cm^2/s.

An approximate expression for the kinematic viscosity is:

$$\upsilon = \frac{40}{20 + T^{O}C} \times 10^{-6} (m^2/s) \qquad 3.20$$

Some values of dynamic viscosity μ are shown in Table 3.3.

Table 3.3: Dynamic viscosity μ of pure water as a function of temperature.

$T(^{O}C)$	μ ($N\,s/m^2$)				
	0	2	4	6	8
0	1.7938×10^{-3}	1.6740×10^{-3}	1.5676×10^{-3}	1.4726×10^{-3}	1.3872×10^{-3}
10	1.3077×10^{-3}	1.2390×10^{-3}	1.1748×10^{-3}	1.1156×10^{-3}	1.0603×10^{-3}
20	1.0087×10^{-3}	0.9608×10^{-3}	0.9161×10^{-3}	0.8746×10^{-3}	0.8363×10^{-3}
30	0.8004×10^{-3}	0.7670×10^{-3}	0.7357×10^{-3}	0.7064×10^{-3}	0.6791×10^{-3}

Effect of concentration on the fall velocity

The influence of sediment concentration on the fall velocity can be expressed as:

$w_O = w(1-c)^{\beta}$, in which c is the volumetric concentration, w is the fall velocity for a single particle, w_O is the fall velocity of particle in a concentration c and β is a function of Re and particle shape. And also function of non-dimensional particle size: $D_* = (\frac{\Delta g D^3}{\upsilon^2})^{1/3}$

where: $\Delta = (\rho_s - \rho)/\rho$. 3.21

For common natural particles (SF is about 0.7):

$\beta = 4.65$ when D_*<40 3.22a

$\beta = 2.35$ when D_*>~8000 3.22b

$\beta = 7.478 D_*^{-0.129}$ when $40 \le D_* \le 8000$ 3.22c

3.2.6 Cumulative frequency curve

The size distribution of sediment particles reflects the intensity of sorting process in river flow and is related to the amount of sediment transported. There are several methods to describe the size gradation, such as frequency histogram, cumulative size-frequency curve and others.

Frequency histogram**:** particle diameter (or its logarithm) is taken as abscissa and the percentage of weight (or number) as the ordinate.

Cumulative size-frequency curve**:** particle diameter (or its logarithm) is taken as the ordinate and the percentage of weight (or number) of sediment particles that is smaller than the given size is taken as the abscissa.

3.3 Sediment transport model

3.3.1 Threshold for bed shear stress

Water flowing over a bed of sediment exerts a force on grains that tend to move or entrain them. The resistance to the entraining action depends on the grain size and its distribution. Shields (1936) suggested that the process of initiation of motion is statistical in nature.

The measure of the threshold of motion can be made using the bed shear-stress. Shields (1936) developed the threshold called Shields parameter θ_{cr}, which is the ratio of the force exerted by the bed shear-stress acting to move a grain on the bed and the submerged weight of the grain. The threshold Shields parameter θ_{cr} is defined as:

$$\theta_{cr} = \frac{\tau_{cr}}{g(\rho_s - \rho)D} \qquad 3.23$$

where τ_{cr} = threshold bed shear-stress, g = gravitational acceleration, ρ_s = sediment density, ρ = water density, D = particle diameter.

This dimensionless parameter θ_{cr} can be plotted against the grain Reynolds number Re_*:

$$\mathrm{Re}_* = u_{*cr} D / \upsilon \qquad 3.24a$$

where $u_{*cr} = (\tau_{cr} / \rho)^{1/2}$ 3.24b

This relationship is famously known as Shields curve and is widely used in determining the critical condition of sediment movement. However, it is inconvenient to use because the unknown u_{*cr} appears on both sides of the equation.

$$D_* = \left(\frac{g(s-1)D^3}{\upsilon^2}\right)^{1/3} \qquad 3.25$$

where $\upsilon = \mu / \rho$, $s = \rho_s / \rho$. Then Shields parameter can be approximately written as the following form:

$$\theta_{cr} = 0.24(D_*)^{-1} \qquad D_* \le 4 \qquad 3.26a$$

$$\theta_{cr} = 0.14(D_*)^{-0.64} \qquad 4 < D_* \le 10 \qquad 3.26b$$

$$\theta_{cr} = 0.04(D_*)^{-0.10} \qquad 10 < D_* \le 20 \qquad 3.26c$$

$$\theta_{cr} = 0.013(D_*)^{0.29} \qquad 20 < D_* \le 150 \qquad 3.26d$$

$$\theta_{cr} = 0.055 \qquad D_* > 150 \qquad 3.26e$$

3.3.2 Threshold current speed

The flow velocity which makes a few particles begin to move is called threshold (or initiation) of motion or incipient motion.

There are a lot of methods developed to predict the threshold (critical) depth-averaged speed U_{cr} for a steady inflow where the river bed is flat, horizontal and un-rippled.

Van Rijn (1984c) developed formulae to calculate the critical mean flow velocity for particles in the range of 100~2000 μm, in water at 15 ^{O}C, $\rho_s = 2650 \ \ kg/m^3$ and $g = 9.81 \ \ m/s^2$:

$$U_{cr} = 0.19(D_{50})^{0.1} \log_{10}^{(4h/D_{90})} \qquad 100 \le D_{50} \le 500\mu m \qquad 3.27a$$

$$U_{cr} = 8.5(D_{50})^{0.6} \log_{10}^{(4h/D_{90})} \qquad 500 \le D_{50} \le 2000\mu m \qquad 3.27b$$

where all units are in metres and seconds. These equations are more difficult to use because they are purely based on experiments.

Soulsby (1997) combined his threshold bed shear-stress formula with the friction law to form a relationship for threshold current speed, which works for any non-cohesive sediment and flow conditions, provided:

$$U_{cr} = 7\left(\frac{h}{D_{50}}\right)^{1/7}\left[g(s-1)D_{50}f(D_*)\right]^{1/2} \qquad D_* > 0.1 \qquad 3.28a$$

where $f(D_*) = \frac{0.30}{1+1.2D_*} + 0.055[1 - \exp(-0.020D_*)]$ 3.28b

This equation is easier to use because it is based on theory.

3.4 River morphology

3.4.1 Classification

Channels are classified as a range of geomorphological channel types. These classifications take consideration of river planform, cross section geometry, longitudinal profile and types of bed materials.

Schumm (1977) showed five basic river types in Figure 3.1 and these types show a relationship between the sediment load, channel stability and channel form. It is convenient to divide the channel form as: straight, meandering, braided and anastomosed channels. In this chapter, meandering and braided channels will be analysed in more details in connection with the brief introduction of straight and anastomosed channels.

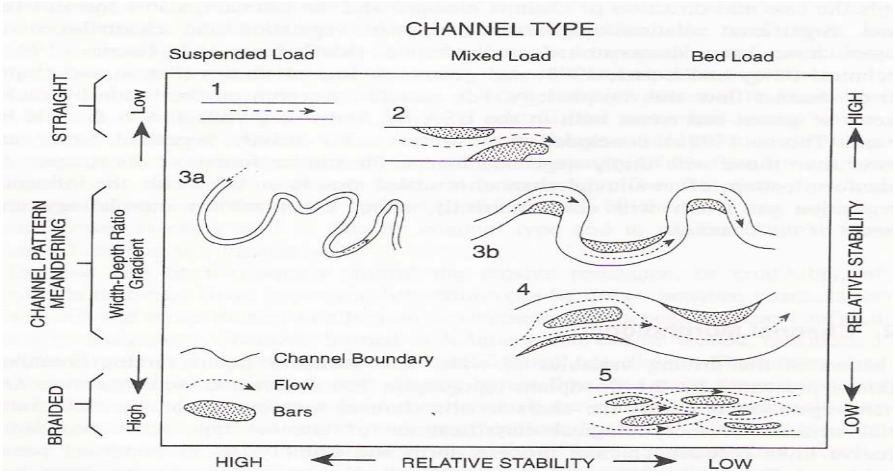

Figure 3.1: Classification of channel pattern based on sediment load and system stability (adapted from Schumm (1977)).

If the sinuosity (channel length/ straight line valley length) of a river channel is less than 1.1, the channel is considered straight. As shown in Figure 3.1, straight channels always have fine suspended sediment.

The braided rivers are separated by braided bars and these bars can be stable when large size particles and vegetation make the bars stable as islands. Banks are resistant to erosion. This type of channel form is regarded as anastomosing.

And in gravel bed rivers, the basic morphological unit: pool-bar exists in all straight, meandering and braided channels. Channel-bed configurations include bedforms and bars. Bedforms include ripples, dunes, and antidunes and remain submerged. Bars include alternate bars, point bars and tributary bars. Bars are alluvial bed deposits and would be exposed during low flows.

3.4.2 Differentiation between braided and meandering channels

Leopold & Wolman (1957) proposed to use the following equation to determine the channel pattern:

$$S = 0.012 Q_b^{-0.44} \qquad 3.29$$

where S = bed slope, Q_b = bank full discharge.

This equation separates braided channels and the meandering channels. A figure of slope against discharge has been used by other researchers to differentiate between meandering and braided channels and boundaries were drawn to distinguish not only areas of braided and meandering, but also areas of meandering and straight.

The relationship between erosion and transporting bank materials is a key element used to differentiate channels patterns (Brotherton, 1979). A channel would be straight when erosion is more difficult than transporting; a channel would be braided when erosion is easier than transporting; meandering is the intermediate state when erosion and transporting are in balance.

3.4.3 Meandering rivers

In this study, model channels developed in the flume were not the real meandering channels but the thalweg meandering. Theory about meandering channels could be used on the thalweg meandering. This is the reason why information about meandering is introduced here.

Relationships

Langbein and Leopold (1966) found that θ is a function of the maximum angle θ_m set at the origin, the downstream distance x and the river length L:

$$\theta = \theta_m \cos\frac{2\pi x}{L} \qquad 3.30$$

where θ = channel direction or orientation angle, θ_m = maximum angle between a channel segment and the mean down valley axis, L = river length (path wave length). This equation describes symmetrical meander paths reasonably well.

It is recognized that there is approximately a constant relationship between meander parameters and channel width. Leopold et al. (1960) observed that the meander length Λ is about 10 times the channel width W and the ratio of wavelength to minimum radius of curvature Λ / R_m for a meandering stream is between 3 and 5. Leopold and Wolman (1960) suggested 4.7 as an average ratio.

Dury (1965) found the relationship between the meander wavelength and discharge, given as:

$$\lambda = 54.3Q_b^{0.5} \qquad 3.31$$

where λ = meander wavelength.

Nixon (1959) related the width, depth and mean velocity to the bank-full discharge in sediment bed rivers:

$$B = 2.99Q^{1/2},\ \ y_0 = 0.55Q^{1/3},\ \ V = 0.61Q^{1/6} \qquad 3.32$$

Charlton et al. (1978) derived similar expressions for gravel bed rivers:

$$B = 3.74Q^{0.45},\ \ y_0 = 0.31Q^{0.40},\ \ V = 0.86Q^{0.15} \qquad 3.33$$

Ackers (1964) found that the best-fit relations describing the morphology of straight channels in medium sand, which carried flows (Q_w) between 0.011 and 0.153 m^3/s, were:

$$A = 0.52Q_w^{0.85},\ \ B = 2.64Q_w^{0.42},\ \ y_0 = 0.20Q_w^{0.43},\ \ V = 1.92Q_w^{0.15} \qquad 3.34$$

where A = cross- section area in m^2, B = width in m, y_0 = depth in m, V = velocity in m/s.

Ackers and Charlton (1970a) indicated that the width of meandering channels on average is twice of straight channels.

River width and depth are also functions of type of sediment and sediment load. Coarse sediments lead to broader and shallower rivers and fine sediments to deeper and narrower streams (Raudkivi, 1998). However, the above equations do not take sediment load into consideration and they are not widely used.

Schumm (1968) analysed a large number of empirical data sets for sand bed rivers and streams and derived the following relationships:

$$\lambda = 1935Q_m^{0.34}M^{-0.74} \qquad r^2 = 0.89 \qquad 3.35a$$

$$\lambda = 618 Q_b^{0.43} M^{-0.74} \qquad r^2 = 0.88 \qquad 3.35b$$

$$\lambda = 395 Q_{ma}^{0.48} M^{-0.74} \qquad r^2 = 0.86 \qquad 3.35c$$

where Q_m = mean annual flow rate, Q_b = bank-full discharge (m^3/s), Q_{ma} = mean annual flood flow rate, M = weighted silt- clay index, given by:

$$M = \frac{S_c B + 2 S_b y_0}{B + 2 y_0} \qquad 3.35d$$

in which S_c, S_b = percentage of silt and clay in channel bed and channel banks, respectively.

Blench's equations took account of bed load transport and the effect of differences in bed and bank material is accommodated by means of a bed and a side factor (Thorne et al., 1997).

For discharge (Q): 0.03- 2800 m^3/s, Sediment discharge (Qs): 30- 100 ppm,

Bed material size (D): 0.1- 0.6 mm, Bank material type: cohesive,

Bedform: ripples- dunes, Bank vegetation: not specified,

Valley slope: not specified, Planform: straight,

Profile: uniform,

Mean width: $W^* = \frac{F_{bc}^{0.5}}{F_s^{0.5}} Q^{0.5}$ （m） 3.36a

Bed depth: $d^* = \frac{F_s^{0.33}}{F_{bc}^{0.66}} Q^{0.33}$ (m) 3.36b

Slope: $S = \frac{F_{bc}^{0.833} F_s^{0.083} \upsilon^{0.25}}{3.63 g Q^{0.166} (1 + \frac{Q_s}{2330})}$ 3.36c

where bed factor F_{bc} and side factor F_s are defined by:

$$F_{bc} = F_b (1 + 0.012 Q_s) \qquad 3.36d$$

$F_b = \frac{V^2}{d^*}(m/s^2)$, and can be approximated by: $F_b = 0.58 D_{50}^{0.5}$ 3.36e

$F_s = \frac{V^3}{W^*}(m^2/s^3)$, or F_s = 0.009 (metric) for loam of very slight cohesiveness, 3.36f

= 0.018 (metric) for loam of medium cohesiveness,

= 0.027 (metric) for loam of very high cohesiveness,

where υ the kinematic viscosity (m^2/s), *Qs* bed load charge in parts per 100 000 by weight, D_{50} is the median particle size (mm).

In order to calculate the Blench regime dimensions, the side factor, sediment concentration, and the bed-material gradation should be known. For meandering channels Blench (Thorne et al., 1997) indicated that right-hand side of the slope Equation 3.36c should be multiplied by a factor *k*. He indicated that the value of *k* varied from 2 for well-developed meanders to 1.25 for straight channels with alternate bars.

Migration and cut-off

If a channel bank is composed of erodible sediment particles, the bank may be eroded and the bank line would advance or retreat. The lateral migration in meandering rivers results from the erosion of the outer bank combined with equivalent sedimentation near the inner bank (Julien, 2002).

The rate of migration is controlled to a large extent by the bend geometry of a river and, in particular, by the channel curvature (r_c/W, where r_c is radius of curvature and *W* is channel width) (Knighton, 1998). The relative migration rate is defined as the annual migration rate

divided by the channel width. The migration process involves various movements: translation, extension, rotation and lobbing and compound growth.

The lateral migration increases as channel sinuosity increases. When the sinuosity and bend amplitude become very large, the downstream transport capacity, channel slope and flow velocity are reduced. A threshold sinuosity may be reached when a river can no longer maintain its shape, then a cut-off develops. Cut-off forms include neck cut-off and chute cut-off. (Knighton, 1998) Cut-offs decrease the sinuosity, increase the slope and velocity (Knighton, 1998).

3.4.4 Braided rivers

Braided rivers are multi-channel forms in which the channels are separated by bars or islands. The characteristic feature of the braided pattern is the repeated division and joining of channels, and the associated divergence and convergence of flow, which contributes to a high rate of fluvial activity relative to other river types (Knighton, 1998). Other primary characteristics of braided channels are also found in natural and laboratory braided channels: 1) straight channel banks, 2) division of the flow into numerous thalwegs separated by bars or islands, 3) a very wide, flat-bottomed, shallow cross section, 4) a steep longitudinal profile, 5) a high concentration of bed load, 6) and a continuous shifting of the positions of the thalwegs (Schumm et al., 1987).

To measure the degree of braiding by the sum of channel lengths in a reach to the reach length:

$$Br = \frac{\text{sum of mid channel lengths of all primary channels in reach}}{\text{mid channel length of widest channel in reach}}$$

From the characteristic features of braided channels, these conditions below are required for the development of braided channels: 1) an abundant bed load, 2) erodible banks, 3) a highly variable discharge, 4) steep valley slope.

3.4.5 Regime theory

Bettess and White (1983) recognized that for a given type of sediment, a river with valley slope (Sv) carrying a particular discharge and sediment load is stable only if the slope has a specific value (Sr). This specific value (Sr) is calculated from the analytical regime theory developed by White et al. in 1982. When:

(a) Sr = Sv, channel would be straight and in equilibrium.

(b) Sr < Sv, equilibrium can be achieved by either:

(i) channel would be meandering because meandering reduces the slope measured along the channel from the slope measured along the valley and channel with sinuosity Sv/ Sr. Or

(ii) channel would be braiding when Sr << Sv, which increases the (regime) slope by sharing the total discharge and sediment load between n smaller channels.

(c) Sr > Sv, river cannot achieve the required equilibrium and erosion or deposition would take place to reach another equilibrium condition.

Bettess and White (1983) indicated that large gravel rivers are more frequently braided than sand rivers of comparable size which are more frequently meandering in nature, and it is unusual to come across a meandering gravel river with a high sinuosity while this is more common for sand rivers. It is uncommon for small streams to be braided in character, see Figure 3.1.

3.4.6 Mountain river morphology

Steps and pools are ubiquitous bed forms in mountain stream channels, occurring where gradients exceed 2% and materials are in the gravel to boulder size range (Chin, 2003). Mountain streams differ from their lowland counterparts in a number of important respects (Knighton, 1998). They develop step-pool morphology in which steps are typically formed from the accumulation of boulders and cobbles which span the channel width, and finer sediments in pools produce a characteristic, repetitive sequence of bed forms.

The development step-pool morphology is strongly influenced by local supply and flow conditions. Besides, step-pool morphology plays a fundamental role in river system because of its hydraulic resistance. It could dissipate large potential energy generated by the steep slope, that otherwise would lead to extreme erosion and channel degradation. The role of step–pools is especially important in confined mountain streams that prohibit lateral adjustments and energy dissipation by meandering and braiding (Chin, 2003). From Chin (2003)'s research, it can be concluded that: steps are an effective energy dissipator at low flows; energy dissipation by steps diminishes at increasing flows; the point at which steps become submerged marks a transition in their role as an energy dissipator to roughness elements in the fluvial system.

3.5 Summary

In this chapter, a review of sediment properties, sediment transport model and channel morphology have been presented. Details have been given regarding the sediment characteristics such as the density, porosity, shape, size, repose angle and fall velocity in section 3.2. After this,

the sediment transport models were introduced in section 3.3. Section 3.4 gave the river morphology: meandering river and braided river, introduced regime theory and mountain streams. The equations for bed-load and suspended sediment transport will be introduced in Chapter 6 together with the bed deformation equation.

Chapter 4

Experimentation methods

4.1 Introduction

This chapter introduces the aims, objectives, materials, equipment and methods for the physical experiments. Section 4.2 explains the aims and objectives. Section 4.3 describes the water supply system. Section 4.4 introduces the flume used for the experiments. Section 4.5 describes sediment chosen and section 4.6 shows the data measurement including velocity measurement, depth measurement and water elevation measurement.

4.2 Aims and objectives of the experiments and the planning

4.2.1 Aims and objectives

- To see how the channel changes by the introduction of spur dike (or other artificial structure in the river) from straight channel to meandering.
- To see how the straight channel develops into a meandering river by an initial small curved beginning with steady flow.
- To study characteristics of channels with meandering thalweg and curved boundaries.
- To study effects of bed slope, flow discharge and cross-section sizes on key channel properties.
- To carry out flume experiments to study channel development with unsteady flow.
- The result can provide theory instruction for navigation and flooding defence projects.
- The physical experiments can be compared against results from numerical modelling.

4.2.2 Plan of experiments to meet study aims

There are two sets of experiments. One set of experiments is carried out using a spur dike to see how it causes morphological change. The other is how channel morphology changes from straight to meandering by the initial bending.

4.2.2.1 The procedure for the first set of experiment

1. Put concrete block at the beginning of channel as a spur dike.

2. Put sand in the flume to 5.0 cm depth and then make the sand bed surface flat.

3. Water elevation in the flume is raised by adding water to the tailbox.

4. Discharge in the channel is raised slowly to the designed rate.

5. Water surface and bed elevations are measured along the channel. Vertical and oblique photographs are taken, planimetric and cross-sectional data will be collected to construct maps and cross sections of the channel. (Photograph will be taken every hour.)

There is no sand feeding and water is recycled after the sediment deposition.

4.2.2.2 The procedure for the second set of experiments

The flume was filled with sand to a depth of 8.0 cm. The surface was flattened to a given slope (the same as the flume), then the middle straight channel was excavated. Detail of preparation is below:

Prepare the channel with wood board: the size of wood board is 120 cm width. Put another small wood board in the middle of the large channel (see Figure 4.15). After finishing channel, the real size of the channel is not the same as the board's size: it has got a larger top width, smaller bottom width but the same height). Figure 4.1 shows the channel made in the flume ready for the experiment.

1. Put the sand surface flat while there is no water.

2. Let small quantity of water flow into flume until water upstream at about 1 cm depth, so all sand is under water, and water can flow out through the sluice-gate.

3. Put the board in the flume with its boundary near the glass flume wall, move the board slowly from upstream to downstream to excavate middle channel and flatten the two sides of banks. The slope of channel bank is the sand repose angle in the water, top and bottom width would be different with the size of wood board, height is the same. It needs to measure size again after channel making.

4. Move the board from the beginning smoothly and slowly again to make the channel better. Make two small sand banks at the end of sand bed with channel in the middle which keep water flowing away from the middle channel while lowering down water level, and trying not destroying the smooth surface.

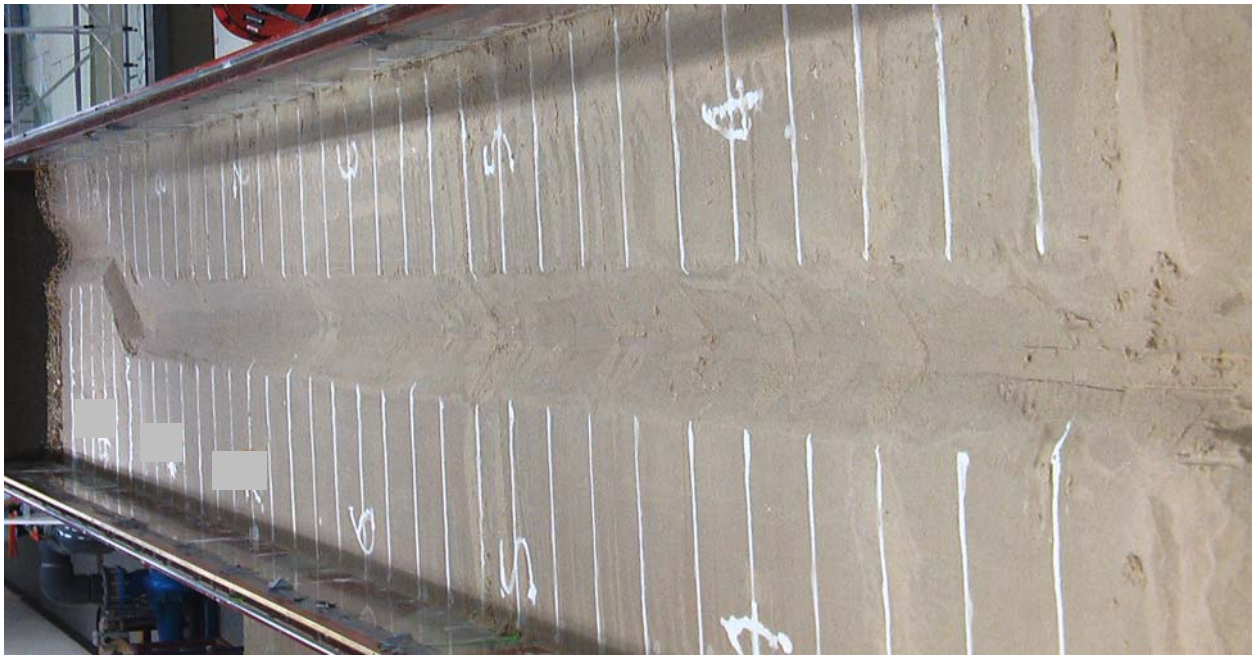

Figure 4.1: Channel ready for experiment.

5. Stop water flowing into flume and lower water level by lowering sluice-gate slowly. The flat sand surface with middle channel can now be seen. Keep lowering the sluice- gate until there is little water in the channel.

6. Leave the sand bed and channel dry for about two days, then dig the upstream channel as designed and also the curved connection. It is important to dry sand for about two days or flowing water in the first minutes would destroy channel banks.

7. Draw white lines with lime water every 20 cm. It is used to mark river boundaries. See picture of flume being ready for use in Figure 4.1.

8. Turn on water to do experiment as designing.

4.3 Water supply system

The following two pictures are showing the flume structure in the lab. One (Figure 4.2) is viewing down the flume from upstream to downstream and the other (Figure 4.3) is viewing it from the side.

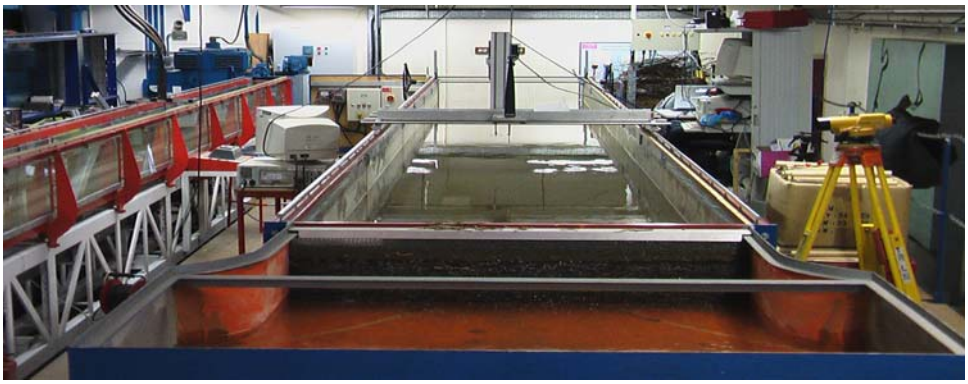

Figure 4.2: The flume viewed from upstream.

Figure 4.3: The flume viewed from the side.

4.4 Flume structure and plan view

Figures 4.4a and 4.4b show the plan and layout of flume for the second set of experiments. In Figure 4.4b, sections A-A and B-B are shown in more detail in Figure 5.1 in Chapter 5. The flume is 10 m long, 1.2 m wide and 0.3 m deep. And 10 m is at the beginning of upstream while 0 m is at the end of downstream.

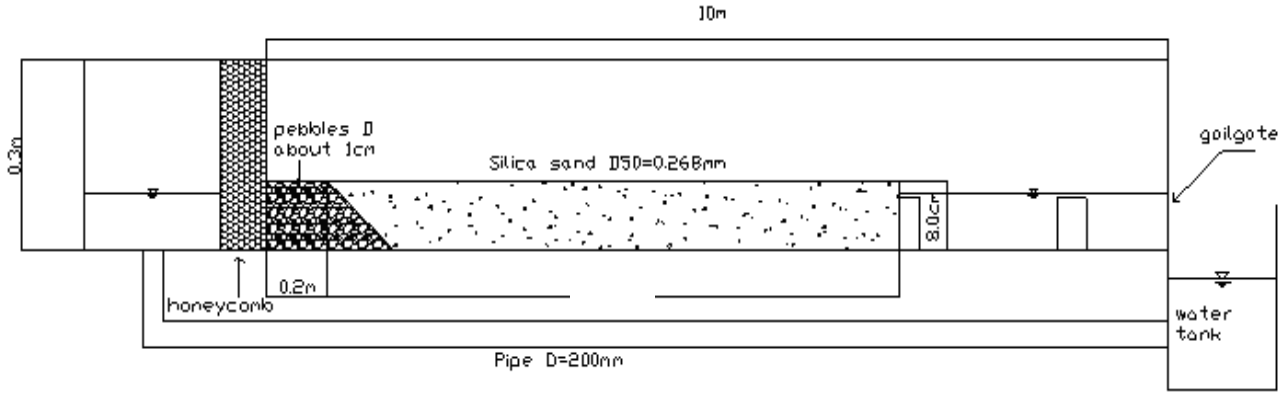

Figure 4.4a: The map for water supply system.

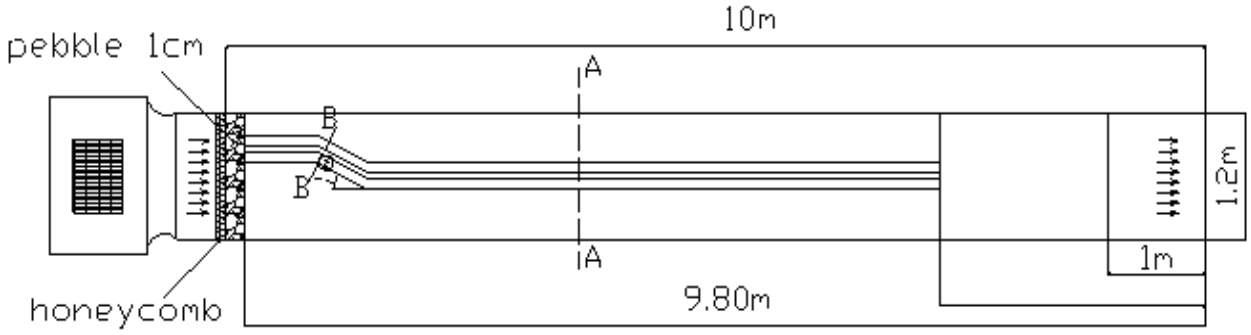

Figure 4.4b: Ichnography of flume.

The first set of experiments

The flume width is 120 cm, length 1000 cm, and a depth of 30 cm. See Figures 4.2 and 4.3. The sediment depth is 5 cm (in the second set of experiments, this is increased to 8.0 cm as shown in Figure 4.4a).

Water comes from pipe below the flume and is then controlled by a honeycomb to make the water velocity more homogenized.

There is a spur dike located at the upstream flume and which is at 1.5 m from the inlet and 8.5 m far from the outlet, see Figure 4.5.

Figure 4.5: The map for the first set of experiments.

The spur dike width is one quarter of the flume width (30 cm). For comparison, the width can be used as 1/3 or 1/5 of flume width. The flume slope can be adjusted, and according to the design, the slope is chosen as 0.005**.**

The second set of experiments

Sand depth is 8.0 cm from 9.8 m to 2.5 m of the flume length. There are pebbles (with diameter of about 1 cm) from 10 m to 9.8 m to prevent sand flowing into the water tank at the upstream. At

the end of the sand bed, there is a brick wall to stop sand flowing out and there is another brick wall at 1.5 m to stop sand flowing into water tank at the downstream. See Figure 4.4a and Figure 4.4b.

4.5 Sediment

The chosen sediment is non-cohesive sediment. Depth of sediment is 5 cm for the first set of experiments and 8.0 cm for the second set of experiments. So with a width of 1.2 m, length of 10 m, the total volume is 0.6-0.9 m^3. Considering the loss during experiments and for a little extra safety ratio, the ordering volume for sediment is 1 m^3. Other researchers used sand with median size D_{50} of 0.56 mm (Schumm et al., 1987), 0.45 mm (Friedkin, 1945), 0.5 mm (Gran and Paola, 2001), 1.25 mm (Jang and Shimizu, 2007), 0.94 mm (Ohmoto, 1998) and 0.6 mm (Michiue and Hinokidani, 1992).

The median size chosen is between 0.2 mm to 0.8 mm. And because the sand would be transported by the flowing water (bed-load and suspended load), if the size is small and velocity is too large, sediment would be completely washed away. Also if the size of silica sand is large and at the same time, the velocity is small, there would be no sediment transport. Water supply ability could reach 55 l/s with a flow depth of 190 mm and the slope at 1:1000. So the maximum velocity (v=Q/ (w×h)) that the flume can provide is shown in Table 4.1.

Table 4.1: The velocity calculation.

Water depth h (m)	Width w=1.2 m and the max velocity (m/s)		
	Q=0.020 m^3/s	Q=0.030 m^3/s	Q=0.055 m^3/s
0.10	0.167	0.25	0.46

0.05	0.333	0.5	0.92

The threshold (critical) depth- averaged speed U_c at different water depths of 5 cm and 10 cm as calculated using different formula.

Г.И.Шамов formula: (Wang et al., 2004):

$$U_c = 1.14\sqrt{\frac{r_{s-}r}{r}gD}\left(\frac{h}{D}\right)^{1/6} \quad 5.1$$

Soulsby (1997) formula for which D_*>0.1

$$f(D_*) = \frac{0.30}{1+1.2D_*} + 0.055[1-\exp(-0.020D_*)] \quad 5.2$$

$$D_* = \left[\frac{g(s-1)}{\upsilon^2}\right]^{1/3} d_{50} \quad 5.3$$

$$U_c = 7\left(\frac{h}{d_{50}}\right)^{(1/7)}[g(s-1)d_{50}f(\mathrm{D}_*)]^{1/2} \quad 5.4$$

with: s=ratio of densities of grain and water.

υ=kinematics viscosity of water.

The results of calculation are shown in the Table 4.2.

Table 4.2: The calculation of critical depth- averaged speed by two different formulae.

Diameter (mm)	By Г.И.Шамов (Wang et al., 2004) formula to calculate the threshold velocity U_c(m/s).		By Soulsby (1997) formula to calculate the threshold current velocity U_c(m/s).
	h=0.05 m	h=0.10 m	h=0.10 m
0.13	0.141	0.158	0.210
0.2	0.163	0.183	0.211

0.35	0.196	0.220	0.220
0.5	0.221	0.248	0.236
0.8	0.258	0.290	0.276

Compare with the critical depth-averaged velocity and the maximum velocity that flume can provide, if sand diameter is chosen as 0.8 mm, water will not make sand transportation. If water depth is 0.05 m, the Acoustic Doppler Velocimeter (ADV) machine cannot work (the minimum water depth requirement). Based on equipment ability and experiment material, the silica sand D_{50} less than 0.8 mm (0.5 mm or 0.2 mm) and water depth as 0.1 m were adopted.

Conclusion: D_{50}=0.5 mm, the critical depth-averaged velocity is 0.25 m/s.

D_{50}=0.2 mm, the critical depth-averaged velocity is 0.18 m/s.

Silica sand could be provided by sand supplier: WBB Minerals and sand size: D_{50}=0.45 mm and D_{50}=0.268 mm. The loose bulk density is 1490 kg.

For D_{50}=0.45mm, the threshold velocity by Г.И.Шамов (Wang et al., 2004) Fomula: U_c=0.24 m/s, by Soulsby (1997) formula: U_c=0.23 m/s.

For D_{50}=0.268 mm, the threshold velocity by Г.И.Шамов (Wang et al., 2004) Fomula: U_c=0.20 m/s, by Soulsby (1997) formula: U_c= 0.20 m/s.

At last, sand with D_{50}=0.268 mm was chosen.

For more information about the sand size, see Tables 4.3 and 4.4. Figures 4.6 and 4.7 show sand's cumulative curve and its percentage.

Table 4.3: Particle size distribution (ISO).

Microns	Passing (%)	Retained (%)		Category
		Full Octave	Half Octave	
8000	100	0.00	0.00	Stones
5600	100	0.00	0.00	Coarse Gravel
4000	100	0.00		
2800	100	0.00		
2000	100	0.00	0.00	Fine Gravel
1400	100	0.00	0.00	Very Coarse Sand
1000	100	0.00		
710	99.90	0.10	1.20	Coarse Sand
500	98.80	1.10		
355	85.20	13.60	57.70	Medium Sand
250	41.10	44.10		
180	11.40	29.70	38.90	
125	2.20	9.20		Fine Sand
90	0.60	1.60	2.10	Very Fine Sand
63	0.10	0.50		
<63	0.00	0.10	0.10	Silt / Clay

Table 4.4: D values for the sand.

D	D95	D90	D85	D60	D50	D25	D20

Size (μm)	413	378	354	289	268	218	207
D	D10	D5	D60 / D10	D90 /D10	D84.1/D15.9	-	-
Size (μm)	174	146	1.7	2.2	1.8	-	-

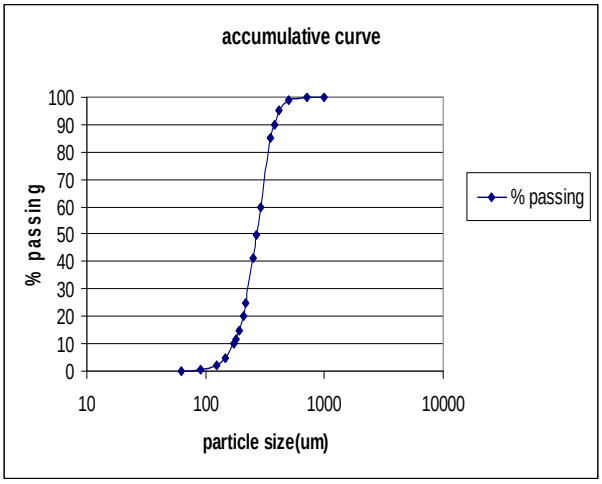

Figure 4.6: The cumulative curve for the sand.

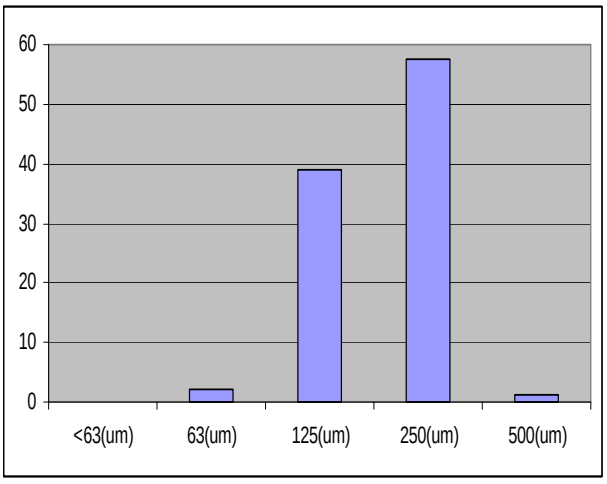

Figure 4.7: The percentage of sand.

4.6 The equipment and data collection

Below is the equipment description and data collection.

4.6.1 Acoustic Doppler Velocimeter (ADV)

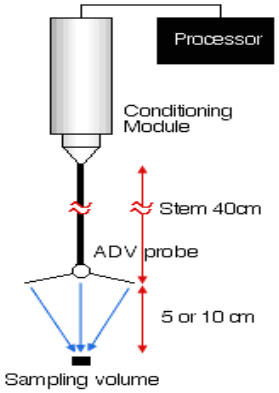

Figure 4.8: The ADV introduction (from: http://biology.st-andrews.ac.uk/serg/adv.htm).

The ADV in the lab of Hydro-environmental Research Centre in Cardiff University was bought from Nortek-AS Company. It is not new and it has been used in several other experiments, but

proved to be in good condition. The ADV and the point gauge which were used in the experiment are shown in Figures 4.9 and 4.10 below.

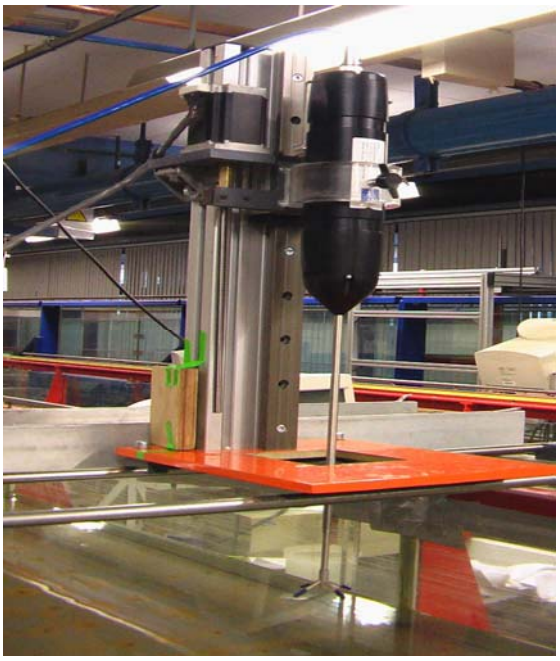

Figure 4.9: The ADV machine.

Figure 4.10: The point gauge.

The ADV probe is controlled by a computer. To make it work well, after the installation of vectrino software on the computer, it is necessary to have a functional test. After preparation, the probe was put in the sanding water in a bucket to test the probe.

The sampling frequency for ADV is 200 HZ. Temperature is set to be close to room temperature and the salinity is 0 (no salt). In this condition, the sound speed can be calculated as 1482.9 m/s at a temperature of 21.20 degrees. The sampling volume is 7 mm.

For this research, to make ensure the measurement was the same level and control easily, the equipment was attached to a movable rack which was parallel with the flume surface and could move on the track, on the top of two sides of flume. See Figure 4.9.

4.6.2 Point gauge and bed profiler

Point gauge that was used to measure water depth in the lab was also attached to a movable rack like the ADV machine. See Figure 4.10.

Also the bed profile would be measured by the HR Wallingford Bed Profiler (Figure 4.11) which is located on two structures and can be moved in horizontal direction. In lateral direction, it can be moved to positions by hand.

The profiler consists of a support beam, a profiler carriage, a probe and a computer. The support beam is mounted over the bed where bed profile is measured. The profiler carriage drives along the support beam and the probe is fitted to the profiler carriage. Except for the drag-arm probe, the probe is driven up and down to maintain a constant distance from the probe sensor to the bed.

Figure 4.11: The bed profiler.

The computer controls the movement of the profiler carriage and the probe and also displays and logs the profile data. (HR Wallingford, 2003)

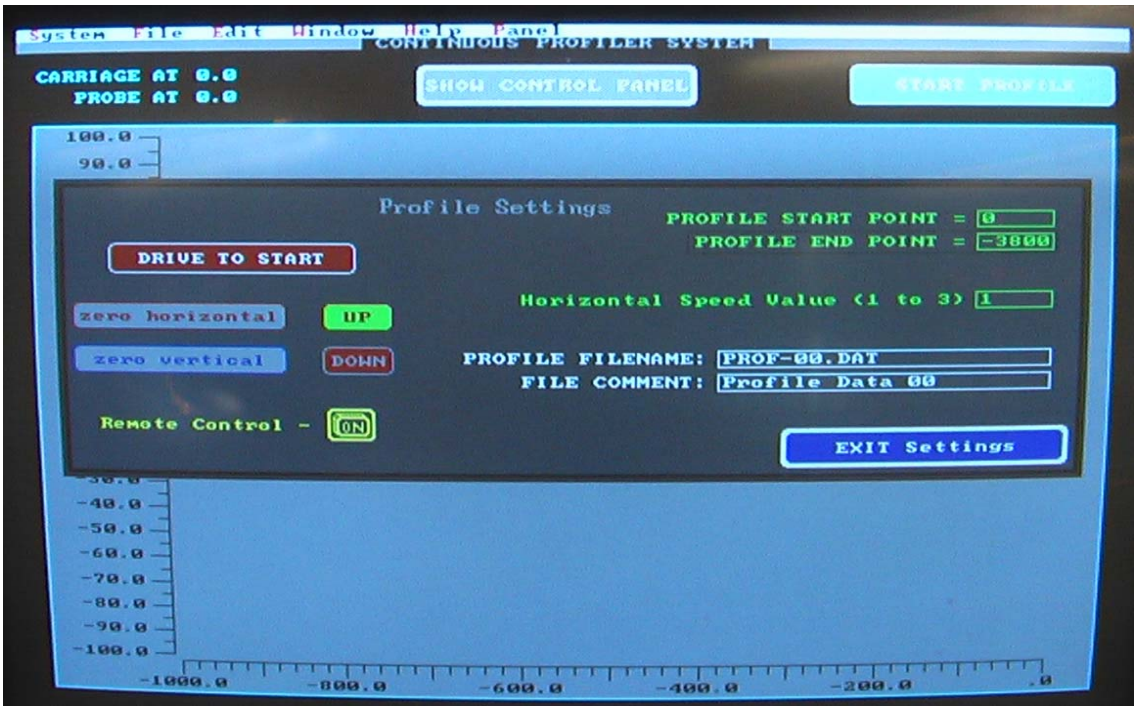

Figure 4.12: Control panel for bed profiler.

The profiler is controlled via two screen displays from a computer and runs with a customised software program. The first sets parameters such as start point, total distance to be travelled, and for incremental profiling the number of steps, step height and so on. The second screen allows the profiling operation to be started and stopped and also displays the profile as it is measured (HR Wallingford, 2003). The control panel on the computer is shown in Figure 4.12.

The bed profiler could measure constantly or step by step (HR Wallingford, 2003). After comparing two methods, the measurement constant is chosen in the experiment because it saves time. Machine measures depth in fixed times and with one chosen moving velocity, distance between two measure points would be slightly different. The bed profiler machine is controlled by computer and parameters are set in the control panel (see Figure 4.12). For experiments here, the bed profiler was moved each 1 cm in lateral directions.

The depths were obtained and stored in .dat format. Because horizontal and vertical readings were taken at discrete time intervals and the data for the continuous profiling programme would not be taken by every 1 cm but different each time. This gives difficulty in obtaining 3-D profiles of channel bed by TECPLOT. With help of the programme which is compiled by FORTRAN 90, depth at fixed points can be interpolated by neighbour points. This programme is attached at the end of the thesis.

4.6.3 Velocity Meter

Velocity is important in experiments and it was measured by Nixon Streamflo Velocity Meter model 430 (See Figure 4.13). The miniature head of the flow sensing probe can be inserted into small channels where it has ability to measure velocities as low as 5.0 cm/s and channel depth should larger than about 2 cm. The sensing probe is a measuring head joined by a slim tube to the plug and socket which connects to the measuring instrument.

Figure 4.13: Nixon Streamflo Velocity Meter model 430.

4.6.4 Discharge control for unsteady inflow

Experiments with unsteady inflow are different to experiments with steady inflow. Discharge was changed by pump engine frequency. And frequency could be changed easily by hand using control panel of SIEMENS Micromaster 430 (see Figure 4.14).

Figure 4.14: Control panel for Micromaster 430 and control panel for valve openness.

Because minimum frequency change can be 0.10 HZ and small frequency change can achieve small discharge change, this method is more accurate than controlling valve openness.

When water tank is full，valve openness is fixed to 15% (see in Figure 4.14), discharge with different engine frequency could be measured by vee weir. Then accurate discharge could be used for experiment (see Table 4.5).

Table 4.5: Discharge with different frequency. (The formulae used for vee weir is: $Q = C_d \times \frac{8}{15}\sqrt{2g}\tan(\theta/2) \times h^{5/2}$ (Chadwick et al., 2004) Where h is water depth above the lowest crossing, here h=H-10.7 (cm), θ is the angle of vee weir, here $\theta = 90^0$, and C_d is the experimentally derived coefficient between Q and Q_{ideal}, $C_d = Q/Q_{ideal}$, here C_d=0.59 for $\theta = 90^0$ Q by m^3/s.)

Frequency (HZ)	Water Height	Vee weirs Depth (D)	h=(H-D) (cm)	q(m^3/s)	q(l/s)

Frequency (HZ)	q(l/s)

	(H) (cm)	(cm)			
15.90	12.95	10.7	2.25	0.000106	0.106
16.10	13.55	10.7	2.85	0.000191	0.191
16.40	14.10	10.7	3.40	0.000297	0.297
16.60	14.50	10.7	3.80	0.000392	0.392
17.00	14.90	10.7	4.20	0.000504	0.504
17.30	15.20	10.7	4.50	0.000598	0.598
17.70	15.50	10.7	4.80	0.000703	0.703
18.10	15.75	10.7	5.05	0.000798	0.798
18.60	16.00	10.7	5.30	0.000901	0.901
19.00	16.20	10.7	5.50	0.000988	0.988
19.50	16.45	10.7	5.75	0.001104	1.104
20.10	16.65	10.7	5.95	0.001203	1.203
20.40	16.85	10.7	6.15	0.001307	1.307
21.10	17.03	10.7	6.33	0.001404	1.404
21.60	17.20	10.7	6.50	0.001500	1.500
22.30	17.38	10.7	6.68	0.001607	1.607
23.00	17.53	10.7	6.83	0.001698	1.698
23.40	17.70	10.7	7.00	0.001806	1.806
24.00	17.85	10.7	7.15	0.001904	1.904
24.60	18.00	10.7	7.30	0.002006	2.006

15.90	0.1
16.10	0.2
16.40	0.3
16.60	0.4
17.00	0.5
17.30	0.6
17.70	0.7
18.10	0.8
18.60	0.9
19.00	1.0
19.50	1.1
20.10	1.2
20.40	1.3
21.10	1.4
21.60	1.5
22.30	1.6
23.00	1.7
23.40	1.8
24.00	1.9
24.60	2.0

25.10	18.13	10.7	7.43	0.002096	2.096		25.10	2.1
25.70	18.27	10.7	7.57	0.002196	2.196		25.70	2.2
26.40	18.42	10.7	7.72	0.002307	2.307		26.40	2.3
27.00	18.55	10.7	7.85	0.002405	2.405		27.00	2.4
27.50	18.68	10.7	7.98	0.002506	2.506		27.50	2.5
28.00	18.80	10.7	8.10	0.002601	2.601		28.00	2.6
28.60	18.92	10.7	8.22	0.002699	2.699		28.60	2.7
29.20	19.05	10.7	8.35	0.002806	2.806		29.20	2.8
29.70	19.15	10.7	8.45	0.002891	2.891		29.70	2.9
30.20	19.30	10.7	8.60	0.003021	3.021		30.20	3.0
31.00	19.38	10.7	8.68	0.003092	3.092		31.00	3.1
31.80	19.50	10.7	8.80	0.003200	3.200		31.80	3.2
32.60	19.60	10.7	8.90	0.003292	3.292		32.60	3.3
33.40	19.72	10.7	9.02	0.003404	3.404		33.40	3.4

4.6.5 Data measurements and records

The first set

1. Use camera to record pictures of change at different stages from vertical and longitudinal direction.

2. At each time stage, measure velocity.

3. Depth of water measurement (h1):

4. Depth of sand measurement:

The height (H) from the bottom of flume to the position of moving rack needs to be measured. After measuring the length (h2) between the water surface and the position of moving rack, the depth of sand (D) is H-h1-h2.

5. Measure the meander wavelength, amplitude, depth, width of channel.

The second set

The boundary line measurement

1. Put the tripod at the end of flume with a camera to record changes of river morphology (Figure 4.15).

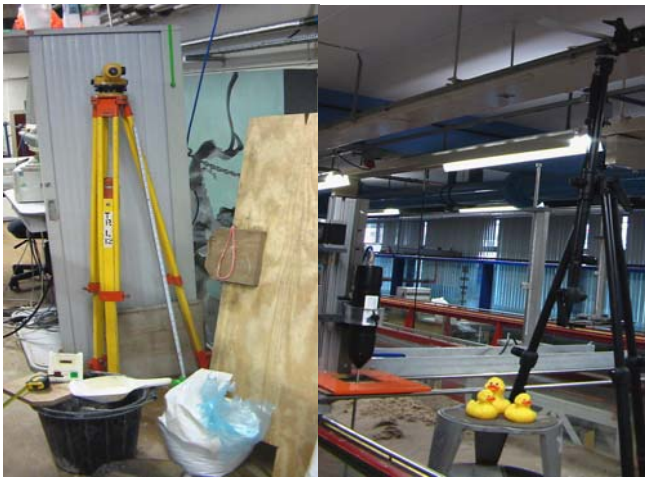

Figure 4.15: The equipment used in the experiments (wood board, tripod, ADV and other tools).

2. After the sand bed became dry on the surface, use lime water to draw the transverse lines. From observation, the morphology change was faster at the first 1 hour and then become slowly. So camera will record every 2 minutes' changes during the first 1 hour and then 5 minutes' changes in the second hour. After 2 hours, the camera records changes by every 10 minutes and half hours if the running continues.

3. Copy pictures from camera to computer and then edit them by AutoCAD. Draw the paralleled lines according to the limed lines on the sand bed surface and draw the Polyline (the name of one type of line in AutoCAD) by river boundaries. Use software CAIC.exe which can transfer the positions of points in Polyline to an excel file. Then draw boundary lines by excel.

These pictures would be compared with results from numerical modelling.

Depth measurement

For depth of channel, at moment, it is not easy to get a timely measurement. The point gauge was used to measure one section, but it was so slow to get 10 points for one section in short time and the condition would change to another one after finish one section. There will be no two sections for comparison at the same time.

The ADV machine can measure water depth when it is deeper than 5 cm and this limits its use. It was tried to measure the depth by filling water slowly in the flume to raise water depth to more than 5 cm after half hour to 1 hour. More details will be presented later. After measurement, flow water away and begin the running as initial condition. After another hour, do the same as before to raise water level for the depth measurement by ADV. It is the same procedure for Bed profiler machine.

4.7 Summary

In this chapter, the materials, equipment and methods that were used in this experimental study were introduced. Experiment aims and objectives were explained in section 4.2. In section 4.3, the water supply system for the flume in the lab was illustrated and section 4.4 shows a plan view of

the flume structure. After that, the characteristic of the main material: sand used in the study was described. This included threshold velocity and particle size distribution analysis. Then in section 4.6, equipment like ADV, the bed profiler, velocity meter, point gauge and discharge control equipment were outlined with their operating methods. The experiment results for this study will be discussed in Chapter 5.

Chapter 5

Results of Physical Experiment

5.1 Introduction

Many experiments with different conditions have been carried out in this study without changing the sand bed. Two different types of tests were designed. One set was designed to test the meander development caused by a spur dike, and the other set was designed to test the meander development resulting from the initial bending. With these two different types of tests, a large number of experiment conditions were conducted using different flume slopes, flow rates and channel sizes. In this chapter, more details of experiments with steady inflow and unsteady inflow will be described and the discussions follow these results.

5.2 Flow rate measurements

Because flow rates in the experiment were small and could not be read directly from the discharge meter, they were measured separately. The flow rate was measured by a vee weir in the flume as shown in Figure 5.1.

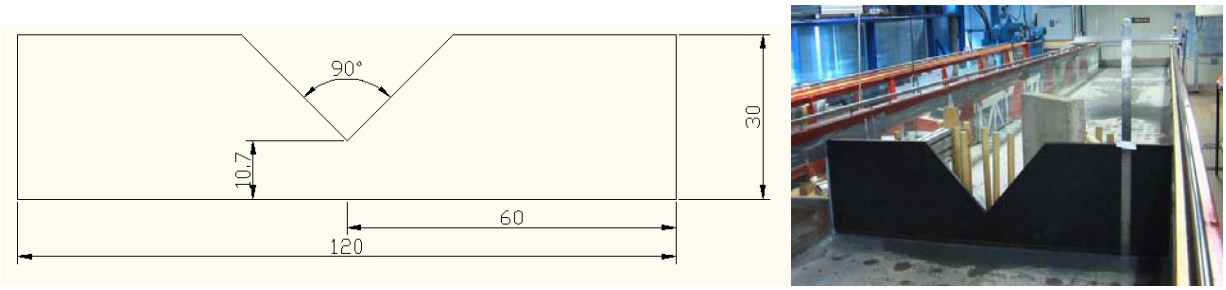

Figure 5.1: Vee weir used to measure flow rate and its setting in the flume (cm).

Then pump was switched on and water flowed with different flow rate. With a point gauge to measure water depth H and then flow rate was calculated with formula below:

$$Q = C_d \times \frac{8}{15}\sqrt{2g}\tan(\theta/2) \times h^{5/2} \quad \text{(Chadwick et al., 2004)} \qquad 5.1$$

Where h is the water depth above the lowest crossing, here h=H-10.7 (cm), θ is the angle of vee weir, here $\theta = 90^0$, and C_d is the experimentally derived coefficient between Q and Q_{ideal}, $C_d = Q / Q_{ideal}$, here C_d=0.59 for $\theta = 90^0$.

After this measurement, the discharge used before becomes clear and tests can be compared with each other easily. At beginning water was collected at the end of flume by container in a period and then measured by scale to get the exact flow rate. Flow rate got in this way had a good agreement with that by calculation from vee weir. Then flow rate was measured directly from the vee weir in this study.

Table 5.1: Measurement of discharge by vee weir.

H (cm)	19.40	17.15	15.52
h (cm)	8.70	6.45	4.82
Discharge (l/s)	3.110	1.472	0.711

5.3 The experiments series B with middle channel whose banks were above water level and with spur dike together

The experiment series A (Tests 1 to 6) were set with a spur dike to see its effect on morphology when the sand was all under water. Results indicated that the spur dike could cause bed erosion and formed a curved inner channel as shown in Figure 5.2.

Figure 5.2: Spur dike in experiments series A for Tests 1- 6.

In reality it is unreasonable and not practicable for this research. Projects use spur dikes to make flow smooth rather than turbulent. It proved that a straight river would have a curving development by the initial bending in upstream. After these tests, channels were excavated in the middle of the sand bed and bending in the upstream was designed for experiments. Tests with straight channel were also carried out for comparison.

5.3.1 Results from the experiments series B

Test conditions for this set are described in Table 5.2.

Table 5.2: Experiments series B: with middle channel whose banks above water level and with spur dike.

Test No	Channel size (cm×cm×cm) -bank slope	Area of cross section(cm^2)	Slope	Q (l/s)	Comment
7	30×30×4-90^0	120	0.003	1.472	Straight channel, feeding sand
	Channel 1				
8	30×22×4-45^0	104	0.010	1.472	Straight channel, no sand feeding

9	30×22×4-45^0	104	0.010	1.472	Bending beginning, no sand feeding
10	30×22×4-45^0	104	0.010	1.472	Bending beginning-sand feeding
11	30×22×4-45^0	104	0.015	1.472	Bending beginning-sand feeding

Channels for these tests were made from attached small wood board when there was no water in the flume and channel size was shown as below. Spur dike was not moved away and channel banks were above water level in experiments (See Figures 5.4- 5.10). Experiments for straight channel without bend upstream were carried out in Tests 7 and 8, while experiments for channel with bend upstream were carried out in Tests 9- 11 in experiments series B.

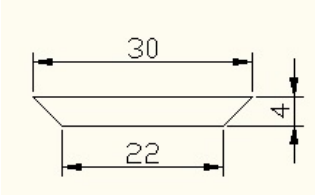

Figure 5.3: Channel size 1 for Tests 7- 11 (cm).

At first, there was a middle straight channel for Test 7, but after 1 hour in Figure 5.4, channel did not have a curving development at all as expected, so in Test 8, flume slope was increased from 0.003 to 0.010, and but again this time channel kept straight as in Figure 5.5. Then a channel with initial bending was made in Test 9 as shown in Figure 5.6. This angle was a trial.

Figure 5.4: Test 7 at 1 h.

Figure 5.5: Test 8 at 1 h.

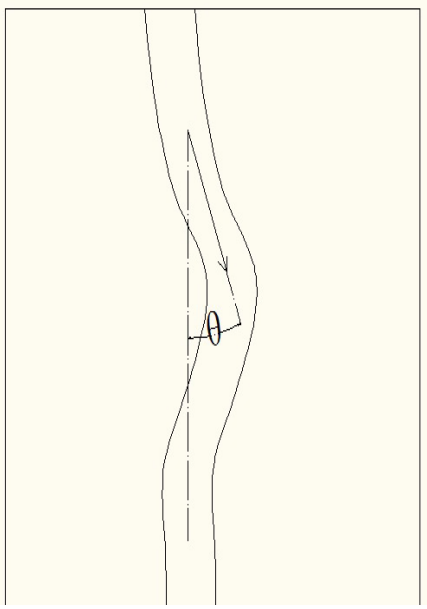

Figure 5.6: Test 9 with bending.

Figure 5.7: Test 9 at 140 min.

Figure 5.8: Test 10 at 150 min.

Figure 5.9: Test 10 at 210 min.

From results shown in Figure 5.7 in Test 9, after 140 minutes, channel did not have obvious lateral development. The angle of initial bending for this test was not large (see in Figure 5.6), so this was the main reason for no meander development. In Test 10, the initial bending angle increased

more, after 150 min as in Figure 5.8, bank boundaries became curved and after 210 min, there was a meandering thalweg in the straight channel as shown in Figure 5.9.

.

The result encouraged having a large bending angle in upstream and keeping the same in experiments series C, D and E. Results also encouraged increasing the flume slope from 0.010 to 0.015 in Test 11. The channel development for Test 11 in Figure 5.10 proved that increased slope not only gave the channel meandering thalweg but also sinuous bank boundaries. The large slope here indicated that it plays a key role on channel development.

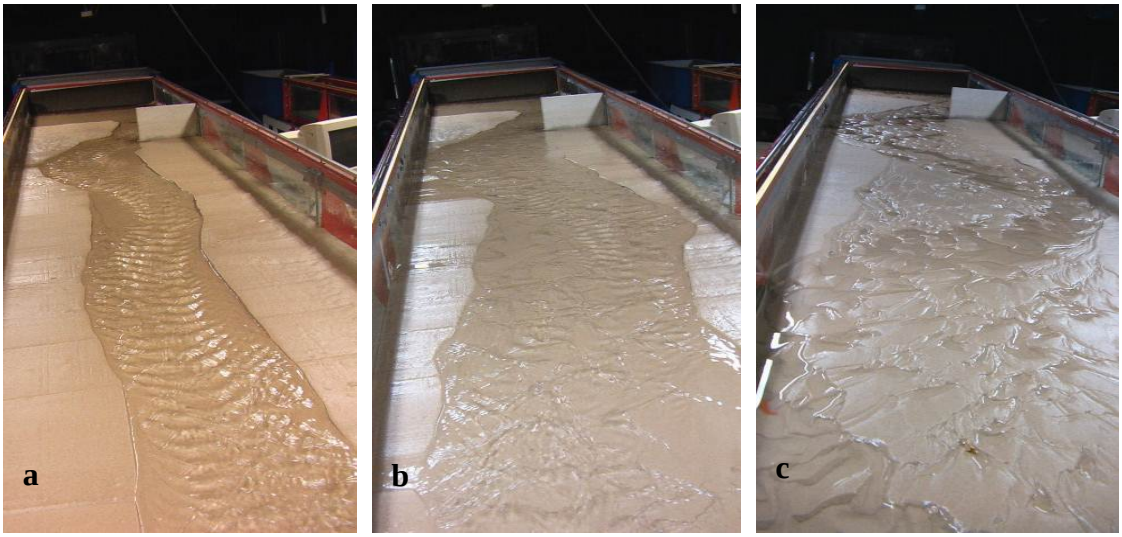

(a) 15 min (b) 60 min (c) 130 min

Figure 5.10: Test 11 at 15 min, 60 min and 130 min with slope 0.015.

In all these experiments from series B, the spur dike did not play a role and the initial bending and slope caused the channel to have a meandering thalweg. Take this into consideration, the spur dike was moved away after Test 11 for experiments series C, D and E.

5.3.2 Discussion from the results of experiments series B

Channel would become wide only when the initial channel was straight, no matter whether slope was 0.003 or 0.010, and there was no meandering trend at all. The largest shear stress (τ) on the bed in straight channel was along the centre. So Schumm et al. (1987) drew the conclusion that shear stress (τ) decreased away from centre and approached zero at the corners of a rectangular channel; therefore, the area of active sediment movement was in the centre of straight channel.

There was an initial bending and a meandering thalweg occurred in Test 10 with slope 0.010. When slope was increased to 0.015 in Test 11, channel not only had a meandering thalweg but also had sinuous boundaries. As it developed, the channel became wider and shallower and channel had an obvious meandering thalweg while boundary lines were not obviously curved.

Experiments from Tests 7-11 indicated that the slope and initial bending were key factors in causing curving thalweg and boundaries.

5.4 The experiments series C, D and E: with middle channel and without spur dike

5.4.1 Setting and results for experiments series C, D and E

In these series, many experiments were carried out. Different channel sizes, flow rates, flume slopes were combined to create different experiment conditions. From the results, these parameters could be found to have varying effects on channel morphology. Tests 12- 14 had a channel size as shown in Figure 5.3 and Test 15 had a little difference. Other tests used the channel size as shown in Figure 5.11. These sizes were made from the same wood board but with a different depth, see details for channel preparation in Chapter 4. They were made under water,

so the bank slope was sand's repose angle: 29^0. Experiment conditions for all test cases are shown in Table 5.3, Table 5.4 and Table 5.5.

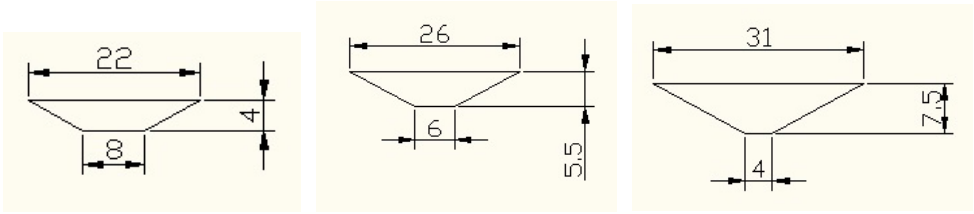

(a) Channel size 2 (b) Channel size 3 (c) Channel size 4

Figure 5.11: Different channel sizes (cm).

Table 5.3: Experiments series C: Tests 12- 15.

Test No	Channel size (cm×cm×cm) bank slope	Area of cross section (cm^2)	Slope	Q(l/s)
12	$30\times22\times5.5\text{-}45^0$	143	0.015	1.472
13	$33\times22\times5.5\text{-}45^0$	151.25	0.015	1.472
14	$33\times22\times5.5\text{-}45^0$	151.25	0.015	1.472
15	$32.5\times17.5\times4\text{-}29^0$	100	0.015	0.711

Table 5.4: Experiments series D: Tests 16-19, 21- 26, 29- 30 with bank slope 29^0.

Test No	Channel size (cm×cm×cm)	Area of cross estion (cm^2)	Slope	Q (l/s)
	Channel 2			
16	22×8×4	60	0.015	1.472 /0.711
17	22×8×4	60	0.015	0.711
18	22×8×4	60	0.015	0.711

19	22×8×4	60	0.015	0.711
	Channel 3			
21	26×6×5.5	88	0.015	3.110
22	26×6×5.5	88	0.015	0.711
23	26×6×5.5	88	0.020	0.711
24	26×6×5.5	88	0.020	0.711/1.472
25	26×6×5.5	88	0.010	0.711
26	26×6×5.5	88	0.010	1.472
	Channel 4			
29	31×4×7.5	131.25	0.010	1.472
30	31×4×7.5	131.25	0.015	0.711/ 1.472

Table 5.5: Experiments series D: Tests 31- 37 with bank slope 29^0 .

Test No	Channel size (cm×cm×cm)	Area of cross section(cm^2)	Slope	Q(l/s)	Time
31	26×6×5.5	88	0.020	0.711	30/30
32	26×6×5.5	88	0.020	1.472	30/30
33	26×6×5.5	88	0.015	1.472	30/30
34	26×6×5.5	88	0.020	1.472 /0.711	30/30
35	31×4×7.5	131.25	0.020	1.472	30/30
36	31×4×7.5	131.25	0.020	3.110	30
37	31×4×7.5	131.25	0.015	1.472	30/30

There were 23 tests in total in Tables 5.3, 5.4 and 5.5. The most important factors for channel morphology are discharge, sediment load and character and valley floor slope. (Schumm et al., 1987) In these tests, the initial conditions (flume slope, channel size, initial entrance bending, flow rate, sand feeding) were changed to compare river morphology development. Some channels just had a meandering thalweg with a straight bank boundary after water supply. Some had obvious sinuosity at the beginning of tests, and then the experiment went on, there was a trend development from meandering to braided.

These developments were analyzed by channels' types: straight, meandering and braided while considering parameters like flow rate, sediment load and character, channel size, water depth and flume slope.

From the experiments, the depth of water was found to be around 3 cm. Sediments parameters were calculated to compare with its critical parameters when the flume slope was 0.015, giving:

τ_{cr} =0.186 *Pa* τ = 4.41 *Pa*

u_{*cr} =0.014 *m/s* u_{*}=0.06 *m/s*

θ_{cr} =0.043 θ=1.018

The comparison shows that parameters from experiments are larger than the critical parameters and sediments can be moved by the flowing water easily.

5.4.2 Description of channel development

5.4.2.1 Straight channels

From other researchers, a straight channel could develop to a meandering one. Nagata et al. (2000) carried out an experiment and confirmed this development. Numerical modelling also had result that the channel developed from straight to meandering. Secondary flow develops spontaneously in straight channels as a result of vortices generated at the boundary walls (Einstein and Shen, 1964; Shen and Komura, 1968). And inequalities from bank roughness induce asymmetry and periodic reversal of the dominant cell, resulting in the formation of a meandering thalweg and alternating bars.

Schumm et al (1987) got results from other researchers: it is impossible to produce any pattern other than straight if the valley slopes below the valley slope 0.003. From Test 18 in Figure 5.12, channels would become wider and shallower only even after 1020 minutes because the initial channel in Test 18 was straight, and slope and flow rate were small. The low slope and small flow rate make the flowing with low energy and produce the straight channel.

Table 5.6: Tests with initial straight channel and result with straight channel.

Test No	Channel size (cm×cm×cm) bank slope	Area of cross section (cm^2)	Slope	Q (l/s)
Tests from experiment Series C				
18	22×8×4- 29^0	60	0.015	0.711
Tests from experiment Series B				
7	30×30×4- 90^0	120	0.003	1.472

8	$30\times22\times4\text{-}45^0$	104	0.010	1.472

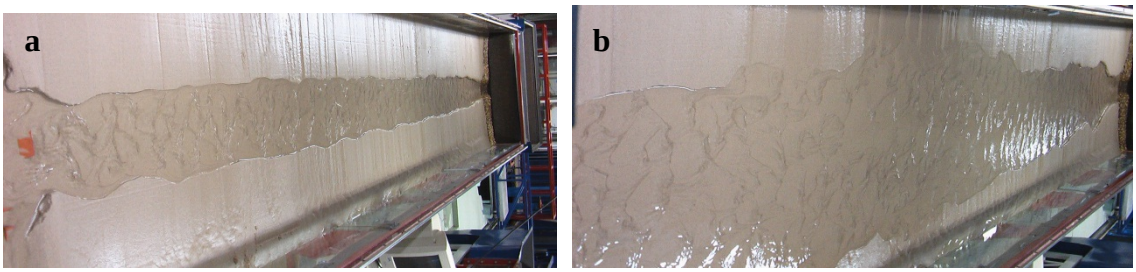

Figure 5.12: Test 18 with initial straight channel at 60 minutes (a) and 1020 minutes (b).

An initially straight channel in Test 18 remained straight because of its small flow rate (0.711 l/s) and slope (0.015). It had the same straight development in Tests 7 and 8 (see Figures 5.4 and 5.5) which had a medium flow rate (1.472 l/s), and a small slope of 0.003 and 0.010. Again the reason for straight channel was that in straight channel, flow with low energy was unable to scour the bed and have a high rate of sediment transportation.

5.4.2.2 Straight channels with meandering thalweg

Channels with this type of development were in Table 5.7, they had an upstream bend. Their developments were not straight like above: by development, channel became wider and shallower, boundary lines did not have obvious meandering, but a little curving, and channel had an obvious meandering thalweg. Tests 11 and 13 are good examples, see Figures 5.13, 5.14. Figure 5.15 shows that there was an obvious sinuous thalweg in Test 11 after stopping water supply.

Table 5.7: Tests with an initial bend upstream and results with a little curving channel and meandering thalweg.

Test No	Channel size (cm×cm×cm) bank slope	Area of cross section (cm^2)	Slope	Q (l/s)
Tests from experiment Series C and D				

13	33×22×5.5-45^0	151.25	0.015	1.472
26	26×6×5.5	88	0.010	1.472
33	26×6×5.5	88	0.015	1.472
	Tests from experiment	Series B		
10	30×22×4-45^0	104	0.010	1.472
11	30×22×4-45^0	104	0.015	1.472

Figure 5.13: Channel development at 60 min (a), 130 minutes (b) in Test 11.

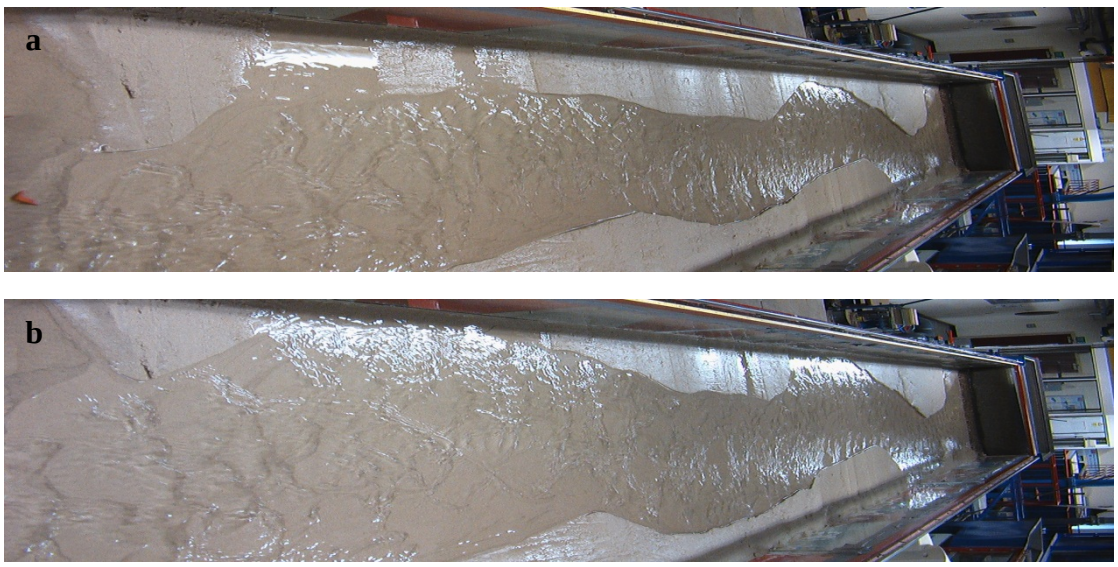

Figure 5.14: Channel development at 60 min (a), 130 minutes (b) in Test 13.

Figure 5.15: The meandering thalweg at 130 minutes in Test 11 after stop water supply.

Compared with Test 8 with slope 0.010, Test 11 had a steep slope 0.015 and a bend upstream. These differences meant that Test 11 had downstream boundary curving and a sinuous thalweg. It proved that with a steep slope and a bend upstream, a meandering boundary would appear. That Test 13 increased channel depth to 5.5 cm from 4 cm in Test 11 told us that: with the same flowing rate and channel slope, a high bank depth/width ratio can provide high energy to erode bank. Results in Figures 5.13 and 5.14 proved that large depth/width ratio can have more erosive ability. In Figure 5.15, the thalweg had a very large bend with high sinuosity when boundaries were a little curved. This is the main characteristic of this type of development.

5.4.2.3 Meandering channels

Channel development with different channel size

Accourding to Schumm et al (1987), a channel's sinuosity will begin to increase from 1 to maximum 1.3 when valley slope is increased from 0.003 to 0.016. That means that below 0.003, it is straight channel and between 0.003 and 0.016, it is meandering, above 0.016, it is braided. With these experiments here, because different tests from Schumm were used, meandering happened at a slope of 0.015, with flow rate of 0.711 l/s for Tests 15, 19 and 22 with channel sizes 1, 2 and 3 separately (see in Table 5.8). Meandering also occured in Test 29 when valley slope was 0.010,

with flow rate of 1.472 l/s and a channel depth of 7.5 cm. Test 22 increased slope from 0.015 to 0.020, which was Test 23. And Test 23 had a more sinuous thalweg compared with Test 22. More details will be shown in Figure 5.22. Below is channel development for Tests 15, 19 and 22 with different channel size.

Table 5.8: Tests 19, 22 and 15 with meandering channels.

Test No	Channel size (cm×cm×cm) bank slope	Area of cross section (cm^2)	Slope	Q (l/s)
19	22×8×4	60	0.015	0.711
22	26×6×5.5	88	0.015	0.711
15	32.5×17.5×4- 29^0	100	0.015	0.711

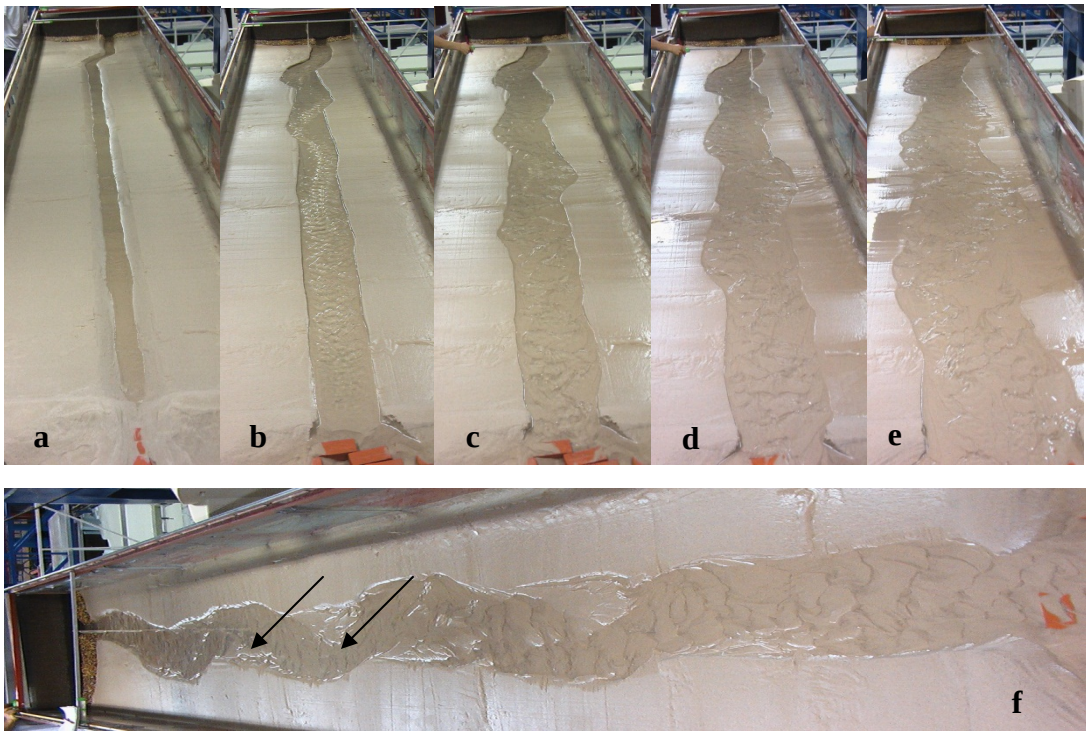

Figure 5.16: Test 19 with channel size 2 ($60\,cm^2$) at 0 min (a), 14min (b), 30 min (c), 60 min (d), 120 min (e) and at 60 min (f) after stop water supply.

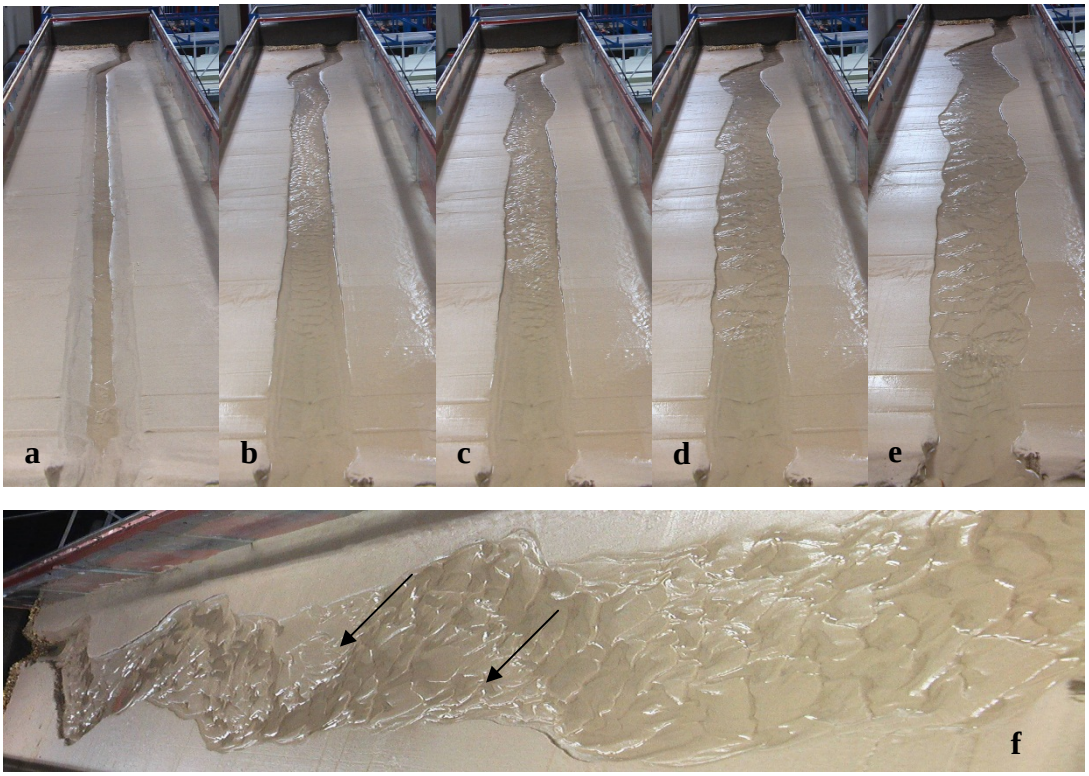

Figure 5.17: Test 22 with channel size 3 ($88\,cm^2$) at 0 min (a), 14min (b), 30 min (c), 60 min (d), 120 min (e), and 300 min (f).

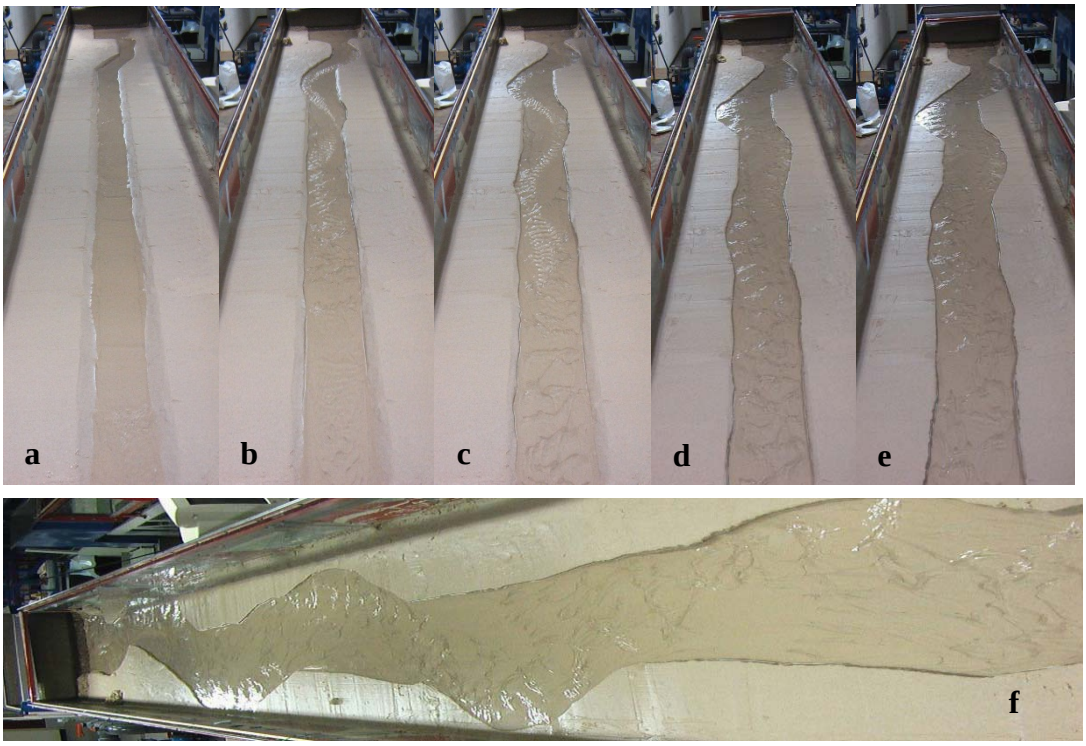

Figure 5.18: Test 15 with channel size 32.5 cm×17.5 cm×4 cm ($100\,cm^2$) at 0 min (a), 14 min (b), 30 min (c), 60 min (d), 120 min (e), and 425 min (f).

From the channel development above with different channel sizes, Test 19, which had the smallest channel size ($60\,cm^2$) had most sinuous boundary lines compared with Tests 22 and 15. Also, from Figure 5.16, it is clear to see that in Test 19 the meander and points bars at 60 min when there was no water supply. With initial bending at the beginning, alternate bars and pool formed. Their existence enhanced the development of meandering. Amplitude at 118 min was larger than that at 60 min but channel was wider and shallower at 2 hours. Pools and crossings came out alternately. The phenomenon of channel development in the lab in Figures 5.16f and 5.17f (the bars by black arrows) were in close agreement with the natural river in Figure 5.19 by the black arrows.

Figure 5.19: The nature river in east Russian from Google map.

In the section of pools and riffle, one side was shallow (point bar) and another side (thalweg) was deep. By spiral flow due to the centrifugal force in meandering, sand was transported from concave to convex. This made the pool develop further. Figure 5.20 shows transverse sections measurement at 1 hour and at 2 hours along the river from 7 m to about 4 m(the upstream is marked as 10 m and flume downstream is marked as 0 m. Flow direction is from 7 m to 4 m).

They showed at 1 hour, that thalweg changed from right to left and then to right again with shallow crossings in the middle. The river planform at 1 hour and 2 hours were shown in Figure 5.16d and 5.16e.

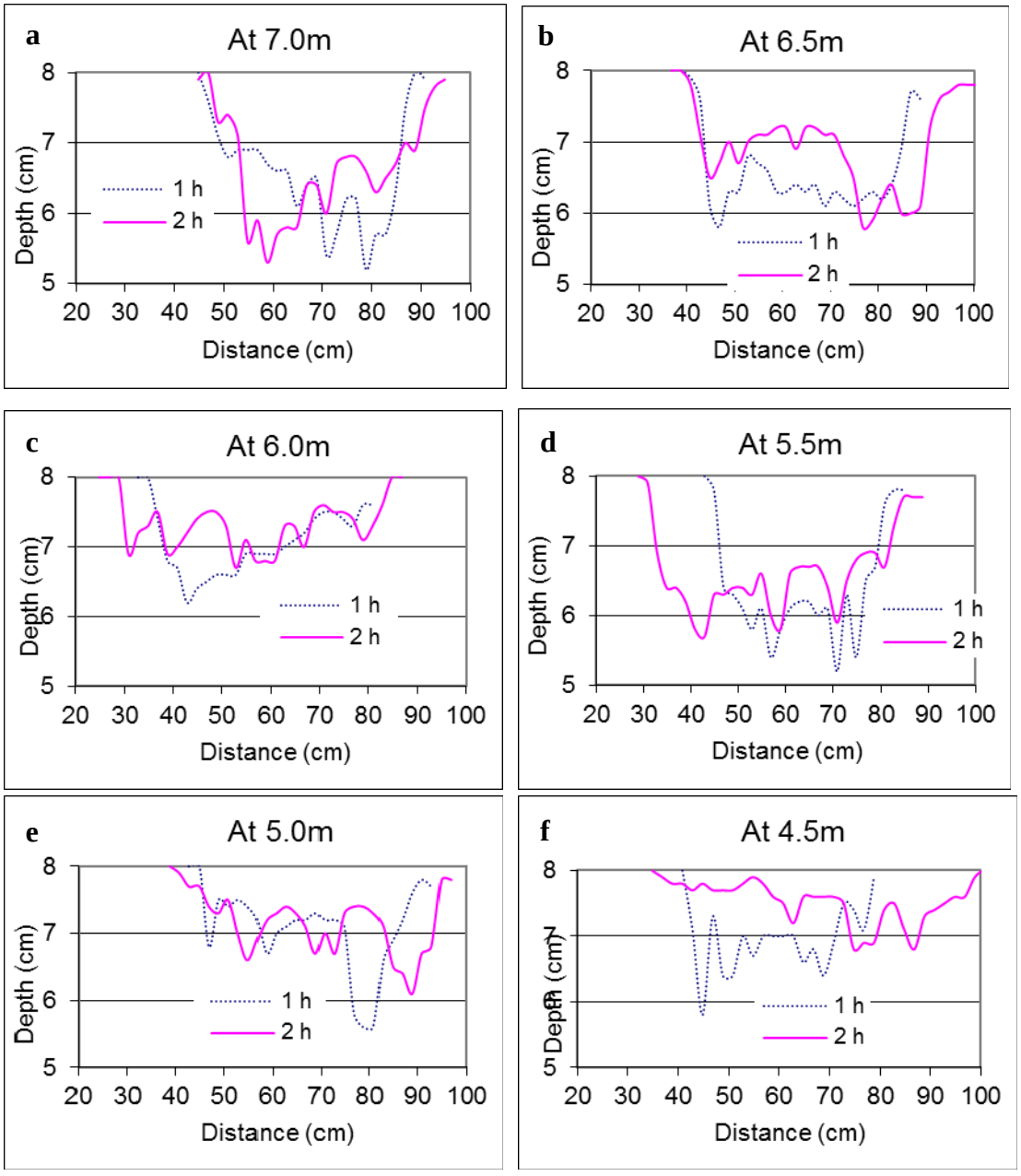

Figure 5.20: Transverse sections at 7 m (a), 6.5 m (b), 6 m (c), 5.5 m (d), 5 m (e) and 4.5 m (f) in Test 19 at 1 h and 2 h.

Taking the section at 5.5 m as an example, widening and shallowing occurred from 1 h to 2 h. The deepest depth at 1 hour was nearly 3 cm, and then at 2 hours, it changed to about 2.3 cm. Channel

width also increased 40 cm from 45 cm to 85 cm in this 1 hour. Channel banks developed further on both sides, meaning there was more sinuosity at 2 hours than at 1 hour.

Figure 5.21 from Knighton (1998) shows Einstein and Shen's model of twin periodically reversing, surface- convergent helical cells to explain the flow structure in alluvial straight channels. In this model, the thalweg changed from right to left and then to right again with shallow crossing in the middle just as the same as Test 19 at 1 h in Figure 5.20. It also shows the flow structure in flume channel.

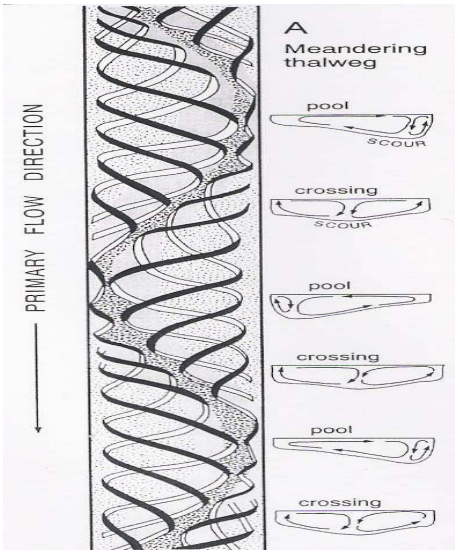

Figure 5.21: Models of flow structure and associated bed forms in straight alluvial channels ((A) Einstein and Shen's (1964) model of twin periodically reversing surface- convergent helical cells, black lines indicate surface currents, and white lines near bed currents.).

Channel development description

There was beginning of thalweg meandering and point bar development in Tests 15, 19 and 22 with a medium flume slope of 0.015. During the test, there was little overflow in Test 19. This

encouraged to increase the channel size to avoid overflow. Point bars (black arrows shown in Figure 5.17) in Test 22 would appear when water level was decreased by stopping water supply. This made increase channel slope to cause much stronger meandering with point bars. Test 23 is the following experiment which had the same flow rate and channel size but a steep slope of 0.020. The trapezoidal cross section's average aspect ratio (width/depth) is 2.9. It gave a good example of how a meandering channel develops from a straight channel with initial bending upstream. Other experiments also had meandering tendency, but not as obvious as in Test 23.

There are white lime lines to indicate distance (see in Figure 5.22). With this flow rate and flume slope, the initial channel size was not its equilibrium size. When water flew into channel, banks began to be eroded and channel became wide and shallow. Due to the bending at the beginning, the small channel size and mainstream changed flowing direction to another bank and this bank was eroded, causing the channel to become wider and shallower. The sinuosity was formed upstream and moved downstream, see Figure 5.22. Then the sinuosity became stronger and enhanced erosion. Sand was deposited to form bars. The resulting channel featured in Figure 5.22a were very similar to a nature river described by Duan and Julien (2005) which meanders downstream, with its amplitude of meandering decreasing in the downstream direction. This is a real river in New Mexico, the lab experiment can model the features of natural rivers.

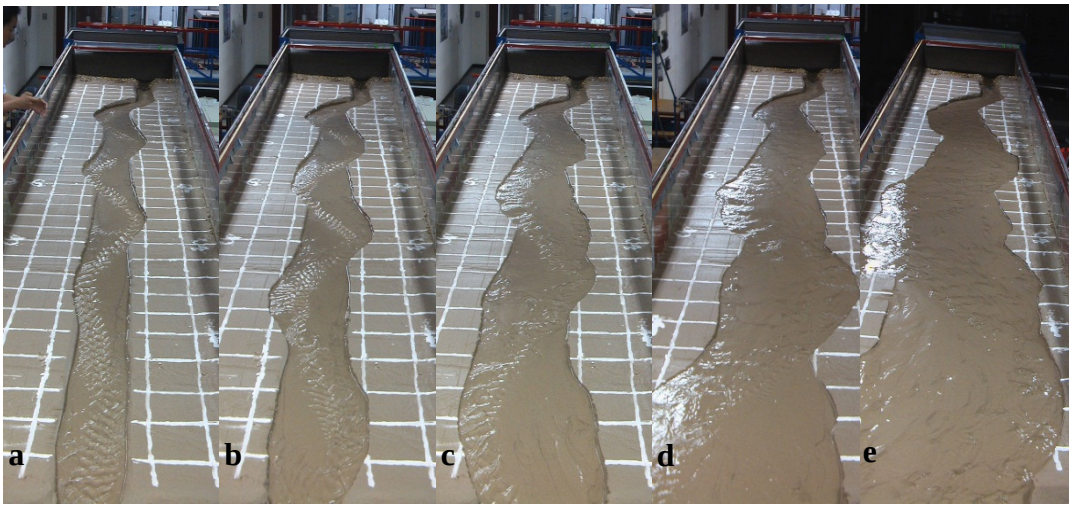

16 min 30 min 60 min 120 min 300 min

Figure 5.22: Test 23 with slope 0.020, flow rate 0.711 l/s and channel size 3 at 16 min (a), 30 min (b), 60 min (c), 120 min (d) and 300 min (e). Flow direction is from up to down.

From Figures 5.22 and 5.23, it can be seen that bend development rate was not the same. At the first 40 minutes, the whole channel developed a bend rapidly, then from 40 minutes to 60 minutes, there was little development upstream (thalweg not obvious) and the thalweg downstream was clear with fast bank erosion (by checking white lines). Then after 60 minutes, the rate of growth decreased dramatically, but width of the channel continued to grow with wave length and growth of amplitude. The reason for these different rates is that the channel became wider upstream to downstream, when upstream was wide and its erosion rate was slow, downstream was narrow and its velocity was large and had strong erosive ability. When downstream became wider than its initial width, flow velocity was small and stream power became separated, and then bend development increased slowly. Channel boundary lines and thalweg in Figure 5.23 show how bend developed from 0 min to 120 minutes.

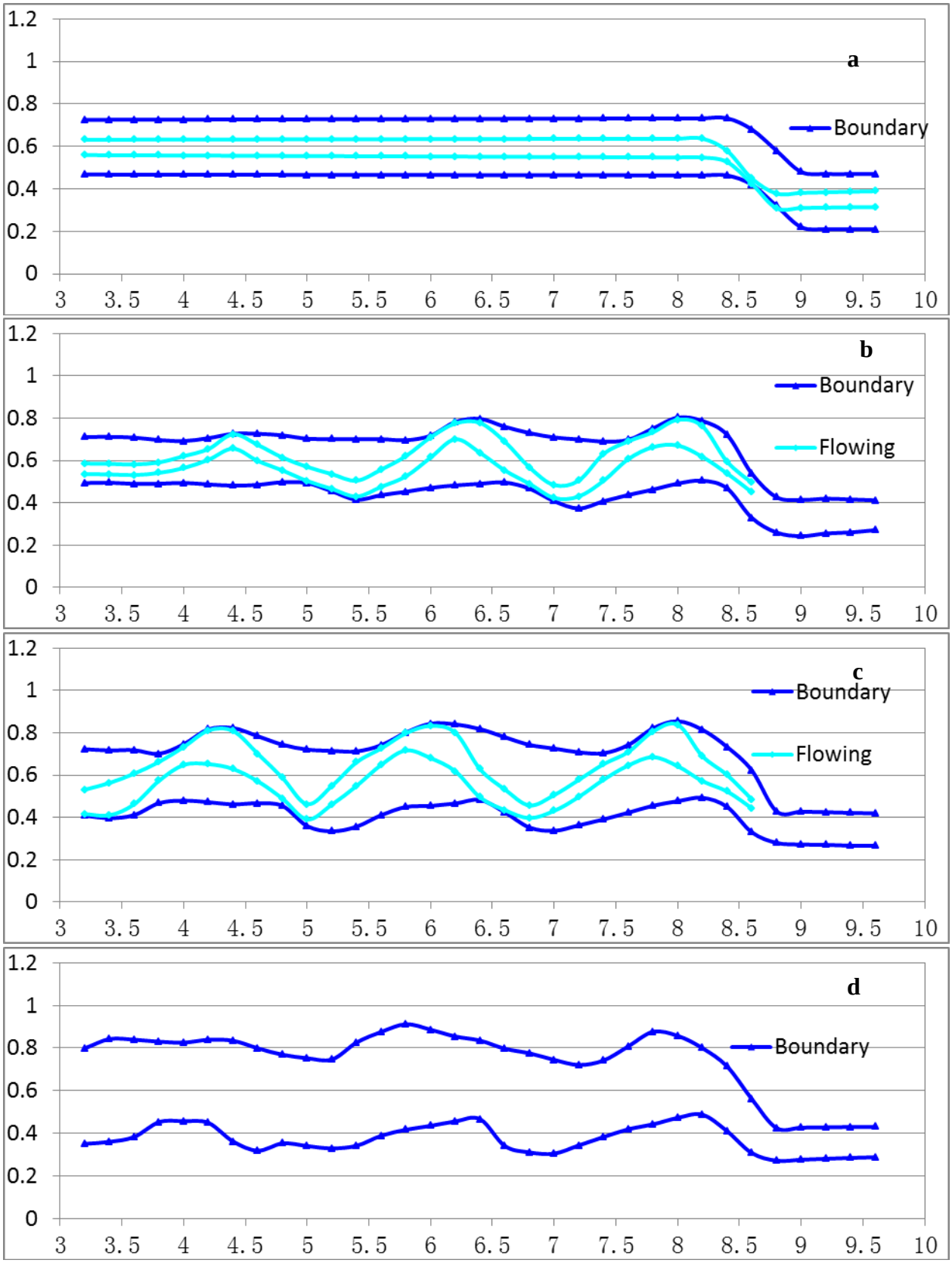
a
Boundary
b
Boundary
Flowing
c
Boundary
Flowing
d
Boundary
1.2
1
0.8
0.6
0.4
0.2
0
3
3.5
4
4.5
5
5.5
6
6.5
7
7.5
8
8.5
9
9.5
10

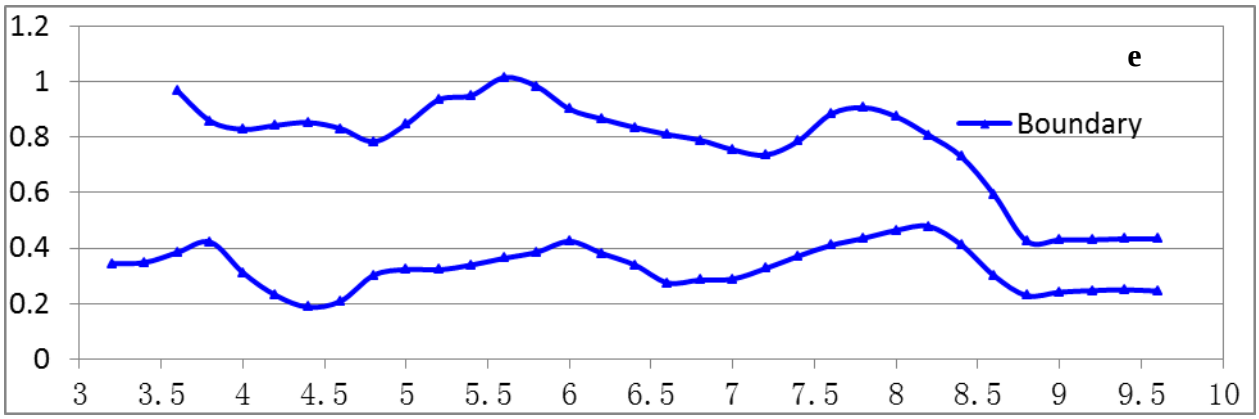

Figure 5.23: Boundary lines and thalweg development in Test 23 at 0 min (a), 16 min (b), 30min (c), 60 min (d) and 120 min (e). Flow direction is from right to left. In transverse: m, in longitudinal: m.

Because of non-cohesive material in tests, point bars in Tests 19, 22 and 23 were not very stable. If there is clay or other cohesive sediment, point bars would be stable when channel migrates away. By developing, flow rate around point bars is small and cohesive material covers the surface of point bars and can then consolidate them. Consolidation plays an important role in the evolution of river channel pattern (Smith, 1998). In that way, a real meandering river would be formed. Here channel type in Tests 19, 22 and 23 could be regarded as type 3b or 4 as in Figure 3.2 in Chapter 3. In these tests, flow rate was steady and other conditions were simple such as homogenous sands and no vegetation. If not, morphology change would be complex: bar would be fixed by vegetation to be an island. Fine sand would be in convex and coarse sand would be in concave. Others (Jang and Shimizu, 2007; Gran and Paola, 2001; Tal et al., 2003) have done research to see how vegetation affects the morphology. For more complicated flow condition, tests with unsteady inflow will be introduced in the next chapter.

5.4.2.4 Braided channels

Braided channels are a product of high energy and the steepest valley slopes. Braided channels have many channels separated by bars and islands. The characteristic feature of braided pattern is the repeated division and joining of channels, and the associated divergence and convergence of flow, which contribute to a high rate of fluvial activity relative to other river types (Knighton, 1998). The braided development would create rapid increase in channel width. The high velocity flowing would erode banks quickly which provide abundant of bed load and bank boundaries keep straight, but flow is divided into many thalwegs by bars and islands. The river becomes very shallow and flat in comparison to its width. Also thalwegs often change without regulation.

There is no obvious braided channel in these series of experiments, but one test showed a trend of braided development: Tests 21 in Figure 5.24. In Figure below, black arrows indicated flowing channels which were separated by shallow bars. This channel development with very large discharge is different from tests described before which had one main thalweg and other branches, with bars and islands separating them.

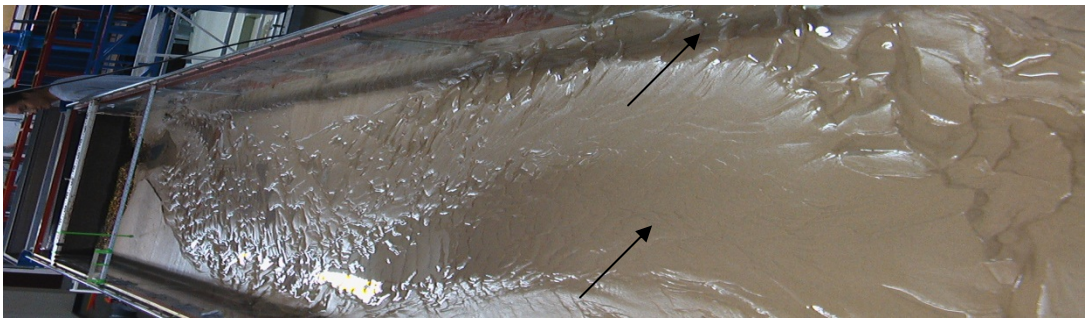

Figure 5.24: Test 21 with slope 0.015, channel size 3 and discharge 3.110 l/s at 60 minutes.

5.4.3 Reproducibility discussion of tests with the same conditions

Channel geometry in sand- bed streams can be described by one set of continuous functions over a wide range of flow conditions (Hickin, 1972). It means that under the same constraints and with the same values of independent variables, channel form should be reproducible. (Schumm et al., 1987) Tests 23, 24 and 31 had the same conditions in the first 30 minutes: flow rate of 0.711 l/s, slope of 0.020, channel size 3 of 26 cm×6 cm×5.5 cm. Their channel forms at 30 minutes are shown in Figure 5.25, and the comparison of Tests 23 and 24 is shown in Figure 5.26.

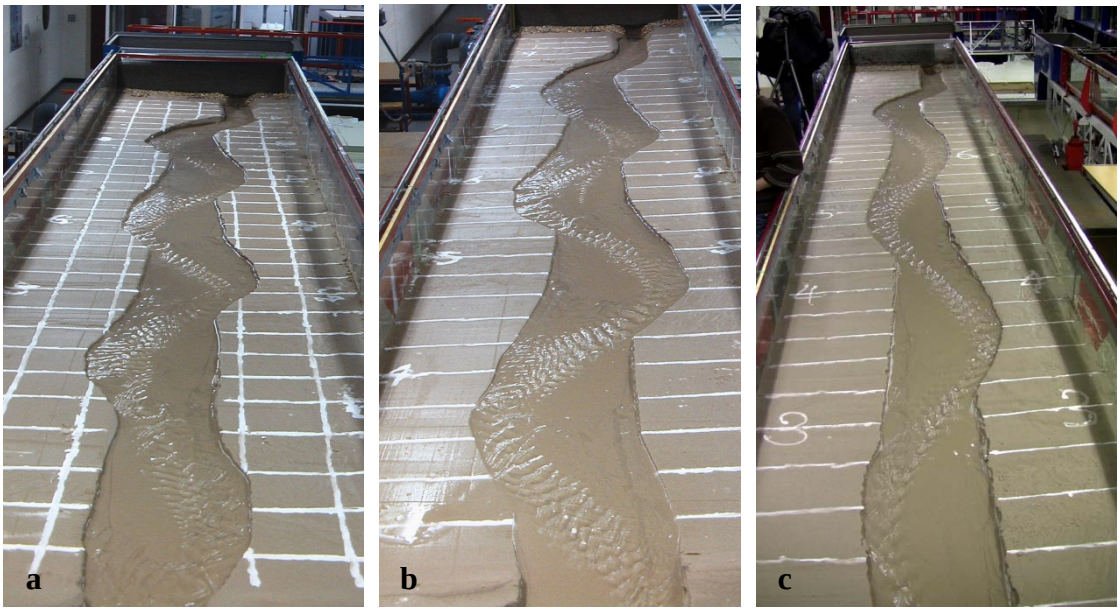

Figure 5.25: Channel geometry at 30 minutes for Tests 23 (a), 24 (b) and 31 (c).

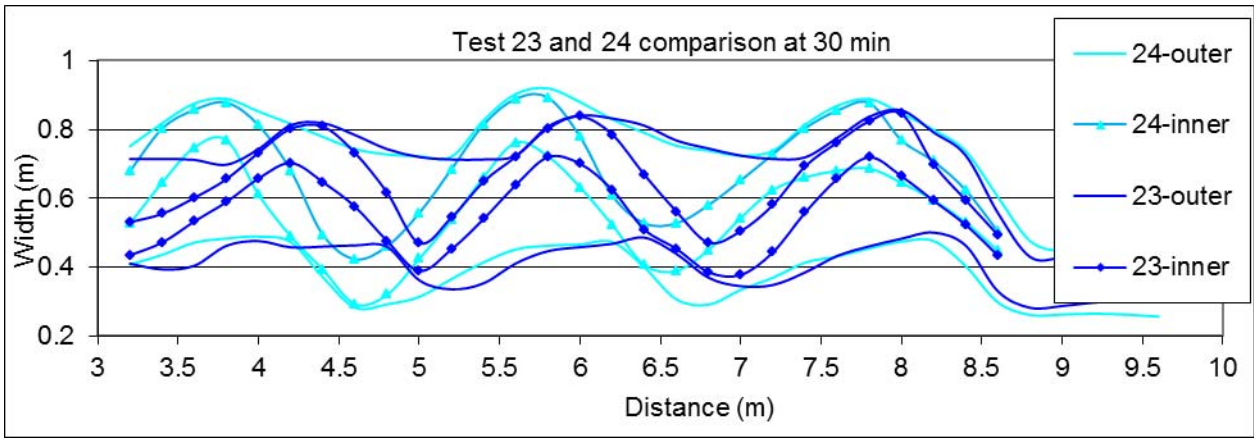

Figure 5.26: A comparison of inner and outer boundaries at 30 minutes for Tests 23 and 24.

It is not easy to compare the difference between these three tests in Figure 5.25 because of the angle of camera, so forms of Tests 23, 24 were drawn together in Figure 5.26 for easy comparison. But Figure 5.25 still shows the same relationship of point bars with meandering thalweg and their positions. Figure 5.26 shows channel development for Tests 23 and 24 with the same conditions at 30 minutes. It can be seen that the trend of development for those two channels is similar. However, there are some differences between them, like meander width and length. The main reason for these differences in curves is that the initial channel was made manually and they could not be made exactly the same. The morphology is controlled by flowing rate, sand characteristic, channel slope and size. If these parameters were the same, morphology would be more consistent. Therefore, the development of a channel is a reproducible process, particularly under laboratory conditions. This is also confirmed by others' experiments and research.

5.4.4 Channel development in longitudinal and lateral direction

5.4.4.1 Cross section development and lateral migration with medium channel

Figure 5.27 is Test 31 at 30 minutes, point bars with a meandering thalweg after stopping water supply clearly showed the effect from upstream bending. Figure 5.28 shows the lateral migration at different time steps. Measurements for the first 30 minutes were at sections of the meander apex, bottom and crossing, and then at 60 minutes, the second measurement was at the same section for easy comparison purpose in Figure 5.29.

In Figure 5.27, phenomena associated with meandering were clearly observed, such as point bars appearing alternately, strong sinuous thalweg, sediment transport passed to downstream and some

deviation towards the bars from the channels due to the secondary effect on the bed. The meandering was temporary and could not last for a long time in this test with non-cohesive sand and point bars could not resist the erosion in the long run. In Figure 5.27b, with point bars above water level, flow seemed to channelize when water was stopped.

Figure 5.27: Test 31 at 30 minutes with water supply (a) and without water supply (b).

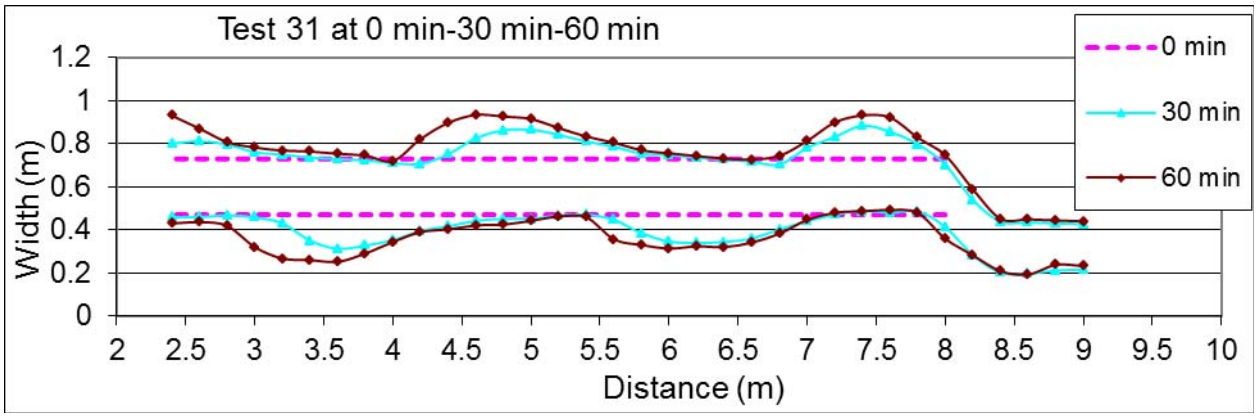

Figure 5.28: Comparison for Test 31 at 0 min, 30 min and 60 min. Flow is from right to left.

In Figure 5.28, in upstream part (5.3 m to 7.8 m), it shows that in the first 30 minutes, the erosion happened seriously, not only on erosion area but also the erosion length in a lateral direction. It was about two times faster than the period from 30 to 60 minutes. But in downstream (2.6 m to 5.3 m), erosion area and lateral length was almost the same for the two half hour periods. This

proves that bank erosion was seriously affected by its upstream bending. In the first 30min, flow from 5.3 m to 7.8 m had strong erosion ability by initial bending and channel in downstream 2.6 m to 5.3 m was not affected. Then at 30 min, channel from 5.3 m to 7.8 m formed bending and provided flowing with erosion ability to channel downstream (2.6 m to 5.3 m). Also at this time upstream was wide and erosion phenomenon was weak.

In Figure 5.29, it is clear to see channel section development from 0 min to 60 min. At 30 minutes, thalweg moved from upstream right side to downstream left side and then right side again with crossing in the middle. The first 30 minutes had almost 85% of lateral migration at the meander apex (see at 6.10 m, 4.90 m and 3.60 m). Crossing at 5.5 m and 4.30 m was different. After 30 minutes, the channel had little migration or no obvious change at 5.5 m, but at 4.30 m, channel was eroded at its left side and had more erosion than the first 30 minutes. The depth had little change in these two 30 minutes. The most erosion happened on the right side, the left side also had small erosion at beginning, but after 30 minutes, there was almost no change on the left side in lateral direction. Bed elevation increased a lot in the first 30 minutes by deposition, the first half hour accounted for most of the deposition. At 30 minutes, point bars and the main channel formed, and then after that there was scour on these bars, then the middle channel bar and secondary channel formed.

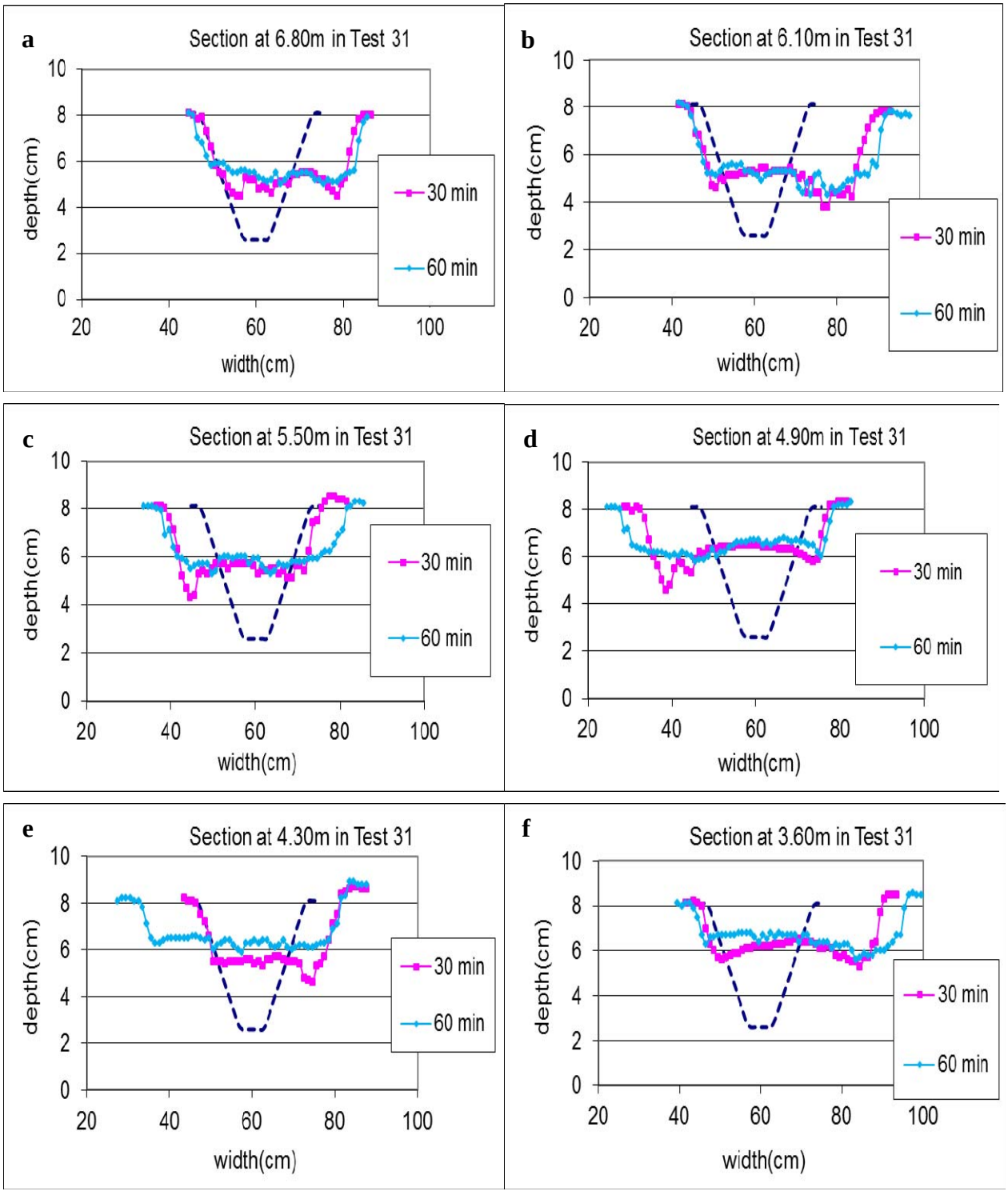

Figure 5.29: Test 31 at 0 min, 30 min and 60 min at sections 6.80 m (a), 6.10 m (b), 5.50 m (c), 4.90 m (d), 4.30 m (e) and 3.60 m (f). Flow is from inside to outside of paper.(Blue lies are the original channels)

5.4.4.2 Channel development with big channel and different slope

Channel morphology was changed by bank erosion and sand transportation or deposition. Bank erosion provided sand source. The cut bank development took place when flowing against banks and banks directed flowing against the opposite banks, causing opposite bank erosion again. Here we can take example from Tests 35 and 37 in Table 5.9 to describe the cut bank development and meander shift. Photographs describing channel development for Tests 35 and 37 are shown below alternately in Figures 5.30 and 5.31.

Table 5.9: Tests 35 and 37 with meandering channels.

Test No	Channel size (cm×cm×cm) bank slope	Area of cross section (cm^2)	Slope	Q (l/s)
35	31×4×7.5	131.25	0.020	1.472
37	31×4×7.5	131.25	0.015	1.472

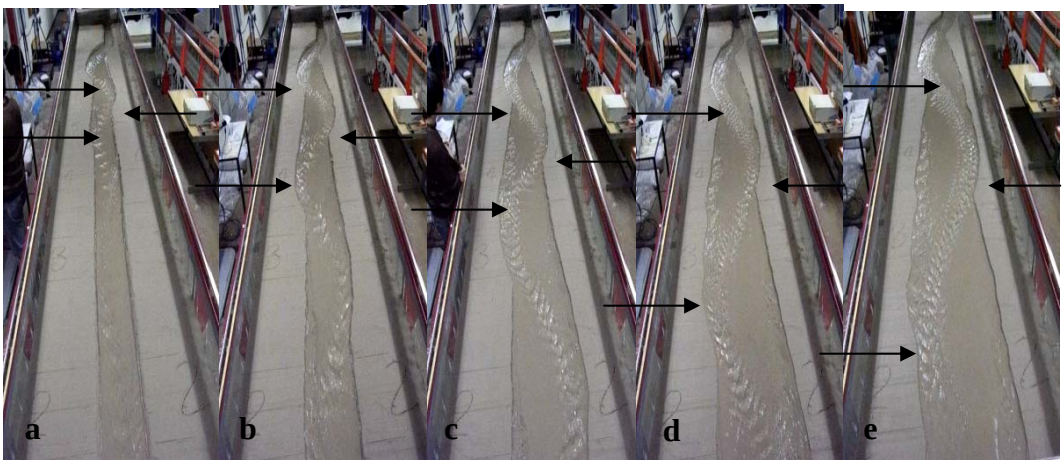

6 min 12 min 18 min 24 min 30 min

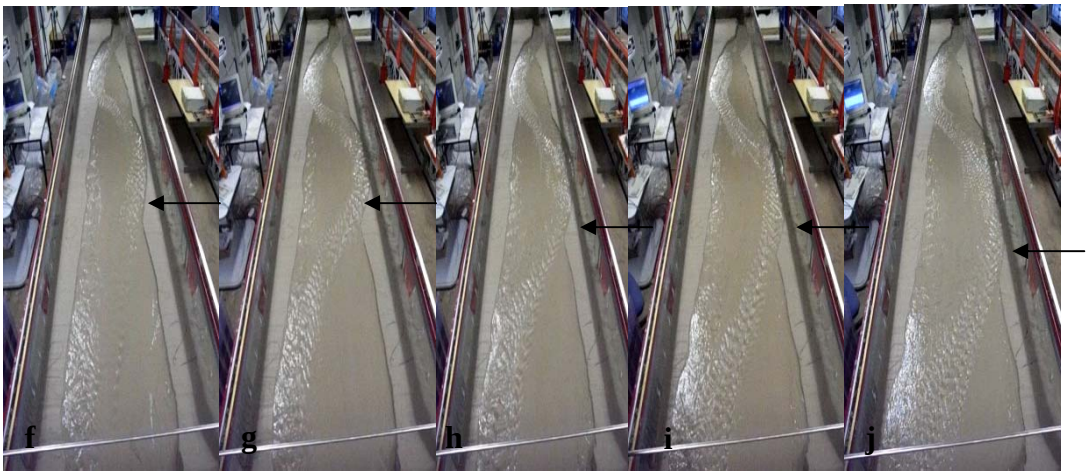

36 min 42 min 48 min 54 min 60 min

Figure 5.30: Cut bank development in 60 minutes for Test 35 (slope: 0.020, discharge: 1.472 l/s, channel size 4).

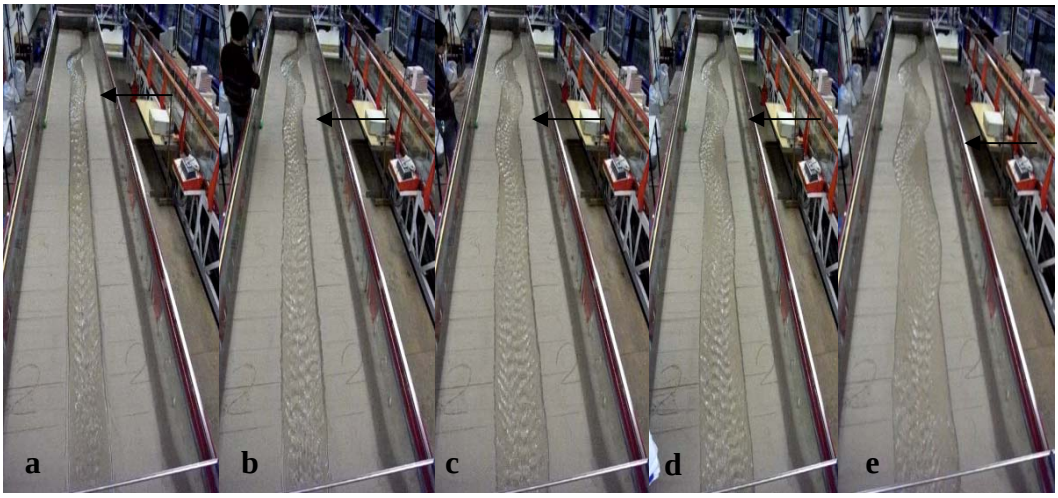

6 min 12 min 18 min 24 min 30 min

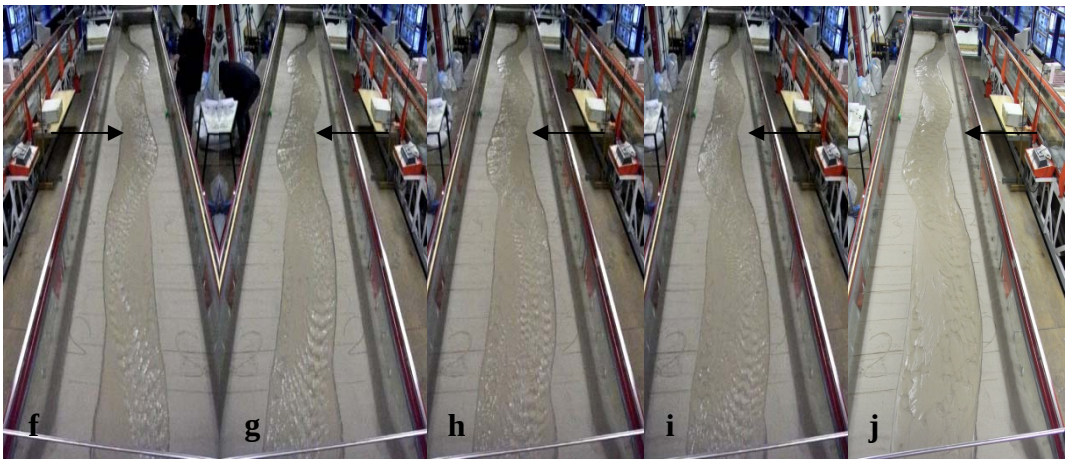

36 min 42 min 48 min 54 min 60 min

Figure 5.31: Cut bank development in 60 minutes for Test 37 (slope: 0.015, discharge: 1.472 l/s, channel size 4).

Tests 35 and 37 had the same big channel 4 (31 cm×4 cm×7.5 cm), and the same discharge of .472 l/s but a different slopes. This made a large difference for channel development as shown in Figures 5.30 and 5.31. The large slope shown in Figure 5.30, the speed of moving sinuous thalweg downstream was faster than in Figure 5.31. Black arrow on channel right indicates the first apex where flowing eroded bank after bending. The position of black arrow moved a little from 5.8 m to 4.8 m from 6 min to 12 min in Test 37 and then, it almost remained still, moving 0.40 m from 4.8 m to 4.4 m in 60 min. This moving speed was slower because flume slope for this test was 0.015. When flume slope was 0.020 in Test 35, the speed of moving sinuous thalweg became faster. The black arrow on the right channel moved from 5.4 m at 6 min to 3.2 m at 30 min and at last moved to 2.4 m at 60 min. This also proves that the rate of bend development was not uniform through time.

Through development, a bar formed. But in Test 35, the length and width of bar after bending did not stop growing in 60 min. At 6 min, the bar length was 1.5 m from 6.5 m to 5.0 m, at 30 min, the bar length was 2.9 m from 5.4 m to 2.5 m and 3.2 m from 4.7 m to 1.5 m. It was different with Test 37. The bar length was 0.9 m at 6 min and at 60 min it was 1.1 m, which did not change a lot in 1 hour because the channel almost reached a stable condition at 30 min, and the channel in Test 35 continued its bend development after 60 min.

Keller (1972) illustrated a five stage model of development for alluvial stream channels in Figure 5.32 and its advantage is that it can be applied to nearly all alluvial channels. Results of channel development in the lab (Tests 35 and 37) can be regarded from stage 1 to stage 3 where dominant

bed forms are pools, riffles and asymmetrical shoals (point bars). Channels in the lab could transform from a straight to a meandering thalweg but they could not develop to stage 4 and 5. As discussed before, if there is vegetation, clay or fine sand to stabilize point bars, the channel would develop to the next two stages- the well-developed meandering channels.

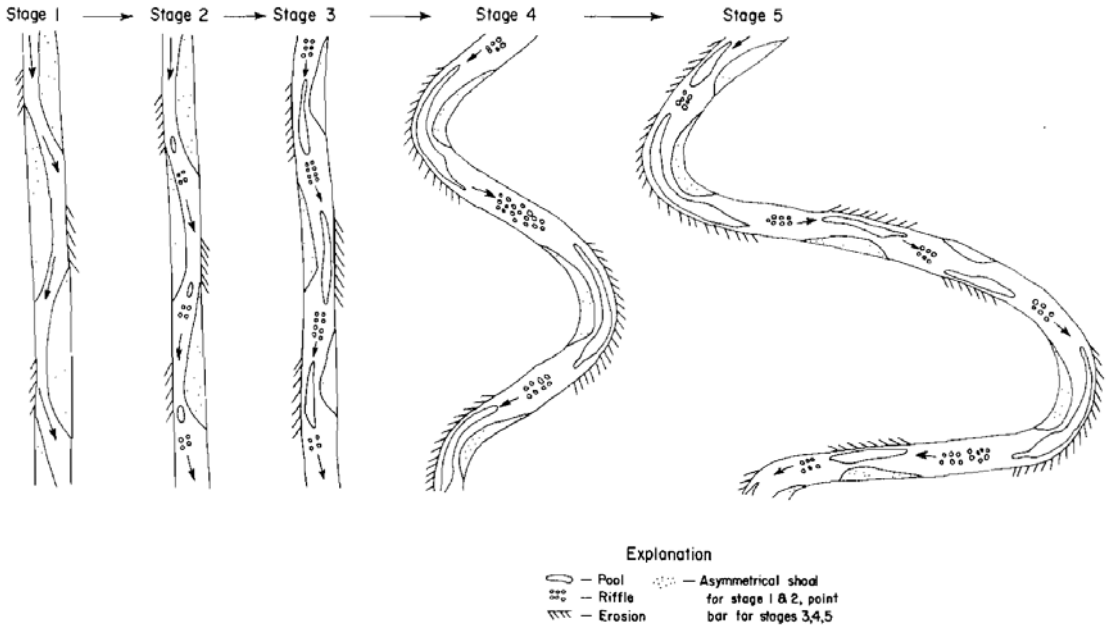

Figure 5.32: Illustration of the five stage model of development for alluvial stream channels by Keller (1972).

The phenomenon of bar formation and bend development here proved the large effect of slope to morphology again. Figure 5.33 shows bank development clearly for Test 23. It had same phenomenon with Test 37 but was clearer with white lines to mark distance.

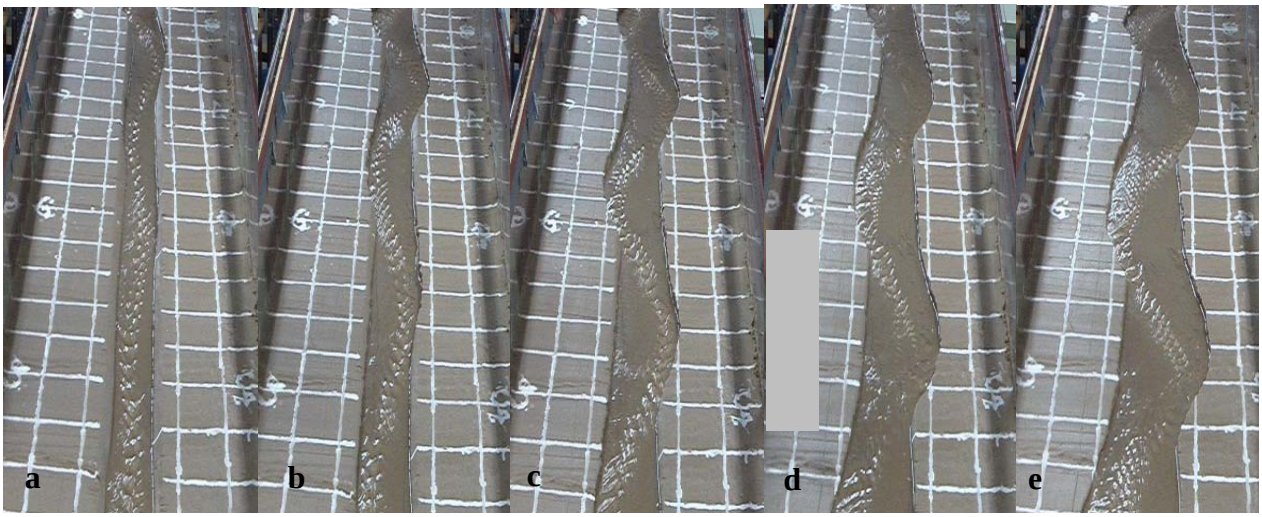

6 min 12 min 18 min 24 min 30 min

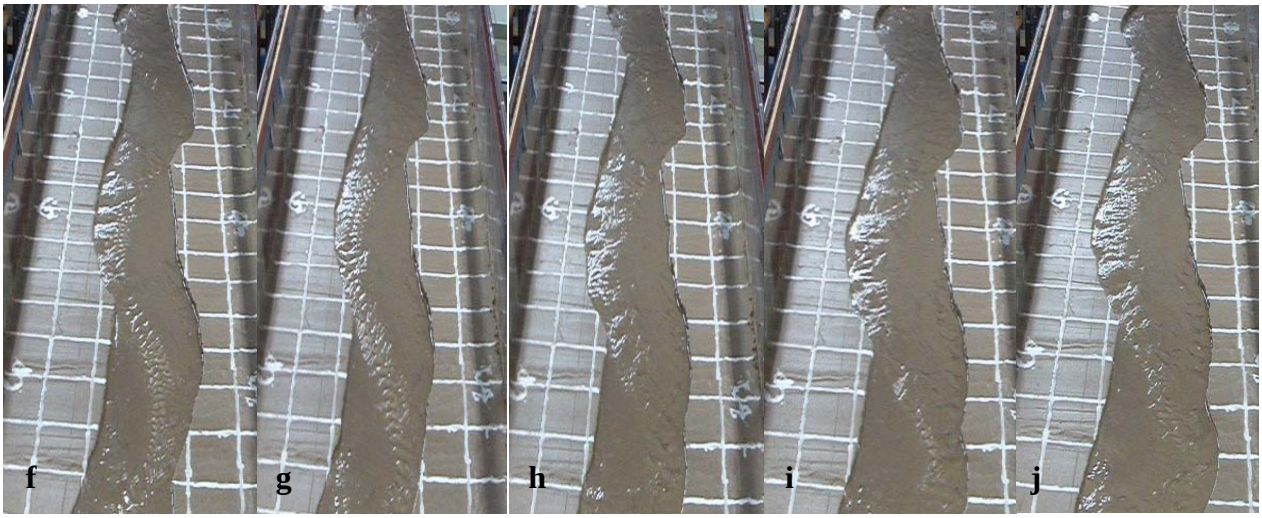

36 min 42 min 48 min 54 min 60 min

Figure 5.33: Bend development in Test 23 (slope: 0.020, discharge: 0.711 l/s, channel size 3: 26 cm×6 cm×5.5 cm).

5.4.5 Controlling parameters

5.4.5.1 Comparison for channels with different slopes

In Table 5.10, Tests 23, 22 and 25 had the same flow rate and channel size but a different slope: Test 23 with 0.020, Test 22 with 0.015 and Test 25 with 0.010. It is clear to see the important effect on morphology by slope in Figures 5.34- 5.36.

Table 5.10: Tests 23, 22 and 25 with meandering channels.

Test No	Channel size (cm×cm×cm) bank slope	Area of cross section (cm^2)	Slope	Q(l/s)	Date
23	26×6×5.5	88	0.020	0.711	5.8
22	26×6×5.5	88	0.015	0.711	5.5
25	26×6×5.5	88	0.010	0.711	5.17

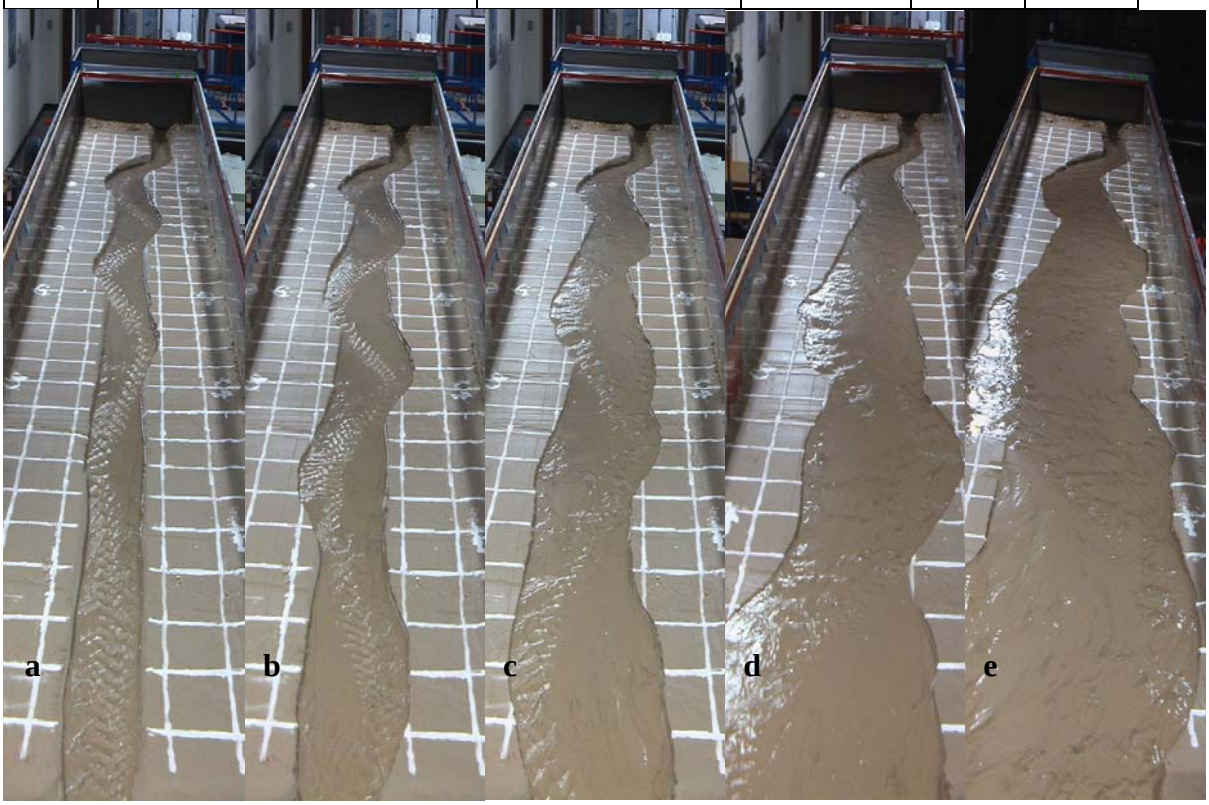

Figure 5.34: Test 23 at 14 min(a), 30 min(b), 60 min(c), 120 min(d) and 300 min(e).

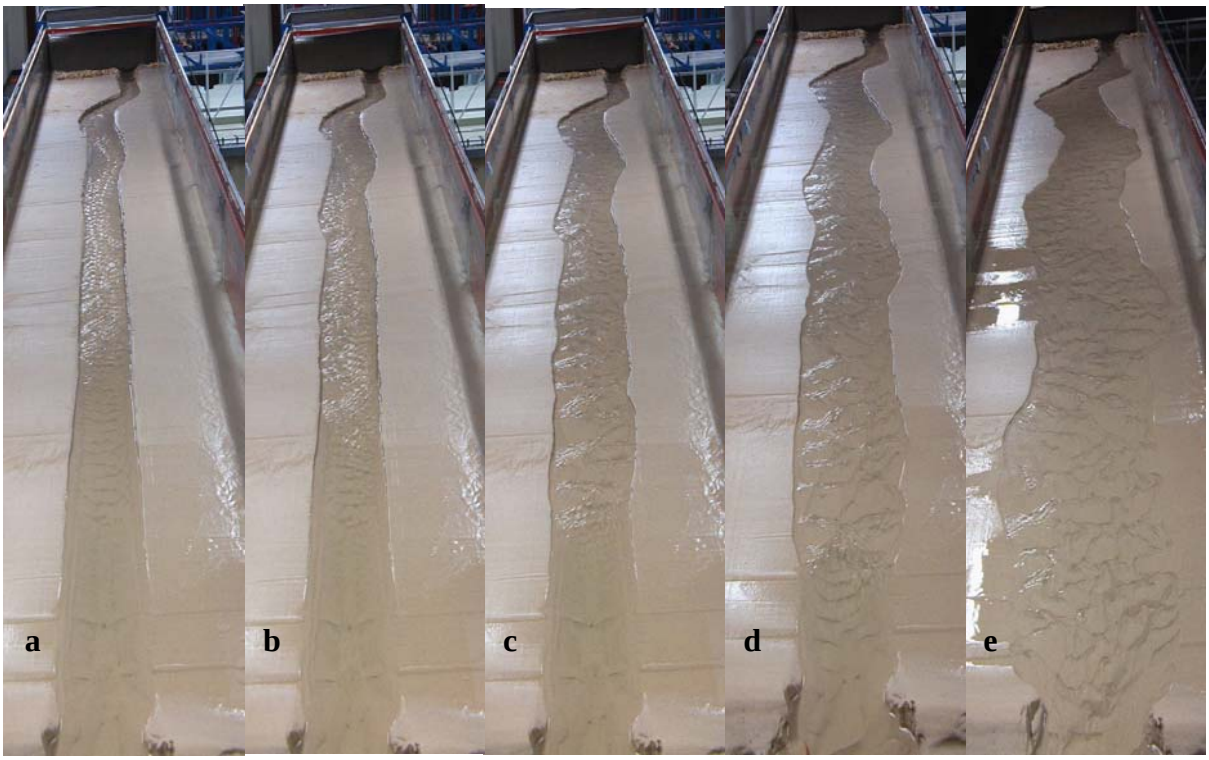

Figure 5.35: Test 22 at 14 min(a), 30 min(b), 60 min(c), 120 min(d) and 300 min(e).

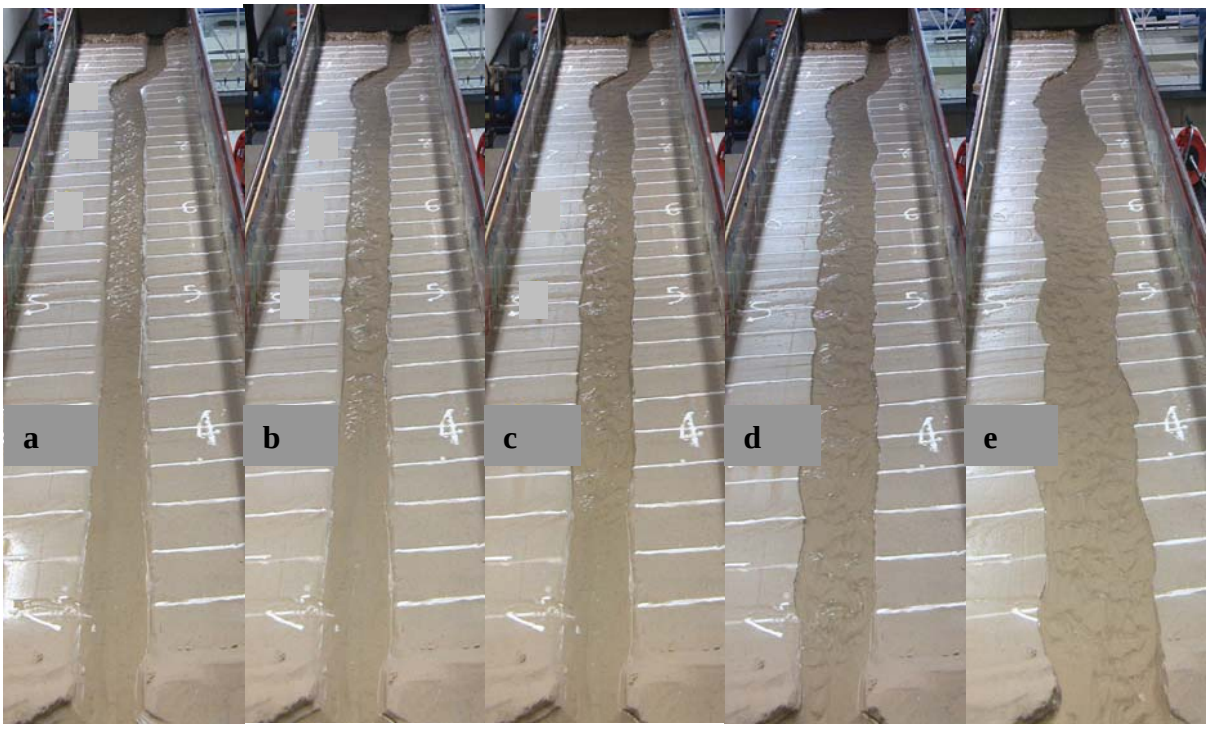

Figure 5.36: Test 25 at 14 min(a), 30 min(b), 60 min(c), 120 min(d) and 300 min(e).

With a large slope in Test 23, the channel developed quickly and became sinuous quickly. But with the flat slope in Test 25,the channel developed very slowly, keeping straight and narrow for a long time. Test 22, with the middle slope, had channel development which was neither fast nor slow, just on an average level.

Conditions of Tests 23, 22, and 25 differ essentially in having different values of Froude number ($Fr = u / \sqrt{gh}$) caused by different slope. Tests 23 (the same as Test 31 in Table 5.5) had a high value of *Fr* (Fr=1.27) which leaded to quick meandering development with high sinuosity, *Fr* for Test 22 was about 1.00 which leaded to channel with low sinuosity and *Fr* for Test 25 was smallest at about 0.60 with almost straight channel development. The velocity for *Fr* was obtained by tracking the particle travelling a certain distance. (It is the same for *Fr* in Tables 5.11 and 5.12; at 7 min, flow rate became stable and channel was still straight after a long distance.)

The bed load sheet could be visible in the channel for cases 22 and 25 in 30 min and 60 min in Figures 5.34- 5.36. Bed load source came from bank collapse and erosion. Bed load was also the main type of sediment transportation.

Channel development in the experiment correlated well with the observation by Schumm and Khan (1971). When slope is small, channel would remain straight and when slope increases, sinuosity would increase, meaning that channel develops in a meandering pattern. When slope continues to increase, channel would become braided. Here Test 23 had a sinuous channel with thalweg meandering. If slope becomes larger, for example: 0.025, channel would develop as braided or trend to braided with many small middle channels.

The slope in these experiments was steeper than those in nature. The modelling rivers' slope was between 0.010 and 0.025 for meandering river, which is nearly 10 times of that of real stream.

5.4.5.2 Comparison for channels with different flow rate

A large slope increases unit stream power (unit stream power: $\rho gQS/w=\tau U=\rho gdSU$, where ρ= density of water, g = accerlation due to gravity, Q = discharge, S = water surface gradient, w = width of river, U =mean velocity, τ= mean shear stress, d = mean flow depth) which enhances erosion ability and increases bank collapse and bed load transportation. Large flow rate could also provide large unit stream power to cause sinuosity. Van den Berg and Bledsoe (2003) agreed that stream power is an appropriate parameter to predict channel patterns: with increasing stream power, channel width increases, and the channel pattern increasingly tends to become braided. Conversely, with a lowering of the stream power, channels tend to become relatively narrow and single-thread. Friedkin (1945) found that meander wavelength, sinuosity, and amplitude increase with discharge. This phenomenon could be observed in Figure 5.37. Tests 31 and 32 had different flow rate (0.711 l/s and 1.472 l/s respectively). And Tests 35, 36 also had different flow rate (1.472 l/s and 3.110 l/s respectively). Their run conditions and results are in Table 5.11. It is clear that Test 32 with large flow rate had larger meander length, width and amplitude than Test 31. Test 36 had the same comparison with Test 35, and did not even have one whole wave in the flume.

Figure 5.37: Tests 31 (a) and 32 (b), Tests 35 (c) and 36 (d) at 30 minutes.

Table 5.11: Results of Tests 31, 32, 35 and 36.

Test No	Slope	Q (l/s)	Bed forms(cm) at 30 min			30 min / 60 min	At 30 min	At 7 min
			Λ	λ	A	L	sinuosity	Fr
31	0.020	0.711	60	250	48	369/ 426	1.54	1.27
32	0.020	1.472	98	285	74	472/ 598	1.64	1.15
35	0.020	1.472	81	450	65	493/ 594	1.30	1.21
36	0.020	3.110	-	-	-	-	-	1.30

S: slope of flume, Λ is amplitude of meandering, λ is length of meandering, A is width of channel, L: Length (cm) of thalweg of one wave (cm), h: channel depth (cm).

5.4.5.3 Comparison for channels with different channel size

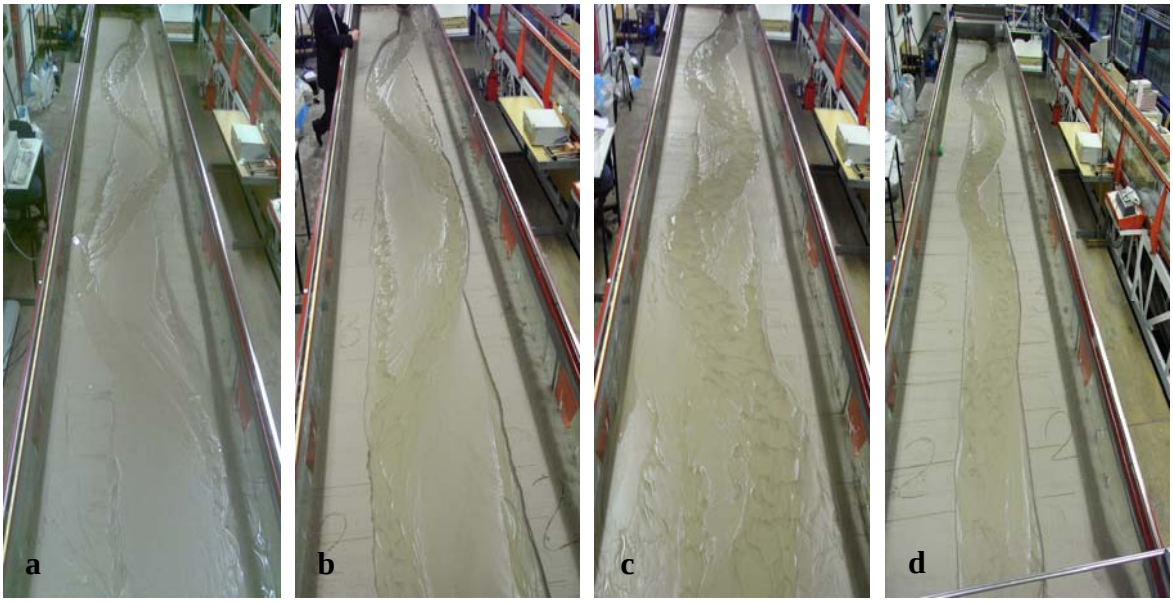

Figure 5.38: Tests 32 (a) and 35 (b), 33 (c) and 37 (d) at 30 minutes.

Channel size especial aspect ratio (average width/ depth) plays an important role in river morphology change. It is recognized by many researchers that the channel pattern is most sensitive to the bankfull width/depth ratio. The small width/depth ratio means water could be concentrated in a small area with large unit stream power (ρgdSU). Also a channel with small width- depth ratio is not its equilibrium condition, and it leads to bank erosion, sand deposition, and finally a total different morphology. Small width/depth ratio has a higher bank and bank collapse could provide lots of sand load for morphology change when bank erosion is a major source of sediment load in many real rivers. This happened in model stream.

Table 5.12: Results of tests with the same discharge.

Test No	Slope	Q	Aspect ratio	Bed forms(cm) at 30 min			30 min/ 60 min	At 30 min	At 7 min		
				Λ	λ	A	L	Sinuosi	V	h	Fr

								ty			
32	0.020	1.472	2.9	98	285	74	472/ 598	1.64	57.1	2.5	1.15
35	0.020	1.472	2.3	81	450	65	493/ 594	1.30	53.7	2	1.21
33	0.015	1.472	2.9	83	300	72	483/ 483	1.61	51.7	3	0.95
37	0.015	1.472	2.3	62	256	51	391/ 436	1.33	60.2	3	1.11

S is slope of flume, Q: flow rate (l/s), Λ is amplitude of meandering, λ is length of meandering, A is width of channel, L: Length (cm) of thalweg of one wave (cm), h: channel depth (cm), V: velocity at 7min (cm/s).

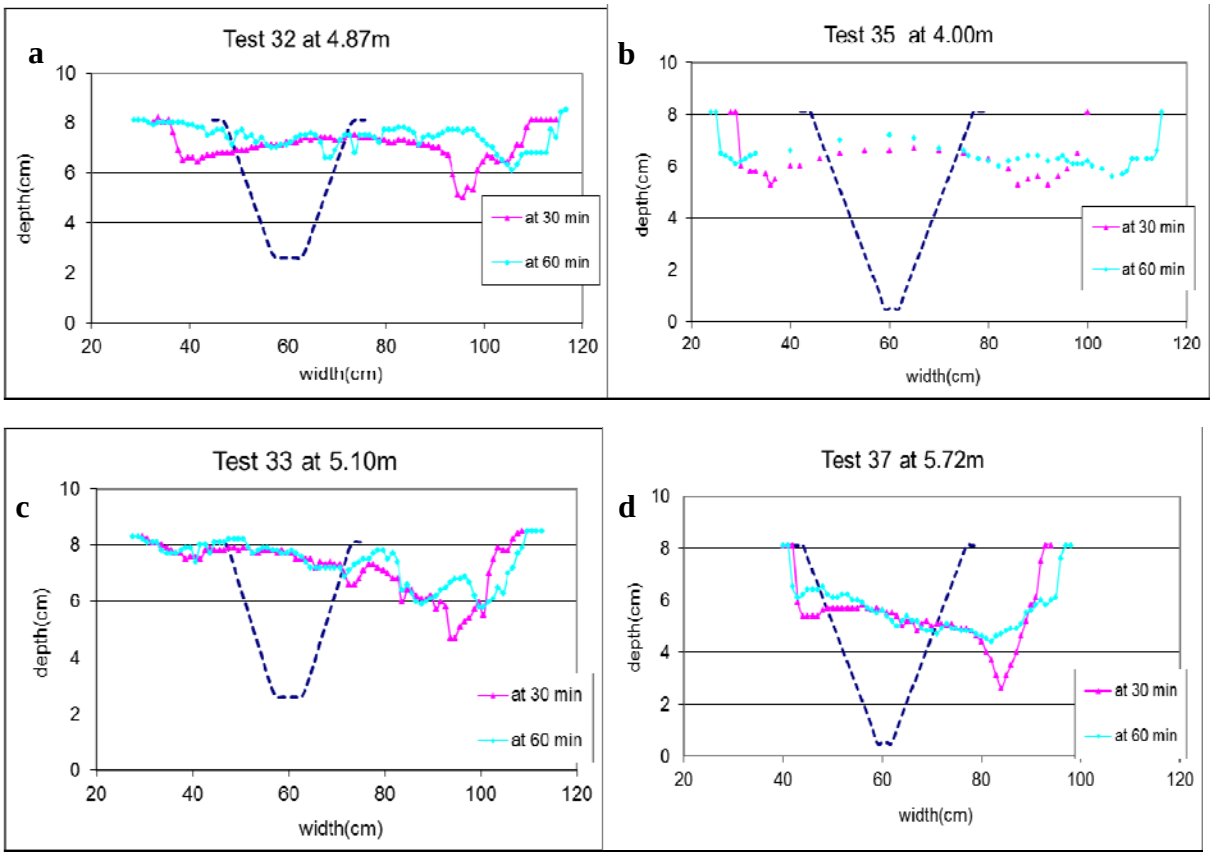

Figure 5.39: Cross section measurement of the first wave apex after bending in Tests 32 (a), 35 (b), 33 (c) and 37 (d). (Blue lines are the original channels)

The comparison can be seen from Figure 5.38 between Tests 32 and 35, Tests 33 and 37. Tests 35 and 37 had a smaller average width/depth ratio with 2.3 and 32 and 33 with 2.9. It is clear to see in Table 5.12 that smaller width/ depth ratio meant that Tests 35 and 37 have smaller sinuosity, smaller meander amplitude and width, but meander length. We also observed the same dependence of the width/depth ratio on the Froude number (*Fr*) again. *Fr* in 35 and 37 were larger than 32 and 33 in Table 5.12. The difference can also be observed from the cross section measurement of the first wave apex after bending in Figure 5.39. Tests 35 and 37, with small width/depth ratio, had a deep and narrow channel.

5.4.5.4 Sediment

Sediment character

Sediment character plays an important role in channel formation, and many researches and observations have proved this influence.

Friedkin (1945) did experiments to demonstrate the effect of varying materials while other conditions remianing the same. Channels with more silt would be deeper and narrower and meander wavelength and amplitude were smaller than channels with less silt.

In Friedkin's experiments, the channel was straight with a meandering thalweg. It was not a real meandering river. But when cohesive clay was added to flowing water, the true meandering channel was formed from a meandering thalweg channel. Many researchers have observed the effect of deposition of cohesive clay. Schumm and Khan (1972), Yi (1965) and Dulal and Shimuzu (2010) observed that the clay could reduce shallow water depth over bars and stabilize

point bar against further erosion, the scour along thalweg lowered water level, and the channel became narrower and deeper with larger sinuosity.

Shimizu et al.'s (1996) test at 95 minutes showed a good result, but author did many tests with different conditions, without one as the same. Result from Friedkin also showed a good meandering form after 3 hours. But Test 23 from author showed a good result after 40 minutes when slope was 0.020, different sand size being the main reason. Friedkin chose 0.45 mm, and Shimizu chose 1.25 mm. Both were larger than authors' choice (0.268 mm). Fine sand has a small threshold current speed and that could make morphology develop quickly.

Smith (1998), Dulal and Shimuzu (2010), Ouchi (1985), Shepherd and Schumm (1974) and Gardner (1983) used cohesive material and their experiments required more time, about 100 times more than non-cohesive materials. Smith took more than 120 hours, Dulal took 29 h to 132 h, Garden's meander took 150 hours. Shepherd and Schumm had 107 hours for the channel.

Sediment load

In this research, the researcher at first thought that sand load would play a very important role in channel morphology, but the effect of sediment load was small, and sediment load had no obvious effect on the channel morphology in this experiment. So after dry sediment was fed by hand at a constant rate at the entrance in some earlier tests, there was no sand load by hand, and sand from bank erosion was the major source of sediment load. This was also observed by other researchers, like Ackers and Charlton (1970a). They pointed out that sediment load is unimportant and has a small independent effect on channel morphology.

5.5 Discussion

5.5.1 Experiment with theory research

Theory from Leopold et al. (1960) showed that:

$$\lambda = CB^n \qquad 5.2$$

Where λ is meander length, B is channel width and C=7.3 or C=12.1 with n=1.1 or 1.09.

The meander length is about 10 times channel width and the average ratio of wavelength to minimum radius of curvature is about 3- 5 (Leopold suggested: 4.7):

$$\lambda \approx 10B \approx 4.7R_m \qquad 5.3$$

where B is channel width, R_m is minimum radius of curvature.

Below it is meander relationship of Tests 23 and 24. Because experiment results had curved boundaries and meandering thalweg, they are both measured and shown in Table 5.13. It proves that the meander of thalweg could satisfy theory of Leopold, but the boundary meander could not. From this result, we can conclude that experiments undertaken in a laboratory flume cannot get a real meandering river but a sinuous thalweg.

Table 5.13: Relationship between meander parameters and channel width.

Relationship	Test 23	Test 23	Test 24	Test 24
	Boundary	Thalweg	Boundary	Thalweg
Degree of sinuosity (measured)	1.15	1.75	1.24	1.67
Ratio of meander length to channel width	5.55	12.8	4.44	14.3

5.5.2 Channel morphology discussion by regime theory

Leopold and Maddock (1953) recognized that stream develops for stability and has a relationship named hydraulic geometry. Regime theory agrees with artificial channels and natural rivers, showing that for a stable alluvial channel of given sediment, if two variables (discharge, sediment concentration, width, depth and slope) are known, the other three could be determined uniquely. Regime theory could also be used to calculate the stable slope for an alluvial river and compared with valley slope to decide whether river would be straight, meandering or braided. From Simons & Albertson (1963) using the regime theory, the stable straight channel width is:

$B = 0.9P = 0.9 \times 6.34Q^{1/2} = 5.706Q^{1/2}$, where P: wetted perimeter.

For flow rate 0.711 l/s in tests 31, B=15.2 cm

Ackers and Charlton (1970a) indicated that the meandering channels average twice the width of straight channels, 2B=30.4 cm>16 cm (average). The original channels were not their stable forms, so sediment from channel bed and banks was transported by flowing for deposition, erosion or washed away to change channel form until a stable channel is formed.

Bettess and White (1983) found that braiding of sand channels is uncommon, particularly for small discharges. Gravel rivers have a strong possibility of braiding, and it is not possible to have large sinuosity as meandering. Sand rivers are frequently meandering in nature. In researcher's experiments, considering sand size, channel slope and flow rate, channel form should be between meandering and braided and that correlated with the experiment results.

Using theories discussed in Chapter 3 about stable channels, the parameters of a stable channel were calculated from different theories and are shown in Table 5.14. The calculations are compared with results from the experiments.

Table 5.14: The comparison for stable channel parameters between theories and experiments

(where Br is channel width and Bm is thalweg width, y_0 is depth, λ is meandering wave length, S is channel slope, V is flowing velocity, A is cross section, P wetted perimeter.)

Discharge (m^3/s)	0.000711(Test 31 at 30 min)	0.001472(Test 37 at 30 min)
Experiment / Theory	Br=0.48 m, Bm=0.16 m y_0=0.010 m, λ=2.50 m S=0.0167	Br=0.51m, Bm=0.26m y_0=0.012 m, λ=2.56 m S=0.0130
$P = 4.8Q^{0.5}$ (Lacey, 1929)	P=0.128 m	P=0.184 m
$\lambda = 54.3Q_b^{0.5}$ Dury (1965)	λ=1.45 m	λ=2.08 m
Nixon (1959) for 27 streams in England and Wales. Q is bankfull discharge	B=0.080 m, y_0=0.049 m, V=0.182 m/s	B=0.115 m, y_0=0.062 m, V=0.206 m/s
Charlton et al. (1978) for 23 gravel bed rivers	B=0.143 m y_0=0.017 m V=0.290 m/s	B=0.199 m y_0=0.023 m V=0.323 m/s
Ackers (1964) for straight channels in medium sand, (Q_w) between 0.011 and 0.153 m^3/s	A=0.001097 m^2 B=0.1257 m y_0=0.009 m V=0.647 m/s	A=0.002036 m^2 B=0.1706 m y_0=0.012 m V=0.722 m/s
Stable channel design by Blench's equations	B=0.1540	B=0.2216

	y_0=0.043 S=0.00147---0.00092	y_0=0.054 S=0.0013---0.00081

From Table 5.14, Bm (thalweg width) could be used to compare with width by calculation. If meandering thalweg is a channel, Lacey's equation is reasonable, and Dury's equation agree well for Test 37 but not 31. Nixon's (1959) theory did not correlate with experiment, the main reason is that their theory is based on natural rivers and Q is bankfull discharge. Charlton et al. (1978) equation gives a good result. Width from Ackers (1964) is lower than that in the experiment. Blench's equation correlates well with experiment results on width, but not on channel slope and depth. From comparison, stable channel size in lab could not easily be designed.

From Bettess and White (1983), the discrepancy between the channel slope required for equilibrium and valley slope makes channel develop as a meandering or braided type. Regime theory is used to calculate the equilibrium river slope and by comparing this with the available valley slope, it is then determined whether river type is straight, meandering or braided. For some reasons, the author did not get the calculation result from analytical regime theory developed by White et al. (1982), but got results from other researchers (see in Table 5.14).

Sv (valley slope) in Test 31 is 0.020 and Sr (equilibrium slope by calculation) by Blench's equation is between 0.00092 and 0.00147, Sv>Sr. Then river could accommodate the discrepancy by meandering and channel slope reduced to 0.0167 in Test 31 at last. There was the same phenomenon in Test 37, Sv=0.015, Sr=0.0013- 0.00081. Channel adjusted its slope as meandering to its equilibrium slope 0.013 at last.

5.5.3 Extremal hypotheses

These theories include: the minimum unit stream power (Yang, 1976), the minimum stream power (Chang, 1979), maximum sediment transport rate (Kirkby, 1977; White et al., 1982), the minimum variance hypothesis, minimum energy dissipation rate (Yang et al., 1981), minimum Froude number (Jia, 1990).

From tests in Table 5.15, it is clear that the slope of flowing channels (Tests 31, 32, 33, 35 and 37) became smaller than its original slope after 30 minutes and slope continued to decrease at 60 minutes, but the decrease rate at the second 30 minutes slowed dramatically compared with the first 30 minutes. Test 34 had an unsteady inflow rate and Test 36 did not get a measurement, but at 30 minutes, they all had a decreasing slope. The development also correlates with the minimum Froude number (Jia, 1990), Fr changed from between 0.95 and 1.27 at 7 min to less than 0.70 at 60 minutes. Channels developed to more stable conditions with minimum unit stream power ($U\tau = \rho gdSU$=minimum).

Table 5.15: Channels' slope and Fr in the second set of experiments

Test No	Slope of flume	Slope of thalweg		Fr	
		30 min	60 min	7 min	60 min
31	0.020	0.0167	0.0159	1.27	<0.70
32	0.020	0.0148	0.0128	1.15	<0.70
33	0.015	0.0109	0.0105	0.95	<0.70
35	0.020	0.0177	0.0156	1.21	<0.70
37	0.015	0.0130	0.0129	1.11	<0.70

5.5.4 Relation between slope and discharge

From the experiment results, we can concluded that slope plays a very important role in morphology change and it can be seen that in Tests 25, 22 and 23, threshold value of slope existed, see Figures 5.34- 36.The slope changed from 0.010 to 0.015 to 0.020 and the channel pattern then changed from straight (Test 25) to meandering thalweg (Test 22) to a well-developed meandering thalweg channel (Test 23).

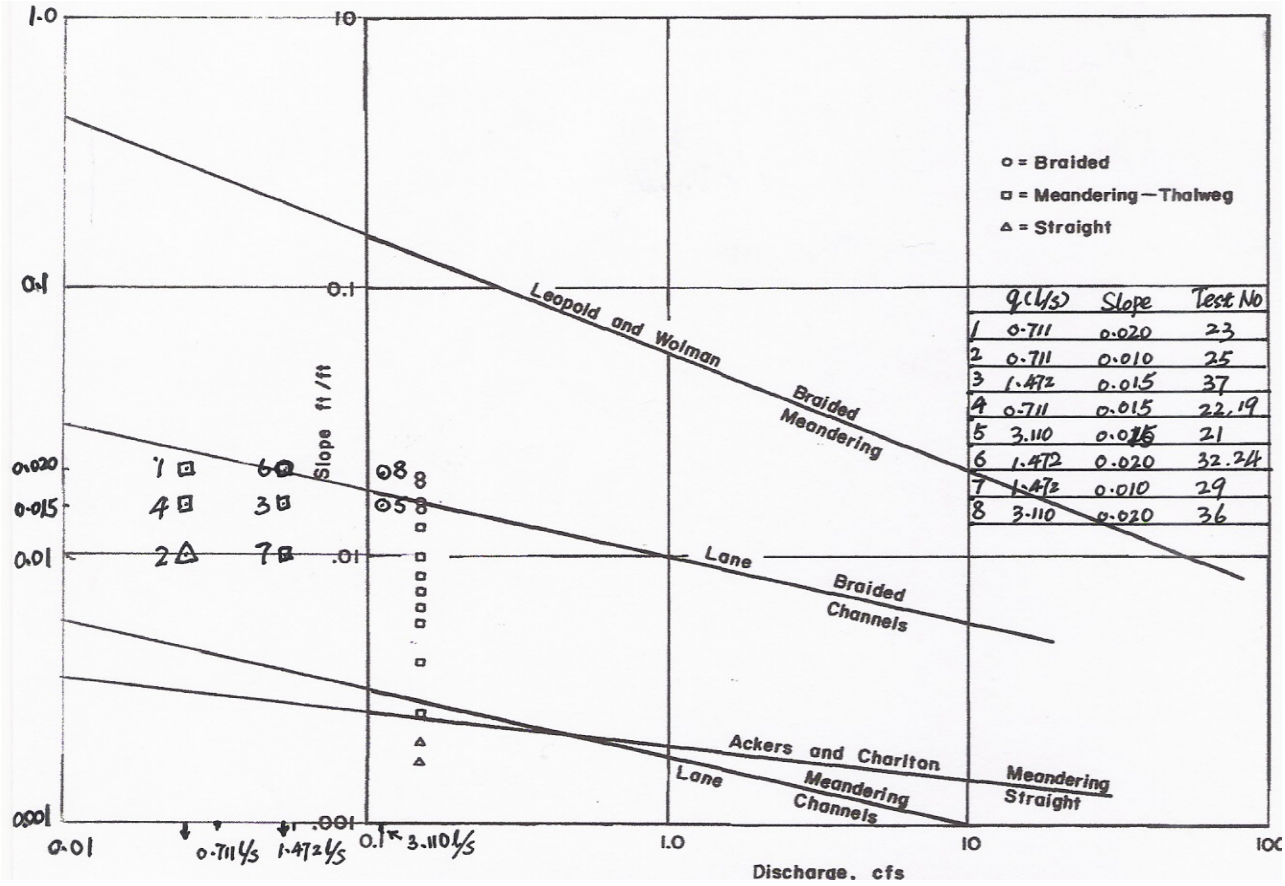

Figure 5.40: Relation between slope and discharge and threshold slopes at each discharge as defined by Lane (1957), Leopold and Wolman (1957), Ackers and Charlton (1971), and Schumm and Khan (1972).

Threshold values of slope at a given discharge have been recognized by other researchers (Schumm and Khan, 1972) and their relations are shown with study's data in Figure 5.40 (point 1 is Test 23, point 2 is Test 25, point 3 is Test 37 and point 4 is Test 22). Lane and Ackers and Charlton curves fit Schumm and Khan's data very well, Lane curve fits this study's meandering thalweg datas very well (points 1, 3, 4 and 7) but point 2 for straight channel. The author also had other points (points 5, 6 and 8) which have tendency to be braided. From Figure 5.40, these points (points 5, 6 and 8) are just at or above Lane's line, but from their channel morphology (see Figure 5.41 below), that were not the exact braided channels but have some characteristics of braided channels, such as multiple channels, separated bars and incision on the surface of large bar.

Figure 5.41: Channel development for Tests 21 (a), 24 (b), 32 (c) and 36 (d).

5.6 Summary

The experiments have been described in this chapter and have shown the important of channel size, sand characters, channel slope and flowing rate.

1. Slope is a key factor in distinguishing straight, meandering and braided channels. Braided channels must have steep slope and coarse sand. Larger slopes or larger flow rates would cause meandering. Steep channel slopes became flat quickly at beginning and then slowed.

2. The essential control factor is the Froude number. A channel with small width/ depth ratio, or a large slope, or a large flow rate which leads to meandering all have large Fr (more than 1). With this test, Fr became smaller and finally less than 0.70. In these meandering thalweg channels, a large Fr caused smaller sinuosity.

3. The cohesive clay plays a key role in stabilizing point bar and in forming real meandering river, not just a sinuous thalweg. Non- cohesive silica sand in this experiment meant that point bars did not lasting long.

4. Bed- load transportation is the main type of sand transportation. Some tests with large flow rates or steep channel slopes had meandering channels or straight channels with meandering thalweg, which were not their stable form, but half-way to braided form or multiple channels. These processes maybe short or long depending on flow rate and channel slope.

5. Sediment load plays an unimportant role in channel morphology and is not independent variable controlled by other factors like slope, discharge and channel size.

6. Sinuous meandering rivers can be modelled in the lab and the resulting model shows many similarities and differences with real rivers. Similarities include ripple-pool form and point bars. The difference is that the slope for the model river was much steeper than that of a real stream.

7. The stable channel size from regime theories correlates with the experiment results, but these theories should be chosen carefully especially considering their range of application.

5.7 Introduction with unsteady inflow

Channel development with steady inflow was introduced in this chapter and here, experiments for channel development with unsteady inflow were described. Unsteady inflow includes gradually varied inflow and rapidly varied inflow. Here, a series of physical experiments conducted with the objective to understand the influence of unsteady inflow using channels in the lab with non-cohesive sediment are reported. For comparison, sediment is material that was used for experiments with steady inflow in past research.

5.8 Experiments with unsteady inflow

Experiments are listed in Table 5.16. There are two types of unsteady inflow for channel experiments. One is increasing gradually, decreasing gradually (Tests D2 and D3, see Figure 5.42) and another one increases suddenly, and decreases suddenly (Test D5, see Figure 5.43, Test D10). Tests D1, D4 had steady inflow 0.6 l/s (see blue lines in Figures 5.42, 5.43). In this way, experiments with steady inflow could compare experiments with unsteady inflow. D1 compares with D2, D3 compares with D4 and D5 in the medium channel. D8, D9 compare with D10 in the large channel.

Table 5.16: Experiments with their test conditions.

Test No	Square (cm^2)	Slope	Q (l/s)	Time (min)
Medium channel			Average	
D1	88	0.020	Steady 0.6 l/s	30
D2	88	0.020	Unsteady 0.6 l/s	30

D3	88	0.020	Unsteady 0.6 l/s	60
D4	88	0.020	Steady 0.6 l/s	60
D5	88	0.020	Unsteady 0.6 l/s	60
D6	88	0.015	Steady 0.6 l/s	60
D7	88	0.025	Steady 0.6 l/s	60
Large channel				
D8	131.25	0.015	Steady 2 l/s	30
D9	131.25	0.015	Steady 2 l/s	60
D10	131.25	0.015	Unsteady 2 l/s	60

5.8.1 Tests with medium channel

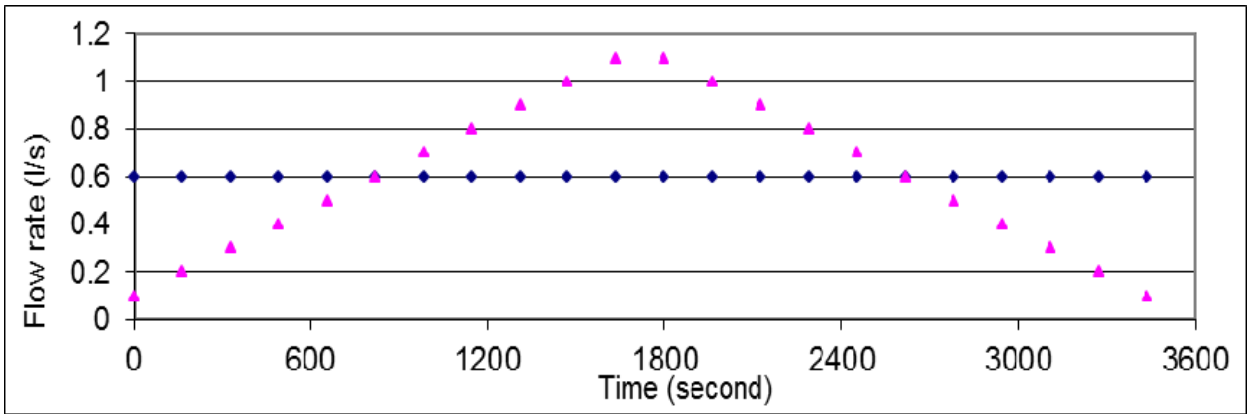

Figure 5.42: Gradual changing discharge (red line) for Tests D2 (30 min) and D3 (60 min).

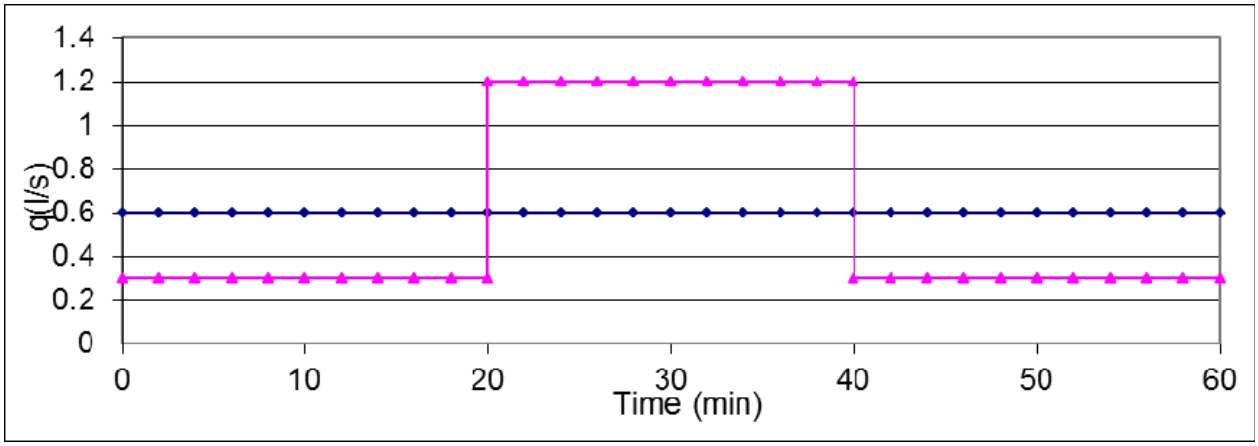

Figure 5.43: Rapidly varied changing discharge (red line) for Test D5 (60 min).

5.8.1.1 Reproducibility of tests with steady inflow and unsteady inflow

Comparison was made between two separate tests with the same flowing conditions. Figure 5.44 is with steady inflow and Figure 5.45 is with unsteady inflow. From the results, it is seen that channel bank lines almost cover each other in upstream and the difference in downstream is small at 15 min, 30 min, no matter whether it is in steady or unsteady inflow. Considering the difference caused by the channel made by hand, the reproducibility of the fluvial channel with steady inflow and unsteady inflow in the lab could be confirmed.

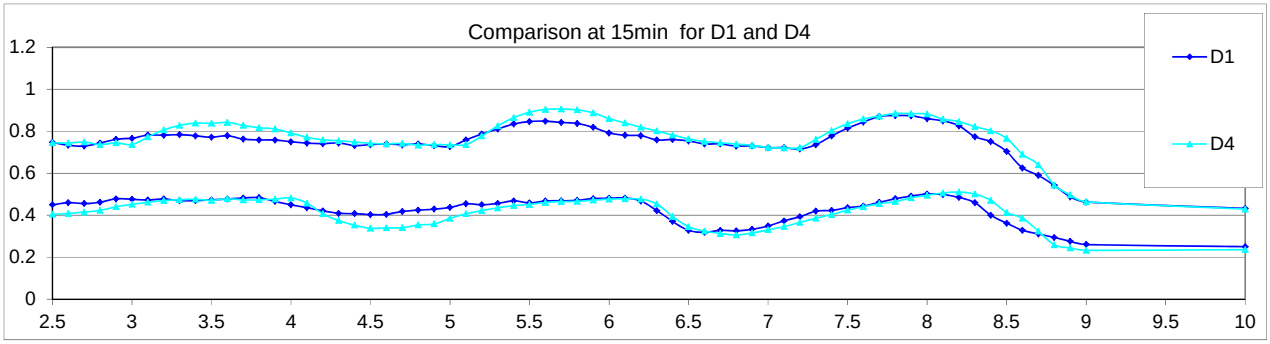

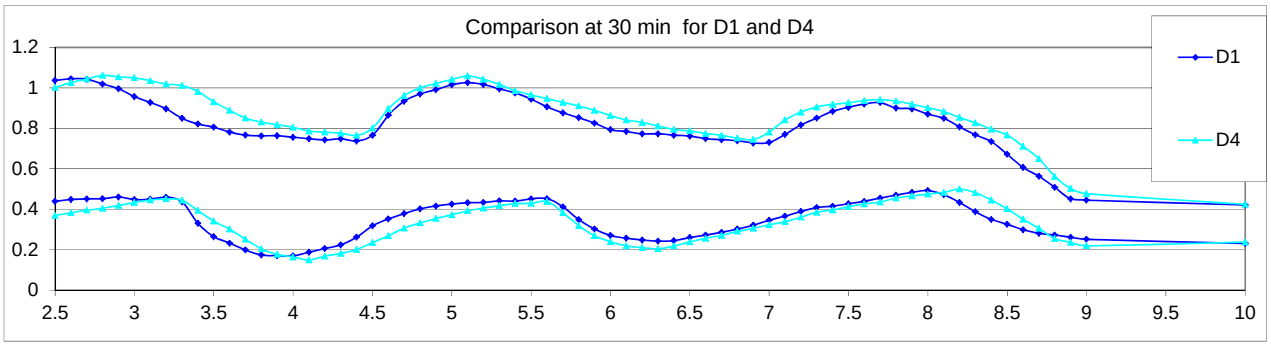

Figure 5.44: Tests D1 and D4 at 15 min and 30 min with the same steady inflow (m).

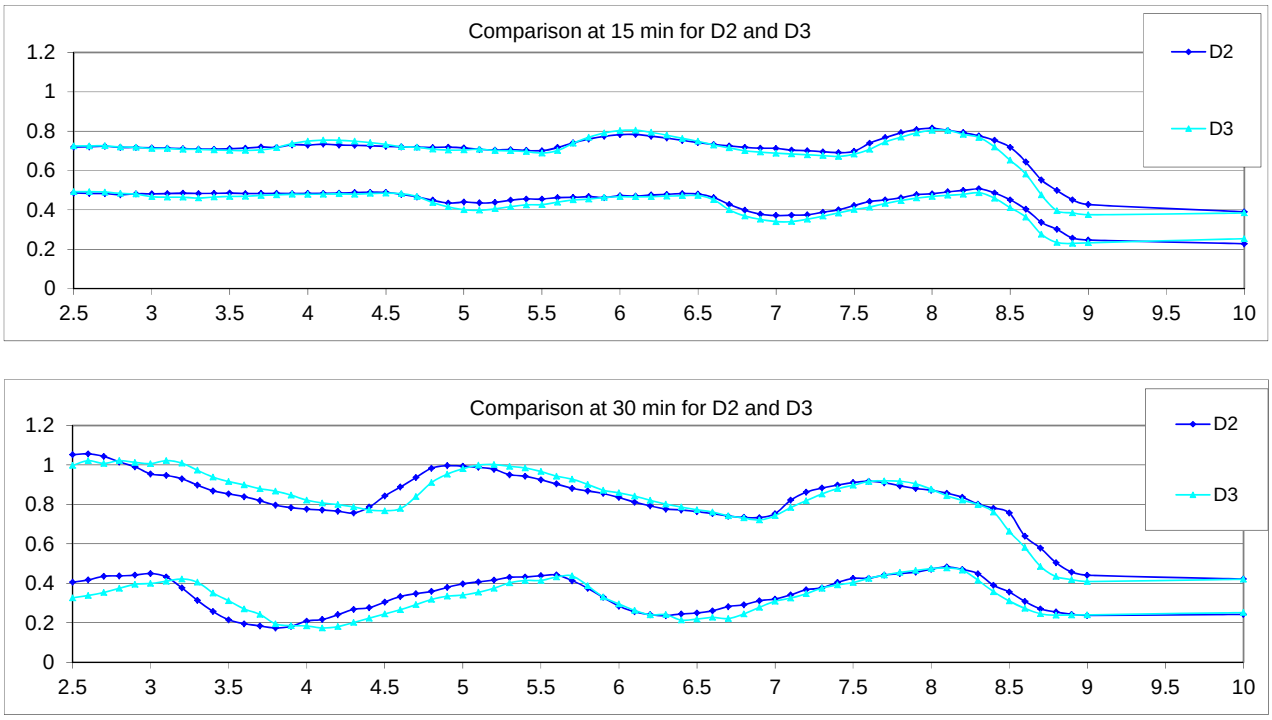

Figure 5.45: Tests D2 and D3 at 15 min and 30 min with the same unsteady inflow (m).

5.8.1.2 Medium channel for tests comparison with steady inflow and unsteady inflow

Channel development from 0 min to 30 min

Figure 5.46 is a comparison between steady inflow, gradually varied inflow and rapidly varied inflow at 15 min and 30 min. D4 is steady inflow, D3 is gradually varied inflow and D5 is rapidly varied inflow.

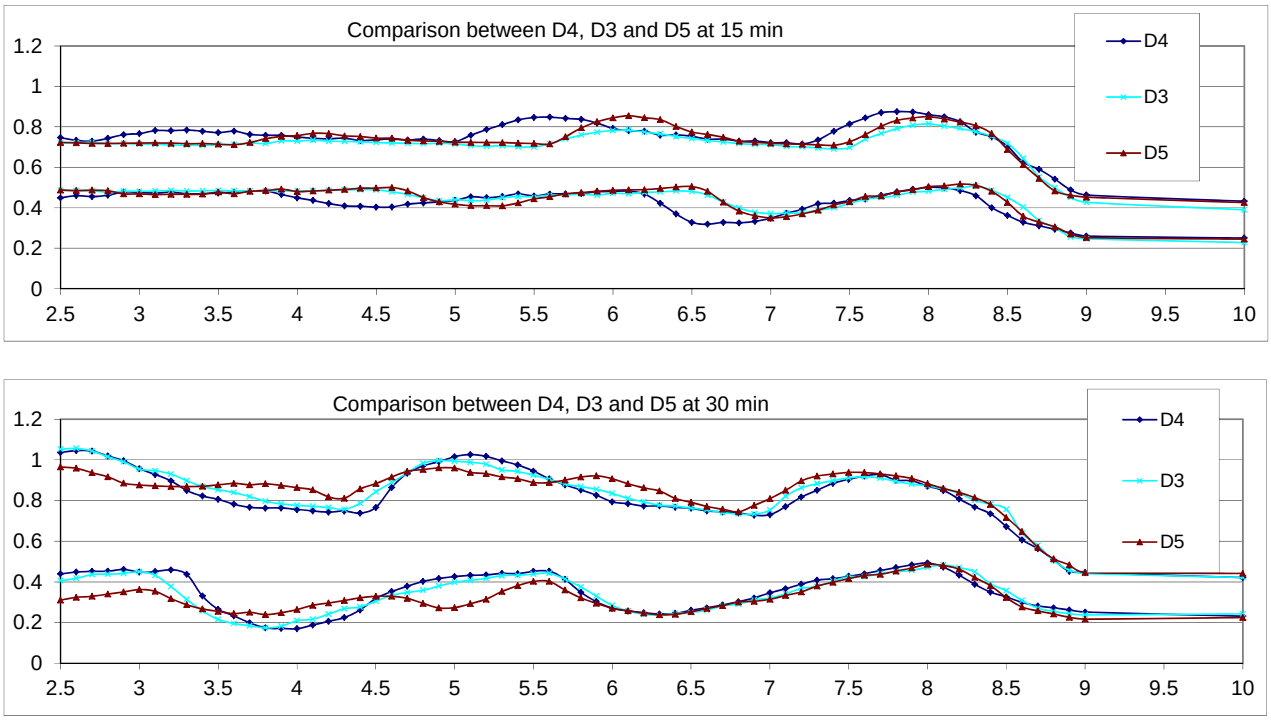

Figure 5.46: Tests D3, D4 and D5 with the same channel size, flume slope but different flow conditions (m).

From flow conditions in Figures 5.42 and 5.43, at 30 min and 60 min, tests with unsteady inflow and steady inflow both had the same total water quantity. Before 15 min, D4 not only had larger flow rate but also larger total water quantity, so D4 had more channel development at 15 min compared with D3 and D5. After 15 min, flow rate for D3 and D5 became larger than D4 and also erosion rates on the bank. At 30min when the total water quantity was the same, D3, D4, D5 right bank line and upstream left bank line was almost at the same place. D5 had little more bank erosion on both sides because of its sudden increase in flow rate. At 30 min, from Table 5.2.2, the average width for D5 was 53 cm which was the widest, while D3 was 50 cm and D4 was narrowest with only 48 cm.

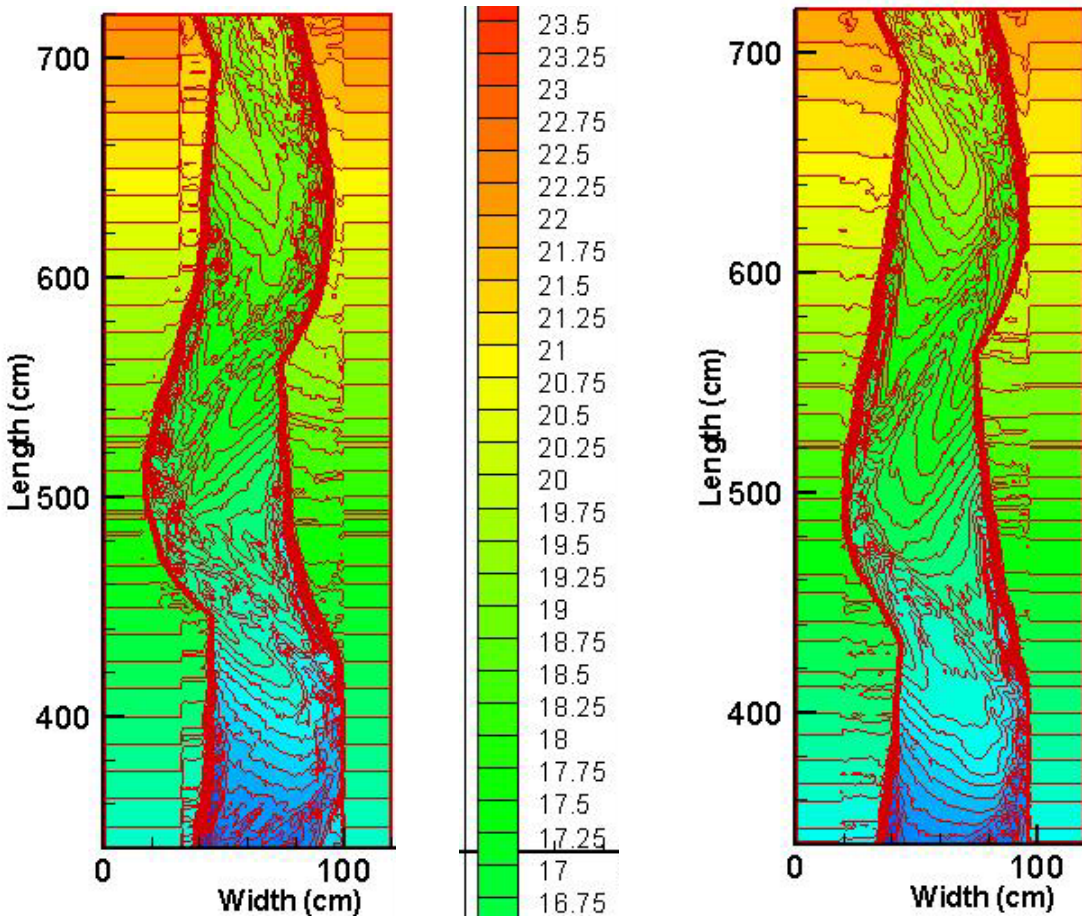

D1 with steady inflow at 30 min D2 with gradually varied inflow at 30 min

Figure 5.47: Bed profile for D1 with steady inflow and D2 with unsteady inflow at 30min (cm).

Figure 5.47 shows bed profiles for D1 and D2 at 30 min. Picture shows flume length from 7.20 m to 3.40 m. It is seen that deeps and shoals located almost at the same place for these two tests and also area for deeps and shoals is the same. The only difference is that the contour for D2 is smoother than D1 because D2 had gradual flow rate change.

Figure 5.48 shows the 3-D of bed profile for Test D1 from measurement and channel from camera picture from the same location. It can be seen that the measurement could describe the real situation accurately. So from measurement, tests can be used to compare with each other easily.

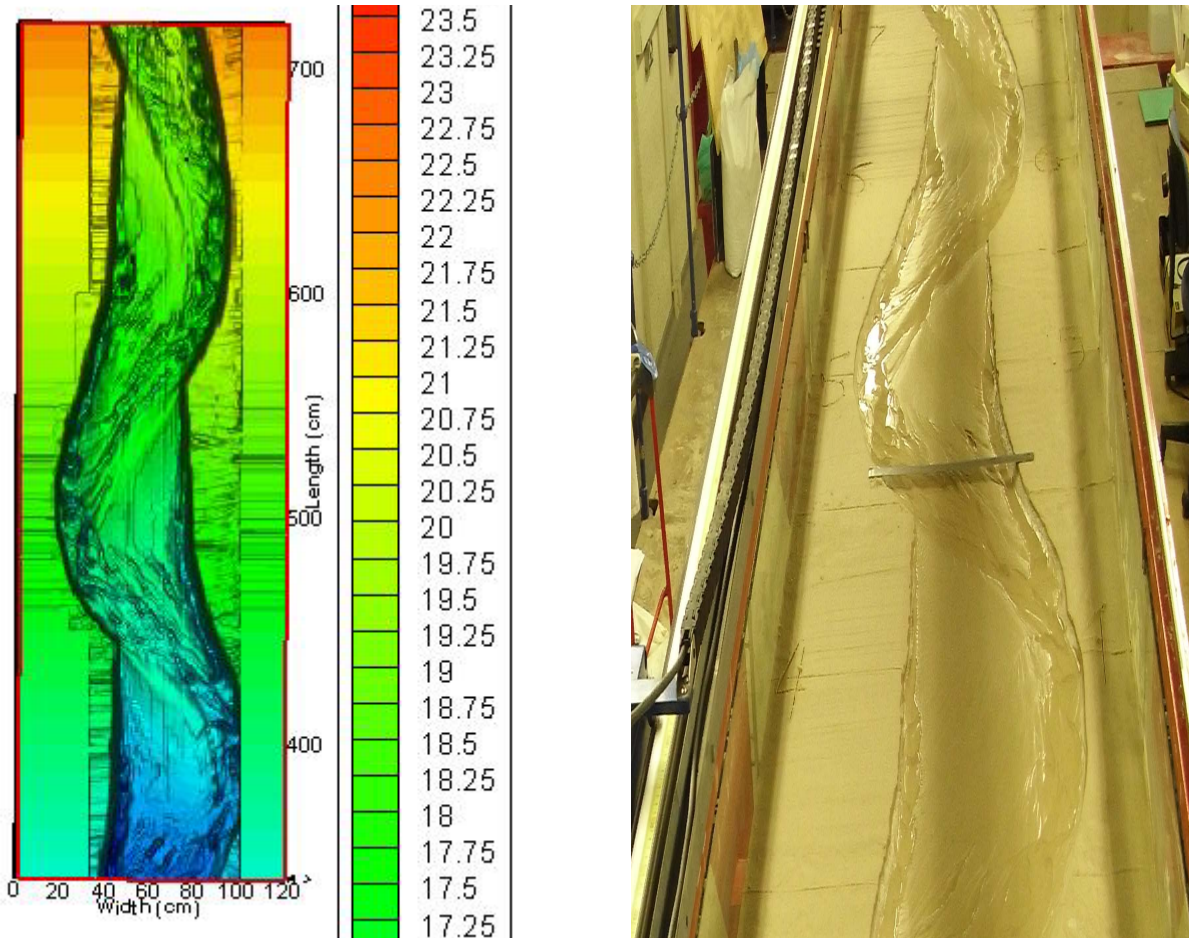

Figure 5.48: 3-D Bed profile and picture of D1 at 30 min after stopping water supply (cm).

Just like the bed profile in Figure 5.47, cross sections for these tests with different running conditions at 30 min also show similar development in Figure 5.49. Especially at 6.3 m, 5.6 m and 5 m, width and depth were covered very well. At downstream, D2's channel was wider but D1 had a deeper channel. This phenomenon also happened at upstream, but not as obvious as downstream. Section developments tell that steady inflow could erode the channel bed and has a deeper channel, unsteady inflow has more effect on bank erosion and makes channel wider.

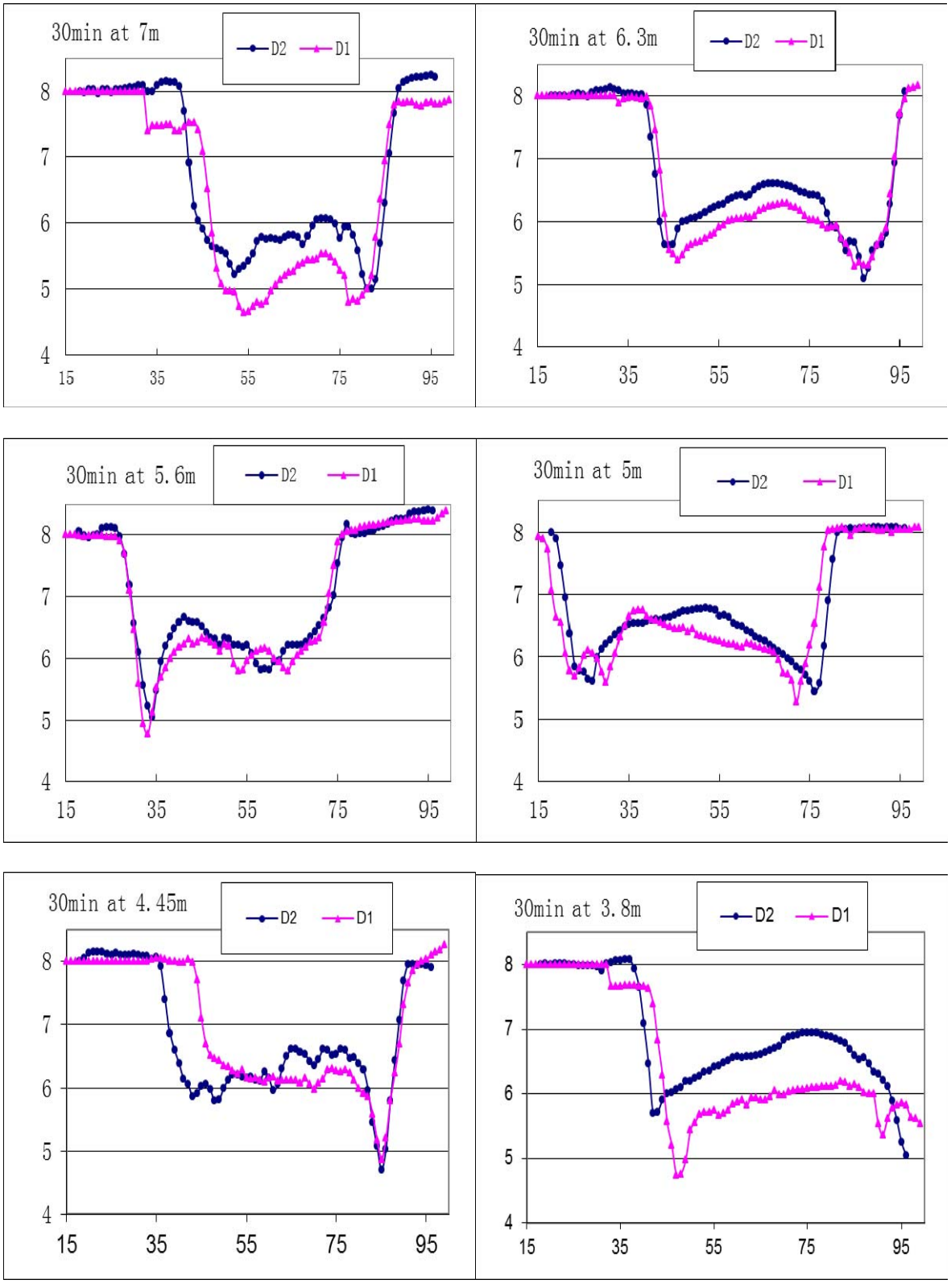

Figure 5.49: Cross sections for Tests D1 (D4) and D2 (D3) at 30 min (cm).

Channel development from 30 min to 60 min

The flow rate for D3, D4 and D5 was described in Figures 5.42 and 5.43. At 30 min, flow rate for D3 reached its peak and then decreased gradually, but in future 15 min observations, flow rate was still larger than steady inflow rate of 0.6 l/s. At 45 min, there was a turning point: flow rate began to be lower than 0.6 l/s. Also test D4 had a steady inflow 0.6 l/s. From 30 min, test D5 would keep 1.2 l/s 10 min, and then at 40 min, it suddenly changed to 0.3 l/s.

The difference of flow rate brings difference bank erosion rates and erosion positions. In Figure 5.50, it is clear to see that at 45 min and 60 min, bank positions were totally different to that at 15 min and 30 min. Test D4 with steady inflow at 45 min was the slowest channel development. D5 had more area in Figure 5.43 which was higher than 0.6 l/s than D3, so D5 got the erosion, D3 was the second and D4 was least in upstream.

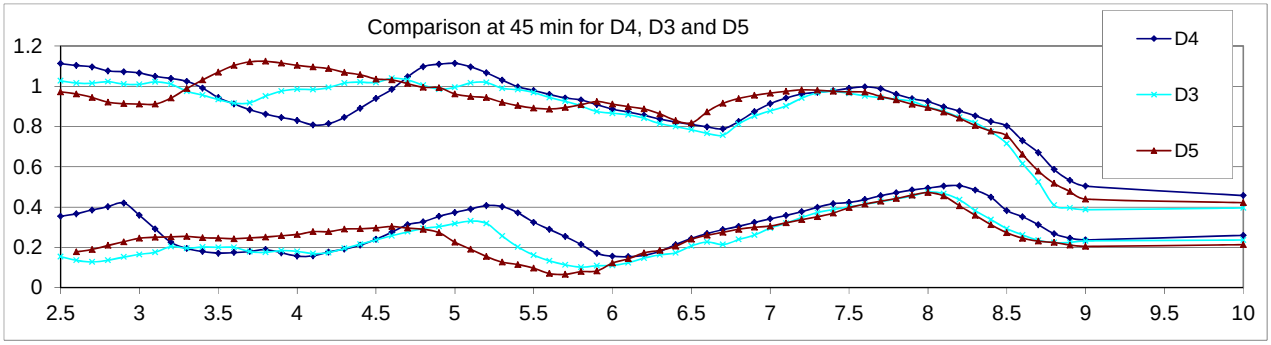

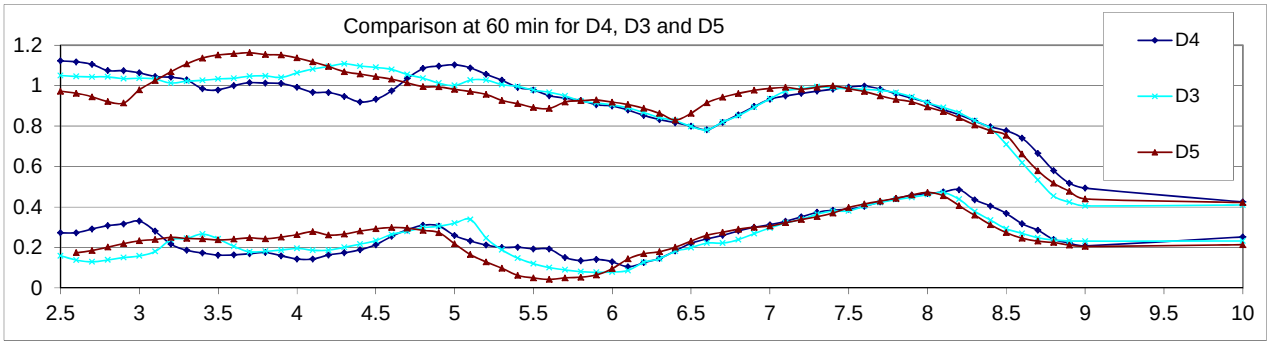

Figure 5.50: Tests D3, D4 and D5 with the same channel size, flume slope but different flow conditions at 45 min and at 60 min.

From 45 min to 60 min, D3 and D4 changed their positions but not D5 in upstream. After 45 min, D5 had the smallest flow rate and slowest erosion rate, its banks almost kept their positions. With more area that could erode bank, D5 got the largest bank erosion at 60 min. After 45 min D4 still had a flow rate that could cause erosion, this made the difference between D3 and D4 smaller. At 60 min, D5 was the widest as 66 cm, D3's channel width increased a lot and reached 65 cm which was almost the same as D5, D4 had the smallest channel again. Unsteady inflow brings a wider channel than steady inflow.

From channel development, it was seen that it was seriously affected by flow rate. When flow rate is too small, bank erosion would not happen, like D3 after 45 min. When flow rate is large enough and creares bank erosion, the channel would develop fast, like Test D4. And if the flow rate is larger and lasts for a while, then channel changes its origin morphology quickly, like D5 in the middle 20 min. The flow process in D3 is like a flooding in nature, and only effective flow causes bank erosion.

Bed profiles for the above tests are shown in Figure 5.51. D5 has a large difference with D3 and D4, where the channel almost became straight after 5.6 m and the right bank reached flume boundary at downstream. It had the widest upstream channel. Distinguishing between upstream point bar and downstream point bar is not clear in D5, not like in D3 and D4. D3 and D4 had similarities in beginning and end of the channel, but not in the middle. D3 had a narrow ripple

length at about 5 m and D4 was longer, because D4 was a steady inflow and its ripple length was stable. Correspondingly, the ripple in D3 was destroyed and rebuilt easily in the main channel. So contours in main channel had a big difference for D3 and D4, and point bar had a similarity. From Figure 5.51, D4 had largest sinuosity, most smooth point bars.

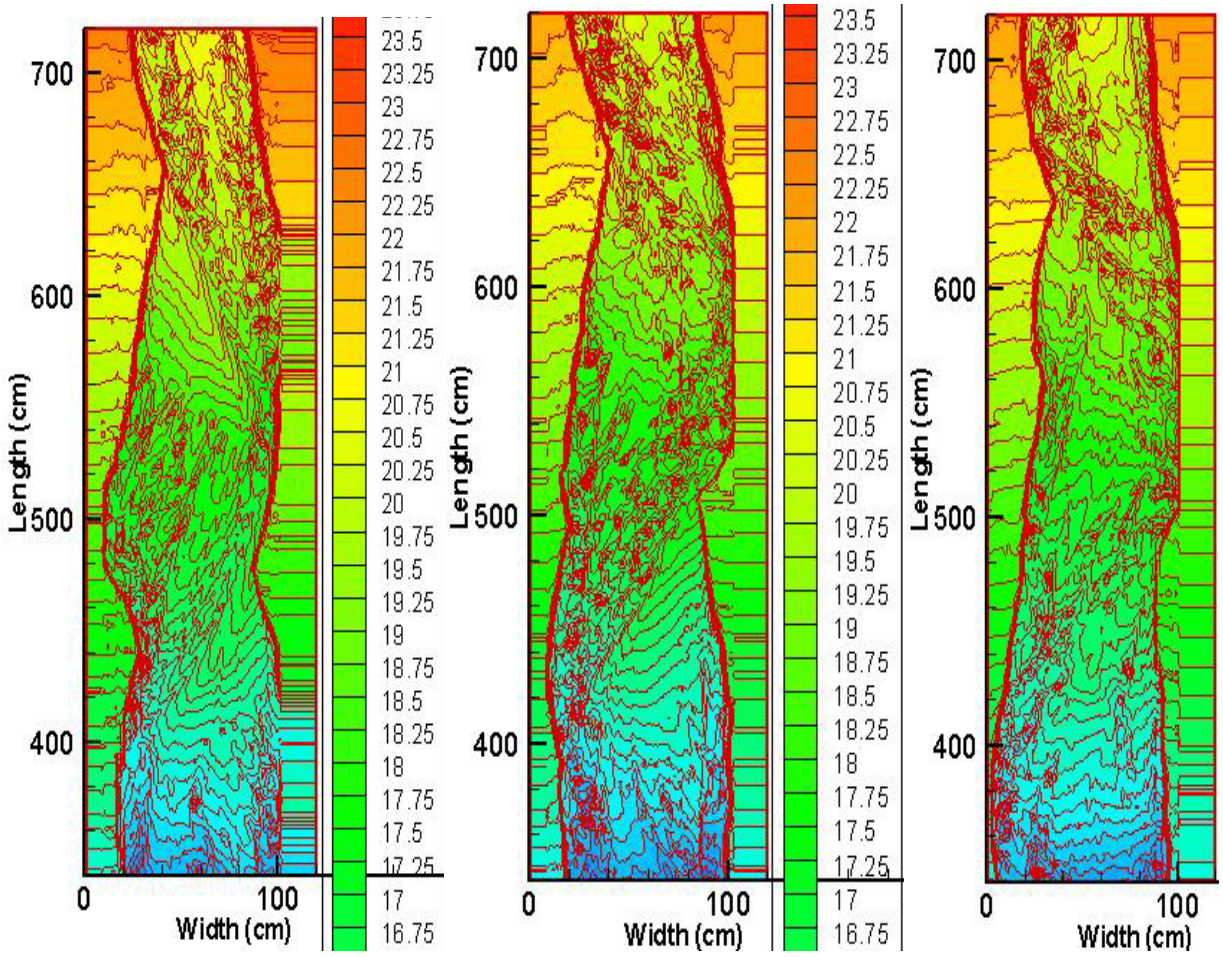

D4: Steady inflow D3: Gradually varied inflow D5: Rapidly varied inflow

Figure 5.51: Channel after stopping water supply and their bed profiles in Tests D4, D3 and D5.

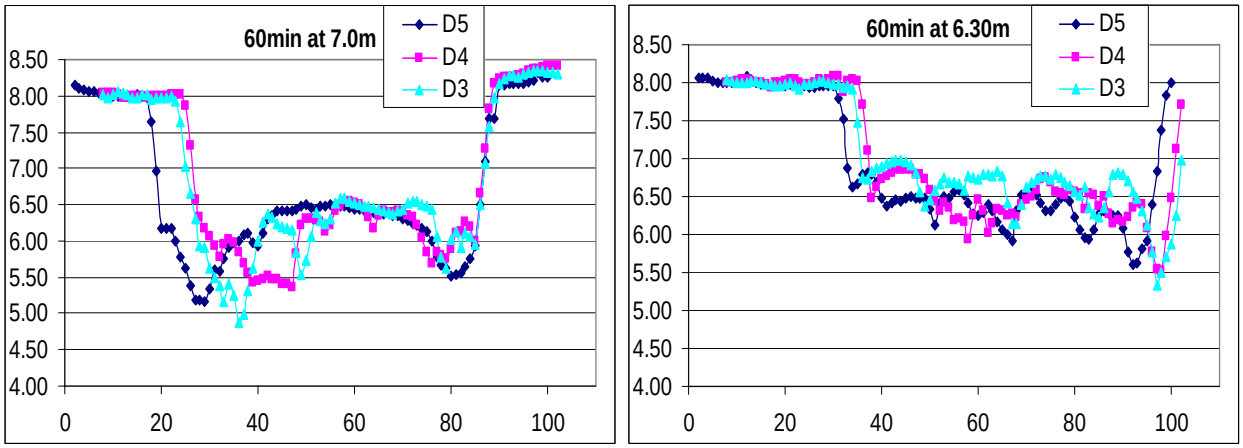

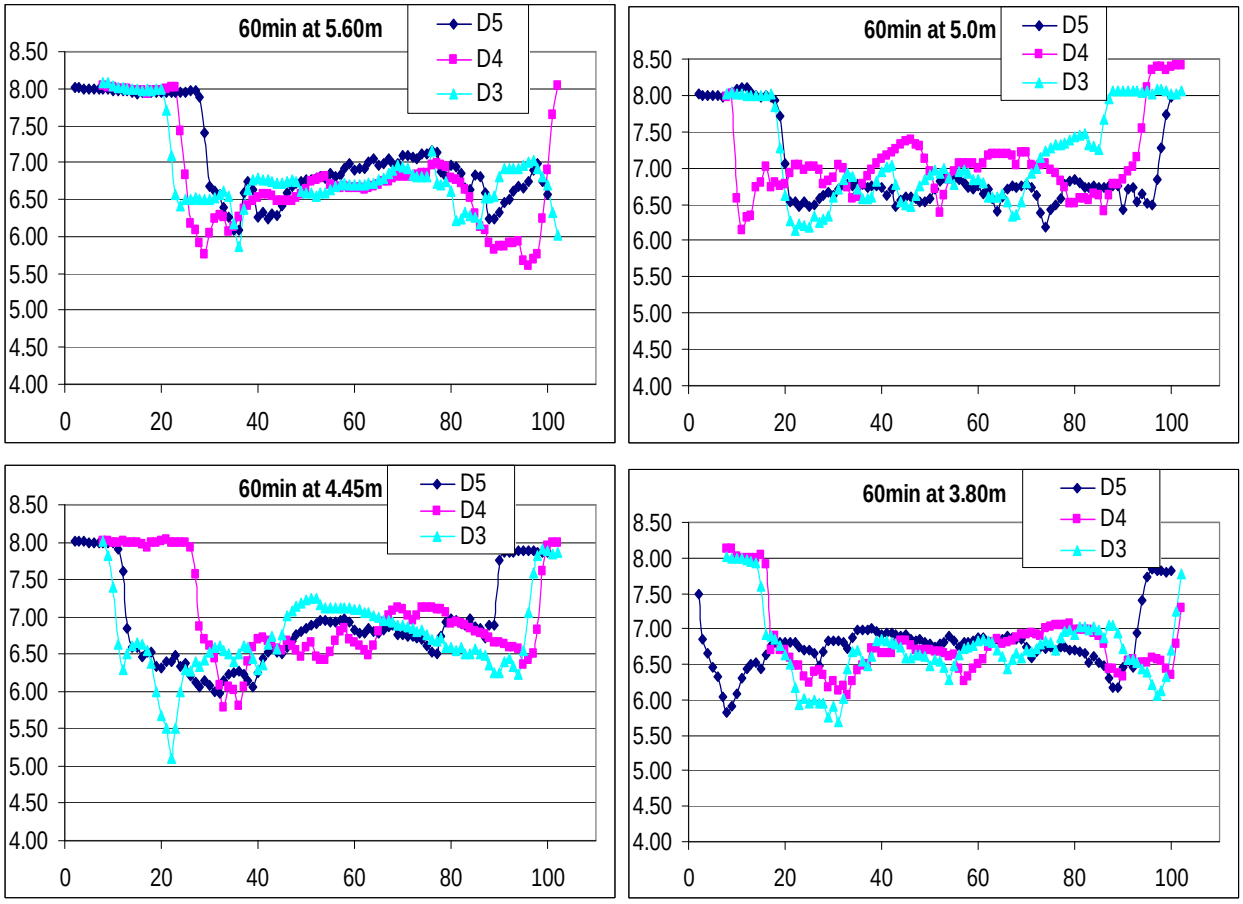

Figure 5.52: Bed profile and cross sections for Tests D4, D3 and D5 (cm).

Also from cross sections in Figure 5.52, D3 with a gradually varied inflow had the deepest main channel. It is not easy to find any regulations on average widths or average depths, because they always changed their positions.

It is concluded from bed profiles, steady inflow produces stable ripples and curved channel banks. Rapidly varied unsteady inflow got straight channel, wider upstream. Gradually varied inflow got unstable ripples in the main channel and deeper main channel. Unsteady inflow brings wider channels than steady inflow.

5.8.2 Tests with large channel

Tests with large channel were also carried out and their flow conditions are described in Figure 5.53. Bed profiles for D9 with steady inflow 2 l/s at 30 min and at 60 min are shown in Figure 5.54.

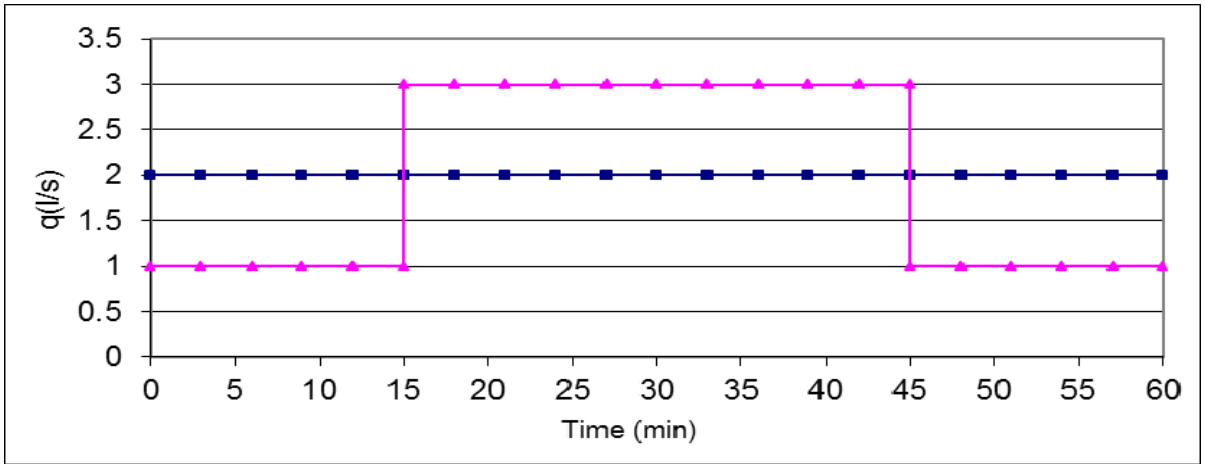

Figure 5.53: Unsteady discharge (red line) for Tests D10 (60 min) and steady inflow (blue line) for D8 (30 min), D9 (60 min).

The relationship for channel at 30 min and 60 min is clear in Figure 5.54. D9 at 30 min was a well-developed channel with meandering thalweg and then at 60min, meander wavelength and amplitude became larger and wider but sinuosity for meandering thalweg became small.

Figure 5.55 shows differences of channel development for Tests D9 and D10. Again it proved that unsteady inflow makes channel wider just like in Figure 5.50. D10 was wider by nearly 1/3 than D9 at 6.5 m and 4.5 m. On average, D10's channel width from bending was larger 11 cm than D9 in Table 5.17.

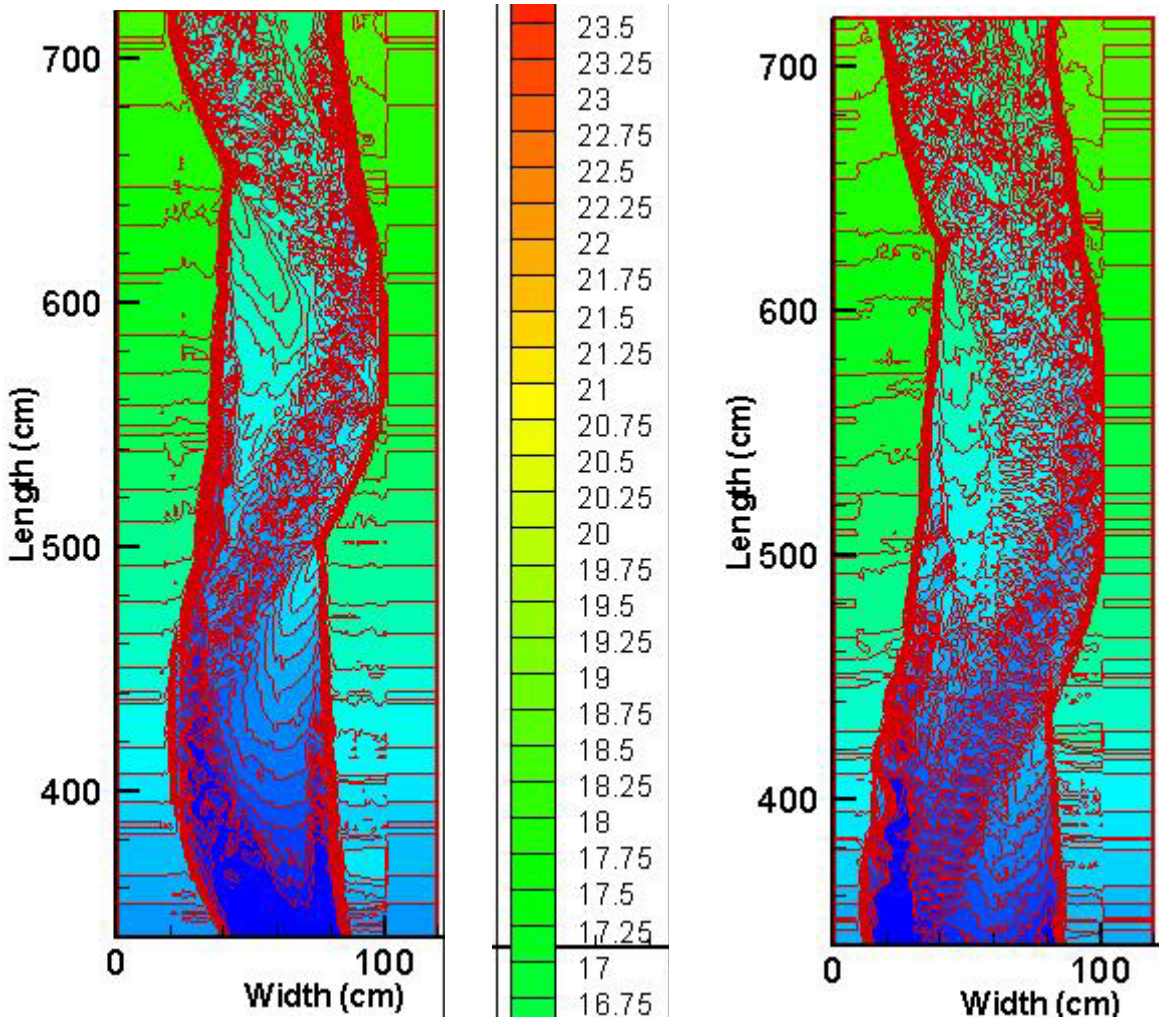

D8 (D9): Steady inflow- 2 l/s- 30 min D9: Steady inflow- 2 l/s- 60 min

Figure 5.54: Channel development for steady inflow 2 l/s in 30 min and in 60 min.

Table 5.17: Channel width comparison between D4 (steady inflow), D3 (gradually varied inflow) and D5 (rapidly varied inflow), D9 (steady inflow) and D10 (rapidly varied inflow).

	D4	D3	D5	D9	D10
Average from bending at 30 min	0.48 m	0.50 m	0.53 m	-	-
Average from bending at 60 min	0.61 m	0.65 m	0.66 m	0.62 m	0.73 m
Increase	0.13 m	0.15 m	0.13 m	-	-
Largest width at 30 min	0.53 m	0.64 m	0.69 m	-	-

Largest width at 60 min	0.83 m	0.89 m	0.87 m	0.76 m	0.96 m

Table 5.17 shows that unsteady inflow made channels wider. In medium channels, D5 and D3, got larger channel width than D4, especially D5 with rapidly varied unsteady inflow having the largest width. It was larger 10% than D4 at 30 min and larger 8% than D4 at 60 min. D3's average width increased more in 30 min than D4 and D5. In the large channel, unsteady inflow again made a wider channel. Difference of largest width is larger a lot than that of average width between D9 and D10. Correspondingly in the medium channel, this difference is almost the same.

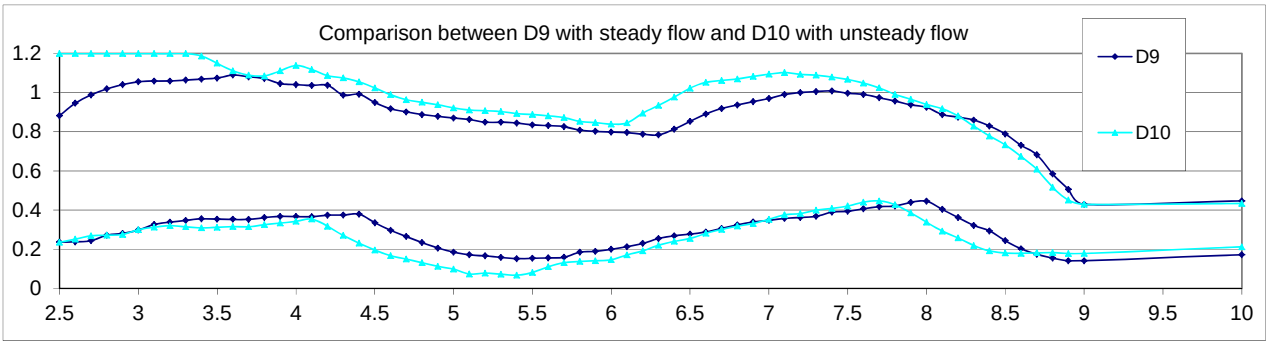

Figure 5.55: Compare channel development for D9 with steady inflow and D10 with unsteady inflow at 60 min.

5.8.3 Sinuosity

Table 5.18: Sinuosities for banks and meandering thalwegs.

Sinuosity		15 min		30 min		45 min	60 min
		up	down	up	down		
D1	Bank line	1.19	1.02	1.23	1.16	-	-
	meandering	1.62	1.15	1.68	1.64	-	-

D2	Bank line	1.13	1.01	1.20	1.14	-	-
	meandering	1.50	1.14	1.79	1.57	-	-
D3	Bank line	1.17	1.04	1.28	1.13	1.17	1.26
	meandering	1.60	1.23	1.60	1.31	1.51	-
D4	Bank line	1.23	1.09	1.29	1.20	1.29	1.22
	meandering	1.75	1.40	1.92	1.40	-	1.43
D5	Bank line	1.29	-	1.17	-	1.13	1.16
	meandering	1.88	-	-	-	-	-
D6	Bank line	1.05	-	1.08	-	1.03	1.03
	meandering	-	-	-	-	-	-
D7	Bank line	1.26	1.19	1.30	-	1.24	1.25
	meandering	1.84	1.70	1.96	-	-	-
D8	Bank line	1.13	1.02	1.18	-	-	-
	meandering	1.46	1.06	1.46	-	-	-
D9	Bank line	1.05	-	1.05	-	1.07	1.08
	meandering	-	-	-	-	-	-
D10	Bank line	1.14	-	1.16	-	1.14	1.15
	meandering	-	-	1.43	-	1.40	-

Sinuosities (S) of banks and meandering thalwegs from different tests are shown in Table 5.18.

From these data, it is seen that:

For the same medium channel with different flow conditions:

At 30 min, S_{steady} (D4)> $S_{gradual\ unsteady}$ (D3)> $S_{rapidly\ varied\ unsteady}$ (D5)

At 60 min, $S_{gradual\ unsteady}$ (D3)> S_{steady} (D4)> $S_{rapidly\ varied\ unsteady}$ (D5)

For the same large channel with different flow conditions:

At 30 min, $S_{rapidly\ varied\ unsteady}$ (D10) >S_{steady} (D9)

At 60 min, $S_{rapidly\ varied\ unsteady}$ (D10) > S_{steady} (D9)

For medium channel with different slope:

At 30 min, S (D7 with slope 0.025)> S (D4 with slope 0.020)> S (D6 with slope 0.015)

At 60 min, S (D7 with slope 0.025)> S (D4 with slope 0.020)> S (D6 with slope 0.015)

From above results, the relationship of sinuosity at 30 min and 60 min did not change their position for channels with different slope and large channels with different flow conditions. D10 with unsteady inflow had larger S (sinuosity) than D9 with steady inflow, and channel with a larger slope got larger S, D7 had largest S and D6 had the smallest.

For medium channel with different flow conditions, D3 and D4 changed their places at 30 min and 60 min, D5 with rapidly varied inflow was always the last. It is different in large channels, D10 with rapidly varied inflow was larger than D9 with steady inflow.

5.8.4 Experiment with theory calculation

From earlier discussion in Chapter 5.5.2: if meandering thalweg is a channel, Lacey's equation is reasonable, Charlton et al. (1978) equation also gives a good result. Dury's results are not good, however. Blench's equation agrees well with experiment results on width, but not on channel slope and depth. Here in Table 5.19, calculations correspond well with the discussion in Chapter 5.5.2 for steady inflow. Table 5.19 also gives relationship of experiment results for unsteady inflow with calculation results for gradually varied inflow and rapidly varied inflow.

Table 5.19: Comparison calculation results with experiment results (where Br is channel width and Bm is thalweg width, y_0 is depth, λ is meandering wave length, S is channel slope, V is flowing velocity).

	Q=0.6 l/S=0.0006 m^3/s	Q=2 l/S=0.002 m^3/s
Experiment results / Calculations	D4: B=0.14 m, λ=2.3 m,s=0.0101 (steady)	D9: B=0.20 m, λ=3.0 m, s=0.0101 (steady)
	D3: B=0.16 m, λ=2.5 m, s=0.0115 (gradual unsteady)	
	D5: B=0.12 m, λ=2.7 m (rapid unsteady)	D10: B=0.23 m, λ=3.1 m, V=0.458 m/s, y_0=0.025—0.03 m (rapidly varied unsteady)
	D6: B=0.30 m, V=0.35 m/s (slope=0.015)	
	D7: B=0.12 m, λ=3.2 m, V=0.30 m/s (slope=0.025)	
Charlton et al. (1978) gravel bed rivers: $B=3.74Q^{0.45}$, $y_0=0.31Q^{0.40}$, $V=0.86Q^{0.15}$	B=0.133, y_0=0.016, V=0.283 For steady: $B=(0.90--1.05)\times B_C$, $V=1.06\times V_C$ For gradual unsteady: $B=1.20\times B_C$ For rapidly varied unsteady: $B=0.90\times B_C$	B=0.228, y_0=0.026, V=0.338 For steady: $B=0.88\times B_C$ For rapidly varied unsteady: $B=1.01\times B_C$ $V=1.36\times V_C$ $y_0=(0.96--1.15)\times y_{0C}$

In Charlton's equation (B_C is calculated width):

For medium channel: $(B_{gradual-unsteady}=1.20\times B_C)>(B_{steady}=0.97\times B_C)>(B_{sudden-unsteady}=0.90\times B_C)$

$(V_{steady}=1.06\times V_C)$

For large channel: $(B_{sudden-unsteady}=1.01\times B_C)>(B_{steady}=0.88\times B_C)$

$$V_{sudden-unsteady} = 1.36 \times V_C \,,\quad y_{0sudden-unsteady} = 1.05 \times y_{0C}$$

Charlton's equation can be edited as:

With middle channel: $B_{steady} = 3.74Q^{0.45}$, $B_{gradual-unsteady} = 4.49Q^{0.45}$, $B_{sudden-unsteady} = 3.37Q^{0.45}$

$$V_{steady} = 0.86Q^{0.15}$$

With large channel: $B_{steady} = 3.29Q^{0.45}$, $B_{sudden-unsteady} = 3.78Q^{0.45}$

$$V_{sudden-unsteady} = 1.17Q^{0.15}\text{,}\quad y_{0sudden-unsteady} = 0.32Q^{0.40}$$

Charlton's equations give a good result for steady inflow on width and velocity. Correspondingly equations for unsteady inflow can be rectified as in Table 5.20.

Table 5.20: Rectified Charlton's equation for gradually varied inflow and rapidly varied inflow.

Charlton's equation for different flow conditions		
Steady flow	Gradually varied inflow	Rapidly varied inflow
$B = B_C$, $V = V_C$, $y_0 = y_{0C}$	$B = 1.20 \times B_C$, $V = 1.20 \times V_C$, $y_0 = 1.20 \times y_{0C}$	$B = 0.90 \times B_C$, $V = 0.90 \times V_C$, $y_0 = 0.90 \times y_{0C}$
$B_{steady} = 3.74Q^{0.45}$ $V_{steady} = 0.86Q^{0.15}$ $y_{0steady} = 0.31Q^{0.40}$	$B_{gradual-unsteady} = 4.49Q^{0.45}$ $V_{gradual-unsteady} = 1.03Q^{0.15}$ $y_{0gradual-unsteady} = 0.37Q^{0.40}$	$B_{sudden-unsteady} = 3.37Q^{0.45}$ $V_{sudden-unsteady} = 0.77Q^{0.15}$ $y_{0sudden-unsteady} = 0.28Q^{0.40}$

Charlton's equations work well for medium channels. But for large channels, equations should be edited with different ratios. Other equations need more data to be rectified for steady inflow and unsteady inflow.

5.9 Conclusion

1. It is seen that depth and shallow located almost at the same place for Tests D1 and D2 and also area for depth and shallow is the same. The only difference is that the contour for D2 is smoother than D1 because D2 had gradual flow rate change.

2. Sections development tells that steady inflow could deepen channels and unsteady inflow has more effect on bank erosion and makes channels wider.

3. It is concluded from bed profiles that steady inflow produces stable ripples, smooth point bars and curved channel banks. Rapidly varied unsteady inflow got a straight channel which was wider upstream. Gradually varied unsteady inflow got unstable ripple in the main channel and the deepest pools.

4. Charlton's equations work well for steady inflow and to make them work well for gradually varied inflow and rapidly varied inflow, Charlton's equations should have a ratio of 1.2 for gradually varied unsteady inflow and 0.9 for rapidly varied unsteady inflow as shown in Table 5.20. It must be emphasized that ratios here were only used in the current study, for other research or real rivers, more investigations are needed.

Chapter 6

Governing equations

6.1 Introduction

In recent years, numerical models have been widely used to predict the hydrodynamic, solute and suspended sediment transport processes in riverine, estuarine, coastal and ground waters. Numerical modelling is increasingly accepted by its time saving and accuracy. In the field of river morphology, computational fluid dynamics (CFD) models have been used to predict the formation, development, and migration of free- forming meander bends.

It is necessary to understand the physical processes that control the movement of solute and mass in the water column before a numerical model is developed to predict the sediment transport processes. Also, in order to predict sediment transport processes, it is necessary to predict the hydrodynamic processes.

This chapter describes the governing equations used to represent the hydrodynamic, solute and sediment transport processes. The equations are based on the conservation of mass and momentum. In the real world, the hydrodynamic, solute and sediment transport processes is three dimensional. The 3-D mass balance equation will be introduced first and then the depth integrated 2-D mass equation. Then the momentum equation will be described. The discretisation will be introduced in Chapter 7.

6.2 Hydrodynamic equations

The 3-D and 2-D governing equations describing the hydrodynamic process of fluid flow are the basis of numerical models used to predict the hydrodynamic, water quality and sediment transport

processes in coastal, estuarine and river waters.

Fluid flow can be described by the conservation laws of mass and momentum within the body of fluid. The mass conservation equation, or the conservation equation of fluid mass, can also be called the continuity equation. The mass conservation requires that the net fluid entering or leaving a control volume in a time interval Δt equals the amount of mass of change within the control volume during Δt. The momentum conservation requires that the sum of the external forces acting on a unit mass equals the rate of change of linear momentum by Newton's second law of motion.

6.2.1 Three dimensional equations

The Navier- Stokes equations for incompressible flows are given below:

$$\frac{\partial u}{\partial t}+u\frac{\partial u}{\partial x}+v\frac{\partial u}{\partial y}+w\frac{\partial u}{\partial z}=X-\frac{1}{\rho}\frac{\partial P}{\partial x}+\nu(\frac{\partial^2 u}{\partial x^2}+\frac{\partial^2 u}{\partial y^2}+\frac{\partial^2 u}{\partial z^2}) \qquad 6.1$$

$$\frac{\partial v}{\partial t}+u\frac{\partial v}{\partial x}+v\frac{\partial v}{\partial y}+w\frac{\partial v}{\partial z}=Y-\frac{1}{\rho}\frac{\partial P}{\partial y}+\nu(\frac{\partial^2 v}{\partial x^2}+\frac{\partial^2 v}{\partial y^2}+\frac{\partial^2 v}{\partial z^2}) \qquad 6.2$$

$$\frac{\partial w}{\partial t}+u\frac{\partial w}{\partial x}+v\frac{\partial w}{\partial y}+w\frac{\partial w}{\partial z}=Z-\frac{1}{\rho}\frac{\partial P}{\partial z}+\nu(\frac{\partial^2 w}{\partial x^2}+\frac{\partial^2 w}{\partial y^2}+\frac{\partial^2 w}{\partial z^2}) \qquad 6.3$$

$$\frac{\partial u}{\partial x}+\frac{\partial v}{\partial y}+\frac{\partial w}{\partial z}=0 \qquad 6.4$$

where ν is the kinematic viscosity of the fluid, *u, v, w* are the instantaneous velocities in the x, y, z directions respectively, ρ is the fluid density, *P* is the instantaneous pressure, g is the gravitational acceleration, *X, Y, Z* are the body forces per unit mass in *x, y, z* directions respectively. Equations 6.1- 6.3 are the momentum conservation equations in the x, y and z

directions respectively. Equation 6.4 is the three-dimensional continuity equation for all kinds of incompressible flows.

6.2.2 Two-dimensional depth integrated equations

6.2.2.1 Two-dimensional depth integrated mass conservation

When the water depth is shallow and the flow velocity shows little variation in the vertical direction, it is appropriate to integrate these equations over the depth of water to obtain two-dimensional equations.

As shown in Figure 6.1, then depth integrated of continuity equation 6.4 gives:-

$$\int_{-h}^{\eta}(\frac{\partial u}{\partial x}+\frac{\partial v}{\partial y}+\frac{\partial w}{\partial z})\partial z=\int_{-h}^{\eta}(\frac{\partial u}{\partial x}+\frac{\partial v}{\partial y})\partial z+w_{\eta}-w_{-h}=0 \qquad 6.5$$

Using Leibnitz Rule:

$$\int_{a}^{b}\frac{\partial f(x,y)dx}{\partial y}=\frac{\partial}{\partial y}\int_{a}^{b}f(x,y)dx-f(b,y)\frac{\partial b}{\partial y}+f(a,y)\frac{\partial a}{\partial y} \qquad 6.6$$

gives for equation 6.6:

$$\frac{\partial}{\partial x}\int_{-h}^{\eta}udz-u_{\eta}\frac{\partial \eta}{\partial x}\Big|_{\eta}+u_{-h}\frac{\partial(-h)}{\partial x}\Big|_{-h}+\frac{\partial}{\partial y}\int_{-h}^{\eta}vdz-v_{\eta}\frac{\partial \eta}{\partial y}\Big|_{\eta}+v_{-h}\frac{\partial(-h)}{\partial y}\Big|_{-h}+w_{\eta}-w_{-h}=0 \qquad 6.7$$

At the bed: $u_{-h}=v_{-h}=w_{-h}=0$ 6.8

Then $\frac{\partial}{\partial x}\int_{-h}^{\eta}udz-u_{\eta}\frac{\partial \eta}{\partial x}\Big|_{\eta}+\frac{\partial}{\partial y}\int_{-h}^{\eta}vdz-v_{\eta}\frac{\partial \eta}{\partial y}\Big|_{\eta}+w_{\eta}=0$ 6.9

At the surface the kinematic free surface condition (namely a particle on the surface will remain on the surface) gives:

$$\frac{d\eta}{dt}\Big|_{\eta}=\left[\frac{\partial \eta}{\partial t}+\frac{\partial \eta}{\partial x}\frac{dx}{dt}+\frac{\partial \eta}{\partial y}\frac{dy}{dt}\right]_{\eta}=\left[\frac{\partial \eta}{\partial t}+u\frac{\partial \eta}{\partial x}+v\frac{\partial \eta}{\partial y}\right]_{\eta}=w_{\eta} \qquad 6.10$$

Substituting in Equation 6.9 gives:

$$\frac{\partial \eta}{\partial t}+\frac{\partial UH}{\partial x}+\frac{\partial VH}{\partial y}=0 \qquad 6.11a$$

Or $$\frac{\partial \eta}{\partial t}+\frac{\partial p}{\partial x}+\frac{\partial q}{\partial y}=0 \qquad 6.11b$$

where: $U=\frac{1}{H}\int_{-h}^{\eta} u dz$ and $V=\frac{1}{H}\int_{-h}^{\eta} v dz$ i.e. depth averaged velocities in the x and y directions respectively, and H= total depth = $h+\eta$, p and q are flow per unit width in the x and y directions respectively, defined as: $UH=p$, $VH=q$.

If there is an inflow or outflow in the studying area, a source or sink term can be added to the right hand side of equation 6.11b to give:

$$\frac{\partial \eta}{\partial t}+\frac{\partial p}{\partial x}+\frac{\partial q}{\partial y}=q_m \qquad 6.11c$$

where q_m is source discharge per unit horizontal area.

6.2.2.2 Two-dimensional depth integrated momentum equations

The momentum equations for an incompressible turbulent flow in a Cartesian co-ordinate system can be integrated over the depth to give the depth integrated momentum equations, with the derivation being detailed in Falconer (1993):

$$\underbrace{\frac{\partial p}{\partial t}}_{term1}+\underbrace{\frac{\partial \beta p U}{\partial x}+\frac{\partial \beta p V}{\partial y}}_{term2}=\underbrace{fq}_{term3}-\underbrace{gH\frac{\partial \eta}{\partial x}}_{term4}+\underbrace{\frac{\rho_a}{\rho}C_w W_x\sqrt{W_x^2+W_y^2}}_{term5}-\underbrace{\frac{gp\sqrt{p^2+q^2}}{H^2C^2}}_{term6}$$
$$+\underbrace{\varepsilon\left[2\frac{\partial^2 p}{\partial x^2}+\frac{\partial^2 p}{\partial y^2}+\frac{\partial^2 q}{\partial x\partial y}\right]}_{term7} \qquad 6.12a$$

$$\underbrace{\frac{\partial q}{\partial t}}_{term1}+\underbrace{\frac{\partial \beta q U}{\partial x}+\frac{\partial \beta q V}{\partial y}}_{term2}=\underbrace{-fp}_{term3}-\underbrace{gH\frac{\partial \eta}{\partial y}}_{term4}+\underbrace{\frac{\rho_a}{\rho}C_w W_y\sqrt{W_x^2+W_y^2}}_{term5}-\underbrace{\frac{gq\sqrt{p^2+q^2}}{H^2C^2}}_{term6}$$
$$+\underbrace{\varepsilon\left[2\frac{\partial^2 q}{\partial x^2}+\frac{\partial^2 q}{\partial y^2}+\frac{\partial^2 p}{\partial x\partial y}\right]}_{term7} \qquad 6.12b$$

where p=UH, q=VH: Discharges per unit width in the x and y directions respectively ($m^3/s/m$)

U, V: Depth averaged velocity components in the x and y directions respectively (m/s) defined as:

$$U = \frac{1}{H}\int_{-h}^{\eta} u dz\,,\quad V = \frac{1}{H}\int_{-h}^{\eta} v dz \qquad 6.13$$

β: Momentum correction factor for a non-uniform vertical velocity profile.

f: Coriolis parameter due to earth's rotation $f = 2\omega\sin\varphi$, with ω is angle rotation speed of the earth and $\omega = 2\pi/(24\times 3600) = 7.27\times 10^{-5}\, radians/s$, φ is geographical angle of latitude of site.

g: Gravity acceleration and g=9.81 m/s^2.

H: Total water depth and $H = \eta + h$, see in Figure 6.2 below.

η: Water surface elevation above datum see in Figure 6.2 below.

h: water depth between bed level and datum see in Figure 6.2 below.

ρ_a: Air density ($\cong 1.292 kg/m^3$).

C: Chezy roughness coefficient ($m^{1/2}/s$).

C_w: Air/fluid resistence coefficient (assumed to be 2.6×10^{-3}, Falconer and Chen (1991)).

ε: Depth averaged turbulent eddy viscosity (m^2/s).

W_x and W_y are the wind velocity component in the x and y direction, respectively,

Further details of the derivation of momentum equations can be found in Falconer (1993).

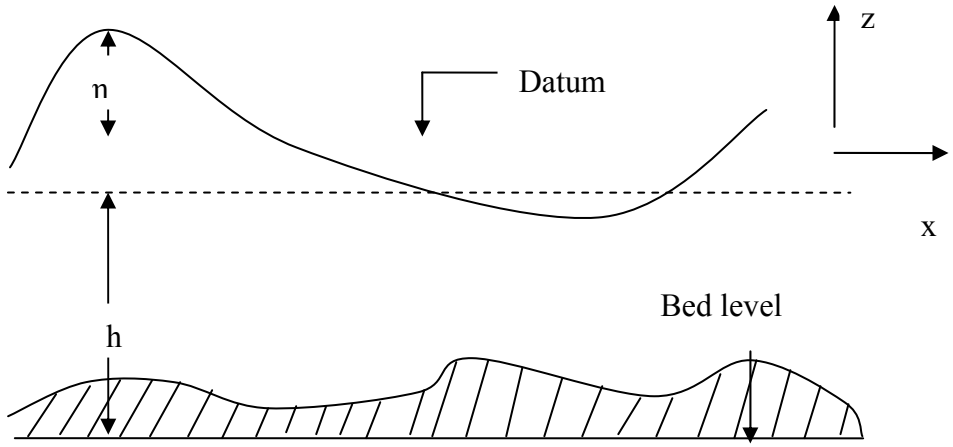

Figure 6.1: Co-ordinate system for depth integrated equations.

Term1: local acceleration.

Term 2: advective or convective acceleration.

Term 3: body force to describe the effect of the earth's rotation on the flow.

Term 4: pressure gradient to represent the action of gravity.

Term 5: wind effect.

Term 6: bed shear stress.

Term 7: the turbulent shear stress.

6.2.2.3 Meaning of different terms and parameters

The momentum correction factor

The momentum correction factor β can be defined as:

$$\beta = \frac{1}{U^2 H}\int_0^H u^2 dz \qquad 6.14$$

where U: depth average velocity, u: local velocity, H: total water depth and z: vertical co-ordinate

In practical model studies, and in the absence of extensive field data, β is generally either set to unity or a specific vertical velocity profile is assumed (see Falconer, 1993).

For the Seventh Power law velocity profile assumption, the value of β is 1.016.

For an assumed logarithmic vertical velocity profile, the value of β can be expressed as:

$$\beta = 1 + \frac{g}{C^2 \kappa^2} \qquad 6.15$$

where C is the Chezy's bed roughness coefficient.

κ is von Karman's constant (κ =0.4)

For an assumed quadratic velocity profile (Falconer& Chen, 1991), the value of β=1.2.

Coriolis parameter due to earth's rotation

The Coriolis term describes the effect of the earth's rotation on the flow. It is dependent on the latitude and the flow velocity and acts at right angle to the flow. It deflects currents in channel and can indirectly influence river alignment and sediment transport. On the coast it affects tidal currents and amplitude, causing the flow to rotate around points of zero amplitude.

Pressure gradient

This term represents the action of gravity and takes into account both the topography and the water elevation. This term contains both the mean depth and water elevation, and the derivative of the water elevation, making the term non-linear. In the case of computational instability, the mean depth may be used instead of mean depth and water elevation. This term usually represents the driving force in tidal flow (Falconer et al., 2001).

Wind effects

From Falconer et al. (2001), wind exerts a drag force as it blows over the water surface, and the shear stress at the air water interface is calculated by assuming that it is proportional to the square of the wind speed at a particular height above the water surface.

The shear stress due to wind action on the water surface is usually expressed as a quadratic function:

$$\tau_{xw} = \gamma \rho_a W_x W_s \qquad 6.16a$$

$$\tau_{yw} = \gamma \rho_a W_y W_s \qquad 6.16b$$

where γ is air- water resistance coefficient and most widely be used as γ=0.0026, ρ_a is air density,

$\rho_a = 1.29 kg/m^3$, W_x and W_y are the wind velocity component in the x and y direction, respectively,

$W_s = \sqrt{W_x^2 + W_y^2}$ is the wind speed measured at 10 m above the water surface.

Bottom friction

The bed shear stress is usually presented in a similar manner to that of uniform flow in open channel. It can be written as in the x direction:

$$\tau_{xb} = \frac{\rho g U \sqrt{U^2 + V^2}}{C^2} \qquad 6.17$$

The bottom friction has a non- linear, retarding effect on the flow. The Chezy coefficient is a semi-empirical bottom friction coefficient, which was originally developed to describe uniform flow in open channels.

The value of Chezy coefficient can be obtained directly:

$30 m^{1/2}/s < C < 100 m^{1/2}/s$

Also, Chezy coefficient can be evaluated from Manning equation:

$$C = \frac{H^{1/6}}{n} \qquad 6.18$$

where n is the Manning roughness coefficient and $0.015 < n < 0.04$.

Alternatively, the Colebrook- White equation can be used to give (Henderson, 1966):

$$C = \sqrt{\frac{8g}{f}} = -18 \log_{10}\left[\frac{k_s}{12H} + \frac{2.5C}{R_e\sqrt{8g}}\right] \qquad 6.19$$

where: f is the Darcy-Weisbach friction coefficient.

R_e is the Reynolds number.

k_s is the Nikuradse equivalent sand roughness size.

Turbulence

From Falconer et al. (2001), the turbulent shear stress refers to the flow resistance associated with the random fluctuation of water in space and time.

Yuan (2007) indicated that the values of the depth averaged turbulent eddy viscosity, E, can either be estimated from field data or, assuming that bed generated turbulence dominates over free shear layer, by a logarithmic velocity profile, such as (Elder, 1959):

$$E = \frac{\kappa}{6} u_* H = 0.0667 u_* H \qquad 6.20$$

where u_* is the bed shear velocity defined as:

$$u_* = \sqrt{\frac{\tau_b}{\rho}} = \frac{\sqrt{g(U^2 + V^2)}}{C} \qquad 6.21$$

τ_b is the bed shear stress.

But Fischer (1973) found from field data that E is greater than that given by Elder (1959), and he found the value from laboratory data was:

$$E = 0.15 u_* H = 0.15 \frac{H}{C} \sqrt{g\left(U^2 + V^2\right)} \qquad 6.22$$

6.3 Equation for sediment transport processes and bed deformation equation

6.3.1 Equation for bed load transport

In the current study the bed load transport is determined using van Rijn's formula (1984a). The model is applicable for the grain size range 0.2 ~ 2.0 mm (or 0 < T < 3):

$$q_b = 0.053 \cdot \frac{T^{2.1}}{D_*^{0.3}} \cdot [(s-1) \cdot g]^{0.5} \cdot D_{50}^{1.5} \cdot \rho_s \qquad 6.23$$

where $s = \rho_s / \rho$ is the specific density; ρ is the density of pure water (= 1000 kg/m^3). D_* is the characteristic (dimensionless) particle diameter and T is the transport stage parameter, which can be calculated using (Yalin, 1972; Ackers and White, 1973):

$$D_* = D_{50} \left[\frac{(s-1) \cdot g}{\nu^2} \right]^{\frac{1}{3}} \qquad 6.24$$

and $$T = \frac{u_*'^2 - u_{*cr}^2}{u_{*cr}^2} \qquad 6.25$$

in which u_{*cr} is the critical shear velocity which can be determined by Shields' diagram, $u_{*cr} = \sqrt{\theta_{cr}(s-1)gD_{50}}$, u_*' is the effective bed-shear velocity (van Rijn, 1984a).

6.3.2 Depth integrated governing equation for suspended sediment transport processes

When a solute is introduced into a fluid body like water, the solute would propagate, dilute and spread as it moves with flow due to the effect of advective, diffusive and dispersive transport processes. The solute can be heat (or temperature), dye pollution, salinity, DO (Dissoloved Oxygen), BOD (Biochemical Oxygen Demand), nutrients etc. The advective- diffusion equation is used to solve the concentration distribution of solute. The advection is a process that the solute moves with the fluid. Diffusion includes the scattering of particles by molecular and turbulent motion. The prediction of suspended sediment transport in a numerical model is generally based on solving the advective-diffusion equation.

For a horizontal or quasi- horizontal flow, the three dimensional solute mass balance equation is integrated over the water depth to obtain the two-dimensional depth integrated advective-diffusion equation giving as (Kocyigit et al., 2005):-

$$\frac{\partial HS}{\partial t}+\frac{\partial HUS}{\partial x}+\frac{\partial HVS}{\partial y}= \\ \frac{\partial}{\partial x}[D_{xx}H\frac{\partial S}{\partial x}+D_{xy}H\frac{\partial S}{\partial y}]+\frac{\partial}{\partial y}[D_{yx}H\frac{\partial S}{\partial x}+D_{yy}H\frac{\partial S}{\partial y}]+E \qquad 6.26$$

where H is the total water depth,

S is the concentration of suspended sediment (kg/m^3),

U, V are the depth- averaged velocity components in x and y direction respectively,

D_{xx}, D_{xy}, D_{yx}, D_{yy} are the depth- averaged dispersion- diffusion coefficients in the x and y directions respectively (m^2/s), which were calculated by an existing formula (Elder, 1959). The net erosion flux per unit area of bed, E, is expressed in the following form:

$$E=\gamma\cdot w_s\cdot(S_e-S) \qquad 6.27$$

where γ is an adjustment coefficient; w_s is the settling velocity of particles (m/s); S_e is the depth-integrated equilibrium concentration, determined from an appropriate sediment transport formula (e.g. the formula by van Rijn (1984b and 2007)). When the sediment flux upwards from the bed due to turbulence and the net sediment flux due to the fall velocity is in equilibrium, $E=0$ or $S_e=S$.

For the equilibrium concentration, the formulation by van Rijn (1984b, 2007) is used in this study:

$$S_e=0.015\cdot\frac{D_{50}}{a}\cdot\frac{T^{1.5}}{D_*^{0.3}}\cdot F\cdot\rho_s \qquad 6.28$$

where F is calculated using Equation 44 in van Rijn (1984b)

$$F = \frac{\left(\frac{a}{H}\right)^{Z'} - \left(\frac{a}{H}\right)^{1.2}}{\left(1-\frac{a}{H}\right)^{Z'} \cdot (1.2 - Z')} \qquad 6.29$$

Z' is the modified suspension number, a is a reference level of sediment profile and it equals to the roughness height. It is the upper edge of the bed load layer ($z = \delta_b$, δ_b = saltation height, z is the vertical coordinate).

6.3.3 Bed deformation equation

For a control volume, the sediment budget equation can be used to predict the area of sediment accretion or erosion. For two-dimensional flows and based on the mass balance concept, the corresponding bed evolution equation is:

$$\frac{\partial h}{\partial t} = -\frac{1}{\rho_s (1-\eta)}\left(\frac{\partial q_{bx}}{\partial x} + \frac{\partial q_{by}}{\partial y} + E\right) \qquad 6.30$$

where ρ_s is the sediment density (ρ_s = 2650 kg/m^3); η is the porosity of bed sediment (η = 0.4 in this study); q_{bx} and q_{by} are components of bed load transport (kg/m/s) in the x and y direction, respectively; E denotes the erosion, or deposition flux (kg/m^2/s). The bed load is related to the hydrodynamic conditions while the flux E is coupled with the suspended sediment concentration.

6.4 Summary

In this chapter, the mass, momentum equations, sediment transportation and bed deformation equations are presented. The different terms and parameters in these equations are discussed. The depth integrated 2-D equations used in the current study are listed below:

1. Continuity equation: Equation 6.11c;

2. Momentum equation: Equations 6.12a and 6.12b;

3. Bed load sediment transport equation: Equation 6.23;

4. Suspended sediment transport equation: Equation 6.26;

5. Bed evolution equation: Equation 6.30.

Chapter 7

Development of 2-D numerical model

7.1 Introduction

The governing equations for the flow, solute and sediment transport processes are introduced in the previous chapter. These equations to be solved are listed below.

1. Two dimensional continuity equation: Equation 6.11c of Chapter 6;

2. Two dimensional momentum equations: Equations 6.12a and 6.12b of Chapter 6;

3. Bed load sediment transport equation: Equation 6.23 of Chapter 6;

4. Suspended sediment transport equation: Equation 6.26 of Chapter 6;

5. Bed evolution equation: Equation 6.30 of Chapter 6.

Then equations are replaced by finite difference equations on the computational mesh based upon the Taylor's series approximation. This process will be introduced in the next section. Also, the secondary flow plays an important role in meandering rivers, which will be discussed in section 7.3. After that bank erosion will be described in section 7.4. In section 7.5, the procedure for the computation is shown and a summary is in section 7.6.

In this model, the bed deformation is simulated based on a two-dimensional hydrodynamic and sediment transport model (Lin and Falconer, 1995). Bank failure is modelled according to the submerged angle of repose, the process of wetting and drying is simulated by an improved method recently developed by Sun and Tao (2010).

7.2 Numerical solution procedure

Equations mentioned in section 7.1 are replaced by finite difference equations on the computational mesh based upon the Taylor's series approximation. There are a number of

methods to express the finite different method like forward, backward or central difference schemes in space and the explicit and implicit solutions in time. The above equations must therefore be divided up in time and space; this process is called discretization: taking the continuous equations and forming discrete segments in time (time step, Δt) and space (grid size, Δx, Δy).

There are three steps to solve the governing equations:

Firstly, the hydrodynamic governing equations are split into two sets of equations in the x and y directions using the methods of fractional steps in space and then an alternating direction implicit finite different scheme (ADI scheme) is used to solve the two sets of discretized equations in a staggered grid.

Secondly, the method of fractional steps in space and the hybrid scheme of explicit and implicit discretization are employed to solve the 2-D sand transport equation. Each time step is divided into two half time steps. For the first half time step, from time level n to n+1/2, values of water elevation, velocity and the solute and sediment concentrations in the x direction are solved implicitly, while other variables in the y direction are expressed explicitly. For the second half time step, from time level n+1/2 to n+1, values of water elevation, velocity in the y direction and solute and sediment concentrations are solved implicitly, while other components in the x direction are now expressed explicitly (Falconer et al., 2001).

For example, in the first half time step for continuity equation and momentum equation, the discretization form can be shown as the following tri-diagonal equations:

$$a_1(i,j)U^{n+\frac{1}{2}}_{i-\frac{1}{2},j} + b_1(i,j)Z^{n+\frac{1}{2}}_{i,j} + c_1(i,j)U^{n+\frac{1}{2}}_{i+\frac{1}{2},j} = d_1(i,j) \qquad 7.1$$

$$a_2(i,j)Z_{i,j}^{n+\frac{1}{2}} + b_2(i,j)U_{i+\frac{1}{2},j}^{n+\frac{1}{2}} + c_2(i,j)Z_{i+1,j}^{n+\frac{1}{2}} = d_2(i,j) \qquad 7.2$$

Thirdly, the bed elevation at each node at the end of the time level can be obtained by solving Equation 6.37 with the explicit scheme. With boundary conditions included, the resulting finite difference equations for each half time step are arranged in a similar way to Equations 7.1 and 7.2 and solved by using the method of Gauss elimination and back substitution. (See Gerald & Wheatly (1994) for details)

The ADI scheme is time-centred and theoretically has no stability constraints. However, to achieve reasonable computational accuracy, the time-step needs to be restricted in relation to the grid-size. A maximum Courant number for the ADI method has been suggested by (Stelling et al., 1986):

$$C = 2\Delta t\sqrt{gH(\frac{1}{\Delta x^2} + \frac{1}{\Delta y^2})} \le 4\sqrt{2} \qquad 7.3$$

where g is the acceleration due to gravity (m/s^2), Δx, Δy, and Δt are grid sizes and the time step, and H is the average depth of flow.

When $\Delta x = \Delta y$, Equation 7.3 will become:

$$\Delta t \le \frac{2\Delta x}{\sqrt{gh}} \qquad 7.4$$

7.3 Bank erosion

Different kinds of soil riverbanks are represented by different erosion mechanisms and modelling methods. River banks could be classified as non-cohesive, cohesive and composite banks. Bank

erosion mechanisms could be classified by controlled conditions as fluvial- controlled and non-fluvial controlled erosion mechanisms. The fluvial controlled erosion mechanisms are caused by scouring action, including lateral erosion by water flow and mass failure due to gravity. The submerged soil on the bank slope is detached, entrained and removed by the near-bank flow, which results in the bank erosion (Xia, Wang and Wu, 2004). Non-cohesive bank material is usually entrained by fluvial force and its submerged weight grain by grain. The main reason for bank failure is sediment erosion on the bottom of banks, and then bank height increases. A non-cohesive bank will fail when the angle of the bank is greater than the submerged repose angle of particle.

The non-fluvial controlled erosion mechanisms are mainly caused by the seepage, piping effect, wind and waves, rapid fall of water level after a high flow event, freezing- thawing and vegetation roots' growth or shrink near the bank. These cause banks reduce their strength and then lead to bank fail. In this study, non-cohesive sand is used as bank material. Fluvial controlled mechanisms play a main role and the submerged angle of repose is an important parameter.

In the models of Jang and Shimizu (2005a, b), Duan and Julien (2005), it is assumed that if the cross-sectional slope of the bank becomes steeper than the submerged angle of repose, any sediment located above the angle is eroded instantly. It has been observed in the laboratory physical experiments that even for non-cohesive sand bank, bank slope is steeper than the submerged angle of repose to some extent. This is thought to be related to the moisture content of the bank, since the submerged angle of repose is measured under water. If the sand bank is partially dry, a rather steep slope can be formed. When more water gradually seeps through the

sand, bank failure then takes place, approximately according to the submerged angle of reposed. This phase lag is important to the evolution of meandering channel. Herein, a characteristic time scale, τ_f, is introduced to represent this temporal process of bank failure, by which the temporal variation of bank slope is assumed to be:

$$S(t) = S_0 + \Delta S \cdot \exp(-t/\tau_f) \qquad 7.5a$$

and $$\Delta S = \max\left(S_0 - S_{cr}, 0\right) \qquad 7.5b$$

In Equations 7.5a and 7.5b, S_0 is the initial bank slope and S_{cr} is the critical slope

$$S_{cr} == \begin{cases} \tan\theta_r & \text{at the submerged bank} \\ \tan(\theta_r + \Delta\theta) & \text{at the water-land interface} \end{cases} \qquad 7.6$$

where θ_r is the submerged angle of repose and $\Delta\theta_r$ is an additional angle for the special location. The impact of the time scale on the river evolution will be discussed in results in the next chapter.

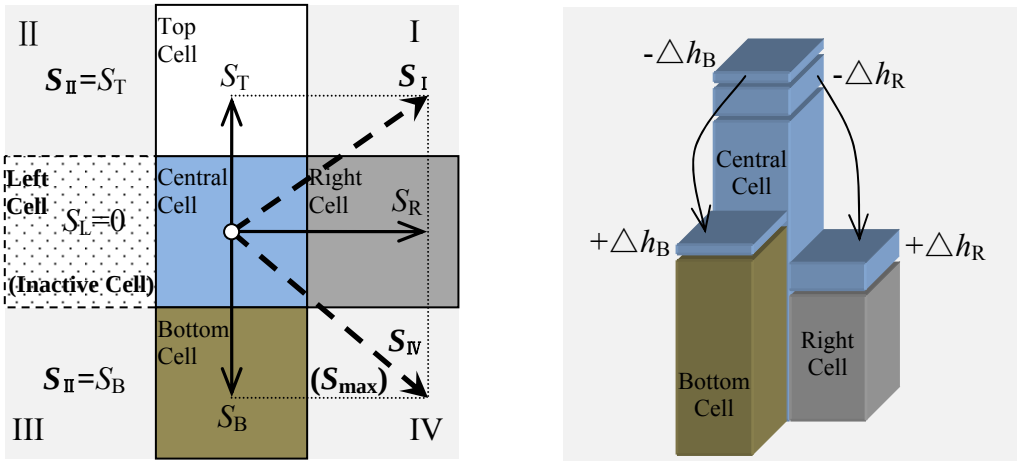

(a) Maximum Bed Slope (b) Bank Failure

Figure 7.1: Schematic diagram of modelling the bank failure.

The bank erosion, including the basal erosion and bank failure (Osman and Thorne, 1988; Darby and Thorn, 1996; Duan and Julien, 2005), was modelled by the following procedure. Firstly, the basal erosion is simulated using the bed deformation by sediment transport models, which was

described in Chapter 6, including both the bed load and suspended load transport. Secondly, the maximum bed slope $S_{\max}$ around a cell is computed. Finally, this slope is compared with the critical bed slope S_{cr} to determine whether bank failure is taking place and the amount of sediment being moved. More details of the procedure for simulating bank erosion are given below.

To estimate whether bank failure will occur in a cell, the maximum bed slope is determined using the information of the four surrounding cells, see Figure 7.1 (a). The adjacent area is divided into four quadrants, I, II, III and IV, and the maximum bed slope is found among the bed slopes in the four quadrants, $S_{\mathrm{I}}, S_{\mathrm{II}}, S_{\mathrm{III}}, S_{\mathrm{IV}}$, written as:

$$S_{\max} = \max\left(S_{\mathrm{I}}, S_{\mathrm{II}}, S_{\mathrm{III}}, S_{\mathrm{IV}}\right) \tag{7.7}$$

with

$$S_{\mathrm{I}} = \sqrt{S_{\mathrm{R}}^2 + S_{\mathrm{T}}^2} \tag{7.8a}$$

$$S_{\mathrm{II}} = \sqrt{S_{\mathrm{T}}^2 + S_{\mathrm{L}}^2} \tag{7.8b}$$

$$S_{\mathrm{III}} = \sqrt{S_{\mathrm{L}}^2 + S_{\mathrm{B}}^2} \tag{7.8c}$$

$$S_{\mathrm{IV}} = \sqrt{S_{\mathrm{B}}^2 + S_{\mathrm{R}}^2} \tag{7.8d}$$

In the above equations, $S_{\mathrm{L}}, S_{\mathrm{R}}, S_{\mathrm{B}}, S_{\mathrm{T}}$ are the bed slopes along the cell system, named as the left ,right, bottom and top slopes respectively, which can be calculated using:-

$$S_{\mathrm{L}} = \max\left(\frac{h_{\mathrm{C}} - h_{\mathrm{L}}}{\Delta x}, 0\right) \tag{7.9a}$$

$$S_{\mathrm{R}} = \max\left(\frac{h_{\mathrm{C}} - h_{\mathrm{R}}}{\Delta x}, 0\right) \tag{7.9b}$$

$$S_{\mathrm{B}} = \max\left(\frac{h_{\mathrm{C}} - h_{\mathrm{B}}}{\Delta y}, 0\right) \tag{7.9c}$$

$$S_{\mathrm{T}} = \max\left(\frac{h_{\mathrm{C}} - h_{\mathrm{T}}}{\Delta y}, 0\right) \qquad 7.9\mathrm{d}$$

where $h_{\mathrm{C}}, h_{\mathrm{L}}, h_{\mathrm{R}}, h_{\mathrm{B}}, h_{\mathrm{T}}$ are the bed elevations at the central, left, right, bottom and top cells, respectively. If a surrounding cell is inactive, such as a dry cell, or a non-loose-bed cell, a zero slope is set. As shown in Figure 7.1 (a), where the left cell is an inactive cell, the slope to the left is set to zero, $S_{\mathrm{L}} = 0$, and consequently the bed slopes in the second and third quadrants will be equal to that in the top and bottom directions, namely $S_{\mathrm{II}} = S_{\mathrm{T}}$ and $S_{\mathrm{III}} = S_{\mathrm{B}}$.

As an example, in Figure 7.1(a) the maximum slope is located in the fourth quadrant, namely:

$$S_{\max} = S_{\mathrm{IV}} = \sqrt{S_{\mathrm{B}}^2 + S_{\mathrm{R}}^2} \qquad 7.10$$

If this maximum bed slope is larger than the critical bed slope S_{cr}, then the bank fails, i.e. some bed material will be transported from the central cell to the bottom and right cells, as shown in Figure 7.1(b). The sediment volumes transferred to the two parts are expressed by the variation of bed elevation, as Δh_{B} and Δh_{R}, since that the spatial steps, Δx and Δy are invariable along the respective coordinate axis. The values of Δh_{B} and Δh_{R} are determined according to the difference between the maximum bed slope $S_{\max}$ and the critical bed slope S_{cr}, by the following formulae:

$$\Delta h_{\mathrm{B}} = \Delta\widetilde{S}\,\frac{S_{\mathrm{B}}}{S_{\max}} \cdot \frac{\Delta y}{2} \qquad 7.11\mathrm{a}$$

$$\Delta h_{\mathrm{R}} = \Delta\widetilde{S}\,\frac{S_{\mathrm{R}}}{S_{\max}} \cdot \frac{\Delta x}{2} \qquad 7.11\mathrm{b}$$

where

$$\Delta\widetilde{S} = \Delta S \cdot \left(1 - e^{-\frac{\Delta t}{\tau_{\mathrm{f}}}}\right) \qquad 7.12\mathrm{a}$$

$$\Delta S = \max\left(S_{\max} - S_{\mathrm{cr}}, 0\right) \qquad 7.12\mathrm{b}$$

In the above equations, ΔS is the difference between the maximum bed slope $S_{\max}$ and the

critical bed slope S_{cr}, while $\Delta\widetilde{S}$ is the slope to be adjusted in the current time step. In Equation 7.12, the time scale τ_f and the critical slope S_{cr}, introduced in Equations 7.5 and 7.6, are applied to the discretized system and coupled with the basic model.

7.4 Secondary flow

It has been found (Seminara, 2006) that at river bends the secondary flow plays an important role on bed deformation (for both erosion and deposition) by transverse sediment transport. Thus it is one of the major dynamic factors of meandering river evolution.

In previous 2-D model studies of bed deformation and bank movement at river bends (Duc et al., 2004; Jang and Shimizu, 2005a, 2005b; Duan and Julien, 2005), the secondary flow was usually taken into account using an empirical formula by Engelund (1974) and Odgaard (1986a):

$$v^s = N_* \cdot \left|\vec{V}\right| \cdot \frac{H}{r} \qquad 7.13$$

where v^s is the near-bed secondary flow speed (m/s); $\vec{V}$ is the primary flow velocity vector (m/s), r is the radius of curvature of the streamline (m); N_* is a coefficient representing the strength of the secondary flow related to the vertical profile of velocity and its value is about 7 based on laboratory measurements. This formula was derived based on the cylinder coordinate system, assuming the river reach to be a circular bend, namely the radius of curvature of streamline is constant (Odgaard, 1986a; Engelund, 1974).

In the present study, a new method is introduced to calculate the near bed secondary flow by linking it to the transverse water level gradient. This method is derived based on the balance of force in the transverse direction, which is the same as the previous research of Odgaard (1986a)

and Engelund (1974), but is based on the Cartesian coordinate system and more importantly, without the constraint of constant radius of curvature.

The surface water flow in rivers is one kind of gravity flow, where the main dynamic factor is produced by the water level gradient, i.e. the pressure gradient. In a straight reach, the direction of negative water level gradient is the same as that of stream line and this pressure gradient plays a role of overcoming the friction and accelerating the flow. On the other hand, at channel bends, the water level gradient does not follow the streamline. At this location, the variation of momentum in the transverse direction causes the water lever at the concave bank to be higher than that at the convex bank. Thus, the water level gradient provides an additional force, i.e. the centripetal force that changes the direction of stream line. In a real water column, under the effect of boundary layer, the velocity at the lower level of a channel is usually smaller than that at the upper level, leading to smaller centrifugal force at the lower level. However, the water level gradient provides the same pressure gradient along the water depth in the same water column. As a result, a relatively larger force at the lower level is produced. Then the near-bed transverse flow is generated by this pressure gradient excess from the concave bank to the convex bank. In this study, a new method of calculating the secondary flow is developed based on above-mentioned principle.

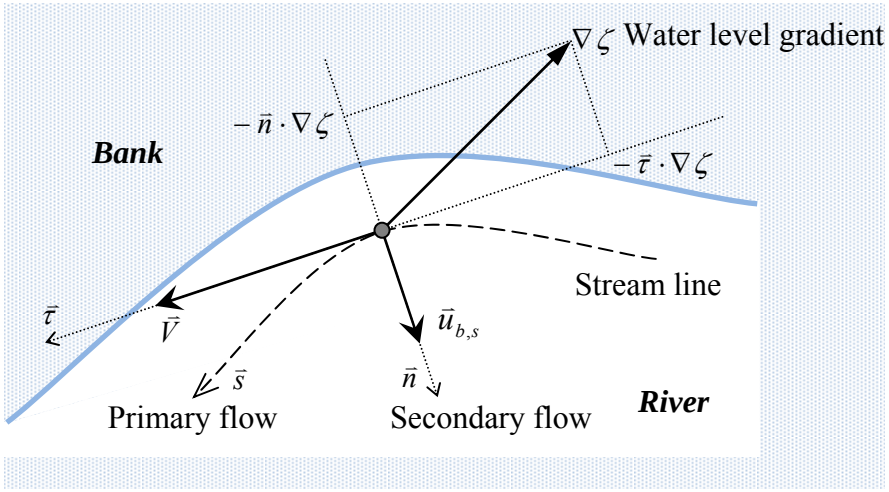

Figure 7.2: Schematic diagram of production of near-bed secondary flow in river bends.

In order to investigate the secondary flow in channel bends, a three dimensional momentum equation based on a local Cartesian coordinate system is used. The origin of the coordinate system is fixed at a reference point along the streamline of a curved reach, see Figure 7.2, where $\vec{\tau}$ is the primary flow direction at this point and $\vec{n}$ is the direction normal to $\vec{\tau}$, namely the direction of secondary flow, with z-axis being the vertical direction. It should be noted that $\vec{\tau}$ is different from $\vec{s}$, the streamline direction. The direction of $\vec{\tau}$ is fixed, while $\vec{s}$ varies with the streamline.

In direction $\vec{n}$, the momentum equation can be written as:

$$\frac{\partial u_n}{\partial t}+\frac{\partial (u_\tau u_n)}{\partial \tau}+\frac{\partial (u_n u_n)}{\partial n}+\frac{\partial (w u_n)}{\partial z} = -g\frac{\partial \zeta}{\partial n}+\frac{\partial}{\partial \tau}\left(\varepsilon_\tau \frac{\partial u_n}{\partial \tau}\right)+\frac{\partial}{\partial n}\left(\varepsilon_n \frac{\partial u_n}{\partial n}\right)+\frac{\partial}{\partial z}\left(\varepsilon_z \frac{\partial u_n}{\partial z}\right) \qquad 7.14$$

where u is the horizontal velocity; w is the vertical velocity; ε is the turbulent eddy viscosity; the subscripts denote the direction. In this equation, the hydrostatic pressure assumption is considered. The superscripts of 'p' and 's' denote the velocity components in the primary flow and secondary flow, respectively. Thus the two velocity components can be written as:-

$$u_\tau = u_\tau^{\mathrm{p}} + u_\tau^{\mathrm{s}} \qquad 7.15a$$

$$u_n = u_n^{\mathrm{p}} + u_n^{\mathrm{s}} \qquad 7.15b$$

It should be noted that $u_\tau^{\mathrm{s}} = 0$ and $u_n^{\mathrm{p}} = 0$, but their spatial derivatives are not zero.

It is further assumed that the secondary flow is quasi-steady and the vertical velocity component is small and its dynamic effect is negligible. Thus the 1st and 4th terms on the left hand side of Equation 7.14 can be neglected. The vertical turbulence-eddy-diffusion term is considered to be much larger than the other horizontal terms, considering the water depth is smaller than the width for most rivers. The primary flow is regarded as the dominant motion, and the advection term can be approximated by the primary flow. Under these assumptions, Equation 7.14 can be simplified as:

$$\frac{\partial(u_\tau^{\mathrm{p}}u_n^{\mathrm{p}})}{\partial\tau}+\frac{\partial(u_n^{\mathrm{p}}u_n^{\mathrm{p}})}{\partial n}=-g\frac{\partial\zeta}{\partial n}+\frac{\partial}{\partial z}\left(\varepsilon_z\frac{\partial u_n^{\mathrm{s}}}{\partial z}\right) \qquad 7.16a$$

The two terms on the left hand side represent the centrifugal force, which is balanced by the pressure gradient, provided by the water level variation and diffusion effect. In past studies, the radius of curvature of streamline, r, is considered to be constant. Thus Equation 7.16a can be written, in the cylindrical coordinate system, as (Engelund, 1974; Odgaard, 1986):

$$-\frac{(u_n^{\mathrm{p}})^2}{r}=-g\frac{\partial\zeta}{\partial n}+\frac{\partial}{\partial z}\left(\varepsilon_z\frac{\partial u_n^{\mathrm{s}}}{\partial z}\right) \qquad 7.16b$$

It should be pointed out that the radius of curvature in Equation 7.13 is coming from the right hand side of Equation 7.16b. However, the constant radius of curvature is hardly held in a real meandering channel. The method of this study is based on Equation 7.16a, instead of Equation 7.16b. In the following derivation, the water level gradient will be reserved with the accelerate term being eliminated, while in previous research the left hand of Equation 7.16b is kept and the pressure gradient is eliminated.

The normalized vertical profile of primary flow is considered to be a function of $f(z)$, such as the traditional power law. Thus the primary flow velocity can be expressed as:

$$u_\tau^{\mathrm{p}}(\tau,n,z,t)=U_\tau^{\mathrm{p}}(\tau,n,t)\cdot f(z) \qquad 7.17a$$

$$u_n^{\mathrm{p}}(\tau,n,z,t)=U_n^{\mathrm{p}}(\tau,n,t)\cdot f(z) \qquad 7.17b$$

where $U_\tau^{\mathrm{p}}(\tau,n,t)$ and $U_n^{\mathrm{p}}(\tau,n,t)$ are the depth-averaged horizontal velocity components in the $\vec{\tau}$ and $\vec{n}$ directions, respectively. Substituting Equation 7.21 into Equation 7.16a gives:

$$f^2(z)\cdot\left(\frac{\partial(U_\tau^{\mathrm{p}}U_n^{\mathrm{p}})}{\partial\tau}+\frac{\partial(U_n^{\mathrm{p}}U_n^{\mathrm{p}})}{\partial n}\right)=-g\frac{\partial\zeta}{\partial n}+\frac{\partial}{\partial z}\left(\varepsilon_z\frac{\partial u_n^{\mathrm{s}}}{\partial z}\right) \qquad 7.18$$

Now integrating Equation 7.18 from bed level h to water surface level ζ gives:

$$\int_h^\zeta f^2(z)\mathrm{d}z\cdot\left(\frac{\partial(U_\tau^{\mathrm{p}}U_n^{\mathrm{p}})}{\partial\tau}+\frac{\partial(U_n^{\mathrm{p}}U_n^{\mathrm{p}})}{\partial n}\right)=-H\cdot g\frac{\partial\zeta}{\partial n}-g\cdot\frac{v^s\left|v^s\right|}{C^2} \qquad 7.19$$

where the bottom friction stress, incurred by the secondary flow, is represented by Chezy coefficient. On the other hand, in order to obtain the near bed secondary flow, Equation 7.18 is integrated over the near bed water column, i.e. from bed h to $h+\alpha H$, giving as:

$$\int_{h}^{h+\alpha H} f^2(z)\mathrm{d}z \cdot \left(\frac{\partial (U_\tau^{\mathrm{p}} U_n^{\mathrm{p}})}{\partial \tau} + \frac{\partial (U_n^{\mathrm{p}} U_n^{\mathrm{p}})}{\partial n} \right) = -\alpha H \cdot g \frac{\partial \zeta}{\partial n} - \beta' \cdot g \cdot \frac{v^s |v^s|}{C^2} \qquad 7.20$$

where α is the proportion of near bed water column and $\alpha \in (0,0.2)$ according to the effective height of bed load; β' is a coefficient used to describe the friction coming from both the bed and the upper layer water. The resistance force coming from upper layer water is considered to be much smaller than that from the bed, thus then it can be assumed that $\beta' \approx 1$.

Eliminating the advection term by combining Equations 7.19 and 7.20 gives:

$$g \cdot \frac{v^s |v^s|}{C^2} = \frac{\alpha(1-\chi)}{\beta' - \alpha\chi} \cdot gH \cdot \left(-\frac{\partial \zeta}{\partial n} \right) \qquad 7.21$$

where χ is defined as:

$$\chi = \frac{\int_{h}^{h+\alpha H} f^2(z)\mathrm{d}z}{\alpha \cdot \int_{h}^{\zeta} f^2(z)\mathrm{d}z} \qquad 7.22$$

It represents the non-uniformity of vertical distribution of primary flow, especially the defect near the bed. Further setting:

$$\lambda^2 = \frac{\alpha(1-\chi)}{\beta' - \alpha\chi} \qquad 7.23$$

Equation 7.21 can be re-written as:

$$v^{\mathrm{s}} = -\lambda C \sqrt{H \left| \frac{\partial \zeta}{\partial n} \right|} \qquad 7.24$$

where the sign of λ is determined by $\frac{\partial \zeta}{\partial n}$ and its absolute value is less than one according to Equation 7.23.

If the vertical profile of primary flow obeys the traditional power law, i.e.:

$$f(z) = \frac{m+1}{m} \cdot \left(\frac{z-h}{H} \right)^{\frac{1}{m}} \qquad 7.25$$

where m is the velocity profile exponent, representing the effect of friction, normally with values ranging from 3 to 7 (Odgaard, 1986). Inserting Equation 7.25 into Equation 7.22 gives:

$$\chi = \alpha^{\frac{2}{m}} \qquad 7.26$$

Considering Equation 7.26 and Equation 7.23, the coefficient λ is estimated to range between 0.0 and 0.3. In this study the value is adjusted within this range.

7.5 Solution procedure for the 2-Dimensional model

The solution procedure for the 2-Dimensional model to simulate the longitudinal and lateral channel deformation can be described as the schematic structure shown in Figure 7.3.

7.6 Summary

A 2-Dimensional model has been developed which consists of a 2-D flow module, a sediment transport module and a bank erosion module. This model is used to simulate lateral bank deformation in the alluvial river. The bank geometry is updated each time step. The key processes of bed deformation, including bed load and suspended load sediment transport, bank failure, secondary flow and wetting and drying are taken into account. The numerical model results by this model will be presented in the next chapter.

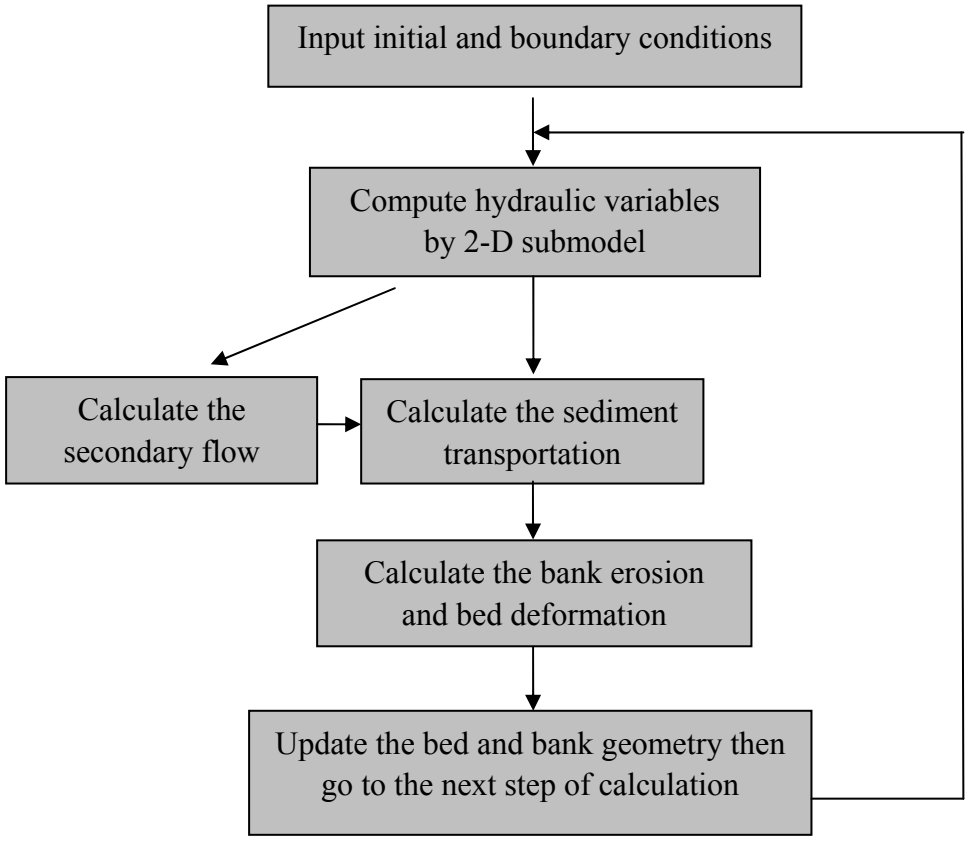

Figure 7.3: Schematic structure for the 2-D model to simulate the longitudinal and lateral channel deformation.

Chapter 8

Numerical model results and comparison with experiments

8.1 Introduction

This chapter describes comparisons between numerical model predictions and physical model results. The numerical model was described in Chapter 7 and physical model was shown in Chapter 5. In modelling predictions with large and medium channels, the simulation results are to compare with experiment results and to analyse channel development process. The numerical model parameters used in this study are: Δt = 0.01 s, Δx=0.02 m, Δy = 0.01 m. The characteristic time scale, τ_f = 1.5 s, and the secondary flow coefficient, λ = 0.13, were determined by the method of trial and error. The model was run in a PC, in which the CPU type is Intel Q9550 with the processor's frequency being 2.83GHz. Each case for 1 hour experiment would consume about 11 hours of computational time.

8.2 Result for numerical modelling with large channel

Experiments with the large channel were carried out for both steady inflow and unsteady inflow conditions. Their test conditions are shown in Table 8.1 and their flow rates are shown in Figure 5.53 in Chapter 5.

Table 8.1: Experimental conditions with large initial channel.

Top width(cm)×bottom width(cm)×height(cm)	Section (cm^2)	Slope	Q(l/s)	Time (min)
D9: 31×4×7.5	131.25	0.015	Steady 2 l/s	60
D10: 31×4×7.5	131.25	0.015	Unsteady 2 l/s	60

8.2.1 Numerical model results, steady inflow (Test D9)

Test D9 was carried out with a steady inflow rate of 2 l/s for 60 min, and its physical model results at 0 min, 15 min, 30 min, 45 min and 60 min are shown in Figure 8.1. The channel development from a straight channel to a meandering one can be clearly seen, which is due to the effect of initial bend upstream.

(a) T=0min (b) T = 15 min (c) T = 30 min (d) T = 45 min (e) T = 60 min

Figure 8.1: Physical model of river development for Test D9.

More details of the physical model results are shown in Chapter 5. Numerical model predictions of horizontal channel evolution, bed forms and section shapes are compared with the experimental data, with the results being described below.

8.2.1.1 Comparison of horizontal channel evolution

The comparison of horizontal evolution between physical and numerical model is shown in Figure 8.2 for T = 0 min, 15 min, 30 min, 45 min and 60 min, respectively.

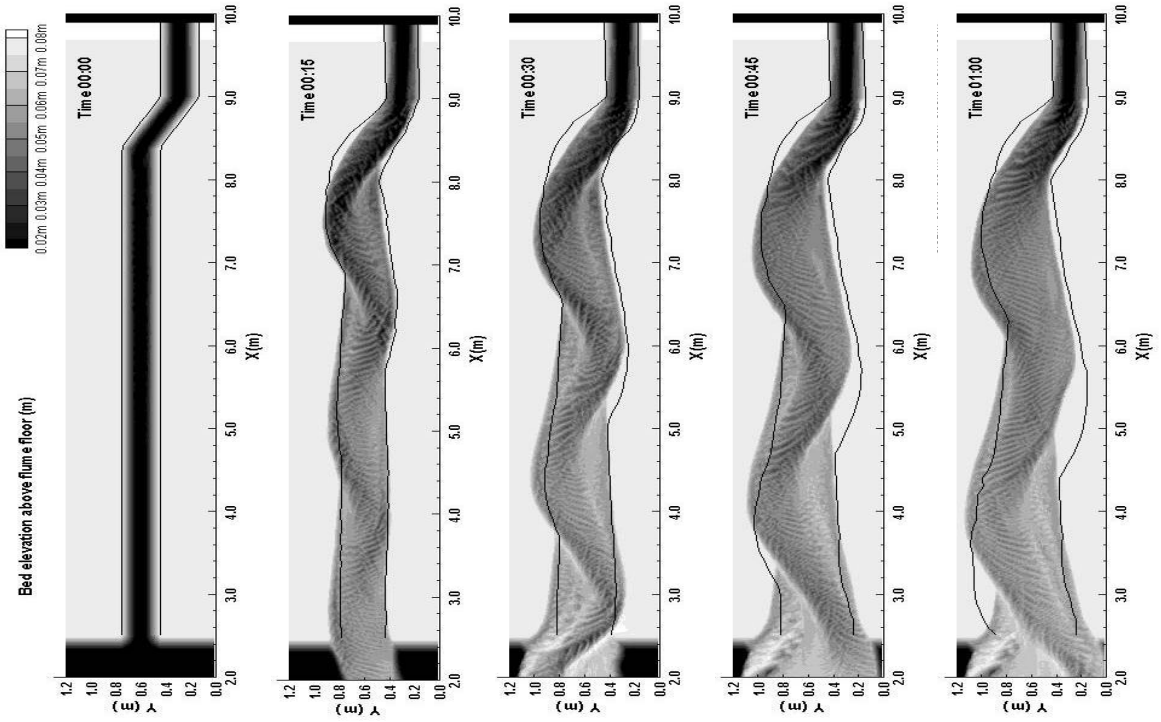

(a) T=0min (b) T = 15 min (c) T = 30 min (d) T = 45 min (e) T = 60 min

Figure 8.2: Comparison of horizontal channel shapes between physical and numerical model results for Test D9. (Solid lines are the channel boundary obtained from physical experimental images.)

The solid lines are bank outlines obtained from the physical model results in Figure 8.1. In the numerical model results the channel became wider and meandering, starting from a narrow straight channel, which agreed well with physical model. The predicted bank boundaries almost covered the experimental bank lines in most of the test area, except in the second apex after the initial bending. The numerical model results lagged behind the physical model at 30 min and this delay became obvious at 60 min. In the numerical model, it is also clear to observe a thalweg similar to the one shown in physical model record. The bed elevation predicted by the numerical model shows that the channel became wider and shallower, which can be further confirmed in the following section. The predicted horizontal movement agreed generally well with the physical model, which indicates that the key processes are simulated adequately by the present model.

8.2.1.2 Comparison of bed forms

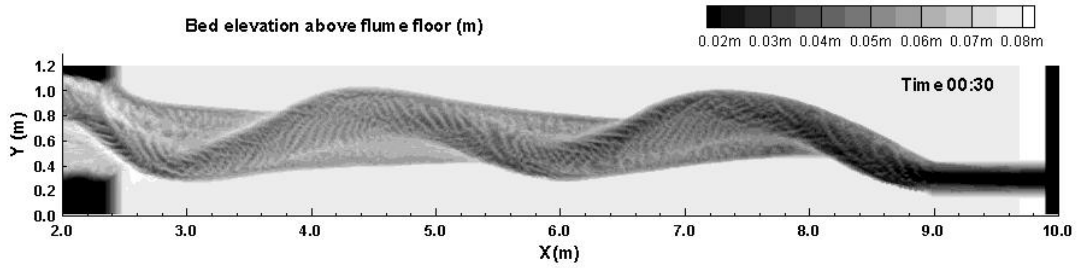

(a) Modelling result at T = 30 min, Test D9

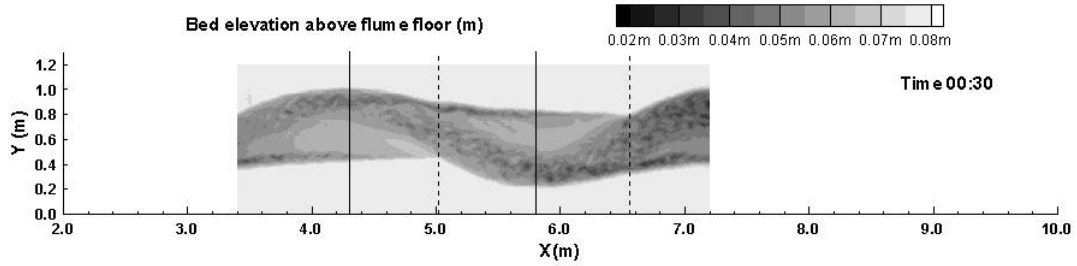

(b) Experiment result at T = 30 min, Test D9

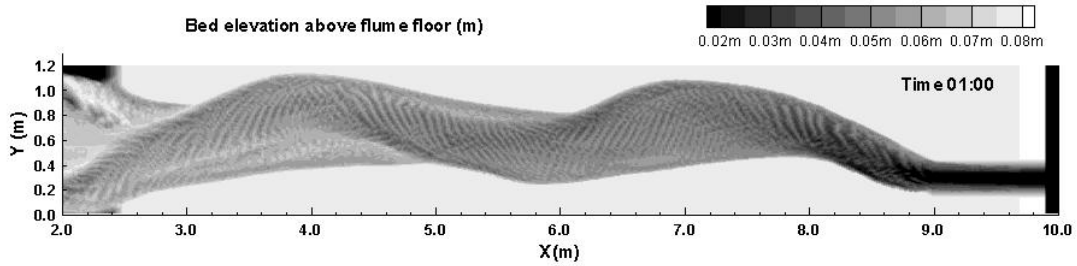

(c) Modelling result at T = 60 min, Test D9

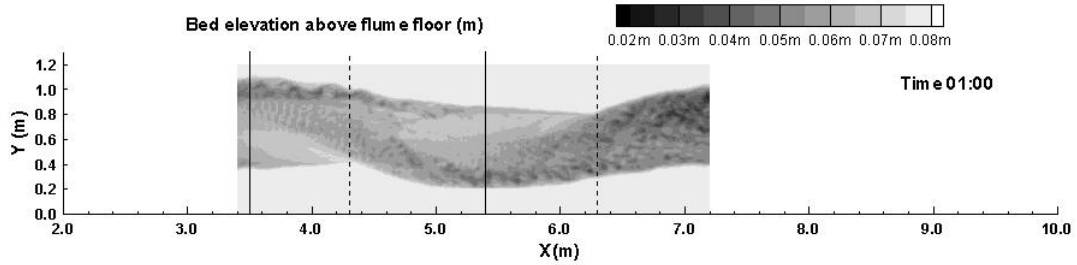

(d) Experiment result at T = 60 min, Test D9

Figure 8.3: Comparison of bed forms by numerical modelling and physical modelling. (Gray scales are used to show the bed elevation above flume floor.)

The bed form comparison is shown in Figure 8.3. It can be seen that properties from the two methods agreed closely at T = 30 min, including the shape of bends, alternate bars and especially

the crossings. At 60 min, the physical model river had a point bar at x = 5.4 m, but the numerical model did not have a point bar there. The overall performance of the numerical results is satisfactory.

8.2.1.3 Comparison of section shapes

The cross-sectional shapes at four characteristic locations A-A, B-B, C-C and D-D: two at crossings (dotted lines A-A and C-C in Figure 8.3) and two at bend apexes (solid lines B-B and D-D in Figure 8.3) are plotted in Figure 8.4. The locations of sections for numerical model are not exactly the same as the physical model. Their positions are at crossings and apexes in model predicted river. In Figure 8.4, the cross-sectional shapes at T = 30 min and 60 min showed that during the channel evolution process the bed level at the initial channel increased due to deposition, while the bed level at the banks reduced due to erosion. Thus a new channel formed. This process has been discussed in physical experiment chapter: the initial cross section was not in balance with a given slope, flow rate and sand size.

The comparison shows a satisfying agreement between the predicted and measured channel widths and depths, the locations of deep and shallow areas, although the numerical model predicted a deeper channel than the physical model. In fact, the difference of channel depths between the physical and numerical models is relatively small; with the prediction is about 20% deeper than the experimental results. The difference in channel widths is also small especially at 60 min.

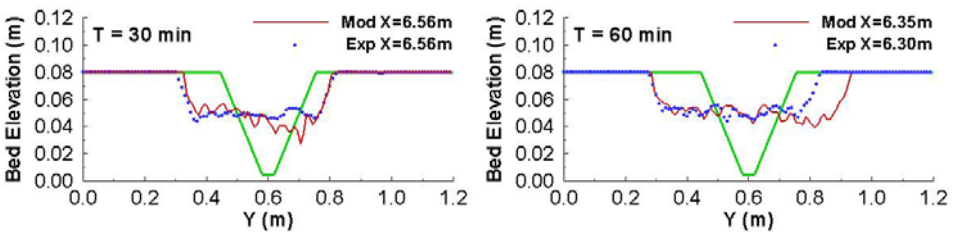

(a) A-A at T=30 min (b) A-A at T=60 min

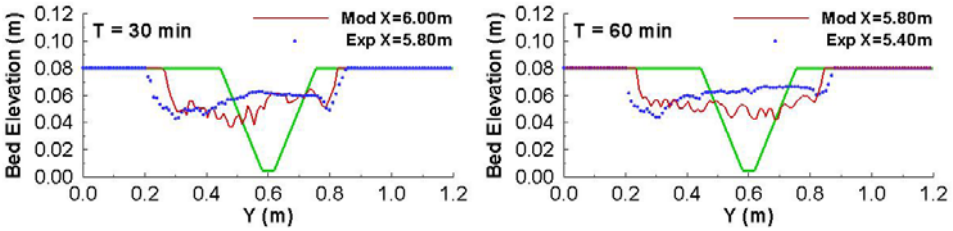

(c) B-B at T=30 min (d) B-B at T=60 min

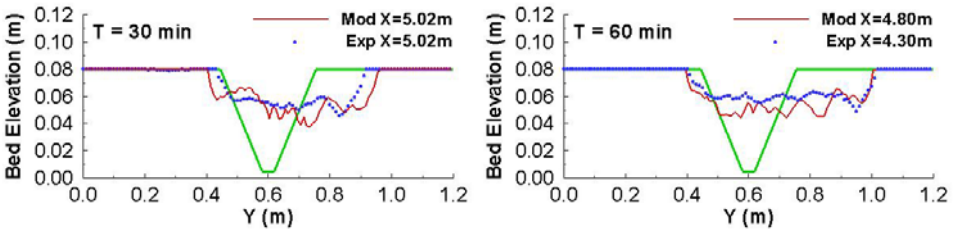

(e) C-C at T=30 min (f) C-C at T=60 min

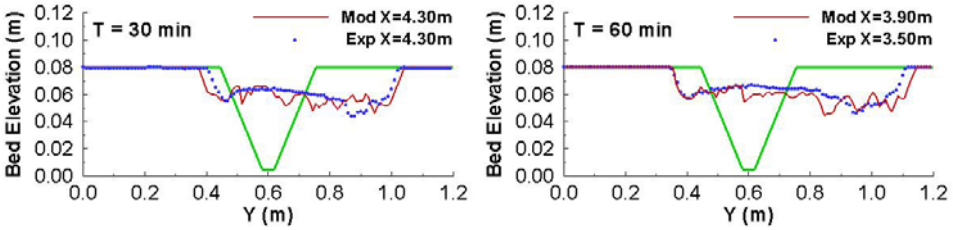

(g) D-D at T=30 min (h) D-D at T=60 min

Figure 8.4: Comparison of section shapes by numerical modelling and physical modelling (Points labelled by 'Exp' are the experimental results; lines labelled by 'Mod' are the modelling results; thick solid lines are the initial section shapes; locations of cross-sections A-A, B-B, C-C and D-D are shown in Figure. 8.3b and 8.3d.

8.2.2 Numerical modelling results, unsteady inflow (Test D10)

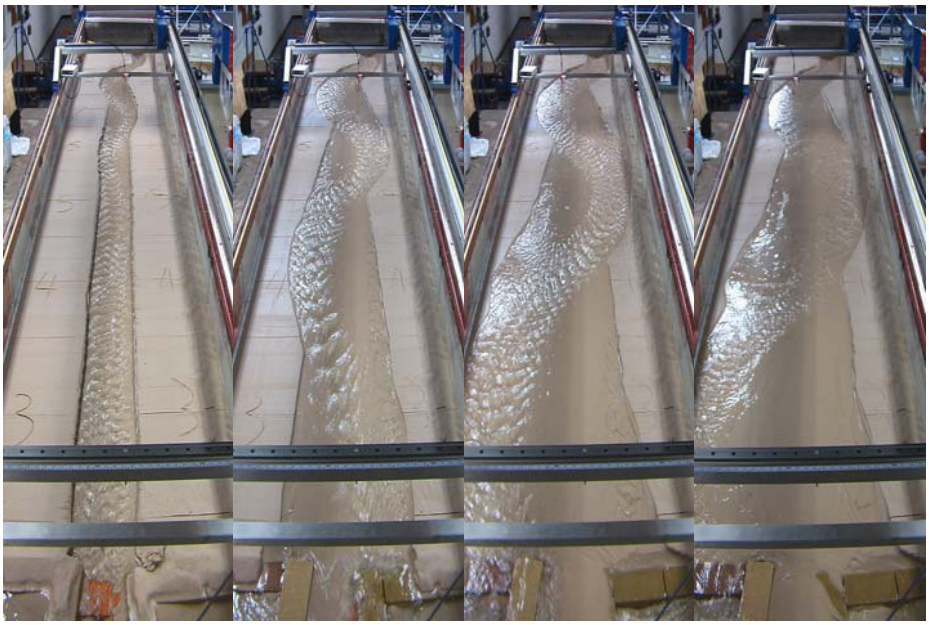

(a): T=15 min (b): T=30 min (c): T=45 min (d): T=60 min

Figure 8.5: Physical experiment, Test D10, from straight channel into meandering one.

Test D10 was carried out with a rapidly varied flow and the channel development process was shown in Figure 8.5. D10 had 1 l/s for 15 min, then 3 l/s for 30 min and 1 l/s for the last 15 min, as shown in Figure 5.53.

8.2.2.1 Comparison of horizontal channel evolution for D10

From Figure 8.6 below it can be seen that the numerical model prediction agrees less well with the physical model. In the first 15 minutes (when the flow rate was 1 l/s), the numerical predicted channel development was slower than the physical model result. The channel kept narrow and straight while the experimental channel showed an initial development of a meandering channel with the width increased. Then when flow rate was increased to 3 l/s, the numerical model gave a quick development until T = 45 min, the computation channel was wider and its thalweg had

larger sinuosity than the experiment channel. After that, the predicted channel kept its width but had a shallower depth.

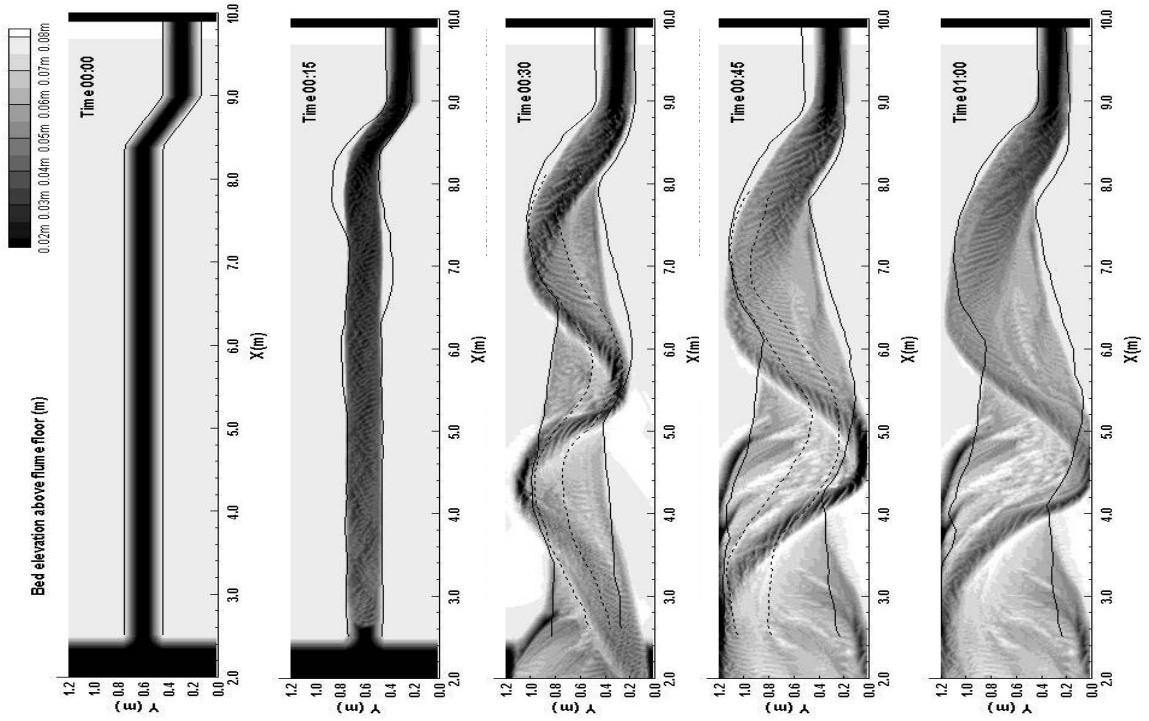

(a) T=0min (b) T = 15 min (c) T = 30 min (d) T = 45 min (e) T = 60 min

Figure 8.6: Comparison of horizontal channel evolution by numerical modelling and physical experiment for Test D10. (Solid lines are the channel boundary obtained from physical experimental images.)

From channel development with numerical model, it is found that when the flow rate was small, the channel development by prediction was slower than experiment, and with large flow rate, the development by prediction were faster than experiment. Channel development is caused by bank erosion which is lead by bed load transport. It means that channel development reflects the bed load transport. That prediction results are sensitive to flow rate shows that bed load transport is also sensitive to flow rate.

8.3 Numerical modelling result for tests with medium channel

In this section, the numerical model has been applied to physical model test cases D3, D4 and D5. Different flow rates were used in these tests and comparisons were made between numerical model predictions and physical model results. Their flow conditions are shown in Figures 5.42 and 5.43 in Chapter 5 and other situations are shown in Table 8.2 below.

Table 8.2: Experiment conditions with medium channel.

Top width(cm)×bottom width(cm)×height(cm)	Section (cm^2)	Slope	Q (l/s)	Time (min)
D3: 26×6×5.5	88	0.020	Gradually varied 0.6 l/s	60
D4: 26×6×5.5	88	0.020	Steady inflow 0.6 l/s	60
D5: 26×6×5.5	88	0.020	Rapidly varied flow 0.6 l/s	60

8.3.1 Numerical modelling results, steady inflow (Test D4)

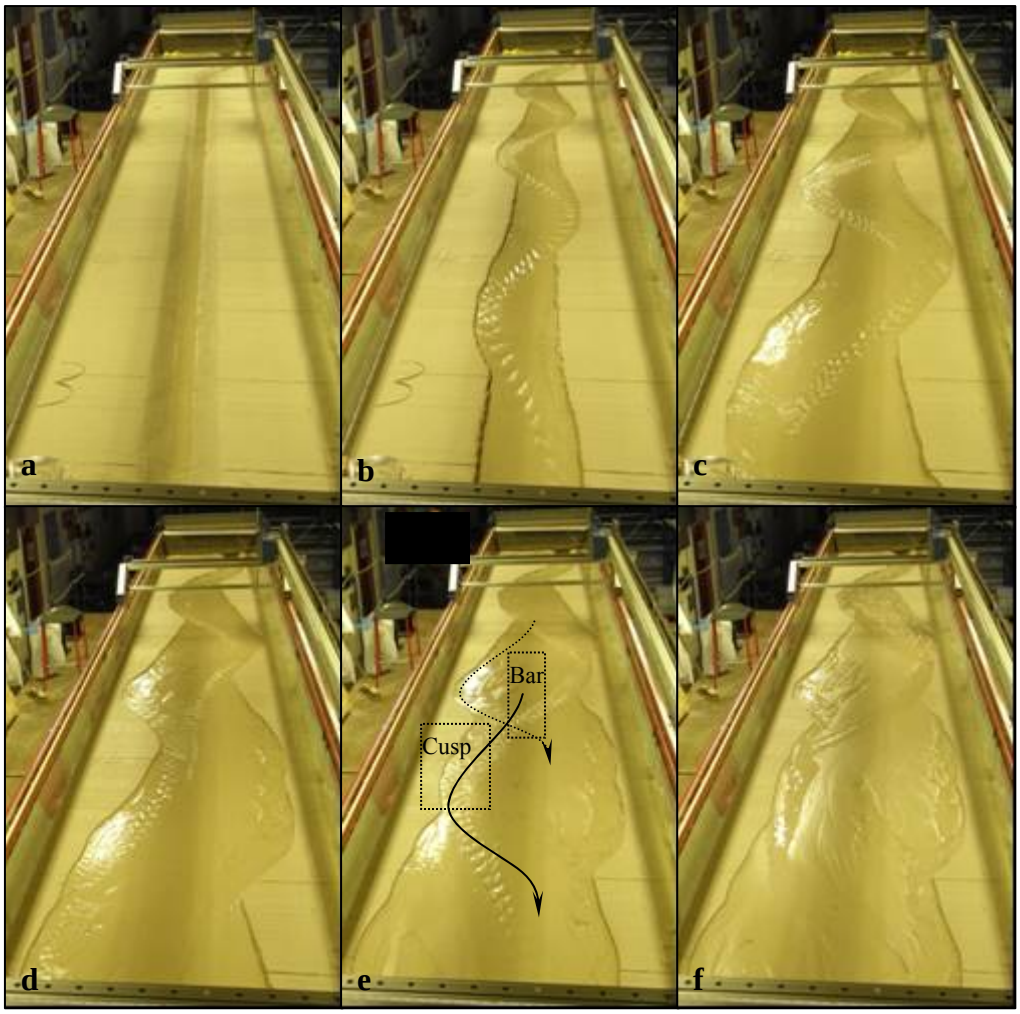

Figure 8.7: Physical experiment of channel development, Test D4 with steady inflow. (a) 0 min; (b) 15 min; (c) 30 min; (d) 45 min; (e) 60 min; (f) after being drained at 60 min.

In this test, flow rate was constant, 0.6 l/s. The channel forms of Test D4 in Figure 8.7 before 30 min showed two types of movement of a meander pattern in a uniform manner: meander sweep and meander swing as described by Schumm et al. (1987). But after 30 min, there was an abrupt downstream shift in the thalweg through the bend. And this formed bars and cusps (see in Figure 8.7e) between the old and new thalweg at the edge of the floodplain. Figure 8.8 shows a

comparison of horizontal evolution between the numerical model predictions and physical model data.

8.3.1.1 Horizontal channel evolution

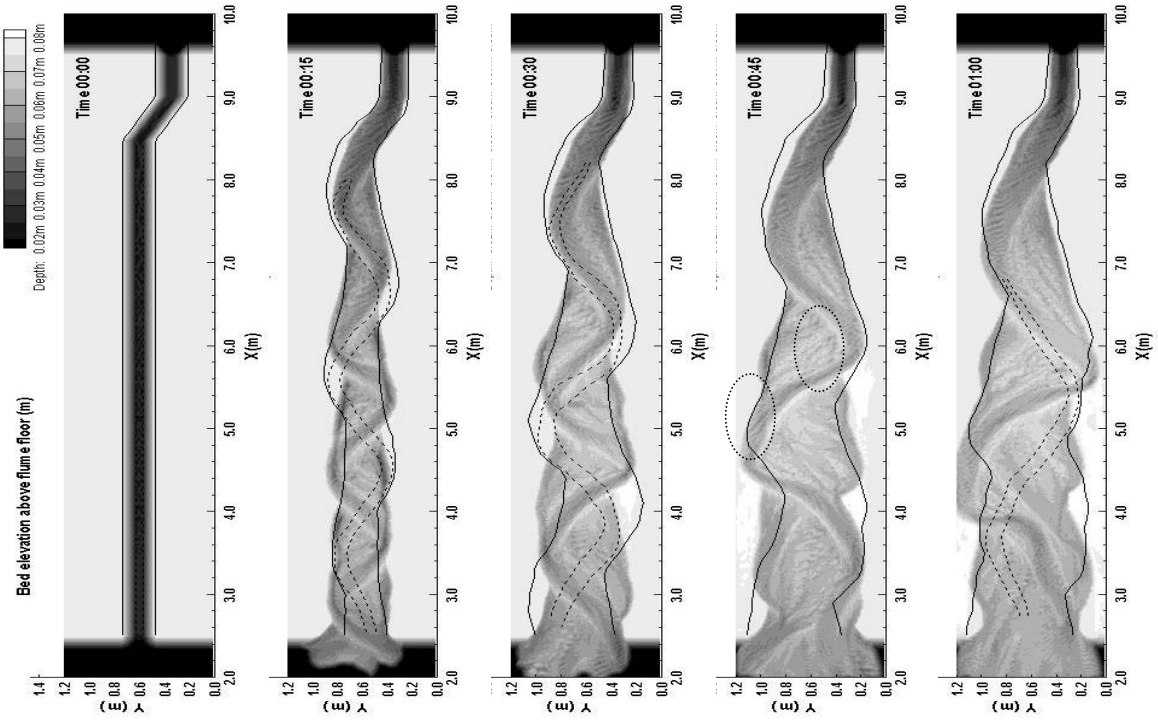

(a) T=0min (b) T = 15 min (c) T = 30 min (d) T = 45 min (e) T = 60 min

Figure 8.8: Comparison of horizontal channel evolution by numerical modelling and physical experiment for Test D4. (Solid lines are the channel boundary obtained from physical experimental images.)

The two types of meander movement: meander sweep and meander swing are modelled successfully by prediction of numerical model as shown in Figure 8.8. Before 30 min, meander shifts forward progressively accompanying with regular bars and dumps. At 30 min, the meander is fully developed, then become unstable: there is an abrupt downstream shift in the thalweg through the bend and forms bars and cusp as shown in Figure 8.8 at 45 min. Prediction of cusp

and meander shift agrees well with physical results as in Figure 8.7. At 60 min, boundary by numerical model reaches the flume wall while boundary by physical model does not. In general speaking, numerical results agreed with physical results in Figure 8.8.

8.3.1.2 Bed forms

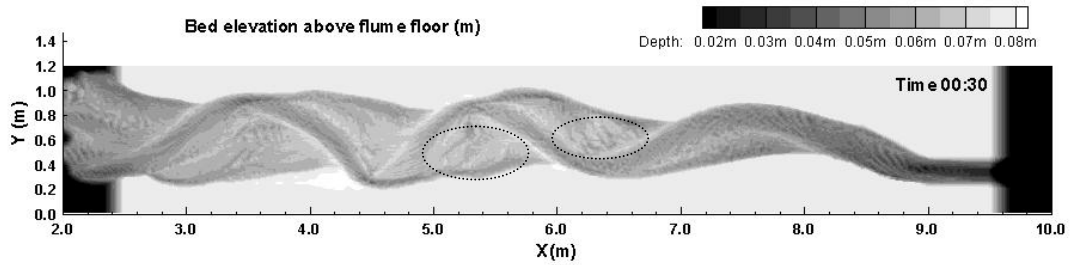

(a) Modelling result at T = 30 min for D4

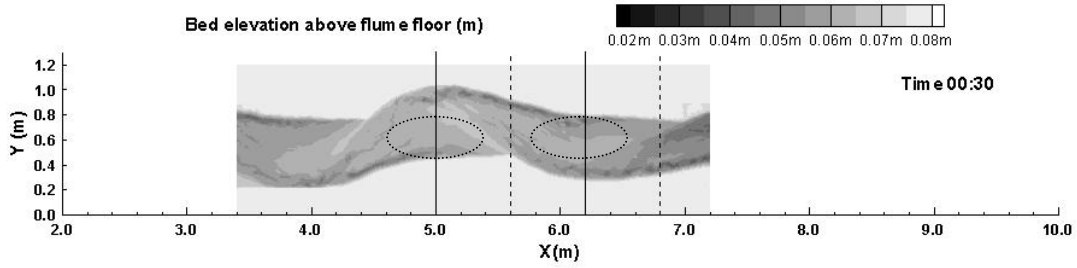

(b) Experiment result at T = 30 min for D4

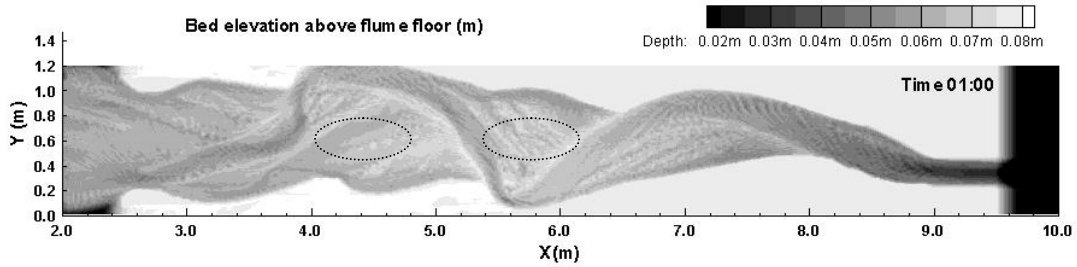

(c) Modelling result at T = 60 min for D4

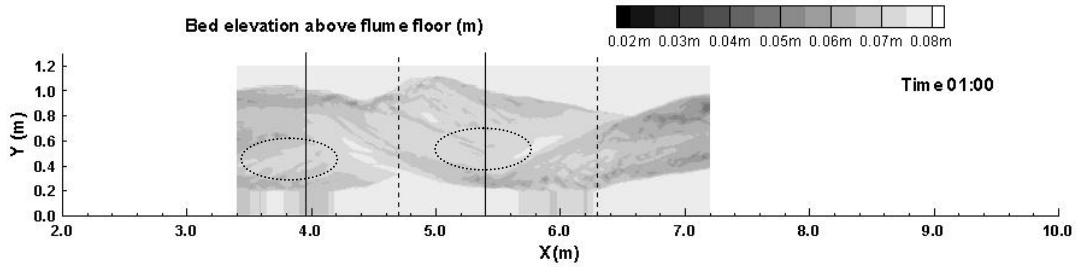

(d) Experiment result at T = 60 min for D4

Figure 8.9: Comparison of bed forms obtained from numerical model and physical experiment, Test D4. (Gray scales are used to show the bed elevation above flume floor.)

Figure 8.9 shows a comparison of model predicted and measured channel bed elevations at T = 30 and 60 min. At T = 30 min, the model predicted point bars are located at the same places as the experiment and their sizes are also similar. The predicted meandering thalweg has a similar curvature as the experiment. However, at T = 60 min, the predicted bars have different sizes and locations from the experiment. The predicted bars are surrounded by a meandering thalweg with a large curvature, while the bars in the physical model are separated by a mild slope meandering thalweg. The development of these bars indicated that two modelling approaches agree generally well.

8.3.1.3 Cross-sectional shapes

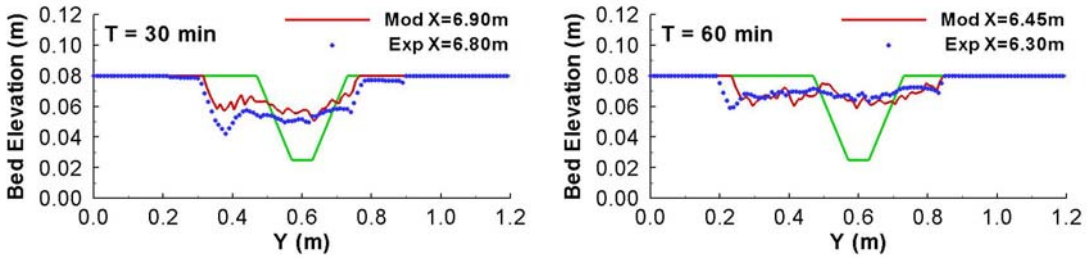

(a) A-A at T=30 min (b) A-A at T=60 min

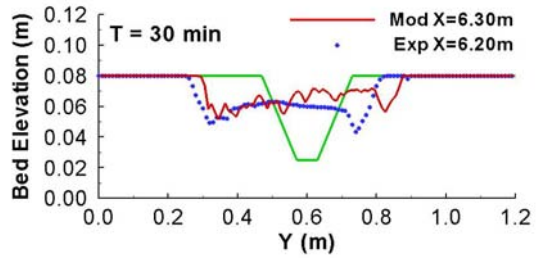

(b) B-B at T=30 min

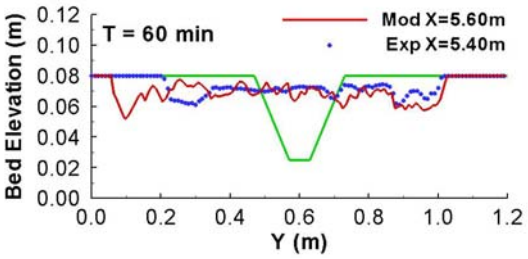

(d) B-B at T=60 min

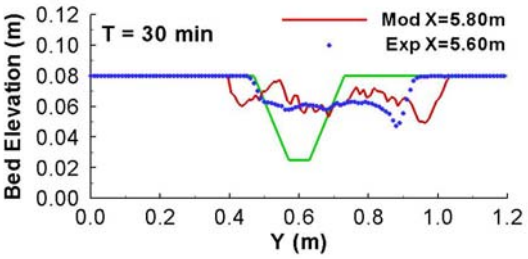

(e) C-C at T=30 min

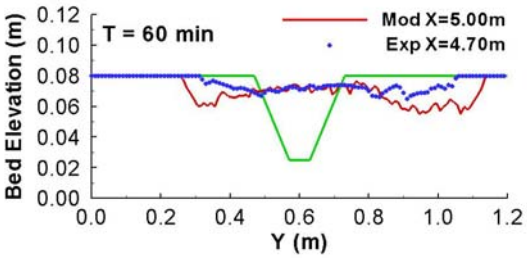

(f) C-C at T=60 min

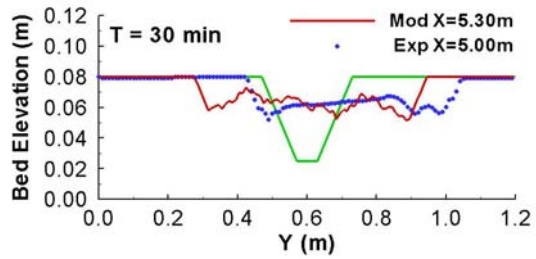

(g) D-D at T=30 min

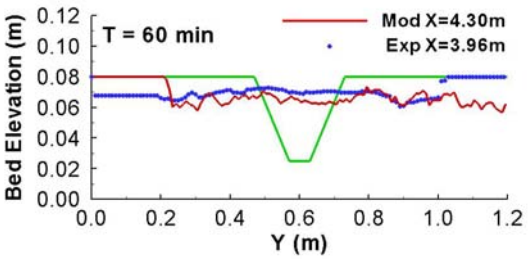

(h) D-D at T=60 min

Figure 8.10: Comparison of section shapes for Test D4 by numerical modelling and physical modelling (Points labelled by 'Exp' are the experimental results; lines labelled by 'Mod' are the modelling results; thick solid lines are the initial section shapes; locations of cross-sections A-A, B-B, C-C and D-D are shown in Figure 8.9b and 8.9d.

The cross-sectional shapes in Figure 8.10 show that the agreement between numerical modelling and physical modelling is satisfactory, and result at T = 30 min is better than that at T = 60 min. At T = 30 min, the difference between the model predicted and measured channel widths is about 12.5%, and predicted result is wider. The value of difference is about 20% at T = 60 min, again the predicted result is wider. At 30 min, the predicted depth is between 0.06 cm and 0.07 cm,

physical depth is between 0.05 cm and 0.07 cm. At 60 min, the model predicted bed level agrees well that that measured.

8.3.2 Numerical modelling results, gradually varied flow (Test D3)

(a): T=15 min (b): T=30 min (c): T=45 min (d): T=60 min

Figure 8.11: Physical experiment development for Test D3 with gradually varied flow.

In Test D3, the flow rate increased from zero at the beginning and reached the highest value at T = 30 min and then decreased to zero at T = 60 min. The outer boundaries have smaller curvatures (see Figure 8.11) than Test D4, because the convex bank would be destroyed more easily by the large flow rate with large erosion ability during T = 15 min- 45 min.

8.3.2.1 Horizontal channel evolution

In Figure 8.12, the numerical model prediction agrees generally well with the physical model after T = 15 min. As discussed earlier, the bed load is sensitive to flow rate: when flow rate is small, channel development is small and slow. That means prediction is underestimating compared with reality, so modelling in 15 min lagged the channel development and after that physical modelling

had a fast approaching with experiment. It is confirmed at 30 min. At T = 45 min, the numerical model predicted a wider channel than the physical model in reaches downstream. Generally speaking, results from two methods agree closely.

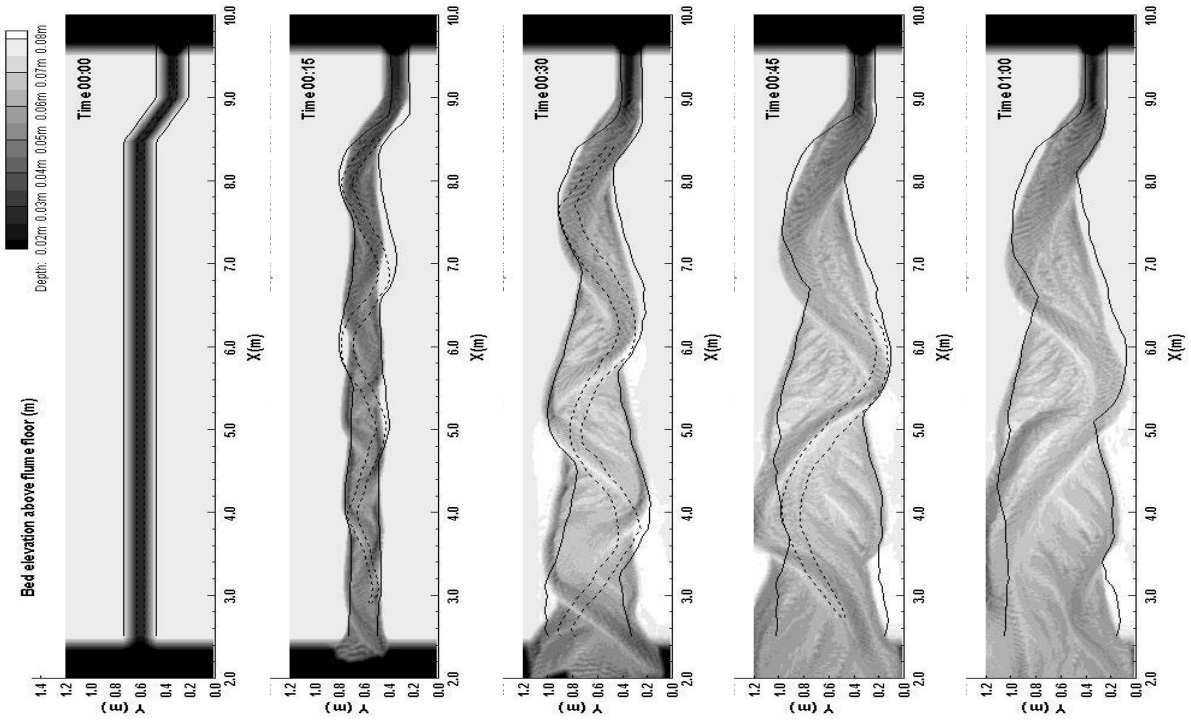

(a) T=0min (b) T = 15 min (c) T = 30 min (d) T = 45 min (e) T = 60 min

Figure 8.12: Comparison of horizontal channel evolution between numerical model predictions and physical model measurements, Test D3. (Solid lines are the channel boundary obtained from physical experimental images.)

8.3.2.2 Bed forms

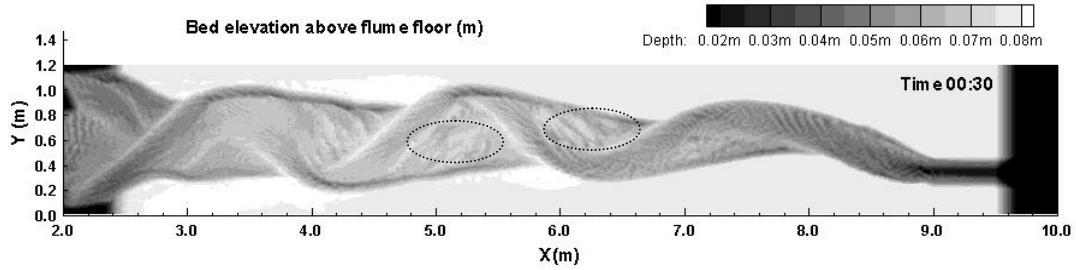

(a) Modelling result for Test D3 at T = 30 min

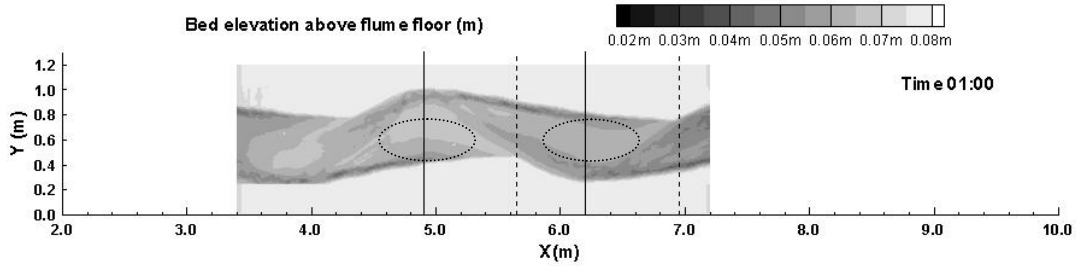

(b) Experiment result for Test D3 at T = 30 min

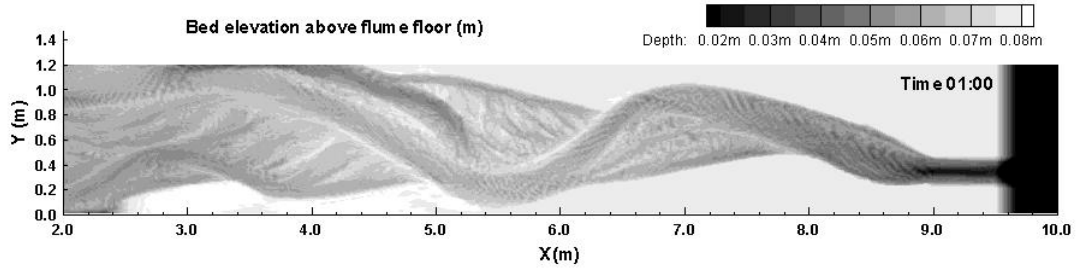

(c) Modelling result for Test D3 at T = 60 min

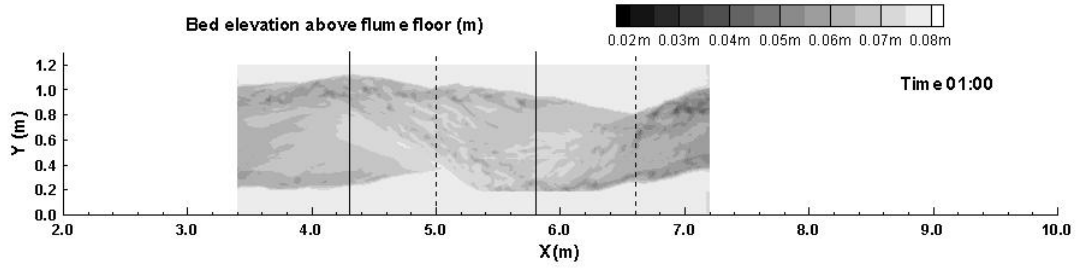

(d) Experiment result for Test D3 at T = 60 min

Figure 8.13: Comparison of bed forms for Test D3 by numerical modelling and physical experiment. (Gray scales are used to show the bed elevation above flume floor.)

It can be seen from Figure 8.13 that at T = 30 min the model predicted channel shape and bed forms agree well with the experiment. The point bars produced from the two methods had similar sizes and locations, the outer boundaries and thalweg lines also had similar shapes. At T = 60 min, numerical model predicted a thalweg, but in the physical model there was not an obvious thalweg in Figure 8.13 (d). The difference can also be observed in Figure 8.11(d).

8.3.2.3 Section shapes

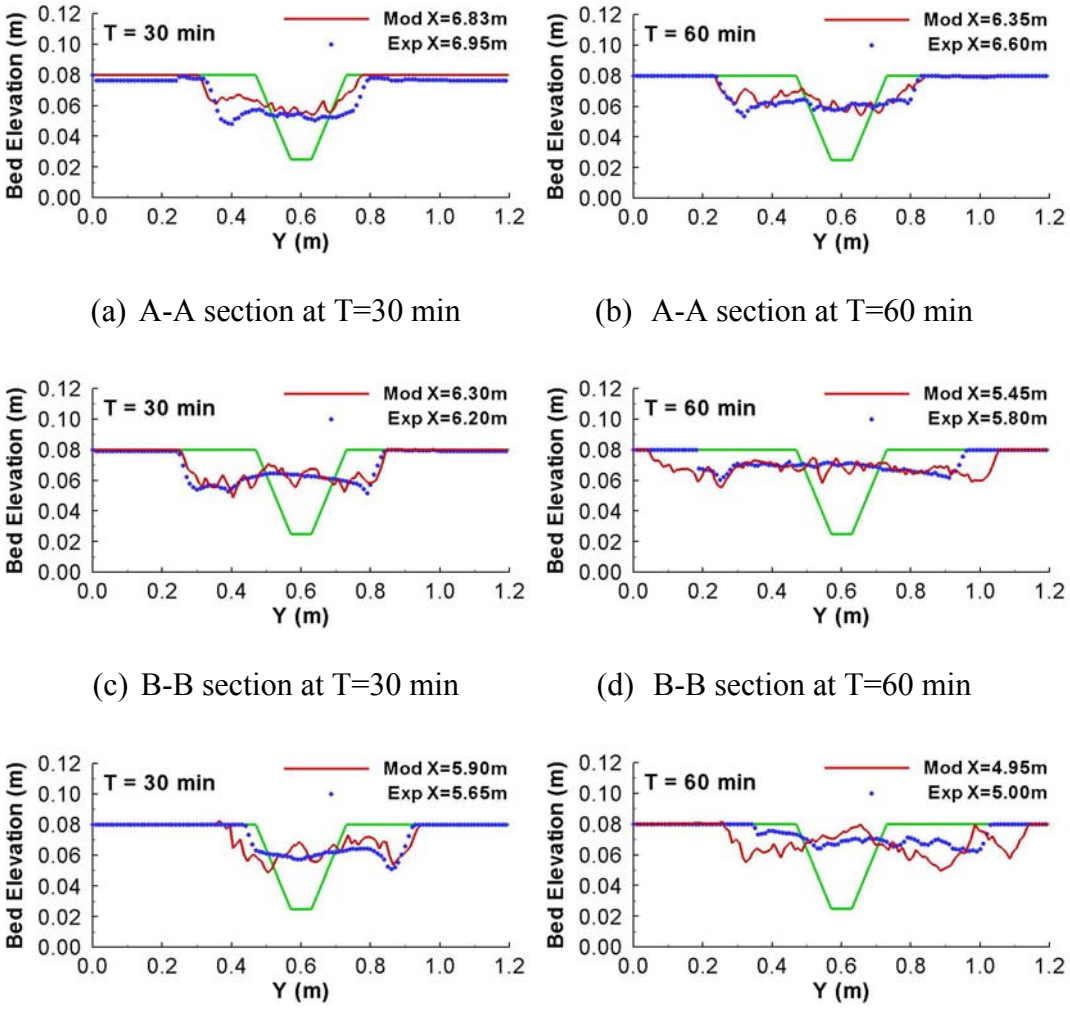

(a) A-A section at T=30 min (b) A-A section at T=60 min

(c) B-B section at T=30 min (d) B-B section at T=60 min

(e) C-C section at T=30 min (f) C-C section at T=60 min

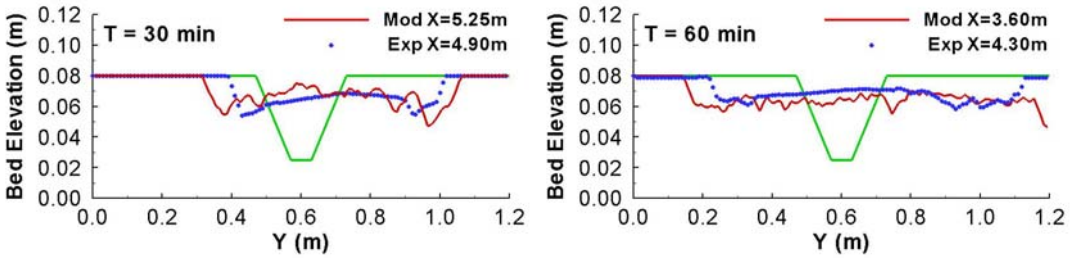

(g) D-D section at T=30 min (h) D-D section at T=60 min

Figure 8.14: Comparison of section shapes for Test D3 by numerical modelling and physical modelling (Points labelled by 'Exp' are the experimental results; lines labelled by 'Mod' are the modelling results; thick solid lines are the initial section shapes; locations of cross-sections A-A, B-B, C-C and D-D are shown in Figure. 8.9b and 8.9d.

The cross-sectional shapes predicted using the numerical model agrees satisfactorily with the physical model. The channel depths, locations of pools and shoals agree well, but the widths have a difference. The numerical model predicted channel width is about 20% larger than the experiment at cross-sections (d), (f), (g) and (h), while at other sections the two methods agree better. At 30 min, the error between predicted and measured results (width and depth) is small and less than 10%. But the error at 60 min is larger.

8.3.3 Numerical modelling results, rapidly varied flow (Test D5)

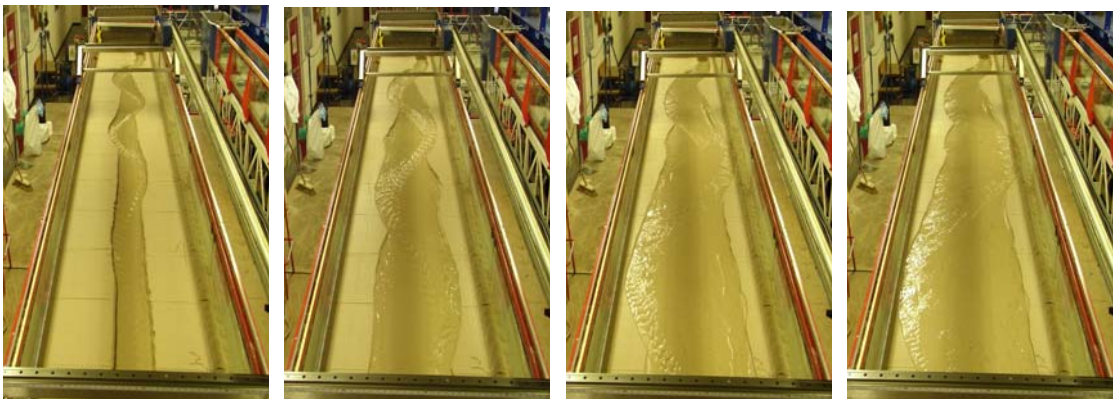

(a): T=15 min (b): T=30 min (c): T=45 min (d): T=60 min

Figure 8.15: Physical experiment development for Test D5 with rapidly varied flow.

In this test, the flow rate was constant, 0.3 l/s for the first 20 min, then increased rapidly to 1.2 l/s and kept constant for another 20 min; later decreased rapidly to 0.3 l/s, keeping 20 min, as shown in Figure 5.43. Experimental results in Figure 8.15 show that D5 had most erosion ability and least curvature in D3, D4 and D5. After 60 min, in D5 one boundary reached the flume wall while D3 and D4 not.

8.3.3.1 Horizontal channel evolution

With a large flow rate lasting for 1/3 of the simulation period (between T = 20 min and 40 min) in Test D5, the channel was eroded rapidly in the lateral direction and the width/depth ratio increased until T = 40 min. During that period, the channel was eroded mostly, see Figure 8.15. After that, channel almost kept its shape because the flow rate was small and channel size was large. The prediction shows a similar channel development trend as the physical model. In the numerical model prediction the channel outer boundaries reached the flume side wall downstream, as in the experiment.

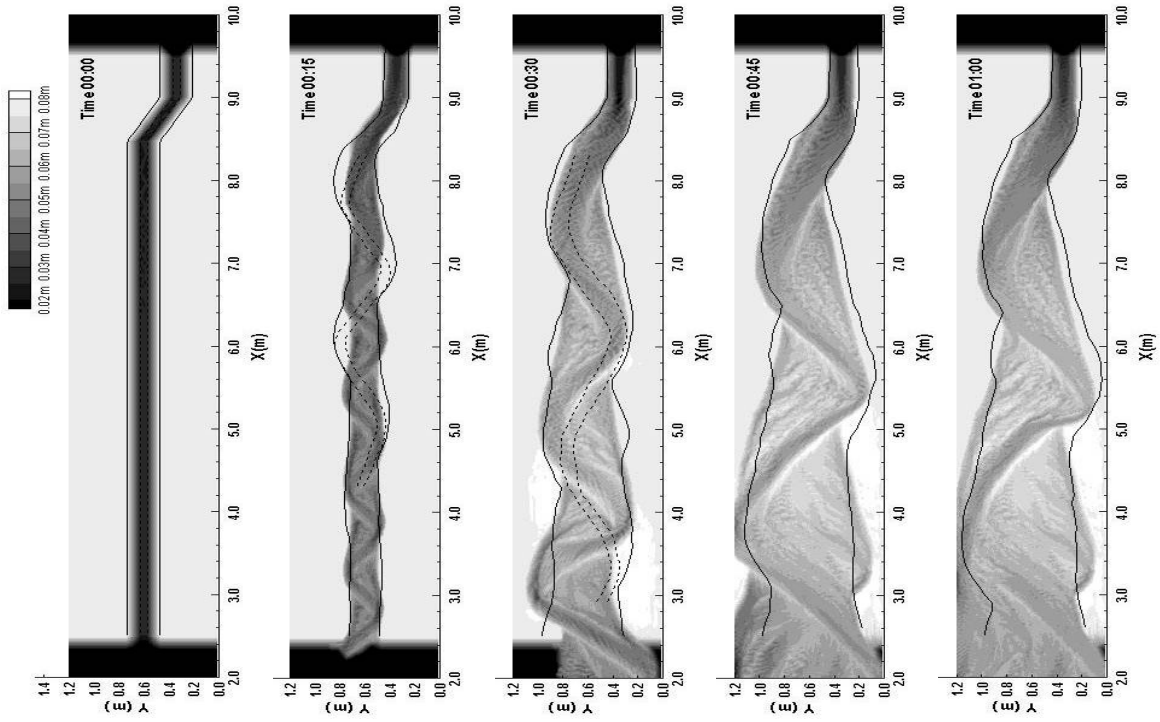

(a) T=0min (b) T = 15 min (c) T = 30 min (d) T = 45 min (e) T = 60 min

Figure 8.16: Comparison of horizontal channel evolution by numerical modelling and physical experiment for Test D5. (Solid lines are the channel boundary obtained from physical experimental images.)

8.3.3.2 Bed forms

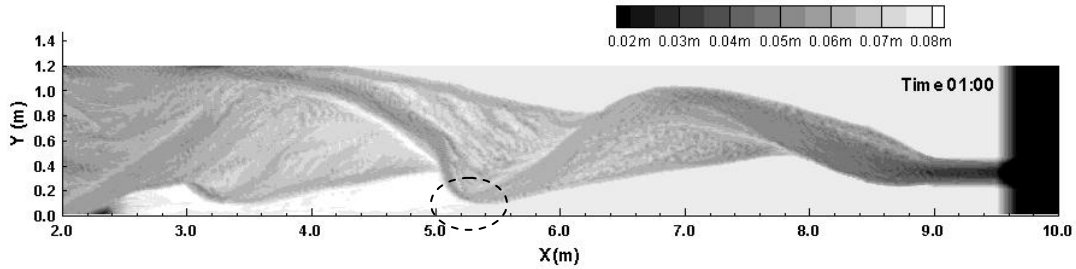

(a) Modelling result for Test D5 at T = 60min

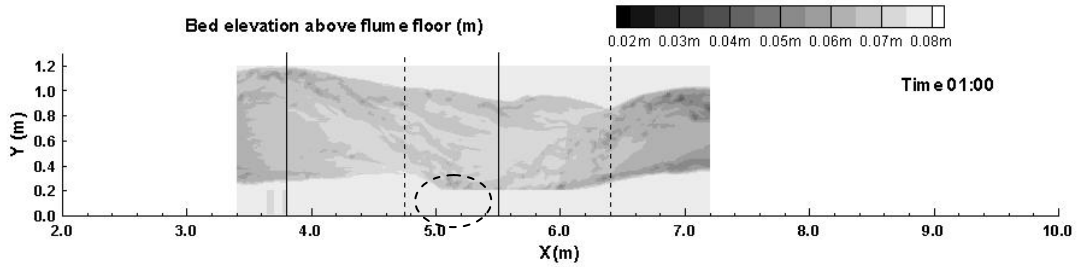

(a) Experiment result for Test D5 at T = 60min

Figure 8.17: Comparison of bed forms for Test D5 by numerical modelling and physical experiment. (Gray scales are used to show the bed elevation above flume floor.)

A comparison of bed levels obtained for the two modelling approaches at T = 60 min is shown in Figure 8.17. The right banks from two methods had the same development trend and they were both eroded seriously and reached one side of the flume wall. The concave banks were eroded as shown by an ellipse in Figure 8.17 at similar positions. Thus, the numerical model prediction agrees well with the experiment.

8.3.3.3 Cross-sectional shapes

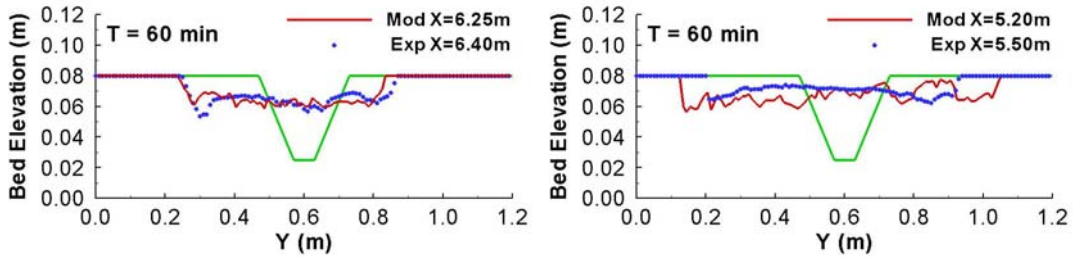

(a) A-A section at 60 min

(b) B-B section at 60 min

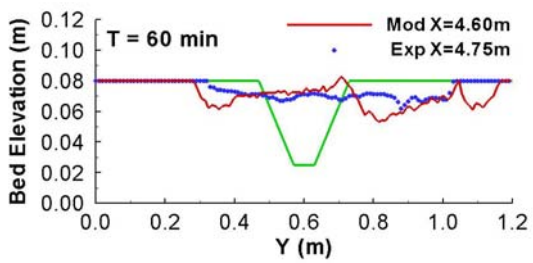

(c) C-C section at 60 min

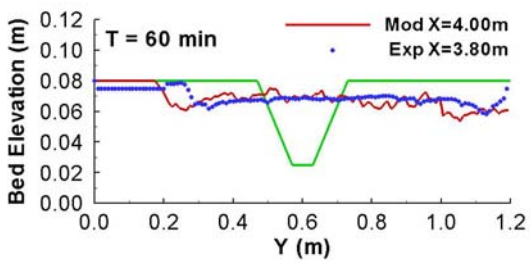

(d) D-D section at 60 min

Figure 8.18: Comparison of section shapes at T = 60 minutes by numerical modelling and physical experiment (Points labelled by 'Exp' are the experimental results; lines labelled by 'Mod' are the modelling results; thick solid lines are the initial section shapes; locations of cross-sections A-A, B-B, C-C and D-D are shown in Figure. 8.17b.

A comparison of cross-sectional shapes by numerical modelling and physical experiment is shown in Figure 8.18. Cross-sections shown in Figures 8.18 (a) and (d) gave the same wide, deep and flat shape. The predicted channels shown in Figures 8.18 (b) and (c) were different from the experiments. It was not flat and the main channel was separated by many branches. Error between predicted and measured data on width is about 30%. During T = 20 min to 40 min, the channel had large flow rate. Because prediction is sensitive to flow rate and overestimate than reality, the numerical modelling amplified this flow rate. As discussed in Chapter 5, a large flow rate could cause the development of braided channels with many branches, as shown in Figures 8.18 (b) and (c).

The numerical modelling could model the characteristics of rapidly varied flow like boundaries curvature, bar position, channel width and depth. The model is sensitive to large flow rate and it would have trend of braided development for channel section shapes.

8.4 Analysis of numerical results with different coefficients

8.4.1 Effect of secondary flow

In order to assess the performance of new secondary flow formula, Equation 7.24 in Chapter 7, a sensitivity analysis was conducted, with the various values of the scale parameter λ (see Equation

7.23 in Chapter 7) being tested. The results at T = 30 min are shown in Figure 8.19, in which picture (b) is the same to the corresponding picture in Figure 8.2.

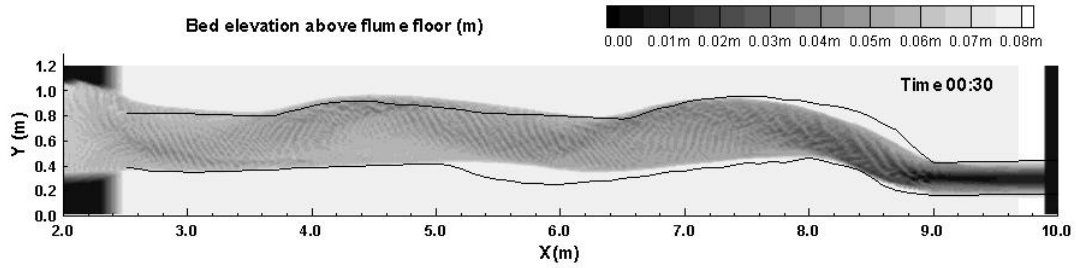

(a) λ = 0.12

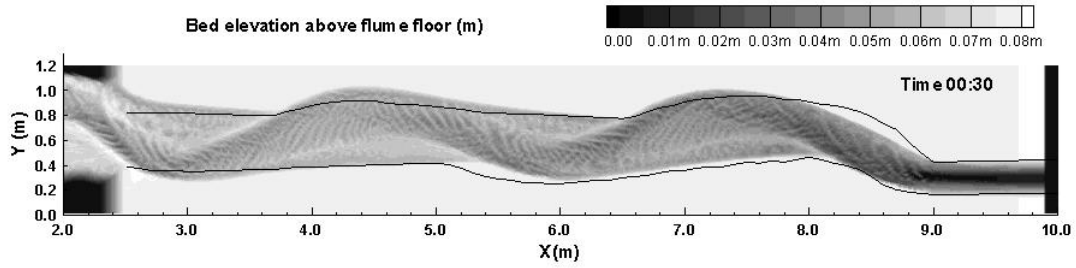

(b) λ = 0.13

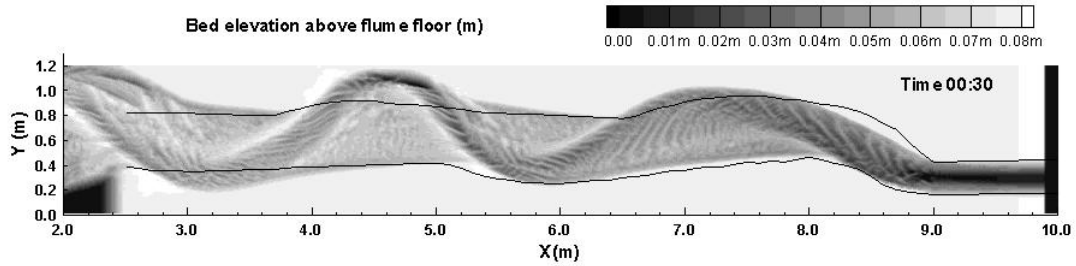

(c) λ = 0.14

Figure 8.19: Channel comparison with various secondary-flow coefficients. (T = 30mins; picture (b) is the same to the corresponding picture in Figure 8.2, Grey scales are used to show the bed elevation above flume floor by numerical modelling; Solid lines are the channel boundary obtained from physical experimental images (Figure 8.1))

It can be seen that the planform at the downstream reach varies distinctly with different coefficients, while the difference is less obvious at the upstream reach. This is thought to be related to the boundary condition of clear water at the inlet, which leads to the deep and steady

channel reach at the upstream end near the inlet (Friedkin, 1945). The comparison shows that the bigger value the λ is, the higher the sinuosity will be, which is caused by the increased sediment transport rate related to the higher secondary flow intensity. At the same time, in the case of higher meander ratio, the meander belt is wider, but the main stream is narrower with lower bed.

8.4.2 Impact of characteristic time scale on bank failure

The experiments were generally undertaken 2 days after the sediment was laid. It was observed from the experiment that if an experiment was carried out just after the sand bed had been formed, without being laid to dry, the evolution of channel would be rather straight without bend being formed. Thus the firmness of the sediment bed is an important factor of the channel forming processes.

The characteristic time scale (τ_f) introduced in Chapter 7, is a factor representing the insistence property. Sensitivity analysis was also carried out to assess the impact of varying τ_f, with its value being set to 0.5 s, 1.0 s, 1.5 s, 5.0 s and 10.0 s, respectively. The results are shown in Figure 8.20, in which, for comparison, picture (c) is the same to the corresponding picture in Figure 8.2.

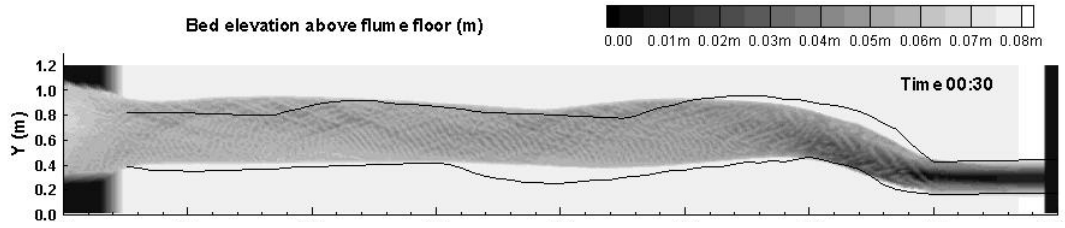

(a) $\tau_f = 0.5$ s

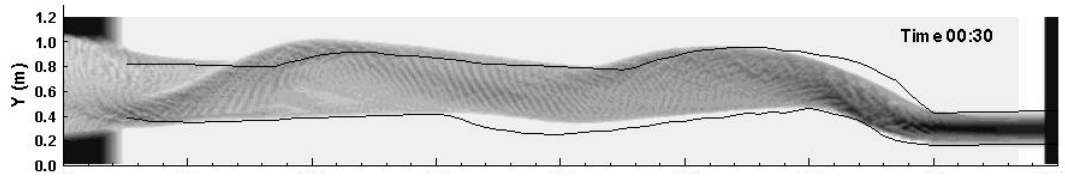

(b) $\tau_f = 1.0$ s

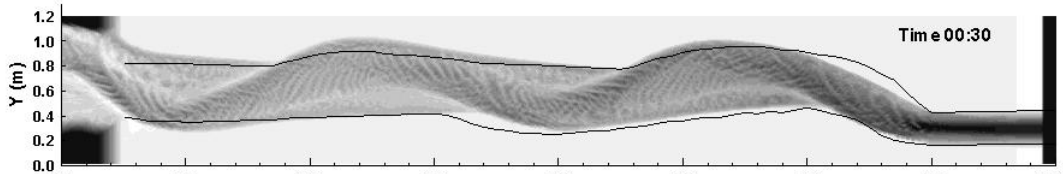

(c) $\tau_f = 1.5$ s

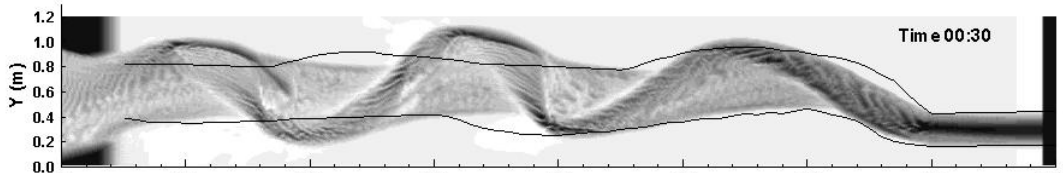

(d) $\tau_f = 5.0$ s

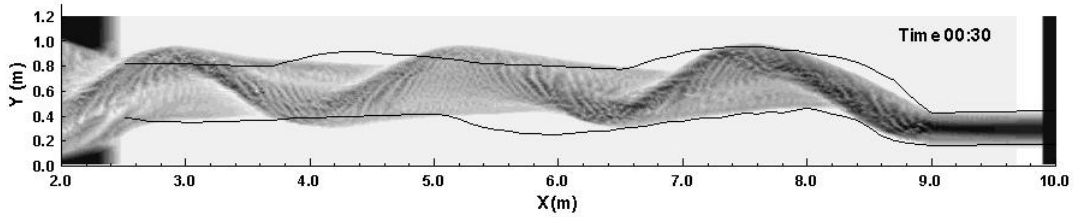

(e) $\tau_f = 10.0$ s

Figure 8.20: Comparison of channel form with various bank-failure time-scales. (T = 30mins; the picture (c) is the same to the corresponding Picture in Figure 8.2**,** Grey scales are used to show the bed elevation above flume floor by numerical modelling; Solid lines are the channel boundary obtained from physical experimental images (Figure 8.1))

Figure 8.20 (a) and (b) show that the channel is rather straight, when τ_f is small, i.e. the bank is less insistent. With the increase of this value, the meander ratio becomes bigger and the meander belt wider, as the bank at front of a bend cannot be eroded immediately and an angle is formed between the main stream and the initial straight channel, as shown by pictures from (a) to (d) in Figure 8.20. However, when the value of τ_f is increased further, seen Figure 8.20 (e), the channel's meander ratio would be reduced. Since the bank is too hard to be eroded in a short time, then a deeper channel is formed. The bank strength related to the vegetation was investigated by

Jang (2005b, 2007b), and it was found that the water depth increased and the width decreased with vegetation. This is similar to the case of a large value of τ_f.

8.5 Summary

In this chapter the numerical modelling results were described for the experiments with steady inflows, gradual varied flows, and rapidly varied flows. The channel sizes were considered (large and medium sizes). The effect of different parameters on channel evolution was also discussed. The numerical model developed in Chapter 7 was used to simulate the channel development processes. The results presented in this chapter showed that the predictions made by this numerical model agree generally well with the physical model measurements. The key characteristics of channel evolution were adequately modelled for different flow rates and channel sizes. These characteristics included the channel width and depth, boundary sinuosity and shape, thalweg sinuosity, point bar positions, locations of erosion and deposition areas. A sensitivity analysis was carried out and it showed that the secondary flow and bank strength are both key parameters in the fluvial channel evolution processes.

Finally, it should be pointed out that parameters used in this study were based on the experimental conditions reported herein. Further calibration, adjustment and development of this model are necessary for other conditions, especially in natural rivers.

Chapter 9

Conclusions and recommendations

9.1 Conclusions

The main objectives of this study are to understand the morphological development in fluvial rivers with meandering thalweg and to develop a numerical model to simulate this process, taking bank erosion and secondary flow into consideration. Chapters 3, 4 and 5 described the development of a physical model of a fluvial river in the laboratory, including sand characteristics, sand transport equations, experimental method and experimental results. A numerical model was developed in Chapters 6 and 7, considering bank erosion and secondary flows. The numerical model is applied to the small model river in the laboratory to study its morphological development. A comparison of results between the physical model and numerical model was given in Chapter 8. This final chapter gives a summary of the main results obtained from this research programme. More detailed discussions about the physical and numerical models can be found in individual chapters.

9.1.1 Physical model of channel development

Flume experiment is an effective method to study channel development. In natural rivers the processes of channel development may take a long time, but in the laboratory these processes can take as little as a few hours or few days. In the current project a series of experiments are carried out in the Hyder Hydraulics Laboratory in Cardiff University. All of the experiments were carried out using non cohesive sand as bank and bed materials. The tests had small, medium and large initial channel section sizes, different flume slopes, steady and unsteady inflows. Diagrams showing the layout of the flume can be found in Figures 4.4a and 4.4b in Chapter 4.

9.1.1.1 Steady inflow

In order to investigate the channel development in the nature for efficient water resource management, reducing hazard, improving benefits from rivers, many physical experiments with steady inflow were carried out in the laboratory to model the fluvial river development. A review of these experiments was given in Chapter 2. A straight trapezoidal section channel with a bending upstream was excavated in the sand bed in the flume to form initial experiment conditions in this study. The channel preparing procedure was described in details in Chapter 4, including the introduction of experiment methods, tools and quipment operation.

The findings from the steady inflow experiments confirmed that a small channel in the laboratory could model many of the characteristics of fluvial rivers in the nature, such as ripple-pool form and point bars. The modelling results showed that in the laboratory, the bed slope for modelling river is much steeper than that in a real river. The physical model provided a good method to study real rivers. In the current study, channels only had meandering thalweg, but they were not real meandering rivers. The main reason is that the sand used as the bed material was non cohesive and point bar could not be stable for a long time after it was formed. The cohesive clay plays a key role to stabilise point bars and to form a real meandering river, not just sinuous thalweg.

At the beginning of channel development, a bank was eroded by the flow at the bend upstream, and then the flow was turned to the bank on the other side of the channel and with the effect of bending to erode that bank. This process continued. Thus a meandering thalweg was formed and

developed along the channel, with alternate pools and bars being formed. The forming process was relatively fast and the channel section shapes became shallow and wide quickly at the beginning. The development gradually became slower both on channel width and depth.

The section shapes in the experiments were measured by an ADV when the flume was filled with water after the experimental operation. This process may have caused slight changes to the bank boundaries but it did not affect the bed profile in the channel. Channel cross-sections were also measured by a point gauge. It is found that using the ADV was more effective. The boundary lines were record by a digital camera. The measured cross-sectional shapes and boundary lines during the channel evolution were presented in Chapter 5.

With the help of above measurement techniques, the reproducibility of the experiments was confirmed. This study investigated the impact of bed slope on channel morphology (in section 5.4.5.1) and confirmed that the slope is a key factor in distinguishing straight, meandering and braided channels. A mild slope would lead to straight channels; a medium slope leads to meandering thalweg channels and a high slope leads to braided channels. The effect of flow rate on channel development was also researched in section 5.4.5.2. A large flow rate had larger meander length, width and amplitude. The cross-sectional area was investigated next. From analysing different controlling parameters, the essential control factor was found to be Froude number. A channel with small width/depth ratio, or a large bed slope, or a large flow rate which leads to meandering all have a large Fr. In the experiments, Fr became smaller and finally less than 0.70. In these meandering thalweg channels, a large Fr caused a smaller sinuosity value.

Experimental results were then discussed with regime theory in section 5.5. Generally speaking, the stable channel sizes from the regime theories agree with the experimental results, but these theories should be carefully chosen, especially considering their ranges of application.

9.1.1.2 Unsteady inflow

In real circumstance, the hydrological condition is more complex, the condition of steady inflow is less common than unsteady inflow. This study investigated the channel morphology with gradually varied flow and rapidly varied flow and compared results obtained under steady inflow conditions.

From the results, it was seen that contour for the case of unsteady inflow is more smooth than steady inflow. Section developments tell that steady inflow could deepen the channel and unsteady inflow has more effect on bank erosion and makes the channel wider.

It is concluded from the measured bed profiles, steady inflow produces more stable ripples, smooth point bars, curved channel banks. Rapidly varied flow produces straight channel, wider upstream. Gradually varied flow produces unstable ripple in the main channel and deepest pools.

Charlton's equations works well for the steady inflow condition and to make them work well for the conditions of gradually varied flow and rapidly varied flow, Charlton's equations should have a ratio as 1.2 for the gradually varied flow and 0.9 for rapidly varied flow, as shown in Table 5.20 in Chapter 5. It must be emphasized that the ratios here were only suitable for the conditions used in current study, for other model rivers or natural rivers, more investigations are needed.

9.1.2 Numerical model

9.1.2.1 Numerical model development

The governing equations used in present study have been given briefly in order to give a clear definition in Chapter 6. The solution processes for these equations were described in Chapter 7, which is the same as DIVAST. Then model was modified to consider the bank erosion and secondary flow effects in the bending areas. In this study, a new method was introduced to calculate the near bed secondary flow by linking it to the transverse water level gradient. This method is based on the balance of force in the transverse direction, which is similar to an existing method, but it is based on the Cartesian coordinate system without the constraint of a constant radius of curvature. The bank erosion model is based on the slope stability theory: when the bank slope is larger than the critical slope, bank failure happens. The new model was applied to physical model to predict the channel evolution process for both steady inflow and unsteady inflow conditions. The numerical results and their comparisons with experimental results were presented in Chapter 8.

9.1.2.2 Numerical model application

From result introduced in Chapter 8, the predictions by this new numerical model agreed generally well with the physical model observations. The key characteristics on channel evolution were adequately predicted for different flow rates and channel sizes, including channel widths and depths, boundary sinuosity and shape, thalweg sinuosity, point bar positions, erosion and deposition place. The manners of meander movement: meander sweep and meander swing are

modelled well. The cusps caused by abrupt downstream shift in the thalweg agree well with physical results. A sensitivity analysis was als carried out and it showed that secondary flow and bank strength are both key parameters in fluvial channel evolution. It must be pointed out that the parameters used in this study are based on experimental condition reported herein. Further calibration, adjustment and development on this model are necessary for other conditions, especially for natural rivers.

9.1.3 Summary of findings

- From the steady inflow flume experiments it has been shown that many of the characteristics of fluvial rivers found in the nature can be represented by the model river in the laboratory. Since non-cohesive sediments were used in this study, the model channel only had curved boundaries with a meandering thalweg, but was not a real meandering river. The experiments are repeatable if the same governing parameters are used.
- From the analysis of different controlling parameters, Froude number is the main controlling factor. A channel with a small width/depth ratio, or a large bed slope, or a large flow rate, leads to a meandering thalweg to occur if there is a large Froude number (more than 1).
- Steady inflow could deepen the channel and unsteady inflow has more effect on bank erosion and makes channel wider. Steady inflow produces stable ripples, smooth point bars, curved channel banks. Rapidly varied flow got a straight channel, which is wider upstream. Gradually varied flow got unstable ripples in the main channel and the deepest pools.

Charlton's equations work well for steady inflow and Charlton's equations should have a ratio for gradually varied flow and rapidly varied flow in this study.

- A new secondary flow model was developed based on the balance of force in the transverse direction, and on the Cartesian coordinate system without the constraint of constant radius of curvature. The bank erosion model is based on the theory of slope stability.
- The predictions of channel characteristics and channel evolution processes by this numerical model agree generally well with the physical model for different flow rates and channel sizes. A sensitivity analysis showed that the secondary flow and bank strength are both key parameters in the fluvial channel evolution.

9.2 Recommendations for future work

Following on from the studies reported herein some shortcomings were identified and the following recommendations are made for future research.

9.2.1 Physical model in the laboratory

- Further full bed profile measurement should be carried out on one test with steady inflow like D4 or D9. In this study, only part of river channel was selected to be measured for comparison purpose. Less attention was focused on the entrance of the channel and bending area because no measurement information was available. The whole channel bed profile measurement could provide opportunity of new finding. Also the full measurement

could compare clearly with numerical results because the numerical model covered the whole area of flume.

- Further experimental studies are still needed to address the deficiencies in the development of small channel in the laboratory, especially in the following situations: (i) the fluvial river morphology changes with much steeper flume slopes, like 0.025, 0.030. (ii) physical experiments for longer period of operation, such as 6 hours or longer, to see further channel development and compare with that in 1 hour, (iii) considering accurate moisture measurements for the channel banks and in different moisture conditions (it could be obtained by different days of drying), further investigations are needed to see its effect.

- More details of measurement are required to help analyse the flow conditions such as Froude number, Reynolds number, these include: (i) flow velocity measurement by a flow meter at different times and at different positions, (ii) channel depth measurement at different times and at different positions, (iii) bed profiles in the longitudinal direction. Further experiments should also be carried out with non-uniform sediments. The sorting effect may be important in the bending sections. It is important to analyse the river curvature effect in the bending sections.

9.2.2 Numerical model development

- To undertake further numerical model simulation to investigate long term channel development trends, especially the thalweg movement, and compare model predictions with short time results presented in this study. To study neck cut-off, chute cut-off and other long term migration phenomena.

- To apply the numerical model developed in this study to natural rivers. At the moment, this model only has been used to simulate the small model rivers in the laboratory and obtained good agreement. In a real situation, the process will be more complex. Thus, further investigation is needed in order to predict the complex situation of a real river.

- Further numerical model enhancements are needed in order to investigate the following situations: (i) river morphological development with steep bed slopes, (ii) channel banks with different moisture contents, (iii) effects of a larger range of flow rates on the channel development and, (iv) wider rivers with free migration in the transverse direction.

REFERENCES

Abrahams, A. D., Li, G. and Atkinson, J. F. (1995). *Step- pool streams: adjustment to maximum flow resistance*. Water resources research. 31, 2593- 602.

Ackers, P. (1964). Experiments *on small streams in alluvium*. J. Hydraulics Div., Am. Soc. Civil Eng. 90, 4, 1-37.

Ackers, P. and Charlton, F. G. (1970a). *Dimensional analysis of alluvial channels with special reference to meander length*. J. Hydraulic Res. 8, 287- 316.

Ackers, P. and Charlton, F. G. (1971). *The slope and resistance of small meandering channels.* Inst, Civ. Eng. Pro., Suppl. 15, pp. 349- 370.

Ackers, P. and White, W. R. (1973). *Sediment Transport: New Approach and Analysis.* Journal of the Hydraulic Division, ASCE. No. HY11.

Bestawy, A. (1997). *Bedload transport and bed forms in steady and unsteady flow.* PhD thesis, Faculteit Toegepaste Wetenschappen. Leuven, Belgium, Katholieke Universiteit Leuven.

Bathurst, J. C., Thorne, C. R. and Hey, R. D. (1979). *Secondary flow and shear stress at river bends.* Journal of Hydraulic Division. ASCE, 105(10), 1277–1295.

Bettess, R., and White, W. R. (1983)**.** *Meandering and braiding of alluvial channels.* Proc. Inst. Civ. Eng., Part 2, London, 75, 525–538.

Brotherton, D. I. (1979). *On the origin and characteristics of river channel patterns*. J. Hydrol. 44 (1979), pp. 211–230.

Chadwick, A., Morfett, J. and Borthwick, M. (2004). *Hydraulics in Civil and Environmental Engineering*. 4th ed. Spon Press, UK.

Chang, H. H. (1979). *Minimum stream power and river channel patterns.* J. Hydrol. 41, 301- 327.

Chang, H. H. (1988). *Fluvial processes in river engineering.* Wiley-Interscience. New York. 432 pp.

Chanson, H. (1999). *The hydraulics of open channel flow- An introduction*. John Wiley & Sons Inc., New York.

Charlton, F. G., Brown, P. M and Benson, R. W. (1978). *The hydraulic geometry of some gravel rivers in Britain.* Hydraulics Research Station, Report IT 180, Wallingford, England.

Chen, D. and Duan, J. G. (2006). *Modelling width adjustment in meandering channels.* Journal of Hydrology. 321. 59- 76.

Cheng, N. S. (1997). *A simplified setting velocity formula for sediment particle.* ASCE J. of Hydraulic Engineering , Vol. 123(2), 149- 152.

Chin, A. (2003). *The geomorphic significance of step–pools in mountain streams*. Geomorphology. 55, 125–137.

Coulthard, T. J., Hicks, D. M. and Van De Wiel, M. J. (2007). *Cellular modelling of river catchments and reaches: Advantages,limitations and prospects*. Geomorphology. 90, 192–207.

Crosato, A. (2008). Analysis and modeling of river meandering. PhD Dissertation, Delft University of Technology, The Netherlands, 251 pp.

Darby, S. E., Alabyan, A. M. and Van De Wiel, M. J. (2002). *Numerical simulation of bank erosion and channel migration in meandering rivers.* Water Resources Research, Vol. 38. No 9. p1163.

Darby, S. E. and Thorn, C. R. (1996). *Development and testing of riverbank-stability analysis.* Journal of Hydraulic Engineering. 122(8), 443- 454.

De Vriend, H. J. (1976). *A mathematical model of steady flow in curved shallow channels.* J Hydraulic Research. 15. 37- 54.

De Vriend, H. (1979). *Flow measurements in a curved rectangular channel*, Internal Report No. 9- 97. Technical report, Laboratory of Fluid Mechanics, Deportment of Civil Engineering, Delft University of Technology.

De Vriend, H. J. (1980). V*elocity redistribution in curved rectangular channels*. J Fluid Mech. Vol 107. 423- 439.

Duan, J. G. and Julien, P. (2005). *Numerical simulation of the inception of meandering channel*. Earth Surface Processes and Land Forms, 30, 1093- 1110.

Duan, G., Wang, S. S. Y. and Jia, Y. (2001). *The applications of the enhanced CCHE2D model to study the alluvial channel migration processes. J. Hydraul. Res.*, 39, 469–480.

Duc, B. M., Wenka, T. and Rodi, W. (2004). *Numerical modelling of bed deformation in laboratory channels.* Journal of Hydraulic Engineering, 130(9): 894-904.

Dulal, K. P. and Shimizu, Y. (2010). *Experimental simulation of meandering in clay mixed sediments.* Journal of Hydroenvironment Research.

Dury, G. H. (1965). *Theoretical implications of underfit streams*. U.S. Geol. Survey, Professional Paper 452- C.

Einstein, H. A. and Shen, H. W. (1964). *A study of meandering in straight alluvial channels*. Journal of Geophysical Research 69 (1964), pp. 5239–5247.

Elder, J. W. (1959). *The dispersion of marked fluid in turbulent shear flow*. Journal of Fluid Mechanics, Vol.5(4), 544-560.

El-Khudairy, M. (1970). *Stable bed profiles in continuous bend.* PhD thesis. Univ of California, Berkeley, Calif.

Engelund, F. (1974). *Flow* and *bed topography in channel bend.* J. Hydrau. Div., Am. Soc. Civ. Eng., 100(11), 1631- 1648.

Engelund, F. and Hansen, E. (1967). *A monograph on sediment transport in Alluvial streams.* Teknisk Forlag, Copenhagen.

Falconer, R. A. (1993). *An introduction to nearly horizontal flows*. In: Coastal Estuarial and Harbour Engineers, Reference Book. M.B. Abbott and W.A. Price (eds). London: E and F.N. Spon Ltd. chapter 2.pp 27-36.

Falconer, R. A. and Chen, Y. (1991). *An improved representation of flooding and drying and wind stress effects in a two-dimensional tidal numerical model.* Proc. Instn Civ Engrs, part 2, 91, 659-678.

Falconer, R. A., Lin, B. L., Wu, Y. and Harris, E. (2001). *DIVAST model user manual.* Cardiff University.

Falconer, R. A., Lin, B. L., Wu. Y. and Harris, E. (2001). *DIVAST model reference manual.* Cardiff University.

Federici, B. and Paola, C. (2003). *Dynamics of channel bifurcations in noncohesive sediments.* Water Resources Research. Vol 39. No 6, 1162.

Fischer, H. B. (1973). *Longitudinal dispersion and turbulent mixing in open channel flow*. Annual Review of Fluid Mechanics, 5: 59-78.

Friedkin, J. F. (1945). "*A laboratory study of the meandering of alluvial rivers*", US Army Engineer Waterways Experiment Station, Vicksburg, Mississippi.

Gao, G. H. (2008). *PhD thesis: Numerical Modelling of Hydrodynamic and Sediment-Bacteria Interaction Processes in Estuarine and Coastal Waters.* Cardiff University.

Gardner, T. W. (1983). *Experimental study of knickpoint and longitudinal profile evolution in cohesive, homogenous material.* Geological Society of America Bulletin 94 (1983), pp. 664–672.

Gerald, C. and Wheatly, P. O. (1994). *Applied numerical analysis*. Addison-Wesley Publishing Company Inc., USA.

Goring, D. and Nikora, V. (2002). Despiking Acoustic Doppler Velocimeter Data. *Journal of Hydraulic Engineering*, Vo.128, No.1 January 1, 2002.

Graf, W. H. and Song, T. (1995). *Bed- shear stress in non-uniform and unsteady open-channel flows*. Journal of Hydraulic research IAHR, 33(5), pp699-704.

Gran, K. and Paola, C. (2001). *Riparian vegetation controls on braided stream dynamics.* Water Resources Research. 37. pp. 3275–3283.

Grant, G. E., Swanson, F. J. and Wolman, M. G. (1990). *Pattern and origin of stepped-bed morphology in high-gradient streams, Western Cascades, Oregon*. Geological Society of America Bulletin 102, 340–352.

Henderson, F. M. (1966). *Open Channel Flow*. Macmillan Co. Ltd. 522p.

Hickin, E. J. (1972). Pseudomeanders and point dunes- a flume study, Am. J. Sci. 272, 762- 799.

Hickin, E. J. and Nanson, G. C. (1975). *The character of channel migration on the Beatton River, northeast B. C., Canada.* Geol. Soc. Am. Bull. 86. 487- 494.

Hickin, E. J. and Nanson, G. C. (1986). *A statistical examination of bank erosion and channel migration in Western Canada*. Bull. Geol. Soc. Am., 97, 497- 504.

Hong, X. T., Ma, S. J. and Guo, Q. W. (1987). *An experimental study on the forming conditions of meandering rivers*. Scientia Geographica Sinica. 1987,7(1), 35-43.

Hooke, J. M. (1979). An *analysis of the processes of river bank erosion*. Journal of Hydrology, 42, 39- 62.

Hooke, J. M. (2007). *Spatial variability, mechanisms and propagation of change in an active meandering river.* Geomorphology. 84, 277- 296.

HR Wallingford. (2003). *Bed Profiler User Manual*.

Ikeda, S., Parker, G. and Kimura, Y. (1988). *Stable width and depth of straight gravel rivers with heterogeneous bed materials*. Water Resource Research, 1988, 24(9): 713-722.

Ikeda, S., Parker, G. and Sawai, K. (1981). *Bend theory of river meanders. Part 1. Linear development.* Jounal of Fluid Mechanics. Vol 112, 363-377.

Jang, C. L. and Shimizu, Y. (2005a). *Numerical Simulation of Relatively Wide, Shallow Channels with Erodible Banks.* Journal of Hydraulic Engineering, Vol. 131, No. 7, 565- 575.

Jang, C. L. and Shimizu, Y. (2005b). *Numerical simulations of the behaviour of alternate bars with different bank strengths.* Journal of Hydraulic Research, 43(6): 596-612.

Jang, C. L. and Shimizu, Y. (2007). *Numerical analysis of braided rivers and alluvial fan deltas.* Engineering applications of computational fluid mechanics. Vol.1, No. 1, pp. 15-24.

Jang, C. L. and Shimizu, Y. (2007). *Vegetation effects on the morphological behaviour of alluvial channels.* Journal of Hydraulic Research, 45(6): 763-772.

Jia, Y. (1990). *Minimum Froude number and the equilibrium of alluvial sand rivers.* Earth Surface Processes and Landforms. 15: 199-209.

Jin, D. and Schumm, S. A. (1986). *A new technique for modelling river morphology*. In: Richards, K.S. (Ed.), Proc. First Internat. Geomorphology Conf. Wiley, Chichester, pp. 680–691.

Johannesson, H. and Parker, G. (1989). *Velocity redistribution in meandering rivers.* Journal of Hydraulic Engineering. 115(8), 1019- 1039.

Julien, P. Y. (2002). *River mechanics*. Cambridge University Press. Cambridge. UK.

Julien, P. J. and Wargadalam, J. (1995). *Alluvial channel geometry: theory and applications*. Journal of Hydraulic Engineering. ASCE. 121.

Kabir, M. R. (1993). *Bed load transport in the unsteady flow.* Faculteit Toegepaste Wetenschappen. Leuven, Belgium, Katholieke Universiteit Leuven, pp 131.

Kalkwijk, J. P. Th. and De. Vriend, H. J. (1980). *Computation of the flow in shallow river bends.* J Hydraulic Research. 18. 327- 343.

Kassem, A. and Chaudhry, M. H. C. (2002). *Numerical modelling of bed evolution in channel bends.* Journal of Hydraulic engineering. ASCE. Vol. 128, NO 5.

Keller, E. A. (1972). *Development of alluvial stream channels: A five- stage model.* Geological Siciety of America Buttetin. 83. 1531- 1536.

Kleinhans, M. G., Schuurman, F., Bakx, W. and Markies. H. (2009). *Meandering channel dynamics in highly cohesive sediment on an intertidal mud flat in the Westerschelde estuary, the Netherlands.* Geomorphology Vol 105, 261- 276.

Kikkawa, H., Ikeda, S. and Kitagawa, A. (1976). *Flow and bed topography in curved open channels.* Journal of Hydraulic Division., ASCE. 102(9), 1327- 1342.

Kirkby, M. J. (1977). *Soil development models as a component of slope models*. Earth Surface Processes, 2, 203-30.

Knighton, A. D. (1973). *Riverbank erosion in relation to streamflow conditions, River Bollin-Dean, Cheshire*. East Midland Geographer, 5, 416- 426.

Knighton, D. (1998). *Fluvial forms and processes: A new perspective*. Arnold, London.

Kocyigit. O., Lin, B. L. and Falconer, R. A. (2005). *Modelling sediment transport using a lightweight bed material*. Maritime Engineering, 158 (MA1) (2005) 3-14 ISSN 1741-7597.

Koutitas, C and Gousidou-Koutita, M. (1986). *A comparative study of three mathematical models for wind generated circulation in coastal areas*. Coastal Engineering, 10(1986) 127-138.

Krone, R. B. (1962). *Flume studies of the transport of sediment in estuarial shoaling processes.* Univ of California, Berkeley, Hydr. Engng. Lab. And Sanit. Engng, Res. Lab. Report.

Kuhnle, Jia and Alonso. (2008). Measured and Simulated Flow Near a Submerged Spur Dike. *Journal of Hydraulic Engineering*, Vol. 134, No. 7, July 2008, pp. 916-924.

Lacey, G. (1929). *Stable channels in alluvium*. Proceedings of the Institution of Civil Engineers, London. 229: 259-292.

Lane, E. W. (1957). *A study of the shape of channels formed by natural streams flowing in erodible materials,* M.R.D. Sediment Series No. 9, U.S. Army Engineer Div., Missouri River, Corps of Engineers, Omaha, Neb.

Langbein, W. B. and Leopold, L. B. (1966). *River meander- theory of minimum variance.* USGS Prof. Paper 422- H, U.S. Geological Survey, Washington, D. C.

Leopold, L. B., Bagnold, R. A., Wolman, R. G. and Brush, L. M. (1960). *Flow resistance in sinuous or irregular channels.* USGS Prof. Paper 282- D, U.S. Geological Survey, Washington, D. C., pp. 111- 134.

Leopold, L. B. and Maddock, T. Jr. (1953). *The Hydraulic Geometry of Stream Channels and Some Physiographic Implications*. U.S. Geological Survey Professional Paper 252, 56p.

Leopold, L. B. and Wolman, M. G. (1957). *River channel patterns: Braided, meandering and straight.* U. S. Geol. Survey Prof. Paper 282- B, pp. 39- 85.

Leopold, L. B., and Wolman, M. G. (1960). *River Meanders*, in Geological Society of America Bulletin, v.71, p.769-794.

Lewalle, J. (2006). Draft of Lecture Notes- Incompressible Fluid Dynamics: Phenomenology, Concepts and Analytical Tools. Syracuse University.

Lin, B. L and Falconer, R. A. (1995). *Modelling Sediment Fluxes in Estuarine Waters Using a Curvilinear Co-ordinate Grid System*. Estuarine, Coastal and Shelf Science, Academic Press Ltd., Vol. 41, pp.413-428.

Madej, M. A., Sutherland, D. G., Lisle, T. E. and Pryor, B. (2009). *Channel responses to varying sediment input: a flume experiment modelled after Redwood Creek, California.* Geomorphology. 103 (2009) 507- 519.

McGraw-Hill of Science and Technology Dictionary. (2003). McGraw-Hill Companies, Inc.

Michiue, M. and Hinokidani, O. (1992). Calculation of 2-dimensional Bed Evolution around Spur-dike. *Annual Journal of Hydraulic Engineering*. JSCE, Vol.36, p61-66 (In Japanese).

Mosselman, E. (1998). *Morphological modelling of rivers with erodible banks.* Hydrol. Process. 12, 1357- 1370.

Murray, A. B. and Paola, C. (1994). *A cellular model of braided rivers.*Nature 371, 54–57.

Murray, A. B. and Paola, C. (1997). *Properties of a cellular braided stream model*. Earth Surface Processes and Landforms 22, 1001–1025.

Nagata, N., Hosoda, T. and Muramoto, Y. (2000). *Numerical analysis of river channel processes with bank erosion*. *J. Hydraul. Eng.*, 126(4), 243–252.

Nanson, G. C. and Hickin, E. J. (1986). *A statistical examination of bank erosion and channel migration in Western Canada.* Bull. Geol. Soc. Am., 97, 497- 504.

Netherlands Summer School. (2008). *International summer school on complex flows, turbulence, morphodynamics and ecology in rivers.*

Nixon, M. (1959). *A study of bankfull discharges of rivers in England and Wales*. Proc. Institution of Civil Engineers. Vol. 12, 157- 175.

Nortek-as. (2004). *User Manual.*

Odgaard, A. J. (1981). Transverse *bed slope in alluvial channel bends*. J. Hydraul. Div., Am. Soc. Civ. Eng., 107(12), 1677- 1694.

Odgaard, A. J. (1986a). *Meander flow model. I: Development.* Journal of Hydraulic Engineering, 112(12): 1117-1136.

Odgaard, A. J. (1986b). *Meander flow model. II: Applications.* Journal of Hydraulic Engineering, 112(12): 1137-1150.

Odgaard, A. J. (1989). *River meander model. I. Development.* Journal of Hydraulic Engineering. 115(11), 1433- 1450.

Ohmoto, T., Hirakawa, R. and Ide, K. (1998). *Responses of Secondary Currents and Sediments to Submerged Groynes.* Annual Journal of Hydraulic Engineer, JSCE, Vol. 42, p1003-1008 (In Japanese).

Olsen, N. R. B. (2003). *Three dimensional CFD modelling of free-forming meander channel.* Journal of Hydraulic Engineering 129 (5), 366–372.

Osman, A. M. and Thorne, C. R. (1988). *Riverbank stability analysis. 1. Theory.* J. Hydraul. Eng., ASCE. 114. 134- 150.

Ouchi, S. (1985). *Response of alluvial rivers to slow active tectonic movement.* Geological Society of America Bulletin 96 (1985) (4), pp. 504–515.

Parker, G. (1983). *Theory of meander bend deformation.* In: Elliott, C. M. (Ed.). River meandering proceeding of ASCE River' 83 Conference, ASCE, pp. 722- 731.

Parker, G. (1998). *River meanders in a tray.* Nature 395, 111- 112.

Parker, G. and Andrew, E. D. (1986). *On the time development of meander bends*. J. Fluid Mech. 162. 139- 156.

Parker, G., Sawai, K. and Ikeda, S. (1982). *Bend theory of river meanders. Part II. Nonliner deformation of finite- amplitude bends.* J. Fluid Mech. 115, 303- 314.

Pizzuto, J. E. (1990). *Numerical simulation of gravel river widening.* Water Resource Research, 1990, 26(9): 1971-1980.

Raudkivi, A. J. (1998). *Loose boundary hydraulics.* A.A.Balkema. Rotterdam, Netherlands.

Preston, R. W. (1985). *Representation of dispersion in two dimensional water flow.* Report No. TPRD/L/2783/N84, Central Electrical Research Laboratories. Leatherhead, England, 1- 13.

Rauen, W. B. (2005). *Physical and numerical modelling of 3-D flow mixing processes in contact tanks.* PhD thesis. Cardiff University.

Rodi, W. (2000). *Turbulence Models and their Application in Hydraulics.* Second edition, International Association for Hydraulics Research, Delft, the Netherlands, 104 pp.

Rozovskii, I. L. (1957). *Flow of Water in Bends of Open Channels (in Russian).* Acad. of Sci. of the Ukrainian SSR, Kiev. (English translation, Isr. Program for Sci. Transl., Jerusalem, 1961.

Rüther, N. and Olsen, N. R. B. (2003). *CFD modelling of alluvial channel instabilities.* Proc. 3rd IAHR Symposium on River, Coastal and Estuarine Morphodynamics. IAHR, Barcelona, Spain.

Rüther, N. and Olsen, N. R. B. (2005a). *Advances in 3D Modelling of Freeforming Meander Formation from Initially Straight Alluvial Channels.* 31st IAHR Congress, Seoul, South Korea.

Rüther, N. and Olsen, N. R. B. (2005b). *Three dimensional modeling of sediment transport in a narrow 90° channel bend*. Journal of Hydraulic Engineering 131 (10), 917–920.

Rüther, N. and Olsen, N. R. B. (2007*). Modelling free-forming meander evolution in a laboratory channel using three-dimensional computational fluid dynamics*. Geomorphology. Vol 89. Issue 3-4. 308- 319.

Schumm, S. A. (1967). *Meander wavelength of alluvial rivers.* Science 157: 1549–1550.

Schumm, S. A. (1968). *River adjustment to altered hydrologic regimen, Murrumbridgee River and paleochannels, Australia*. U.S. Geol, Survey Prof. Paper 598, 65 pp.

Schumm, S. A. (1977). *The fluvial system*. Wiley, New York, 338 pp.

Schumm, S. A. (2005). *River variability and complexity*. Cambridge University Press, UK.

Schumm, S. A. and Khan, H. R. (1971). *Experimental study of channel patterns*, Nature 233, 407-409.

Schumm, S. A. and Khan, H. R. (1972). *Experimental study of channel patterns*, Geol, Soc. Am. Bull. 83, 1755- 1770.

Schumm, S. A., Mosley, M. and Weaver, W. (1987). *Experimental fluvial geomorphology*. Wiley. New York.

Seminara, G. (2006). *Meanders.* Journal of Fluid Mechanics, 554: 271-297.

Shao, X. J. and Wang, X. K. (2005). *Introduction to river mechanics*. Qinghua University. China. (in Chinese)

Shen, H. W. and Komura, S. (1968). *Meandering tendencies in straight alluvial channels.* J. Hydraulics Div. A.S.C.E, 94, 997–1016.

Shepherd, R. G. and Schumm, S. A. (1974). *Experimental study of river incision.* Geological Society of America Bulletin 85 (1974), pp. 257–268.

Shields, A. (1936). *Anwendung der Ahnlichkeits- Mechanik und der Turbulenzforschung auf die Geschiebebewegung, Preussische Versuchsanstalt fur Wasserbau und Schiffbau.* Berlin, Heft.

Shimizu, Y., Hirano, N. and Watanabe, Y. (1996). *Numerical calculation of bank erosion and free meandering.* Annu. J. Hydr. Engrg. JSCE, 40, 921–926 (in Japanese).

Simons, D. B. and Albertson, M. L. (1963). *Uniform water conveyance in alluvial material*. Trans. Am. Soc. Civl Engineers, Vol. 128/I, 65- 167.

Silva, A. (1995). *Turbulence flow in sine-generated meandering channel*. PhD thesis, Queen's building, Kinston, Ontario, Canada.

Smith, C. E. (1998). *Modelling high sinuosity meanders in a small flume*. Geomorphology, 25, 19-30.

Soulsby, R. (1997). *Dynamics of marine sands: a manual for practical applications.* Thomas Telford Publications. London.

Sparks, T. (2007). *PhD thesis: Integrated surface water- groundwater modelling linking surface water and groundwater using DIVAST- SG*. Cardiff University.

Stelling, G. S., Wiersma, A. K. and Willemse, J. B. T. M. (1986). P*ractical Aspects of Accurate Tidal Computations*. Journal of Hydraulic Engineering 112: 802-817.

Sun, J. and Tao, J. H. (2010). *A New Wetting and Drying Method for Moving Boundary in Shallow Water Flow Models.* China Ocean Engineering, 24(1) 79-92.

Sun, T., Meakin, P., Jøssang, T. and Schwarz, K. (1996). *A simulation model for meandering rivers.* Water Resources Research 32(9): 2937–2954.

Sun, T., Meakin, P. and Jøssang, T. (2001a). *A computer model for meandering rivers with multiple bedload sediment sizes. 1. Theory.* Water Resources Research 37(8): 2227–2241.

Sun, T., Meakin, P. and Jøssang, T. (2001b). *A computer model for meandering rivers with multiple bedload sediment sizes. 2. Computer simulations.* Water Resources Research 37(8): 2243–2258.

Tal, M., Gran, K. B., Murray, A. B., Paola, C. and Hicks, M. (2004). *Riparian vegetation as a primary control on channel characteristics in multi-thread rivers*. Eds. Bennett, SH, Collison, AJC, Simon, A, Riparian Vegetation and Fluvial Geomorphology, Water Science and Application, v. 8, p. 43-58.

Taylor, W. (1968). Film notes for secondary flow. Education development center, Inc.

Thompson, A. T. (1986). *Secondary flows and the pool-riffle unit: a case study of the processes of meander development.* Earth Surface Processes and Landforms 11: 631-641.

Thorne, C. R. (1982). *Processes and mechanisms of river bank erosion*. In: Hey, R. D., Bathurst, J. C. and Thorne, C. R., (Eds), Gravel- bed rivers. Wiley, Chichester, 227- 259.

Thorne, C. R., Hey, R. D. and Newson, M. D. (1997). *Applied fluvial geomorphology for river engineering and management*. John Wiley &Sons Ltd. Chichester. England.

Thorne, C. R. and Osman, A. M. (1988a). *The influence of bank stability on regime geometry of natural channels.* In: White, W. R. (ED.), International Conference on River Regime. Hydraulic Research Limited, John Wiley, Chichester, 135- 147.

Tominaga, A., Liu, J., Nagao, M. and Nezu, I. (1995). *Hydraulic characteristics of unsteady flow in open channels with flood plain*. The 26th Congress of IAHR, HYDRA 2000, Thomas Telford London.

Valentine, E. M. and Ershadi, C. (2003). *A laboratory study of alluvial channels with unsteady flow*. XXX IAHR Congress, Thessaloniki, Theme C, pp39- 48.

Van den Berg, J. H. and Bledsoe, B. P. (2003). *Comment on Lewin and Brewer (2001): ''Predicting channel patterns''*. Geomorphology, 53, (2003), 333–337.

van Rijn, L. C. (1984a). *Sediment transport , Part I: Bed load transport*. J. Hydraulic Engineering, ASCE, Vol. 110, 1431- 1456.

van Rijn, L. C. (1984b). *Sediment transport , Part II: Suspended load transport*. J. Hydraulic of Engineering, ASCE, Vol. 110, 1613- 1641.

van Rijn, L. C. (1984c). *Sediment transport , Part III: Bed forms and alluvial roughness*. J. Hydraulic Engineering, Vol. 110, 1733- 1754.

van Rijn, L. C. (1993). *Principles of Sediment Transport in Rivers, Estuaries and Coastal Seas*. Aqua Publications, Netherlands.

Voulgaris, G. and Trowbridge, J. (1997). *Evaluation of the Acoustic Doppler Velocimeter (ADV) for Turbulence Measurements*. Journal of Atmospheric and Oceanic Technology. Vo. 15, March, 1997.

Wahl, T. (2000). *Analyzing ADV Data Using WinADV*. Water Resources. ASCE.

Wang, G. Q., Xia, J. Q. and Wu, B. S. (2008). *Numerical Simulation of Longitudinal and Lateral Channel Deformations in the Braided Reach of the Lower Yellow River*. Journal of Hydraulic Engineering, Vol. 134, No. 8, August 1, 2008.

Wang, X. K., Shao, X. J., Wang, G. Q. and Wu, B. S. (2004). *River Mechanics*. Science publisher. Beijing. (In Chinese)

White, W. R., Bettess. R. and Paris, E. (1982). *Analytical approach to river regime*. J. Hydraulic. Div. ASCE. Vol. 108. NO. HY 10, Oct.

Whittaker, J. G. (1987). *Sediment transport in step- pool streams.* In Thorne, C. R., Bathurst, J.C. And Hey, R.D. (eds), Sediment transport in gravel- bed rivers. Chichester. Wiley, 545- 70.

Xia, J. Q., Wang, G. Q. and Wu, B. S. (2004). *Two-dimensional numerical modelling of the longitudinal and lateral channel deformations in alluvial rivers*. Science in China Ser. E

Engineering & Materials Science 2004 Vol.47 Supp.I 199—211.

Xia, J. Q., Wang, G. Q. and Wu, B. S. (2005). *The braided river morphology development and its numerical modelling.* China Water Resources and Hydro-power Press, Beijing. (In Chinese)

Wang, X. K., Shao, X. J., Wang, G. Q. and Wu, B. S. (2004). *River Mechanics*. Science publisher. Beijing. (In Chinese)

Shao, X. J. and Wang, X. K. (2005). *Introduction to river mechanis*. Qinghua University. China. (In Chinese)

Yalin, M. S. (1972). *Mechanics of Sediment Transport.* Pergamon Press, New York, N. Y., pp. 54-61.

Yang, C. T. (1976). *Minimum unit stream power and fluvial hydraulics*. J. Hydrauli. Div. 102, 769- 784.

Yang, C. T., Song, C. S. and Woldenberg, M. J. (1981). *Hydraulic Geometry and Minimum Rate of Energy Dissipation.* Water Resources Research, Vol. 17, No. 4, 1014-1018.

Yang, L. (2005). *Development of Hydroinformatics Software Tool Enteric BacteriaTransport Modelling Associated With Sediment Transport*. PhD Thesis. Cardiff University.

Yi, X. L. (1965). *The reason for forming meandering river and experiment research on bed deformation*. ACTA GEOGRAPHICA SINICA. Vol 31, No 4. Dec 1965. China Academic Journal Electronic Publishing House. (In Chinese)

Yuan, D. K. (2007). *Development of an integrated hydro-environmental model and its application to a Macro- tidal estuary.* PhD thesis. Cardiff University.

Zanke, U. (1982). *Grundlagen der Sedimentbewegung*. Springer- Verlag.

Zimmermann, C. and Kennedy, J. F. (1978). *Transverse bed slope in curved alluvial streams.* J Hydraulic. Div., Am. Soc. Civ. Eng., 104(1), 33-48.

Appendix 1: Programme for experimental data

```
!
!           This programme is used to deal with data from experimental measurements which are
not in correct order. The programme puts data in correct order with time.
!
!     The requirement for input data is from large to small and minus.
!


PROGRAM DATA_UNIFITED
    implicit none
    INTEGER I,J,K,N,M,IOCHK,SIZE01,SIZE02
    REAL, PARAMETER::ERROR = 0.00001
    REAL, ALLOCATABLE :: REFET(:), EXPT(:), EXPDATA(:), CALDATA(:)
    REAL(8) :: MINL,TEMP,MAXWID,WIDTEP01,WIDTEP02,MAXWP,MAXL,MAXQ
    CHARACTER(LEN=20) :: INPUTFILE = "INPUT.TXT", INPUTFILE01 = "INPUT01.txt"
    CHARACTER(LEN=20) :: OUTPURFILE = "OUTPUT.txt"
    CHARACTER(LEN=30) :: OUTPURFILE2 = "OUTPUT2.txt"


    CHARACTER(LEN=1) O
    CHARACTER ASD,ASDF
    LOGICAL ALIVE
!
```

```
!    REFET       : REFERENCED TIME
!    EXPT        : EXPERIMENTAL TIME
!    EXPDATA     : EXPERIMENTAL DATA
!    CALDATA     : CALCULATED DATA
!
!


     INQUIRE(FILE = INPUTFILE, EXIST = ALIVE)
          IF(.NOT.ALIVE)THEN
          WRITE(*,*)TRIM(INPUTFILE),"    DOESN'T EXIST OR WRONG FILENAME."
          STOP
     END IF


     OPEN (10, FILE = INPUTFILE)
     OPEN (11, FILE = INPUTFILE01)
     OPEN (20, FILE = OUTPURFILE)
     OPEN (30, FILE = OUTPURFILE2)
!
!    To calculate the number of data in section measurement and to set the variable array
!
     DO
          READ(10,'(O)', IOSTAT=IOCHK) O
```

```
        IF (IOCHK < 0) EXIT
        SIZE01 = SIZE01 + 1
    END DO
    REWIND (10)
    IF(SIZE01 .LT. 1)THEN
        WRITE(*,*)TRIM(INPUTFILE),"    IS AN EMPTY FILE OR DATA WRONG."
        STOP
    END IF
    ALLOCATE (REFET(SIZE01),CALDATA(SIZE01))

    DO
        READ(11,'(O)', IOSTAT=IOCHK) O
        IF (IOCHK < 0) EXIT
        SIZE02 = SIZE02 + 1
    END DO
    REWIND (11)
    IF(SIZE02 .LT. 1)THEN
        WRITE(*,*)TRIM(INPUTFILE01),"    IS AN EMPTY FILE OR DATA WRONG."
        STOP
    END IF
    ALLOCATE (EXPT(SIZE02-2),EXPDATA(SIZE02-2))
!
```

```
!     Read the data from file for section measurement and store them in different arrays separately.
!
      SIZE02=SIZE02-2

      READ(11,*)
      READ(11,*)
      DO I=1,SIZE01
          READ(10,*) REFET(I)
      END DO

      DO J=1,SIZE02
          READ(11,*) EXPT(J),EXPDATA(J)
      END DO
!
!     If the input data is minus and then change it to be positive.!
      DO I=1,SIZE01
          REFET(I) = -REFET(I)
      END DO

      DO J=1,SIZE02
          EXPT(J) = -EXPT(J)
          EXPDATA(J) = -EXPDATA(J)
```

```
      END DO

!
!     The interpolation begins by linear interpolation.
!
      DO I=1,SIZE01
          DO J=1,SIZE02
              IF (REFET(1).LE.EXPT(1).AND.REFET(SIZE01).GE.EXPT(SIZE02)) THEN
                  IF (REFET(I).LE.EXPT(1)) THEN
                      CALDATA(I) =
((EXPT(1)-REFET(I))*EXPDATA(2)-(EXPT(2)-REFET(I))*EXPDATA(1))/((EXPT(1)-REFET(
I))-(EXPT(2)-REFET(I)))
                  ELSE IF (REFET(I).GT.EXPT(J-1).AND.REFET(I).LE.EXPT(J)) THEN
                      CALDATA(I) =
EXPDATA(J-1)+(REFET(I)-EXPT(J-1))*(EXPDATA(J)-EXPDATA(J-1))/(EXPT(J)-EXPT(J-1)
)
                  ELSE IF (REFET(I).GE.EXPT(SIZE02)) THEN
                      CALDATA(I) =
((EXPT(SIZE02)-REFET(I))*EXPDATA(SIZE02-1)-(EXPT(SIZE02-1)-REFET(I))*EXPDATA(
SIZE02))/((EXPT(SIZE02)-REFET(I))-(EXPT(SIZE02-1)-REFET(I)))
                  ENDIF
```

```
            ELSE IF (REFET(1).GE.EXPT(1).AND.REFET(SIZE01).LE.EXPT(SIZE02))
THEN
                IF (REFET(I).GT.EXPT(J).AND.REFET(I).LE.EXPT(J+1)) THEN
                    CALDATA(I) =
EXPDATA(J)+(REFET(I)-EXPT(J))*(EXPDATA(J+1)-EXPDATA(J))/(EXPT(J+1)-EXPT(J))
                ENDIF

            ELSE IF (REFET(1).GE.EXPT(1).AND.REFET(SIZE01).GE.EXPT(SIZE02))
THEN
                IF (REFET(I).GT.EXPT(J-1).AND.REFET(I).LE.EXPT(J)) THEN
                    CALDATA(I) =
EXPDATA(J-1)+(REFET(I)-EXPT(J-1))*(EXPDATA(J)-EXPDATA(J-1))/(EXPT(J)-EXPT(J-1)
)
                ELSE IF (REFET(I).GE.EXPT(SIZE02)) THEN
                    CALDATA(I) =
((EXPT(SIZE02)-REFET(I))*EXPDATA(SIZE02-1)-(EXPT(SIZE02-1)-REFET(I))*EXPDATA(
SIZE02))/((EXPT(SIZE02)-REFET(I))-(EXPT(SIZE02-1)-REFET(I)))
                ENDIF

            ELSE IF (REFET(1).LE.EXPT(1).AND.REFET(SIZE01).LE.EXPT(SIZE02))
THEN
                IF (REFET(I).LE.EXPT(1)) THEN
```

```
                    CALDATA(I) =
((EXPT(1)-REFET(I))*EXPDATA(2)-(EXPT(2)-REFET(I))*EXPDATA(1))/((EXPT(1)-REFET(
I))-(EXPT(2)-REFET(I)))
                ELSE IF (REFET(I).GT.EXPT(J).AND.REFET(I).LE.EXPT(J+1)) THEN
                    CALDATA(I) =
EXPDATA(J)+(REFET(I)-EXPT(J))*(EXPDATA(J+1)-EXPDATA(J))/(EXPT(J+1)-EXPT(J))
                ENDIF


            ENDIF
        ENDDO
!
!   Data output and change between positive and negative data!
        WRITE(20,20) (-CALDATA(I)+308+80)/10
        WRITE(*,20) (-CALDATA(I)+308+80)/10
        WRITE(30,20) (-CALDATA(I)+308+80)/10+(720-REFET(I)/10)*0.020
    ENDDO


10  FORMAT(A12)
20  format(f12.4)
STOP
END
```

Appendix 2: Experiment with theory calculation

In Lacey's equation (P_C is calculated wetted perimeter, when channel is wide and shallow, wetted perimeter is channel width):

Medium channel: $(P_{gradual-unsteady} = 1.33 * P_C) > (P_{steady} = 1.17 * P_C) > (P_{sudden-unsteady} = 1.00 * P_C)$

Large channel: $(P_{sudden-unsteady} = 1.04 * P_C) > (P_{steady} = 0.91 * P_C)$

The Lacey's equation could be edited as:

With medium channel: $P_{steady} = 5.62Q^{0.5}$, $P_{gradual-unsteady} = 6.38Q^{0.5}$, $P_{sudden-unsteady} = 4.8Q^{0.5}$

With large channel: $P_{steady} = 4.37Q^{0.5}$, $P_{sudden-unsteady} = 4.99Q^{0.5}$

In Charlton's equation (B_C is calculated width):

For medium channel: $(B_{gradual-unsteady} = 1.20 * B_C) > (B_{steady} = 0.97 * B_C) >$

$(B_{sudden-unsteady} = 0.90 * B_C)$

$(V_{steady} = 1.06 * V_C)$

For large channel: $(B_{sudden-unsteady} = 1.01 * B_C) > (B_{steady} = 0.88 * B_C)$

$$V_{sudden-unsteady} = 1.36 * V_C, \quad y_{0sudden-unsteady} = 1.05 * y_{0C}$$

Charlton's equation can be edited as:

With middle channel: $B_{steady} = 3.74Q^{0.45}$, $B_{gradual-unsteady} = 4.49Q^{0.45}$, $B_{sudden-unsteady} = 3.37Q^{0.45}$

$$V_{steady} = 0.86Q^{0.15}$$

With large channel: $B_{steady} = 3.29Q^{0.45}$, $B_{sudden-unsteady} = 3.78Q^{0.45}$

$$V_{sudden-unsteady} = 1.17Q^{0.15}, \quad y_{0sudden-unsteady} = 0.32Q^{0.40}$$

In Ackers's equation (B_C is calculated width):

For medium channel: $(B_{gradual-unsteady} = 1.37 * B_C) > (B_{steady} = 1.11 * B_C) >$

$(B_{sudden-unsteady} = 1.02 * B_C)$

$V_{steady} = 0.47 * V_C$

For large channel: $(B_{sudden-unsteady} = 1.18 * B_C) > (B_{steady} = 1.03 * B_C)$

$$V_{sudden-unsteady} = 0.60 * V_C, \quad y_{0sudden-unsteady} = 1.99 * y_{0C}$$

Acker's equation could be edited as:

With medium channel:

$B_{steady} = 2.93 Q_w^{0.42}$, $B_{gradual-unsteady} = 3.62 Q_w^{0.42}$, $B_{sudden-unsteady} = 2.69 Q_w^{0.42}$

$V_{steady} = 0.90 Q_w^{0.15}$

With large channel:

$B_{steady} = 2.72 Q_w^{0.42}$, $B_{sudden-unsteady} = 3.12 Q_w^{0.42}$

$$V_{sudden-unsteady} = 1.15 Q_w^{0.15}, \quad y_{0sudden-unsteady} = 0.40 Q_w^{0.43}$$

In Blench's equation:

For medium channel: $(S_{gradual-unsteady} = 12.24 * S_C) > (S_{steady} = 10.75 * S_C)$

For large channel:

$(S_{steady} = 13.0 * S_C)$

$$(B_{sudden-unsteady} = 0.88 * B_C) > (B_{steady} = 0.77 * B_C), \quad y_{0sudden-unsteady} = 0.46 * y_{0C}$$

Blench's equation could be edited as:

With medium channel: $W^*_{steady} = \frac{F_{bc}^{0.5}}{F_s^{0.5}} Q^{0.5}$, $S_{steady} = \frac{10.75 F_{bc}^{0.833} F_s^{0.083} \nu^{0.25}}{3.63 g Q^{0.166} (1 + \frac{Q_s}{2330})}$

$$W^*_{gradual-unsteady} = 1.14\frac{F_{bc}^{0.5}}{F_s^{0.5}}Q^{0.5},$$

$$S_{gradual-unsteady} = \frac{12.24F_{bc}^{0.833}F_s^{0.083}\nu^{0.25}}{3.63gQ^{0.166}(1+\frac{Q_s}{2330})}$$

$$W^*_{sudden-unsteady} = 0.86\frac{F_{bc}^{0.5}}{F_s^{0.5}}Q^{0.5}$$

With large channel: $W^*_{steady} = 0.77\frac{F_{bc}^{0.5}}{F_s^{0.5}}Q^{0.5}$, $S_{steady} = \frac{13.0F_{bc}^{0.833}F_s^{0.083}\nu^{0.25}}{3.63gQ^{0.166}(1+\frac{Q_s}{2330})}$

$$W^*_{sudden-unsteady} = 0.88\frac{F_{bc}^{0.5}}{F_s^{0.5}}Q^{0.5},$$

$$d^*_{sudden-unsteady} = 0.46\frac{F_s^{0.33}}{F_{bc}^{0.66}}Q^{0.33}$$

Table 5.2.5: Comparison of calculated results with experimental results (where Br is channel width and Bm is thalweg width, y0 is depth, λ is meandering wave length, S is channel slope, V is flowing velocity, A is cross section, P wetted perimeter).

	Q=0.6L/S=0.0006 m^3/s	Q=2L/S=0.002 m^3/s
Experiment results / Calculations	D4: B=0.14m, λ=2.3m,s=0.0101 (steady)	D9: B=0.20m, λ=3.0m, s=0.0101 (steady)
	D3: B=0.16m, λ=2.5m, s=0.0115 (gradually varied flow)	
	D5: B=0.12m, λ=2.7m (rapidly varied flow)	D10: B=0.23m, λ=3.1m, V=0.458m/s, y0=0.025-0.03m (rapidly varied flow)
	D6: B=0.30m, V=0.35m/s (slope=0.015)	

	D7: B=0.12m, λ=3.2m, V=0.30m/s (slope=0.025)	
$P = 4.8Q^{0.5}$ (Lacey, 1929)	P=0.12 For steady: $P = 1.17 * P_C$ For gradually varied: $P = 1.33 * P_C$ For rapidly varied: $P = 1.00 * P_C$	P=0.22 For steady: $P = 0.91 * P_C$ For rapidly varied: $P = 1.04 * P_C$
$\lambda = 54.3Q_b^{0.5}$ Dury (1965)	λ =1.33 For steady: $\lambda = 1.73 * \lambda_C$ For gradually varied: $\lambda = 1.88 * \lambda_C$ For rapidly varied: $\lambda = 2.03 * \lambda_C$	λ =2.43 For steady: $\lambda = 1.23 * \lambda_C$ For rapidly varied: $\lambda = 1.27 * \lambda_C$
Charlton et al. (1978) gravel bed rivers: $B = 3.74Q^{0.45}$, $y_0 = 0.31Q^{0.40}$, $V = 0.86Q^{0.15}$	B=0.133, y0=0.016, V=0.283 For steady: $B = (0.90 - -1.05) * B_C$, $V = 1.06 * V_C$ For gradually varied: $B = 1.20 * B_C$ For rapidly varied: $B = 0.90 * B_C$	B=0.228, y0=0.026, V=0.338 For steady: $B = 0.88 * B_C$ For rapidly varied: $B = 1.01 * B_C$ $V = 1.36 * V_C$ $y_0 = (0.96 - -1.15) * y_{0C}$
Ackers (1964) straight channels in medium sand, (Q_w) between 0.011 and 0.153 m^3/s, were: $A = 0.52Q_w^{0.85}$,	B=0.117, y0=0.00823, V=0.631 For steady: $B = (1.02 - -1.20) * B_C$, $V = 0.47 * V_C$ For gradually varied: $B = 1.37 * B_C$	A=0.00264, B=0.194, y0=0.0138, V=0.756 For steady: $B = 1.03 * B_C$ For rapidly varied:

$B = 2.64Q_w^{0.42}$, $y_0 = 0.20Q_w^{0.43}$, $V = 1.92Q_w^{0.15}$	For rapidly varied: $B = 1.02 * B_C$	$B = 1.18 * B_C$ $V = 0.60 * V_C$ $y_0 = (1.81 - -2.17) * y_{0C}$
Bench equation: Mean width: $W^* = \frac{F_{bc}^{0.5}}{F_s^{0.5}} Q^{0.5}$ （m）， Bed depth: $d^* = \frac{F_s^{0.33}}{F_{bc}^{0.66}} Q^{0.33}$ (m) Slope: $S = \frac{F_{bc}^{0.833} F_s^{0.083} \nu^{0.25}}{3.63 g Q^{0.166} (1 + \frac{Q_s}{233}}$	Mean width: 0.14, Bed depth: 0.040 Slope: 0.0007516*2=0.0015032 0.0007516*1.25=0.0009395 For steady: $B_{steady} = B_C$, $S_{steady} = 10.75 * S_C$ For gradually varied: $B_{gradual-unsteady} = 1.14 B_C$, $S = 12.24 * S_C$ For rapidly varied: $B_{sudden-unsteady} = 0.86 B_C$	Mean width:0.26, Bed depth: 0.060 Slope: 0.00062 2S=0.00124 1.25S=0.000775 For steady: $S = 13.0 * S_C$ $B = 0.77 * B_C$ For rapidly varied: $B = 0.88 * B_C$ $y_0 = (0.42 - -0.50) * y_{0C}$

Charlton’s equations give a good result for steady flow on width and velocity.